

MODELING THE TRANSVERSE RESPONSE OF  
SHORT BRIDGES SUBJECTED TO EARTHQUAKES

BY  
CHATDANAI WISSAWAPAISAL AND MARK ASCHHEIM

## ABSTRACT

The transverse response of short bridges is often critical to their seismic performance. When transverse displacements are large, damage to substructure columns may occur, often in the form of plastic hinges, shear failures, or lap splice failures. A significant component of the transverse response is due to the dynamic response of the embankment. Current design provisions (ATC-32 1996, Caltrans 1999) neglect this contribution entirely, and other researchers have only investigated linear models of embankment contribution (Wilson and Tan 1990; Werner et al. 1993; Goel 1997). This report focuses on the modeling of short bridges to improve estimates of column displacement demands. In particular, improved approach-embankment models are developed based on seismic response data recorded at two short bridges in California. The models are nonlinear and can be used in conjunction with software programs such as DRAIN-2DX and DRAIN-3DX. One model explicitly considers the piles and embankment soils, while a second, simpler, model considers only the embankment soils. Both models are calibrated to the recorded California bridge data. The more complex model is used to generate response data for representative Illinois bridges, and this data is used to calibrate the simpler model for Illinois bridges.

Furthermore, when transverse demands are excessive, one mitigation technique is the use of conventional elastomeric bearings to seismically isolate the superstructure. Nonlinear models for Illinois Type I, II and III elastomeric bearings are developed. The effectiveness of the bearings for reducing column displacement demands is addressed by analytical studies. These studies consider potential effects of cold temperatures on bearing stiffness.

Procedures for modeling the embankment and pile contributions, as well as the elastomeric bearings, are described. Current practice for modeling other bridge components is summarized. Finally, an Appendix contains sample input files for use with DRAIN 3DX (Prakash and Powell 1993).

## ACKNOWLEDGMENTS

This report was prepared first as a doctoral dissertation by the first author in partial fulfillment of the requirements for the Ph.D. degree in Civil Engineering at the University of Illinois, Urbana. The research was conducted under the supervision of the second author. Thanks are due to the other members of the doctoral committee: Professors Neil M. Hawkins, Douglas A. Foutch, and James H. Long for their helpful suggestions and recommendations.

We gratefully acknowledge Professor Youssef Hashash for his helpful suggestions concerning the approach-embankment model; Dr. M. Karshenas, Mr. Ralph E. Anderson and Mr. Iraj I. Kaspar at the Illinois Department of Transportation for their helpful suggestions and for providing plans of Illinois bridges; Vladimir Grazier of the Division of Mines and Geology at the California Department of Conservation for specially preparing and releasing data recorded at the Meloland Road Overcrossing; Stuart D. Werner for his helpful suggestions; and Edgar Black for his help with various computer codes.

## TABLE OF CONTENTS

CHAPTER	Page
1	INTRODUCTION..... 1
	1.1 Problem Statement..... 1
	1.2 Object and Scope..... 2
	1.3 Organization..... 2
2	REVIEW OF APPROACH-EMBANKMENT AND ABUTMENT MODELS..... 4
	2.1 Overview..... 4
	2.2 Description of Instrumented Bridges..... 5
	2.2.1 Meloland Road Overpass (MRO)..... 5
	2.2.2 Painter Street Overcrossing (PSO)..... 6
	2.3 Current Practice..... 6
	2.4 Proposed Models for the Approach-Embankment and Abutment..... 6
	2.4.1 Linear Models..... 6
	2.4.2 Equivalent-Linear Model..... 11
	2.4.3 3D-Nonlinear Models..... 12
	2.4.4 Other Approaches..... 13
	2.5 Summary..... 14
3	DEVELOPMENT OF IMPROVED APPROACH-EMBANKMENT MODELS..... 22
	3.1 Introduction..... 22
	3.2 Methodology..... 23
	3.3 Modeling of MRO and PSO..... 23
	3.3.1 Modeling of the Meloland Road Overpass..... 24
	3.3.2 Modeling of the Painter Street Overcrossing..... 24
	3.4 Soil-Pile Model..... 25
	3.4.1 Model Description..... 25
	3.4.2 Model Verification..... 30
	3.4.3 Model Calibration..... 30
	3.5 Soil-Slice Model..... 31
	3.5.1 Model Description..... 31
	3.5.2 Model Calibration..... 32
	3.6 Use of Principal Component Analysis to Observe Inelastic Mode Shape..... 32
	3.7 Determination of $L^*$ for Slab-on-Girder Bridges..... 33
	3.7.1 Bridge Description..... 33
	3.7.2 Calibration of Simple Slice Model for Slab-on-Girder Bridges..... 34

CHAPTER	Page
3.8 Summary.....	36
4 REVIEW OF ELASTOMERIC BEARING BEHAVIOR AND MODELING.....	117
4.1 Overview.....	117
4.2 General Characteristics.....	118
4.3 Mechanical Characteristics.....	119
4.4 DIS Lead-Rubber Isolators.....	122
4.5 Sliding Bearing.....	123
4.6 Illinois Bearings.....	124
4.6.1 Modeling of Type I Bearings.....	125
4.6.2 Modeling of Type II Bearings.....	127
4.6.3 Modeling of Type III Bearings.....	127
5 MODELING OF BRIDGE COMPONENTS.....	137
5.1 Introduction.....	137
5.2 Modeling of Bridge Deck.....	138
5.3 Modeling of Bridge Bents.....	139
5.3.1 Nonlinear Static Push-Over Analysis.....	139
5.3.2 Displacement Capacity.....	140
5.4 Modeling of Bridge Pier Foundation.....	142
5.5 Modeling of Bridge Abutment.....	143
6 EFFECTIVENESS OF ELASTOMERIC BEARING FOR REDUCING ILLINOIS BRIDGE COLUMN DISPLACEMENT DEMANDS.....	147
6.1 Introduction.....	147
6.2 Bridge Description.....	148
6.3 Ground Motions.....	149
6.4 Analytical Model.....	149
6.4.1 Displacement Demands in Conventional Bridges.....	150
6.4.2 Effectiveness of Elastomeric Bearing at Reducing Column Displacement Demands at Normal and Low Temperatures.....	153
6.4.3 Response Comparison between ATC-32 Recommendation for Abutment Modeling vs. Improved Approach-Embankment (Soil-slice) Model.....	154
6.5 Summary.....	155
7 SUMMARY.....	196
7.1 Overview.....	196
7.2 Development of Approach-Embankment Models.....	197

CHAPTER	Page
7.3 A Simplified Version of the Approach-Embankment Model.....	198
7.4 Development of the Bearing Models.....	198
7.5 Effectiveness of Elastomeric Bearings for Reducing Illinois Bridge Column Displacement Demand.....	199
7.6 Recommendations for Future Research.....	199
 APPENDIX A	
MODULUS REDUCTION AND DAMPING CURVE FROM THE MODEL.....	201
 APPENDIX B	
EXAMPLE FILES.....	206
 BIBLIOGRAPHY.....	238

## LIST OF TABLES

Table		Page
2.1	Description of Different Abutment and Embankment Models.....	15
3.1	List of Recorded Motions at MRO and PSO to be Used in Model Calibration.....	37
3.2	Section Properties of MRO.....	37
3.3	Section Properties of PSO.....	37
4.1	HITEC Results for Temperature Effects on Bearings.....	128
6.1	Description of Earthquakes Used in the Analysis.....	156
6.2	Drift Capacity of Pier Column.....	156
6.3	Maximum Relative Displacement for the “As-Built” Bridge.....	156
6.4	Maximum Relative Displacement for the “Fixed Bearing” Bridge.....	157
6.5	Case Study of Low Temperature Effect on Bearings.....	157
6.6	Summary of Peak Displacement Response in All Eight Cases (Table 6.5)....	158



## LIST OF FIGURES

Figure	Page
2.1 Bridge Configuration and Strong Motion Instrumentation (Werner et al. 1990).....	16
2.2 Painter Street Overcrossing, Rio Dell, California.....	16
2.3 Embankment Configuration (Wilson and Tan 1990a).....	17
2.4 Finite Element Model Including Abutment Stiffness (Wilson and Tan 1990b).....	17
2.5 Transverse Mode Shape Components (Werner et al. 1990).....	17
2.6 Finite Element Model of MRO (Werner 1993).....	18
2.7 Recommended Modal Damping Ratios (Werner 1993).....	18
2.8 Variation of Damping with AFP (Goel 1997).....	19
2.9 Schematic View of Equivalent Linear Design Model of the Painter Street Overcrossing with Embankment Detail (Price 1997).....	19
2.10 Detailed Model of the Painter Street Overcrossing Bridge System (McCallen and Romstad 1994b).....	20
2.11 Representation of Deck-Abutment-Backwall Foundation Interaction (Siddharthan et al. 1998).....	20
2.12 Boundary Forces and Moments on the Abutment (Siddharthan et al. 1998).....	21
2.13 Comparison between Computed and Measured Transverse Abutment Stiffness.....	21
3.1 Analytical Model of MRO.....	38
3.2 Analytical Model of PSO.....	38
3.3 Approach-Embankment Cross-Section.....	39
3.4 Illustration of Soil-Pile Model.....	39
3.5 Implementation of Soil-Pile Model.....	40

Figure	Page
3.6a Approach-Embankment Slice.....	41
3.6b Shear Deformation in Each Soil Layer.....	41
3.7a Iwan Spring.....	41
3.7b Stress-Strain Relationship of Iwan Spring.....	41
3.8a Iwan Springs in Parallel.....	41
3.8b Use of Iwan-Type Springs to Represent Non-Linear Hysteretic Behavior of Soils.....	41
3.9a Dimension of a Layer of an Approach-Embankment.....	42
3.9b Schematic View of the First Three Steps to Generate the Shear Springs.....	42
3.10 Ranges of Approach-Embankment Thickness ( $L^*$ ) for Soil-Pile Model Calibrated to MRO and PSO along with the Ratio Between the Calculated and the Recorded Peak Relative Displacement at Pier.....	43
3.11 1992 Main Event on PSO ( $L= 2$ m.), Soil-Pile Model.....	44
3.12 1992 Main Event on PSO ( $L= 3$ m.), Soil-Pile Model.....	45
3.13 1992 Aftershock #1 on PSO ( $L= 2$ m.), Soil-Pile Model.....	46
3.14 1992 Aftershock #1 on PSO ( $L= 3$ m.), Soil-Pile Model.....	47
3.15 1979 Imperial Valley Earthquake on MRO ( $L= 2$ m.), Soil-Pile Model.....	48
3.16 1979 Imperial Valley Earthquake on MRO ( $L= 3$ m.), Soil-Pile Model.....	49
3.17 1992 Aftershock #2 on PSO ( $L= 5$ m.), Soil-Pile Model.....	50
3.18 1992 Aftershock #2 on PSO ( $L= 9$ m.), Soil-Pile Model.....	51
3.19 1986 Main Event on PSO ( $L= 7$ m.), Soil-Pile Model.....	52
3.20 1986 Main Event on PSO ( $L= 12$ m.), Soil-Pile Model.....	53
3.21 1986 Aftershock on PSO ( $L= 8$ m.), Soil-Pile Model.....	54
3.22 1986 Aftershock on PSO ( $L= 14$ m.), Soil-Pile Model.....	55

Figure	Page
3.23 1987 Main Event on PSO (L= 9 m.), Soil-Pile Model.....	56
3.24 1987 Main Event on PSO (L= 16 m.), Soil-Pile Model.....	57
3.25 Soil-Slice Model.....	58
3.26 1992 Main Event on PSO (L= 1 m.), Soil-Slice Model.....	59
3.27 1992 Main Event on PSO (L= 2 m.), Soil-Slice Model.....	60
3.28 1992 Aftershock #1 on PSO (L= 1 m.), Soil-Slice Model.....	61
3.29 1992 Aftershock #1 on PSO (L= 2 m.), Soil-Slice Model.....	62
3.30 1979 Imperial Valley Earthquake on MRO (L= 1 m.), Soil-Slice Model.....	63
3.31 1979 Imperial Valley Earthquake on MRO (L= 2 m.), Soil-Slice Model.....	64
3.32 1992 Aftershock #2 on PSO (L= 3 m.), Soil-Slice Model.....	65
3.33 1992 Aftershock #2 on PSO (L= 7 m.), Soil-Slice Model.....	66
3.34 1986 Main Event on PSO (L= 4 m.), Soil-Slice Model.....	67
3.35 1986 Main Event on PSO (L= 9 m.), Soil-Slice Model.....	68
3.36 1986 Aftershock on PSO (L= 5 m.), Soil-Slice Model.....	69
3.37 1986 Aftershock on PSO (L= 11 m.), Soil-Slice Model.....	70
3.38 1987 Main Event on PSO (L= 6 m.), Soil-Slice Model.....	71
3.39 1987 Main Event on PSO (L= 13 m.), Soil-Slice Model.....	72
3.40 Ranges of Approach-Embankment Thickness ( $L^*$ ) for Soil-Slice Model Calibrated to MRO and PSO along with the Ratio Between the Calculated and the Recorded Peak Relative Displacement at Pier.....	73
3.41 Ranges of Approach-Embankment Thickness ( $L^*$ ) for Soil-Pile and Soil-Slice Model Calibrated to MRO and PSO.....	74
3.42a First PCA Mode Shape (PGA = 0.09 g.).....	75
3.42b First PCA Mode Shape (PGA = 0.12 g.).....	76

Figure	Page
3.42c First PCA Mode Shape (PGA = 0.16 g.).....	77
3.42d First PCA Mode Shape (PGA = 0.20 g.).....	78
3.42e First PCA Mode Shape (PGA = 0.52 g.).....	79
3.42f First PCA Mode Shape (PGA = 0.54 g.).....	80
3.43 First PCA Mode Shape (PGA = 0.30 g.).....	81
3.44 A Typical Illinois Bridge.....	82
3.45 Analytical Model of an Illinois Bridge.....	82
3.46 Ranges of Approach-Embankment Thickness ( $L^*$ ) for Soil-Slice Model for Illinois Bridges.....	83
3.47 1992 Main Event on IL-1, L= 2 m. (Soil-Slice Model), L= 2 m. (Soil-Pile Model).....	84
3.48 1992 Main Event on IL-1, L= 3 m. (Soil-Slice Model), L= 3 m. (Soil-Pile Model).....	85
3.49 1992 Aftershock #1 on IL-1, L= 2 m. (Soil-Slice Model), L= 2 m. (Soil-Pile Model).....	86
3.50 1992 Aftershock #1 on IL-1, L= 3 m. (Soil-Slice Model), L= 3 m. (Soil-Pile Model).....	87
3.51 1979 Imperial Valley Earthquake on IL-1, L= 2 m. (Soil-Slice Model), L= 2 m. (Soil-Pile Model).....	88
3.52 1979 Imperial Valley Earthquake on IL-1, L= 3 m. (Soil-Slice Model), L= 3 m. (Soil-Pile Model).....	89
3.53 1992 Aftershock #2 on IL-1, L= 3 m. (Soil-Slice Model), L= 5 m. (Soil-Pile Model).....	90
3.54 1992 Aftershock #2 on IL-1, L= 7 m. (Soil-Slice Model), L= 9 m. (Soil-Pile Model).....	91
3.55 1986 Main Event on IL-1, L= 4 m. (Soil-Slice Model), L= 7 m. (Soil-Pile Model).....	92

Figure	Page
3.56 1986 Main Event on IL-1, L= 9 m. (Soil-Slice Model), L= 12 m. (Soil-Pile Model).....	93
3.57 1986 Aftershock on IL-1, L= 5 m. (Soil-Slice Model), L= 8 m. (Soil-Pile Model).....	94
3.58 1986 Aftershock on IL-1, L= 11 m. (Soil-Slice Model), L= 14 m. (Soil-Pile Model).....	95
3.59 1987 Main Event on IL-1, L= 6 m. (Soil-Slice Model), L= 9 m. (Soil-Pile Model).....	96
3.60 1987 Main Event on IL-1, L= 13 m. (Soil-Slice Model), L= 16 m. (Soil-Pile Model).....	97
3.61 1992 Main Event on IL-2, L= 2 m. (Soil-Slice Model), L= 2 m. (Soil-Pile Model).....	98
3.62 1992 Main Event on IL-2, L= 3 m. (Soil-Slice Model), L= 3 m. (Soil-Pile Model).....	99
3.63 1992 Aftershock #1 on IL-2, L= 2 m. (Soil-Slice Model), L= 2 m. (Soil-Pile Model).....	100
3.64 1992 Aftershock #1 on IL-2, L= 3 m. (Soil-Slice Model), L= 3 m. (Soil-Pile Model).....	101
3.65 1979 Imperial Valley Earthquake on IL-2, L= 2 m. (Soil-Slice Model), L= 2 m. (Soil-Pile Model).....	102
3.66 1979 Imperial Valley Earthquake on IL-2, L= 3 m. (Soil-Slice Model), L= 3 m. (Soil-Pile Model).....	103
3.67 1992 Aftershock #2 on IL-2, L= 3 m. (Soil-Slice Model), L= 5 m. (Soil-Pile Model).....	104
3.68 1992 Aftershock #2 on IL-2, L= 7 m. (Soil-Slice Model), L= 9 m. (Soil-Pile Model).....	105
3.69 1986 Main Event on IL-2, L= 4 m. (Soil-Slice Model), L= 7 m. (Soil-Pile Model).....	106

Figure	Page
3.70 1986 Main Event on IL-2, L= 9 m. (Soil-Slice Model), L= 12 m. (Soil-Pile Model).....	107
3.71 1986 Aftershock on IL-2, L= 5 m. (Soil-Slice Model), L= 8 m. (Soil-Pile Model).....	108
3.72 1986 Aftershock on IL-2, L= 11 m. (Soil-Slice Model), L= 14 m. (Soil-Pile Model).....	109
3.73 1987 Main Event on IL-2, L= 6 m. (Soil-Slice Model), L= 9 m. (Soil-Pile Model).....	110
3.74 1987 Main Event on IL-2, L= 13 m. (Soil-Slice Model), L= 16 m. (Soil-Pile Model).....	111
3.75 Ranges of Approach-Embankment Thickness ( $L^*$ ) for California vs. Illinois Bridges (Figure 3.40 vs. Figure 3.46).....	112
3.76 Response Comparison Between Different Models Subjected to 1992 Main Event on IL-2.....	113
3.77 Response Comparison Between Different Models Subjected to 1986 Main Event on IL-2.....	114
3.78 Comparison of First PCA Mode Shape for IL-2 Bridge Subjected to 1992 Main Event.....	115
3.79 Comparison of First PCA Mode Shape for IL-2 Bridge Subjected to 1986 Main Event.....	116
4.1 Effect of Temperature on Crystallization Rate (Murray and Detenber 1961).....	129
4.2 Effect of Temperature on Stiffness (Murray and Detenber 1961).....	129
4.3 Increase in Shear Stiffness with Exposure Time (Hours) to -13 F (-25 C) (Eyre and Stevenson 1991).....	130
4.4 Effect of Freeze-Thaw Cycles on Low Temperature Stiffening (Eyre and Stevenson 1991).....	130
4.5 Force Displacement Relationship for DIS Lead-Rubber Isolators (Dynamic Isolation System 1993).....	131

Figure	Page
4.6 Teflon-Stainless Steel Slider Showing Dimensions (Kelly and Chalhoub 1990).....	132
4.7 Elastomeric and TFE Elastomeric Expansion Bearings used in Illinois (Jacobsen 1977).....	133
4.8 Coefficient of Friction vs. Vertical Pressure for Laminated Elastomeric- TFE Sliding Bearing (Jacobsen 1977).....	134
4.9 Modeling of Type I Bearing (Without Teflon Sliding Surface).....	135
4.10 Modeling of Type II Bearing (With Teflon Sliding Surface).....	135
4.11 Modeling of Type III Bearing with Sequence of Model Construction.....	136
5.1 A Representative Four-Span Bridge Commonly in Illinois.....	144
5.2 Ranges of Deck Moment of Inertia Used in the Model.....	144
5.3 Nonlinear Static-Pushover Analysis for Multiple Pier-Columns.....	145
5.4 Flexure Contribution to Column Yield Displacement.....	145
5.5 Pier Foundation Spring p-y Analysis .....	146
6.1a A Model Bridge.....	159
6.1b Map of Illinois Showing Three Bridge Sites.....	160
6.2 Design Spectra for the Three Bridge Sites.....	161
6.3 Scaling of the Earthquake Spectra for Knox County, Soil Type B.....	162
6.4 Scaling of the Earthquake Spectra for Knox County, Soil Type D.....	163
6.5 Scaling of the Earthquake Spectra for Knox County, Soil Type E.....	164
6.6 Scaling of the Earthquake Spectra for Marion County, Soil Type B.....	165
6.7 Scaling of the Earthquake Spectra for Marion County, Soil Type D.....	166
6.8 Scaling of the Earthquake Spectra for Marion County, Soil Type E.....	167
6.9 Scaling of the Earthquake Spectra for Massac County, Soil Type B.....	168

Figure	Page
6.10	Scaling of the Earthquake Spectra for Massac County, Soil Type D..... 169
6.11	Original Time-History Records..... 170
6.12	Scaled Time-History Records..... 171
6.12	Scaled Time-History Records..... 172
6.13	Two-Dimensional Bridge Model for the “As-Built” Bridge..... 173
6.14	Two-Dimensional Bridge Model for the “Fixed Bearing” Bridge..... 173
6.15	Elastic Mode Shape of the “As-Built” Bridge..... 174
6.16	Elastic Mode Shape of the “Fixed Bearing” Bridge..... 174
6.17	Hysteresis for the “As-Built” Bridge at Knox County, IL. Soil Type B..... 175
6.18	Hysteresis for the “As-Built” Bridge at Knox County, IL. Soil Type D..... 176
6.19	Hysteresis for the “As-Built” Bridge at Knox County, IL. Soil Type E..... 177
6.20	Hysteresis for the “As-Built” Bridge at Marion County, IL. Soil Type B..... 178
6.21	Hysteresis for the “As-Built” Bridge at Marion County, IL. Soil Type D..... 179
6.22	Hysteresis for the “As-Built” Bridge at Marion County, IL. Soil Type E..... 180
6.23	Hysteresis for the “As-Built” Bridge at Massac County, IL. Soil Type B..... 181
6.24	Hysteresis for the “As-Built” Bridge at Massac County, IL. Soil Type D..... 182
6.25	Hysteresis for the “Fixed Bearing” Bridge at Knox County, IL. Soil Type B..... 183
6.26	Hysteresis for the “Fixed Bearing” Bridge at Knox County, IL. Soil Type D..... 184
6.27	Hysteresis for the “Fixed Bearing” Bridge at Knox County, IL. Soil Type E..... 185
6.28	Hysteresis for the “Fixed Bearing” Bridge at Marion County, IL. Soil Type B..... 186



Figure	Page
6.29 Hysteresis for the “Fixed Bearing” Bridge at Marion County, IL. Soil Type D.....	187
6.30 Hysteresis for the “Fixed Bearing” Bridge at Marion County, IL. Soil Type E.....	188
6.31 Hysteresis for the “Fixed Bearing” Bridge at Massac County, IL. Soil Type B.....	189
6.32 Hysteresis for the “Fixed Bearing” Bridge at Massac County, IL. Soil Type D.....	190
6.33 Two-Dimensional Bridge Model with ATC-32 Abutment.....	191
6.34 Two-Dimensional Bridge Model with Approach-Embankment Model.....	191
6.35 Peak Transverse Displacement Responses of Various Bridge Components (Cases 1-4 -- ATC-32 Model).....	192
6.36 Peak Transverse Displacement Responses of Various Bridge Components (Cases 5-8 -- Soil-Slice Model).....	193
6.37 Comparison of First PCA Mode Shape for “Low” Level of Shakings.....	194
6.38 Comparison of First PCA Mode Shape for “High” Level of Shakings.....	195

## CHAPTER 1

### INTRODUCTION

#### 1.1 Problem Statement

Although seismicity in the New Madrid region is not given as much attention as seismicity in the West Coast, the seismic threat is real and significant. A reasonable goal is that bridges used in the transportation infrastructure must not collapse during an earthquake. For typical short span bridges, the transverse response is critical and the column therefore must be capable of accommodating the imposed displacement demand. The displacement demand at bridge bents is dominated by the dynamic response of the approach-embankment, which includes the foundation soil that supports the abutments at each end of the bridge. This subject has been studied by many researchers recently (Wilson and Tan 1990; Werner et al. 1993; Sweet and Morrill 1993; McCallen and Romstad 1994; Price 1997; and Siddharthan et al. 1998); and several abutment/embankment models have been proposed. However, these models have several drawbacks, described in Chapter Two. An improved approach-embankment model is described to improve column displacement estimates in Chapter Three.

The column displacement demand often may be reduced by using elastomeric bearings at the deck-substructure interface. Conventional rubber bearings have been widely used in Midwestern bridges to accommodate temperature movement since the 1970s. These bearings may be useful for seismically isolating the deck, and thus may be effective for reducing substructure demands during earthquakes. An analytical model for these bearings is described in Chapter Four. The effectiveness of the bearings for

reducing column displacement demands is addressed in analytical studies reported in Chapter Six.

## 1.2 Object and Scope

This study has several objectives:

- (1) To develop an approach-embankment model, to better predict the displacement demand in bridge piers. This part of the study focuses on the transverse response of short bridges, since this often is critical to pier columns. Due to the sparseness of recorded data, the approach-embankment model is calibrated to data obtained from two bridges in California (Painter Street Overcrossing (PSO) and Meloland Road Overpass (MRO)). Then a simpler version of the new model is introduced and calibrated to analytical results developed for Illinois bridges using the more complex approach-embankment model.
- (2) To develop analytical models for the conventional elastomeric bearings used widely in Illinois.
- (3) To investigate analytically the effectiveness of these bearings in reducing bridge column displacement demand.

## 1.3 Organization

There is a total of 7 chapters. Chapter One is an introduction. Chapter Two is a literature review of existing approach-embankment and abutment models developed by several investigators. Chapter Three describes the development of improved approach-

embankment models. This chapter includes the model development methodologies, description of the models, verification of the models, and calibration of the models.

Chapter Four reviews elastomeric bearing behavior and existing models. The behavior and mechanical characteristics of elastomeric bearings is presented as background material, and analytical models for the three types of bearings normally used in Illinois are introduced. Chapter Five describes the modeling of other bridge components according to current recommendations. These recommendations are used in Chapter Six to investigate the effectiveness of elastomeric bearings for reducing column displacement demands in representative Illinois bridges. This chapter describes the bridges, ground motions, and analytical results concerning the effect of elastomeric bearings on bridge response. Chapter Seven summarizes the work and principal findings.

## CHAPTER 2

### REVIEW OF APPROACH-EMBANKMENT AND ABUTMENT MODELS

#### 2.1 Overview

The dynamic characteristics of the foundation soil that supports the abutments at each end of a bridge can have a significant influence on the seismic response of short- and medium-span highway bridges (Wilson and Tan 1990). There are several issues involving abutment/embankment modeling: (1) whether the model includes the flexibility of the soil embankments; (2) whether the soil load-deformation relations are modeled as linear, equivalent linear, or nonlinear; (3) whether material damping is modeled as equivalent viscous or is accounted for directly in the nonlinear hysteretic response of the material; (4) whether the inertial mass of the soil is included; and, (5) whether the model takes into account pile-soil interaction.

Current design provisions (Caltrans 1999) and recommendation (ATC-32 1996) neglect the embankment flexibility but provide guidelines for modeling the flexibility of the abutment wingwalls. In general, this is not sufficient to capture the embankment contribution to transverse response. The Caltrans (1999) and ATC-32 (1996) recommendation are described in this chapter along with recent proposals for modeling the embankments. The improved seismic design criteria recommended for California bridges (ATC-32 1996) models the abutment wingwall stiffness but there is no recommendation on how to model the approach embankment, which includes the foundation soil that supports the abutments at each end of the bridge.

The only known records of bridge response to strong ground motions are those recorded at the Meloland Road Overpass (MRO) and Painter Street Overpass (PSO),

which were instrumented by California Strong Motion Instrumentation Program (CSMIP). Data from these bridges has been used in many relevant research studies (Werner et al. 1987; Douglas et al. 1990; Wilson and Tan 1990; Sweet and Morrill 1993; McCallen and Romstad 1994; Goel and Chopra 1997; and Price 1997). These bridges experienced several earthquakes of varying magnitude. The contribution of abutment/embankment system to the overall dynamic response of the bridge system has been studied by many investigators (Wilson and Tan 1990; Werner et al. 1993; Sweet and Morrill 1993; McCallen and Romstad 1994; Maroney et al. 1994; Goel 1997; Price 1997; and Siddharthan et al. 1998). The differences between each model are summarized in Table 2.1. These modeling approaches are examined below starting from the simplest linear model, ending with a 3-D nonlinear model.

## 2.2 Description of Instrumented Bridges

### 2.2.1 Meloland Road Overpass (MRO)

MRO is a prestressed concrete box-girder bridge that is continuous over two spans of 104 ft. each. The superstructure is supported on monolithic abutments and a single central column. Piles supporting the abutments and single column are timber, having little embedment into the reinforced concrete pile caps. The California Strong Motion Instrumentation Program (CSMIP) instrumented the bridge with 26 channels of strong-motion instrumentation (Porter 1983) on the superstructure, abutments, and free-field, as shown in Figure 2.1. Accelerations were recorded during the 1979 Imperial Valley earthquake having Richter Magnitude ( $M_L$ ) = 6.4. No damage to the bridge was observed.

### 2.2.2 Painter Street Overcrossing (PSO)

PSO is a continuous two span, post-tensioned, reinforced concrete box-girder bridge near Rio Dell, California. It has unequal spans, of length 146 and 119 ft., with two columns at the center bent. The deck is skewed 39 degrees. The east abutment is monolithic; an expansion joint is present at the west abutment. The expansion joint has a shear key to prevent translation in the skew direction. As shown in Figure 2.2, the bridge was instrumented by CSMIP in 1977. Acceleration response was recorded in 6 earthquakes ranging in magnitude between 4 and 7, the largest being the April 1992 Cape Mendocino earthquake having moment magnitude ( $M_w$ ) = 7.0.

### 2.3 Current Practice

Current design provisions (Caltrans 1999) and recommendation (ATC-32 1996) suggest that the abutment wingwall stiffness is calculated based on passive earth pressure of 7.7 ksf. The wall is assumed to be effective up to 8 ft. depth. The effective width for cantilever wall is limited to 5 ft. One wingwall is assumed to be fully effective, whereas another one was only 1/3 as effective. The ultimate passive pressure is mobilized at 0.01-0.025 times the wall height. The pile stiffness of 40 kips/in per pile is used. These are the recommendations which help designers in modeling of the abutments.

### 2.4 Proposed Models for the Approach-Embankment and Abutment

#### 2.4.1 Linear Models

Wilson and Tan (1990a, 1990b) modeled the approach-embankment as a trapezoidal-shaped embankment cross section, as shown in Figure 2.3, based on a linear

elastic plane-strain analysis. They derived a unit transverse stiffness,  $k_t$ , by considering only shear deformations under a static load applied at the top of the abutment slice. The abutment slice is divided horizontally into infinitesimal layers. The shear deformations are integrated over the height of the embankment. In this approach, the transverse stiffness is determined to be

$$k_t = \frac{2SG}{\ln\left(1 + 2S\frac{H}{W}\right)} \quad (2.1)$$

where  $G$  = shear modulus of soil

$S$  = slope of embankment sides

$H$  = embankment height

$W$  = embankment width at the top

Wilson and Tan assumed the transverse stiffness can be obtained by multiplying the unit transverse stiffness by the length of the abutment wingwall. They applied this method to analyze the Meloland Road Overpass (MRO). The finite element model used in the analysis is shown in Figure 2.4 (Wilson and Tan 1990b). In matching the time-history displacement response, Wilson and Tan reported that the simplified model was accurate when equivalent viscous damping within the range of 25-45 percent was used on the system. The results point out that the damping ratio of the embankment soil system is very high and that the fundamental symmetric transverse mode, having large amplitudes at the abutments, is the dominant mode. No recommendation was given as to how much damping should be used in the analysis of other bridges. This method does not include inertial mass of the embankment or consider pile-soil interaction. No consideration is given to the stiffness of the abutment as a structural component.



Werner et al. (1987) studied the dynamic response of the MRO in the 1979 Imperial Valley earthquake. Using system identification (Katafygiotis 1991), the investigators found that the vertical response at mid-span is dominated by vertical deformation of the bridge deck, whereas the transverse mode is predominantly controlled by support motions at the abutment. Werner et al. (1990) subsequently conducted full-scale dynamic testing of the MRO, using a hydraulic ram connected to the bridge deck. For the relatively small static force applied by the ram transverse to the bridge, displacements were dominated by deck deformation. However, for the recorded response to the Imperial Valley earthquake (PGA at the site equal to 0.30 g.), the transverse displacement response was dominated by embankment deformations, as shown in Figure 2.5. This was attributed primarily to the nonlinear behavior of the bridge embankments under the strong shaking intensities and duration of the Imperial Valley earthquake.

Werner (1993) proposed guidelines for modeling the dynamic properties of the approach embankment. This model is shown schematically in Figure 2.6. In the transverse direction, the superstructure rests on a foundation spring that is supported on the embankment. The embankment is modeled as a point mass supported on a transverse embankment spring. All the springs are linear, and the transverse stiffness of the embankment spring,  $k_{ye}$ , is given as

$$k_{ye} = \frac{\frac{4}{p} SGd}{\ln\left(1 + 2S \frac{H}{W}\right)} \quad (2.2)$$

The embankment mass,  $M_e$ , is given as

$$M_e = \frac{\mathbf{r}_s^2 (W + SH) Hd}{4} \quad (2.3)$$

where each variable is as defined previously and

$\rho_s$  = mass density of the soil embankment

$d$  = an effective length of the embankment taken as  $\frac{1}{4}$  of the total length of the bridge deck.

The transverse stiffness given by Equation 2.2 is equivalent to Wilson and Tan's unit transverse stiffness applied to a length of embankment equal to  $2d/\pi$ , about one-sixth of the total length of the bridge. The embankment mass is equal to the volume of the trapezoidal embankment wedge with length equal to  $d/4$  or about one-sixteenth of the total length of the bridge deck.

Werner recommended that this transverse stiffness be used in a linear model in conjunction with a modal damping ratio that is a function of the modal amplitudes of the first transverse and vertical mode shapes. He defined a soil structure interaction (SSI) parameter,  $\theta$ , for a mode as

$$\mathbf{q} = \frac{\mathbf{f}_{ha}}{\mathbf{f}_{hb} + \mathbf{f}_{hv}} \quad (2.4)$$

where  $\phi_{ha}$  = average of absolute transverse horizontal modal amplitudes at the abutment

$\phi_{hb}$  = maximum transverse horizontal modal amplitude along the bridge deck

$\phi_{hv}$  = maximum vertical modal amplitude along the bridge deck

The empirical correlation between the SSI parameter,  $\theta$ , and damping ratio,  $\beta$  is shown in Figure 2.7 for the Meloland Road Overpass. It can be seen that the damping ratio increases with increasing transverse displacement at the abutment. The response computed using Werner's model with recorded motions as input compares well with observed bridge performance at MRO (Werner 1993).

The drawback of Werner's method is that it is not general. It is calibrated to MRO empirically and relies on rational approximations which may or may not extrapolate well to other bridges. Even though the model accounts for both mass and stiffness of the embankment, the nonlinear soil-structure interaction and energy dissipation at the abutment are "smeared" into an enhanced viscous damping applicable to the entire system. Thus, longer bridges would be expected to be less influenced by hysteretic damping at the abutment, but appropriate damping values for such bridges are unknown. Furthermore, it would be desirable to consider pile stiffness and site soil properties, which may differ from those at the MRO.

Goel (1997) used a system identification method to identify the MRO's period and damping ratio as a function of time. He found that the transverse period of the bridge depended mainly on the level of shaking. The period elongated and the effective viscous damping increased as the intensity of shaking increased. Goel observed that a large movement at the bridge abutment may increase the displacement demands on the central bent while for lower levels of shaking or for usual service conditions, the abutment stiffness is larger, and thus transverse deformation of the bridge deck would dominate. This finding is consistent with the transverse mode shapes reported by Werner et al. (1990).

Goel defined the abutment flexibility parameter,  $AFP$ , as

$$AFP = \frac{\Delta_A}{\Delta_A + \Delta_D} \quad (2.5)$$

where  $\Delta_D$  = modal amplitude at the central pier including in-plane deformation of the deck

$\Delta_A$  = modal amplitude at the central pier excluding in-plane deformation of the deck

The empirical correlation between AFP and system damping ratio is shown in Figure 2.8. This relationship is empirical and is based only on recorded MRO data. For the preceding linear procedures, it is unclear how to extrapolate the result when analyzing bridges with different configurations, or for different intensities of ground motion.

#### 2.4.2 Equivalent-Linear Model

Price (1997) studied the approach-embankment soil contribution to dynamic response of short bridges including MRO and PSO, and proposed an equivalent-linear bridge embankment model. This model takes into account the nonlinearity of soils, soil-structure interaction, 3-D response near the bridge abutment, and scattering of incident seismic energy in the vicinity of the embankment. The model was developed using basic embankment and superstructure properties.

Price's model of the PSO is shown schematically in Figure 2.9. The embankment was originally modeled in 2-D but later modified to a more practical 1-D equivalent-linear shear beam model. The bridge superstructure and piers are modeled using linear elastic elements. The abutment backwall and wingwalls are considered rigid, massless, and bonded to the top of the embankment. Only the approach embankment provides flexibility at the bridge abutment. The embankment model is assumed to represent footing, pile cap, wingwall, and pile contributions to the transverse abutment stiffness. The analysis is done in the frequency domain. The soil properties of the embankment are modified after each iteration until compatibility between the maximum shear strains

computed within the embankment and the strains generated in the equivalent linear model is achieved. Energy dissipation at the abutment is accounted for by increasing effective viscous damping as a function of the maximum shear strains.

The model was able to predict the peak recorded response quantities such as the abutment reactions and the relative pier displacement accurately for various levels of ground motions for the PSO. The most sensitive parameters were found to be the modulus reduction curve and the shear wave velocity of the embankment soils. Although the equivalent-linear model does not require such increase in damping with respect to mode shapes as is required in the Werner model (Werner 1993), the strain-energy weighted sum method used to compute modal damping ratios is difficult to use with standard finite element analysis programs.

#### 2.4.3 3D-Nonlinear Models

Sweet and Morrill (1993) and McCallen and Romstad (1994a, 1994b) analyzed the PSO using a detailed three-dimensional model of the bridge-soil system. In McCallen and Romstad's model, the soil embankments were modeled with solid finite elements and the bridge superstructure was modeled with shell and beam elements, as shown in Figure 2.10. Soil stress-strain behavior was modeled using a Ramberg-Osgood model with parameters selected to match Seed's modulus reduction and damping curves (Seed et al. 1984). The detailed nonlinear model represented the recorded time-history response of the PSO well. Sweet and Morrill (1993) used a nonlinear finite element method to model the "soil island" which supports the bridge superstructure and foundations. They considered nonlinear soil material behavior, the opening and closing of gaps between

foundation components and soil, and radiation damping. They recommended direct modeling of the soil with solid elements in place of simple soil springs.

#### 2.4.4 Other Approaches

Siddharthan et al. (1998) proposed a linear secant stiffness approach to represent seat type abutments in seismic analysis through the use of translational springs in the longitudinal and transverse directions, as shown in Figure 2.11. Figure 2.12 shows the boundary forces and moments on the abutment. The linear secant stiffness is derived by estimating the force required to cause a given displacement, considering nonlinear pile-soil interaction, and active and passive soil conditions.

Siddharthan's model was calibrated to field test results for a pseudo-statically loaded large scale abutment (Maroney et al. 1994). The comparison between computed and measured transverse abutment stiffness is shown in Figure 2.13. It is evident from Figure 2.13 that close agreement between computed and measured transverse abutment stiffness was achieved. Nevertheless, in a linear secant stiffness representation of the bridge-abutment-backfill, the assigned viscous damping is very influential on the transverse response of the bridge. Siddharthan made no recommendations as to how much viscous damping should be used in conjunction with each spring or how the bridge would respond under dynamic excitation. Siddharthan modeled the abutment, and not the approach-embankment.

## 2.5 Summary

Several abutment and embankment models were described for use in dynamic response analysis of a bridge. These models have shortcomings, described in Section 2.4. A practical model is sought that considers the nonlinear dynamic response of the approach-embankment and pile-soil interaction, to address bridges having different span lengths, superstructure types, soils, piles, etc. Such a model is developed in Chapter Three.

Table 2.1 Description of Proposed Abutment and Embankment Models.

Research Study	Dynamic Response of Soil Embankment			Pile-Soil Interaction
	Material Modeling	Material Damping	Inertial Soil Mass	
Wilson and Tan (1990)	Linear	Equivalent Viscous	None	None
Werner et al. (1993)	Linear	Equivalent Viscous	Considered	Considered
Sweet and Morrill (1993) McCallen and Romstad (1994)	Nonlinear	Hysteretic	Considered	Considered
Price (1997)	Equivalent Linear	Equivalent Viscous	Considered	None
Siddharthan et al. (1998)	None	None	None	Considered



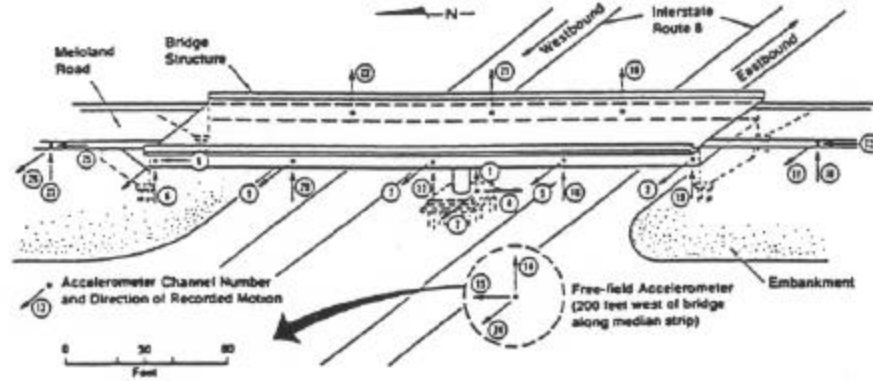


Figure 2.1 Bridge Configuration and Strong Motion Instrumentation (Werner et al 1990)

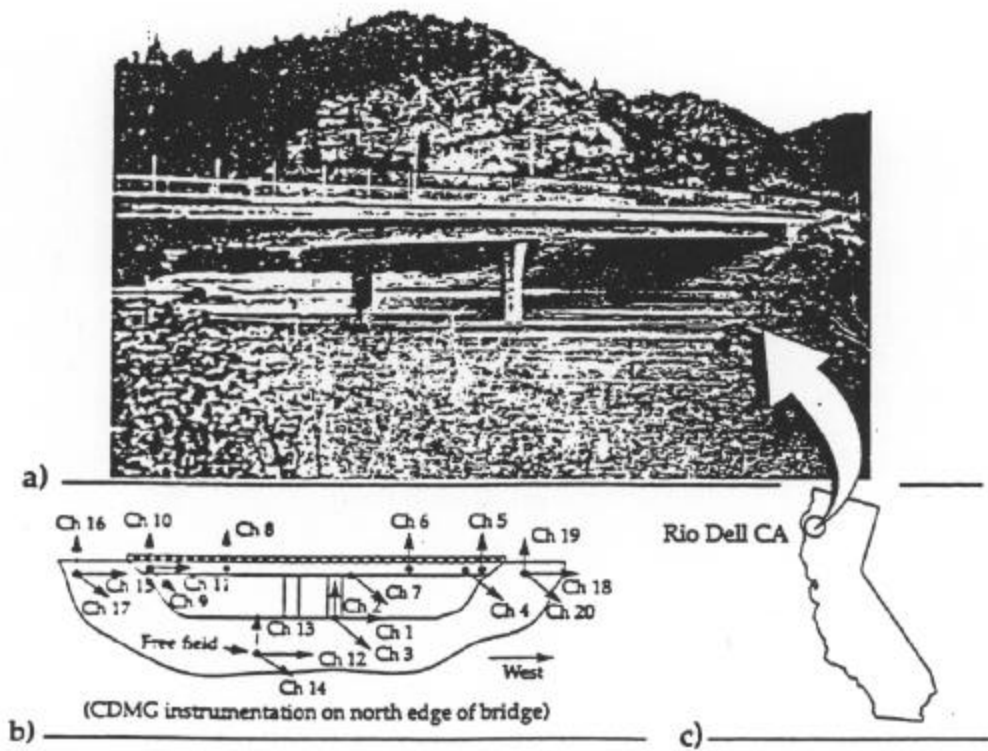


Figure 2.2 Painter Street Overcrossing, Rio Dell, California a) Bridge Photo, South Side of Bridge Shown; b) CDMG Instrumentation Array; c) Bridge Location (McCallen and Romstad 1994b)

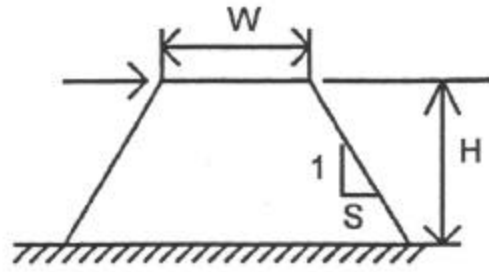


Figure 2.3 Embankment Configuration (Wilson and Tan 1990a)

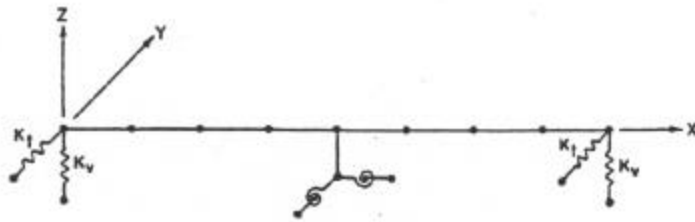


Figure 2.4 Finite Element Model Including Abutment Stiffness (Wilson and Tan 1990b)

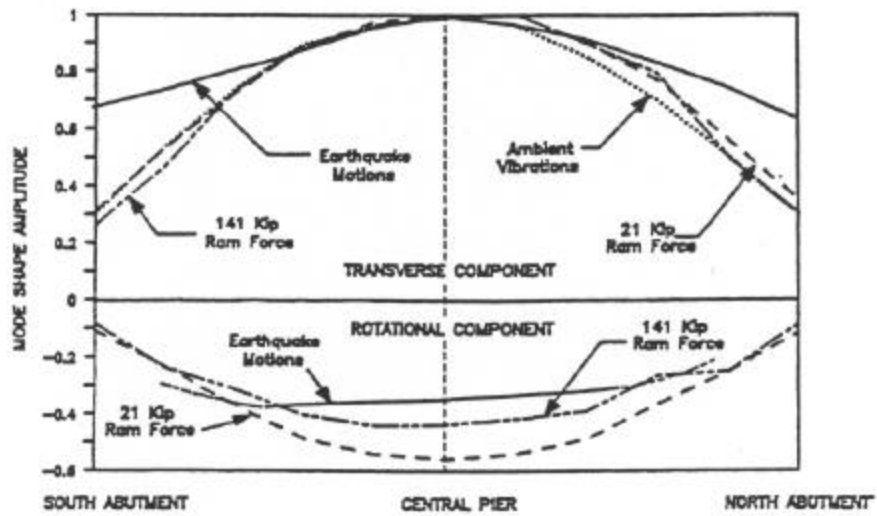


Figure 2.5 Transverse Mode Shape Components (Werner et al. 1990)

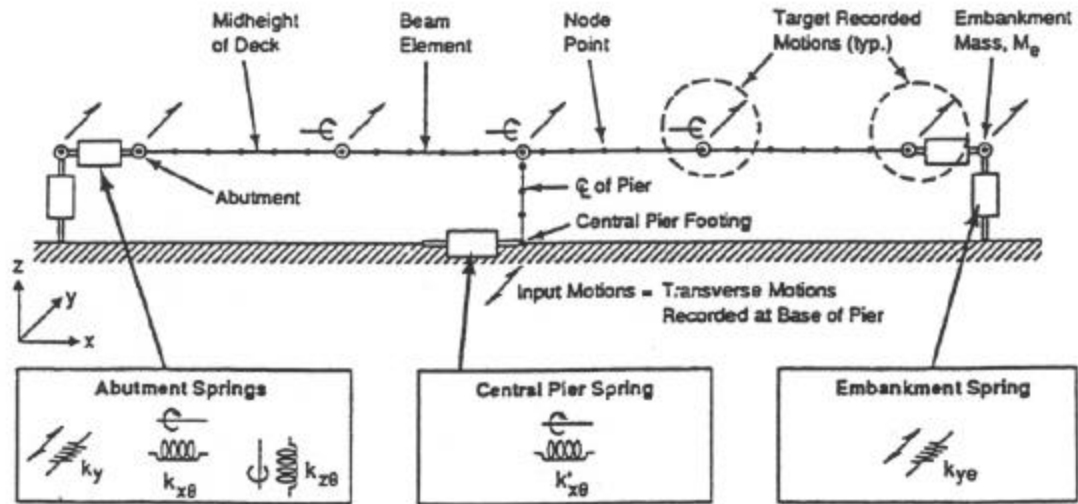


Figure 2.6 Finite Element Model of MRO (Werner 1993)

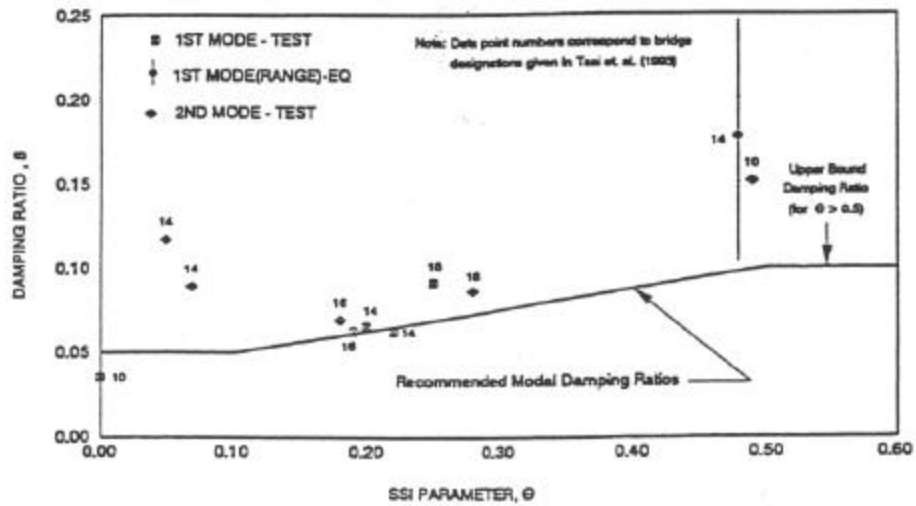


Figure 2.7 Recommended Modal Damping Ratios (Werner 1993)

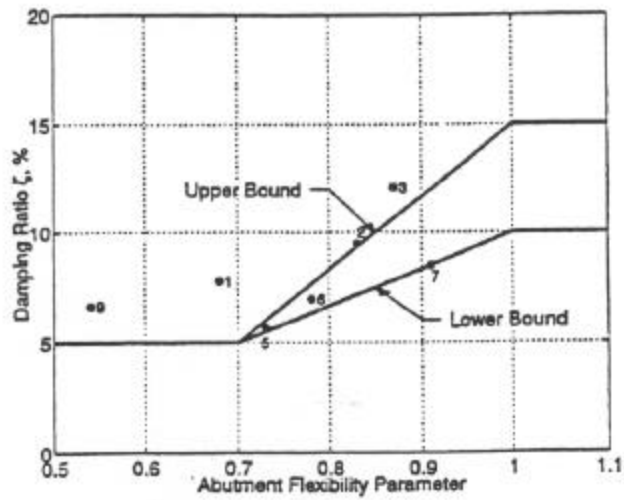


Figure 2.8 Variation of Damping with AFP (Goel 1997)

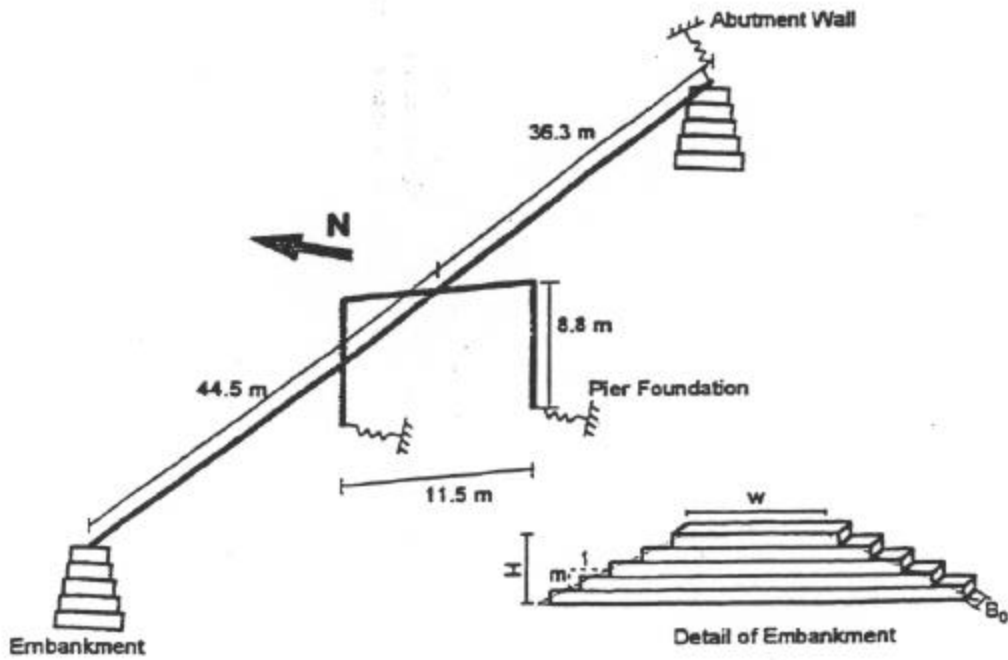


Figure 2.9 Schematic View of Equivalent Linear Design Model of the Painter Street Overcrossing with Embankment Detail (Price 1997)

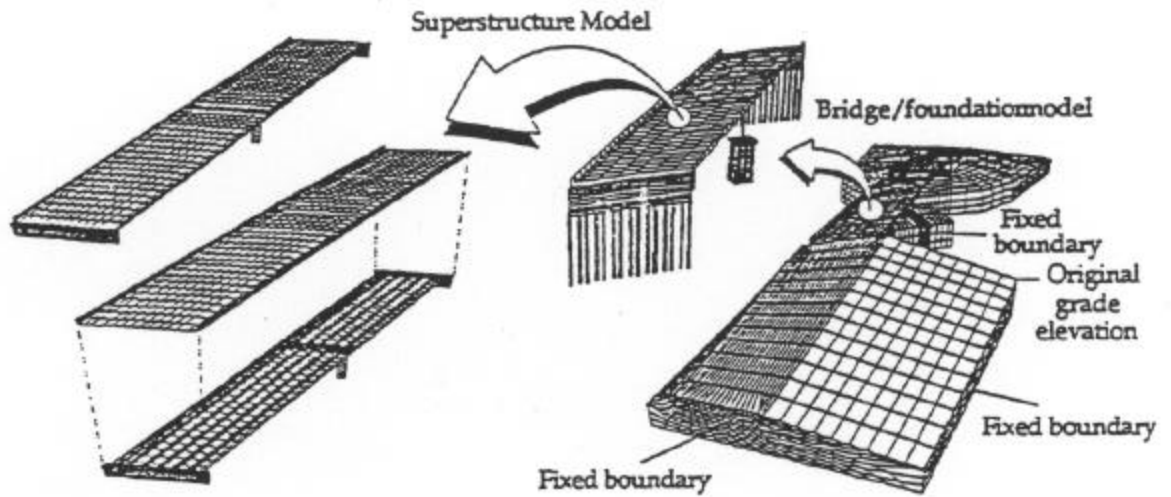


Figure 2.10 Detailed Model of the Painter Street Overcrossing Bridge System (McCallen and Romstad 1994b)

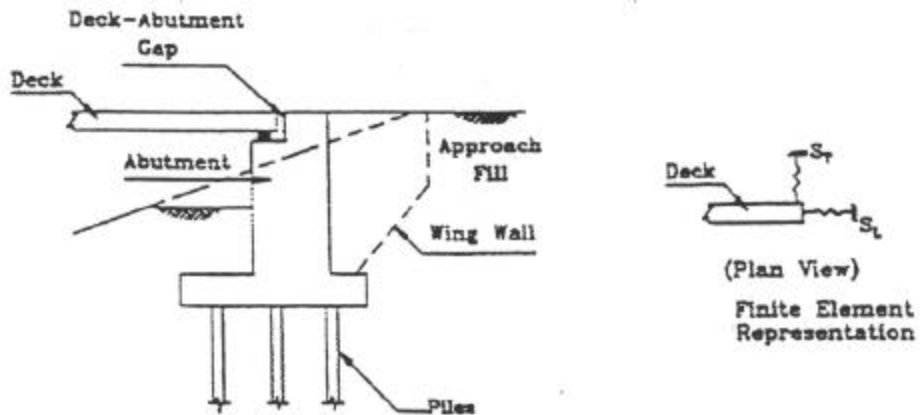


Figure 2.11 Representation of Deck-Abutment-Backwall Foundation Interaction (Siddharthan et al. 1998)

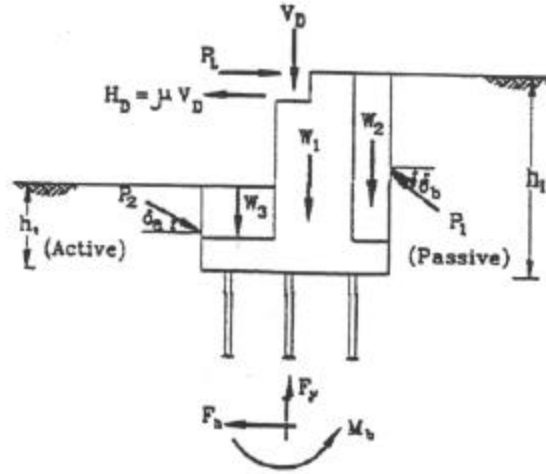


Figure 2.12 Boundary Forces and Moments on the Abutment (Siddharthan et al. 1998)

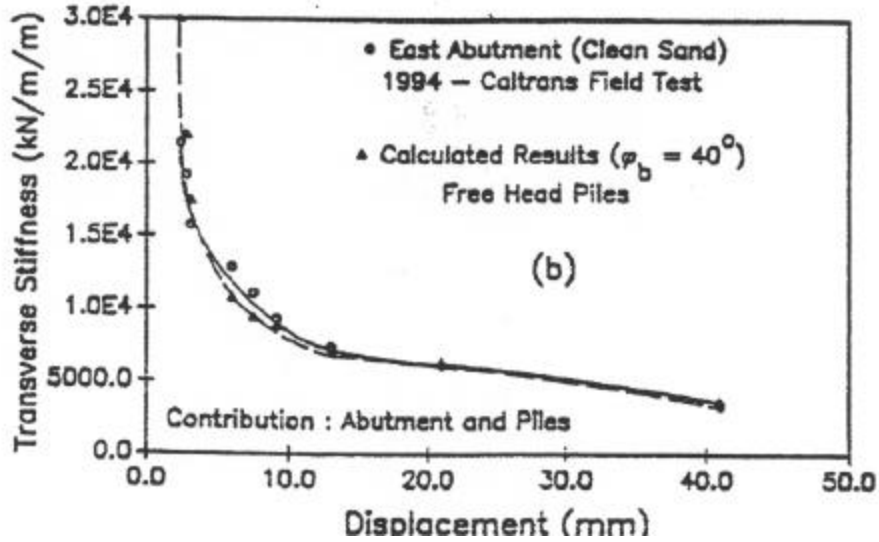


Figure 2.13 Comparison between Computed and Measured Transverse Abutment Stiffness: Abutment and Pile Contribution (Siddharthan et al. 1998)

## CHAPTER 3

## DEVELOPMENT OF IMPROVED APPROACH-EMBANKMENT MODELS

3.1 Introduction

Several existing approach-embankment models and their shortcomings were discussed in Chapter Two. Important considerations include the dynamic response of the soil embankment and interaction between the piles and surrounding soils. The computed dynamic response of the soil embankment depends on the modeling of material properties (linear/nonlinear), damping (equivalent viscous/hysteretic), inertial soil mass, and the degree of nonlinearity. Some approach-embankment models (Wilson and Tan 1990, Price 1997) do not consider pile-soil interaction at the abutment. Siddharthan's model (1998) considers pile-soil interaction but ignores the dynamic response of the approach-embankment. Since soil damping in the vicinity of the abutment is more hysteretic in nature than it is linear viscous, the linear approach-embankment models (Werner et al. 1993, Goel 1997) that use enhanced viscous damping in a linear model of the system do not accurately represent the soil damping at the abutment. Moreover, these models are calibrated to the small data set of recorded responses (Meloland Road Overpass (MRO) and Painter Street Overcrossing (PSO)) and may lack generality for use with different bridge configurations, span lengths, and relative mass distributions.

In this section, a practical nonlinear approach-embankment model is developed to make more accurate predictions of pier transverse displacement demands for a broader class of bridge configurations, span lengths, and mass distributions. This model incorporates the nonlinear hysteretic properties of the soil and includes the dynamic response of the approach-embankment and pile-soil interaction at the abutment. Two models are developed. The more complex model is calibrated to recorded data, which is available for California bridges but not Illinois bridges. A simpler model is then developed, and is calibrated both to the

California bridge data as well as to synthetic data generated for Illinois bridges using the more complex model. This Chapter describes the development of these models.

### 3.2 Methodology

The approach-embankment model is termed the “soil-pile” model. This model explicitly represents the dynamic response of the approach-embankment soil and pile-soil interaction at the abutment. The model relies on standard engineering techniques to establish model properties and is empirically calibrated to the recorded response from MRO and PSO. These techniques consider the embankment dimensions, basic soil properties such as unit weight, plasticity index, and low-strain shear wave velocity of soil, and the properties of the soil below the abutment piles.

A simpler model termed the “soil-slice” model also is developed in this chapter. The soil-slice model explicitly models the dynamic response of the approach-embankment; soil-pile interaction at the abutment is not considered explicitly, but is “smeared” into the approach-embankment model properties. This model is calibrated to the recorded response at MRO and PSO, and to analytically computed responses for typical Illinois bridges.

### 3.3 Modeling of MRO and PSO

The MRO and PSO bridges are described in Chapter 2. Both bridges are typical short bridges in California spanning over two- or four-lane highways. They were heavily instrumented with strong motion accelerometers by the California Strong Motion Instrumentation Program (CSMIP). MRO and PSO were shaken by a combined total of 7 earthquakes. The strongest of these was the 1992 Petrolia earthquake (magnitude 6.4), with  $PGA = 0.54$  g measured in the free-field near the bridge. Table 3.1 lists the recorded motions used in model calibration.



Both bridges were modeled using DRAIN-3DX (Prakash et al. 1993), a non-linear dynamic response analysis program. Three-dimensional idealizations of MRO and PSO are shown in Figure 3.1 and 3.2 respectively. The models were subjected simultaneously to ground motions having components in three orthogonal directions: transverse, longitudinal, and vertical.

### 3.3.1 Modeling of the Meloland Road Overpass

MRO is a symmetric prestressed concrete box-girder bridge, described in Chapter Two. No damage to the bridge was observed after the 1979 earthquake. The reinforced concrete box-girder and a single central column of the MRO were modeled as stick beams using elastic beam-column elements. The elements were located along the centroidal axes of the members. Mass was lumped at each node; a large number of nodes was used to admit higher modes into the response. The bridge dimensions were obtained from the drawings. Section properties are summarized in Table 3.2. The stiffnesses of base pier springs at the central pier reported by Douglas et al. (1990) are very similar to the ones reported by Maragakis et al. (1994) for MRO. A preliminary analysis showed that a fixed pier could be used in place of these stiffnesses with only a minor effect on bridge response; consequently the pier was modeled as fixed.

### 3.3.2 Modeling of the Painter Street Overcrossing

PSO is an asymmetric bridge with 39 degrees skew as described in Chapter 2. The east abutment is monolithic but the west abutment has an expansion joint. The post-tensioned reinforced concrete box-girder, bents, and piers were modeled as stick beams using elastic beam-column elements. For the bent cap, rigid end offsets were assumed for the full depth of the members; thus the stiffness of the bent cap increased by three orders of magnitude.

At the east abutment of PSO, the backwall connection to the pile cap is monolithic. Thus, in addition to the approach-embankment model which is used at the east and west abutments, a backwall spring is placed at the east abutment to model the soil resistance to the backwall. Goel and Chopra (1997) reported the “actual” capacity of the backwall to be about 5300 kN, determined from the recorded motions considering the dynamic equilibrium of the road deck. If this capacity is mobilized at 2.5 percent of wall height (  $0.025 * 8 \text{ ft.} * 12 \text{ in./ft.} = 2.4 \text{ in.}$ ) according to ATC-32’s recommended idealization, the spring constant for the backwall is equal to  $8.7 \times 10^4 \text{ kN/m.}$  (  $5300 \text{ kN.} / (2.4 \text{ in.} * 0.0254 \text{ m./in.})$  ). Based on McCallen and Romstad (1994), the global dynamic response of PSO is not sensitive to the pier foundation stiffness, so each of the central columns was modeled as fixed at their bases. Section properties are summarized in Table 3.3.

### 3.4 Soil-Pile Model

#### 3.4.1 Model Description

A generic approach-embankment cross-section and elevation are shown in Figure 3.3. Figure 3.4 shows a schematic model. In this model, the height of the approach-embankment is taken as the distance from the top of the pile cap at pier closest to the embankment, to the center of the deck slab. The approach-embankment crest width is the actual width, at least equal to the width of the roadway. A plain strain model of the embankment slice is used. The slice is divided into horizontal layers; only shearing deformations within each layer are considered. The top layer extends from the top of the embankment to the bottom of the abutment pile cap as shown in Figure 3.5. It is assumed that the soil between abutment wingwalls moves along with the abutment, and provides little or no additional resistance. The resistance of the top layer is due to shearing deformations of soil only. Soil mass in each layer is lumped at the middle of the layer. Shear springs connect each layer mass. These shear

springs represent simple shear deformations in each layer. At each soil layer, non-linear p-y springs connect the piles to the embankment soil. Below the original grade, only p-y springs provide soil resistance to piles. From a parametric study on layer discretization, the number of embankment soil layers has little effect on the computed bridge response for models having four or more layers. Thus, a minimum of four layers of the embankment soil is recommended. The p-y springs are determined, using conventional engineering approaches leaving the only “unknown” to be the thickness of the slice (in the direction of the road alignment). The slice thickness is determined empirically to match the recorded response of PSO and MRO; the thickness of the wedge affects both the mass and stiffness of the approach-embankment.

The schematic model shown in Figure 3.5 was implemented. The figure illustrates that a rigid link is used to connect the top and bottom nodes of each layer. Shear springs are placed between each layer connecting adjacent rigid links. Each layer mass is lumped at the center of the link. The abutment mass and the top layer soil mass are lumped at the center of the top link. The pile consists of elements connecting at nodes. The section properties of the pile are those of a single pile multiplied by the number of piles, assuming that the piles are well spaced, and therefore have negligible interaction. P-y springs connect each pile node to each layer soil mass. Conventional p-y analysis on the half space of soil is used for pile nodes below the original grade, to account for the flexibility of the soil below grade. Enough p-y springs below grade (along the length of the pile) should be used so that the distance between each spring is no more than the distance between the p-y springs above the original grade. Free-field ground motions were applied to the nodes shown as fixed in Figure 3.5. (The ground motions measured at the ground surface were used at each location along the pile length.)

Determination of the shear springs requires knowledge of the approach-embankment dimensions, the low-strain shear modulus, and the modulus reduction curve. A simple shear deformation is assumed for each layer of the embankment wedge as shown in Figure 3.6a and 3.6b. Iwan (1973) suggested the use of elastic spring with a Coulomb unit (a sliding frictional unit) for modeling the nonlinear hysteretic behavior of soil as shown in Figure 3.7a and 3.7b. Taylor et al. (1978) later used these springs in parallel as shown in Figure 3.8a and 3.8b in one-dimensional site response analysis. Multiple springs can be used to model a hyperbolic stress-strain behavior for soil as shown in Figure 3.8b (Taylor et al. 1978).

Consider a soil layer in Figure 3.6b, in greater detail as shown in Figure 3.9a.

where  $W$  = width of the section

$Z$  = height of the section

$L$  = thickness of the section

$G$  = shear modulus of soil at strain  $\gamma$

$\delta$  = shear displacement

The stiffnesses of the shear springs can be determined by the following procedure:

### Step 1

Divide the abutment wedge into horizontal layers and determine the soil section dimensions and soil properties. The soil properties needed are the low strain shear modulus,  $G_0$ , and the modulus reduction curve. ( $G/G_0$  v.s.  $\gamma$ ) The low strain shear modulus may be inferred from field wave velocity measurements, or free vibration tests (Seed and Idriss 1970). The modulus reduction curve can be obtained from studies on samples of the actual soil or may be inferred from existing studies such as Sun and Seed (1988) and Vucetic and Dobry (1991).

Discrete points are chosen to represent the curve.

Step 2

Determine the secant stiffness,  $K_{\text{sec}}$ , and the corresponding displacement,  $\delta$ , for each layer

from

$$K_{\text{sec}} = \frac{GWL}{Z} \quad (3.1)$$

$$\mathbf{d} = \mathbf{g}Z \quad (3.2)$$

Step 3

Determine the force-displacement relationship (F vs.  $\delta$ ) from

$$F = K_{\text{sec}} \mathbf{d} \quad (3.3)$$

The first three steps are shown schematically in Figure 3.9b.

Step 4

Determine the parameters for the elastoplastic element. Taylor et al. (1978) derived these parameters from the relationship between shear modulus,  $G$ , and strain amplitude,  $\gamma$ .

Similarly, these parameters can be derived from the secant moduli at various displacements.

For an elastoplastic element as shown in Figure 3.7a.

where  $R$  = yield force

$K$  = loading and unloading stiffness

$K_{\text{eff}}$  = effective secant element stiffness

$\Delta$  = displacement

$\Delta_y$  = yield displacement

$$K_{\text{eff}} = K \quad \text{for} \quad \Delta < \Delta_y \quad (3.4)$$

$$K_{eff} = \frac{R}{\Delta_y} \quad \text{for} \quad \Delta = \Delta_y \quad (3.5)$$

$$K_{eff} = \frac{R}{\Delta} = \frac{\Delta_y K}{\Delta} \quad \text{for} \quad \Delta > \Delta_y \quad (3.6)$$

More generally, for  $n$  elastoplastic elements in parallel, sequenced in order of increasing values of  $R$ , the effective stiffness is a summation over all elements:

$$K_{eff} = \sum_{j=1}^n K_j \quad \text{for} \quad \Delta \leq \Delta_{yj} \quad (3.7)$$

$$K_{eff} = \sum_{j=1}^{i-1} \frac{R_j}{\Delta} + \sum_{j=i}^n K_j \quad \text{for} \quad \Delta = \Delta_{yi} \quad (3.8)$$

where  $\Delta_{yi}$  = the yield displacement of the  $i^{\text{th}}$  element

$$\text{Thus, } K_{eff} = \frac{1}{\Delta_{yi}} \sum_{j=1}^{i-1} \Delta_{yj} K_j + \sum_{j=i}^n K_j \quad (3.9)$$

where  $K_{eff,i}$  = the secant stiffness when the  $i^{\text{th}}$  element is at the point of slipping

$$K_{eff,1} = K_1 + K_2 + \dots + K_n$$

$$K_{eff,2} = \frac{\Delta_{y1}}{\Delta_{y2}} K_1 + K_2 + \dots + K_n$$

$$K_{eff,i} = \frac{\Delta_{y1}}{\Delta_{yi}} K_1 + \frac{\Delta_{y2}}{\Delta_{yi}} K_2 + \dots + K_i + \dots + K_n \quad (3.10)$$

or

$$\{K_{eff}\} = [A]\{K\} \quad (3.11)$$

Using  $K_{sec}$  and  $\delta$  from step 2,  $\{K\}$  can be solved. The Coulomb resistances can be found from

$$R_i = \Delta_{yi} K_i \quad (3.12)$$

Finally, the soil mass in each layer can be determined from

$$M = \mathbf{r}V \quad (3.13)$$

where  $\mathbf{r}$ = unit weight of soil

V = section volume.

Likewise, several elastoplastic springs in parallel can be used to construct non-linear p-y springs for the soil-pile interaction. In this study, four nonlinear springs were used for each p-y spring. Site soil properties should be used to obtain the best estimate of the p-y spring properties following established engineering methods (see Section 5.4).

### 3.4.2 Model Verification

Shear springs in the soil-pile model are composed of arrays of elastoplastic elements to represent the shape of the soil stress-strain curve. Verification that the modulus reduction curve and material damping ratio curve correlate well with the experimental data (Seed and Idriss 1970, Sun et al. 1988, Vucetic and Dobry 1991) is provided in Appendix A.

### 3.4.3 Model Calibration

The soil-pile model was calibrated to the recorded response at MRO and PSO. Soil properties were obtained from the construction drawings and a paper by Maragakis et al. (1994). The DRAIN-3DX models are shown in Figures 3.1 and 3.2, as discussed earlier in Section 3.3. The only unknown was the thickness of the approach-embankment to be modeled. A total of 7 ground motions (Table 3.1) were applied to the model. The ranges of approach-embankment thickness ( $L^*$ ) which result in a “good” match between the recorded and the computed bridge relative displacement response and absolute acceleration are plotted in Figure 3.10. The selection of  $L^*$  that resulted in a good match was determined by

inspection. Of interest were both the frequency in the high amplitude range and the peak relative displacement of the central pier. Peak relative displacements were within 20 percent of measured values for all earthquakes except the Imperial Valley 1979, and 1986 Cape Mendocino earthquake. Price (1997) also had difficulty matching the 1986 record although the relative peak displacement was so small (~ 0.5 cm.) as to be of little importance in practical cases. The difficulty with matching response may be caused by: (1) differences in the normalized modulus reduction curve assumed versus the more accurate curve that could be obtained from tests on the embankment soil; (2) the assumed low strain shear modulus of the embankment soil; and (3) settlement of embankment fill below the abutment would affect the embankment soil's low strain shear modulus. The computed response is sensitive to these factors. Figures 3.11-3.24 show the comparison between the recorded and the computed relative displacement and absolute acceleration time-history at the top of the central pier for all the points in Figure 3.10. It should be noted that there are also parameters other than PGA which can be used to plot against  $L^*$ . PGA was used since it is a simple parameter that roughly indicates the level of ground motions. For a given PGA, an average between the upper and lower bound  $L^*$  may be used. Figure 3.10 shows a trend of consistent decrease in  $L^*$  with PGA. This suggests localization of plasticity with stronger earthquakes, causing the embankment nearest the abutment to “decouple” from the remainder of the embankment as the response intensity increases.

### 3.5 Soil-Slice Model

#### 3.5.1 Model Description

A simplified version of the soil-pile model was developed. The simplified “slice” model is calibrated to the MRO and PSO recorded response data and to synthetic data generated using the soil-pile model for a slab-on-girder bridge more representative of Central



U.S. construction. Because soil-pile interaction is not modeled explicitly, different values of  $L^*$  are required. The chief advantage of the model is that it has fewer components and is easier to implement than the previous model. A schematic representation of the model is shown in Figure 3.25. The derivation of shear springs is the same as described in the previous section, with only  $L^*$  determined empirically.

### 3.5.2 Model Calibration

The soil-slice model was calibrated to the MRO and PSO using the same set of ground motions that were used for the soil-pile model (Table 3.1). The comparison between the calculated and the recorded responses is shown in Figures 3.26-3.39. The ranges of the approach-embankment thickness ( $L^*$ ) which give the closest match are shown in Figure 3.40. A comparison of the plot of  $L^*$  vs. PGA for the soil-pile and soil-slice models is shown in Figure 3.41. The soil-slice model requires a smaller  $L^*$  than the soil-pile model to provide for the flexibility introduced by the piles.

### 3.6 Use of Principal Component Analysis to Observe Inelastic Mode Shape

Principal component analysis (PCA) is a statistically-based technique that is used to generate mode shapes based on response data that best represent how the structure responds in the given time. Unlike linear elastic multistory buildings where the first elastic mode shape is usually the dominant mode, the PCA mode shape for short bridges depends significantly on the geometry and section properties of the bridge, and changes with the degree of nonlinearity of the approach-embankment. PCA mode shapes are treated individually for each case.

Using the PCA technique, the first PCA mode shapes of the soil-pile and soil-slice models for each ground motion, using the best-fit  $L^*$  (the average between the upper and

lower limits) were plotted against the PCA mode shapes determined for the recorded response data, ATC-32 abutment, and fixed abutment in Figures 3.42a - 3.42f for PSO bridge, and Figure 3.43 for MRO bridge. In most cases, the PCA mode shapes from the soil-pile model are more similar to those obtained from the recorded data than those obtained using the soil-slice model. Considering the recorded response alone, deck deformation is prominent in the low PGA cases. As for cases with high PGA, embankment response is more prominent, with the deck deformation being relatively minor. In some cases, there is rotation about the vertical axis. Deck deformation is less evident in the soil-pile model than the soil-slice model, which may result from the added pile flexibility in the soil-pile model. The above observations coincide with the strain dependent characteristics of the modeled soil; the soil is stiffer for lower PGA but softer with the larger strains occurring under higher PGA. These results are consistent with the transverse mode shape components of MRO bridge by Werner et al (1990), Figure 2.5, and suggest that the soil-pile and the soil-slice models are closer to measured response than the ATC-32 and fixed abutment models.

### 3.7 Determination of $L^*$ for Slab-on-Girder Bridges

#### 3.7.1 Bridge Description

Several prominent differences exist between typical bridges in the central U.S. and those in California. Most bridges in the central U.S. consist of multiple-steel or concrete girders supporting a concrete deck, unlike the concrete box-girders used in PSO and MRO and in numerous other California bridges. A single concrete pier is often used in California, whereas multiple concrete columns with a crash wall are more popular in at least some central U.S. states. Monolithic abutments are common in California, while seat-type abutments are more commonly found in Illinois. In both states, 1 ft. diameter cast-in-drilled-hole (CIDH) piles are used. These are concrete piles encased in circular steel tube. These

newer Illinois bridges may have a longer embedment length of pile tip into the pile cap than California bridges (1-2 ft. vs. 2-3 in.).

### 3.7.2 Calibration of Simple Slice Model for Slab-on-Girder Bridges

A representative slab-on-girder bridge (Figure 3.44) was provided by the Illinois Department of Transportation (IDOT). The bridge was used in model calibration to estimate embankment thickness ( $L^*$ ) for soil-slice model. Because no records of response of such bridges to strong ground motions are available, response was simulated using the more complex soil-pile model. The synthetic response was used to calibrate  $L^*$  for the soil-slice model. Two different foundation conditions were assumed. The first case (IL-1) corresponded to Route 743 bridge in Scott County, IL. The IL-1 bridge was founded on 6 H-piles (HP310 x 79) with 0.9 m. concrete encasement at pile tip. Embankment soils and the foundation soils are mostly silty clay with undrained shear strength ranging from 25 to 90 kPa. The second case (IL-2) corresponded to Route 310 bridge in Madison County, IL. The IL-2 abutment was founded on 13 CIDH piles (0.3 m. in diameter), drilled into fine sands having friction angle ranging from 34 to 43 degrees. The analytical model of this bridge is shown in Figure 3.45 for two cases that were chosen. Both IL-1 and IL-2 were subjected to the same suite of 7 ground motions, recorded at the MRO and PSO sites. The soil-pile model with recommended  $L^*$  as shown in Figure 3.10 was used as a baseline model. Ranges of  $L^*$  for the soil-slice model for IL-1 and IL-2 that result in the best match to the baseline model are shown in Figure 3.46; peak relative displacements were within 20 percent. The time history results for each point in Figure 3.46 are shown in Figure 3.47 - 3.60 for IL-1, and Figure 3.61 - 3.74 for IL-2. Ranges of approach embankment thickness ( $L^*$ ) determined for the soil-slice model for California bridges and the representative Illinois bridges (Figure 3.40 vs. Figure 3.46) are compared in Figure 3.75. The major difference is in the high PGA ranges

where  $L^*$  for the Illinois bridges is higher than  $L^*$  for the California bridges. This indicates that pile-soil interaction is more important in California bridges and is compensated for by a decrease in  $L^*$  for the soil-slice model. The Illinois bridges were modeled with fixed pile-cap connections because of the longer pile tip embedment into the pile cap, thus a larger  $L^*$  was necessary to capture this stiffness using a soil-slice model.

To establish the importance of modeling the dynamic response of the approach-embankment for Illinois bridges, comparisons were made among bridges with different abutment models as shown in Figure 3.76 and 3.77. In Figure 3.76, the relative displacement time-histories at the pier for IL-2 are compared for models using (a) soil-slice model, (b) ATC-32 abutment model, and (c) fixed abutment, for the 1992 Cape Mendocino/Petrolia (Main Event), having PGA  $\sim 0.54$  g. Figure 3.77 shows the same bridge subjected to 1986 Cape Mendocino (Main Event) having PGA  $\sim 0.16$  g. It is evident that the fixed abutment model highly underestimates pier displacement demand especially in the larger 1992 earthquake. The ATC-32 abutment model also underestimates pier displacement demand in the 1992 earthquake but gives reasonable results for the pier displacement demand in the smaller 1986 earthquake. Thus, to estimate deck displacement response, it is important to model the approach-embankment for short bridges, especially for larger earthquakes. For longer bridges or for bridges with expansion joints within the span, the dynamic response of the approach-embankment will have diminished importance. Such bridges are outside the scope of the present study, and require further study.

The comparisons of PCA mode shape for IL-2 bridge subjected to 1992 Main Event (see Figure 3.76) and 1986 Main Event (see Figure 3.77) are shown in Figures 3.78-3.79. Again, the PCA mode shape from an ATC-32 abutment is closer to the PCA mode shape from the soil-slice model for “low” level of shakings (1986 Main Event), but quite different for “high” level of shakings (1992 Main Event). This is because unlike the nonlinear springs

used in the soil-slice model, ATC-32 adopts linear springs that are unable to capture the stiffness degrading characteristics of the approach-embankment soil at larger strains. It should be noted that the in-plane deck deformation is significant in this bridge because of much lower in-plane deck stiffness compared with MRO and PSO. The deck deformation is more pronounced when stiffer abutments are used (ATC-32), while the more flexible approach-embankment models result in less deck deformations, but larger relative pier drifts.

### 3.8 Summary

This chapter presented the soil-pile approach-embankment model and a simplified version known as a soil-slice model. In the soil-pile model, both dynamic response of the approach-embankment and pile-soil interaction at the abutment are taken into account, while only the dynamic response of the approach-embankment is considered in a soil-slice model.

Both models were calibrated to the recorded response from Meloland Road Overpass (MRO) and Painter Street Overcrossing (PSO). The ranges of approach-embankment thickness ( $L^*$ ) to be used in both models were suggested based on comparisons with empirical data. In general, the models are capable of producing a “good” match between the recorded and the computed bridge relative displacement response and absolute acceleration. The capability of the model is limited to the accuracy of: (1) the assumed low strain shear modulus of the embankment soil; and (2) the assumed normalized modulus reduction curve as opposed to the more accurate curve which can be obtained from tests on the embankment soil. Recommended values of  $L^*$  decrease with PGA, apparently due to localization of damage (inelasticity) within the embankment. The results from these calibrations were used as a base-line model to determine approximate ranges of approach-embankment thickness ( $L^*$ ) for use with representative slab-on-girder bridges modeled with the soil-slice model.

Table 3.1 List of Recorded Motions at MRO and PSO to be Used in Model Calibration.

Bridge	Earthquake	Date	Mag. ( $M_L$ )	PGA (g.)
MRO	Imperial Valley	10/15/79	6.4	0.30
PSO	Cape Mendocino (Main Event)	11/21/86	5.1	0.16
PSO	Cape Mendocino (Aftershock)	11/21/86	5.1	0.12
PSO	Cape Mendocino	07/31/87	5.5	0.09
PSO	Cape Mendocino/Petrolia (Main Event)	04/25/92	6.4	0.54
PSO	Cape Mendocino/Petrolia (Aftershock #1)	04/26/92	6.2	0.52
PSO	Cape Mendocino/Petrolia (Aftershock #2)	04/26/92	6.4	0.20

Table 3.2 Section Properties of MRO.

	$A_{gross}(m^2)$	$I_{strong}(m^4)$	$I_{weak}(m^4)$	$J(m^4)$
Slab	4.346	35.89	1.94	5.29
Column	1.824	0.2648	0.2648	0.5296

Table 3.3 Section Properties of PSO.

	$A_{gross}(m^2)$	$I_{strong}(m^4)$	$I_{weak}(m^4)$	$J(m^4)$
Slab**	7.90	156.0	3.3	10.1
Column	1.92	0.15	0.15	0.59
Bent	2.91	0.72	0.68	1.06

\*\* Salveson 1991.

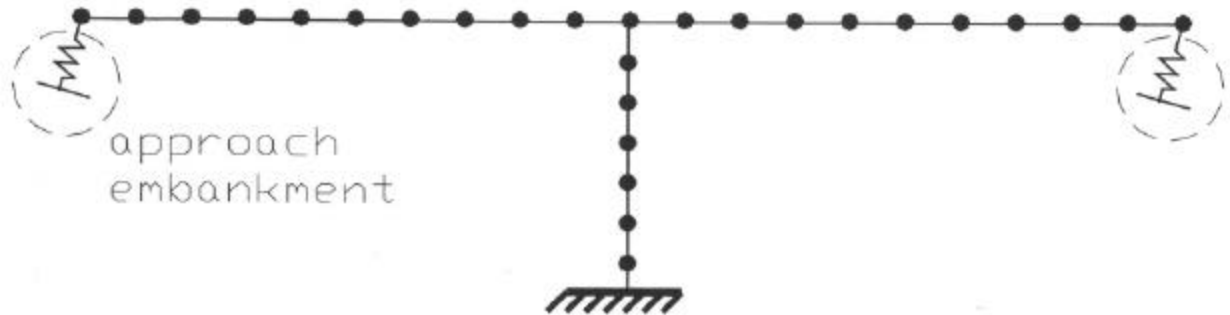


Figure 3.1 Analytical Model of MRO

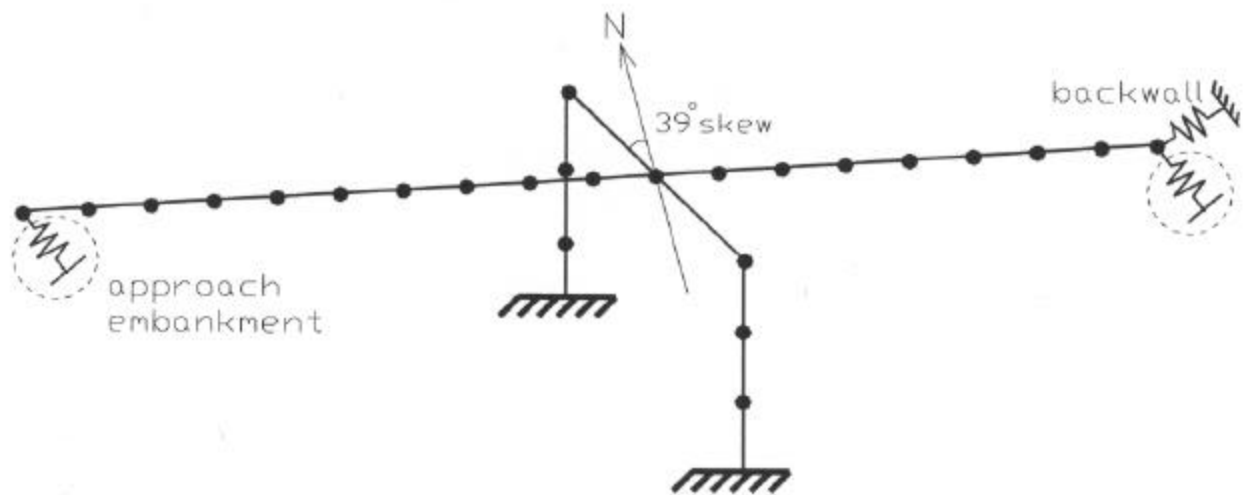


Figure 3.2 Analytical Model of PSO

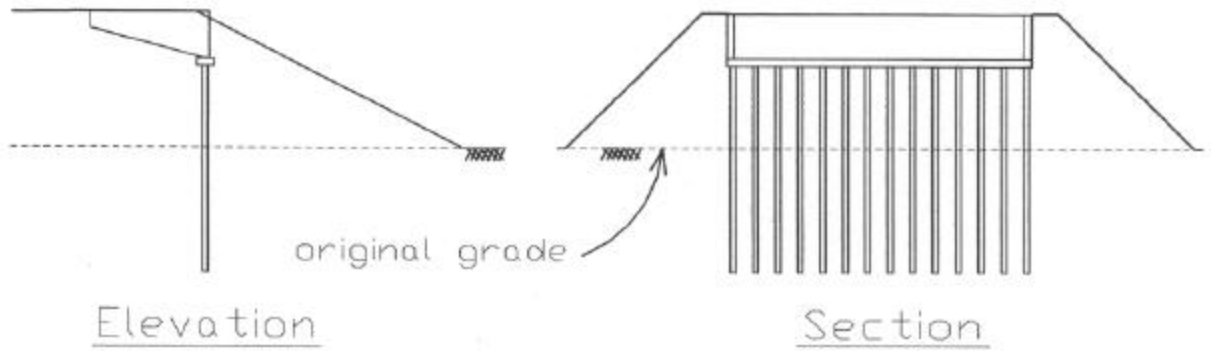


Figure 3.3 Approach-Embankment Cross-section

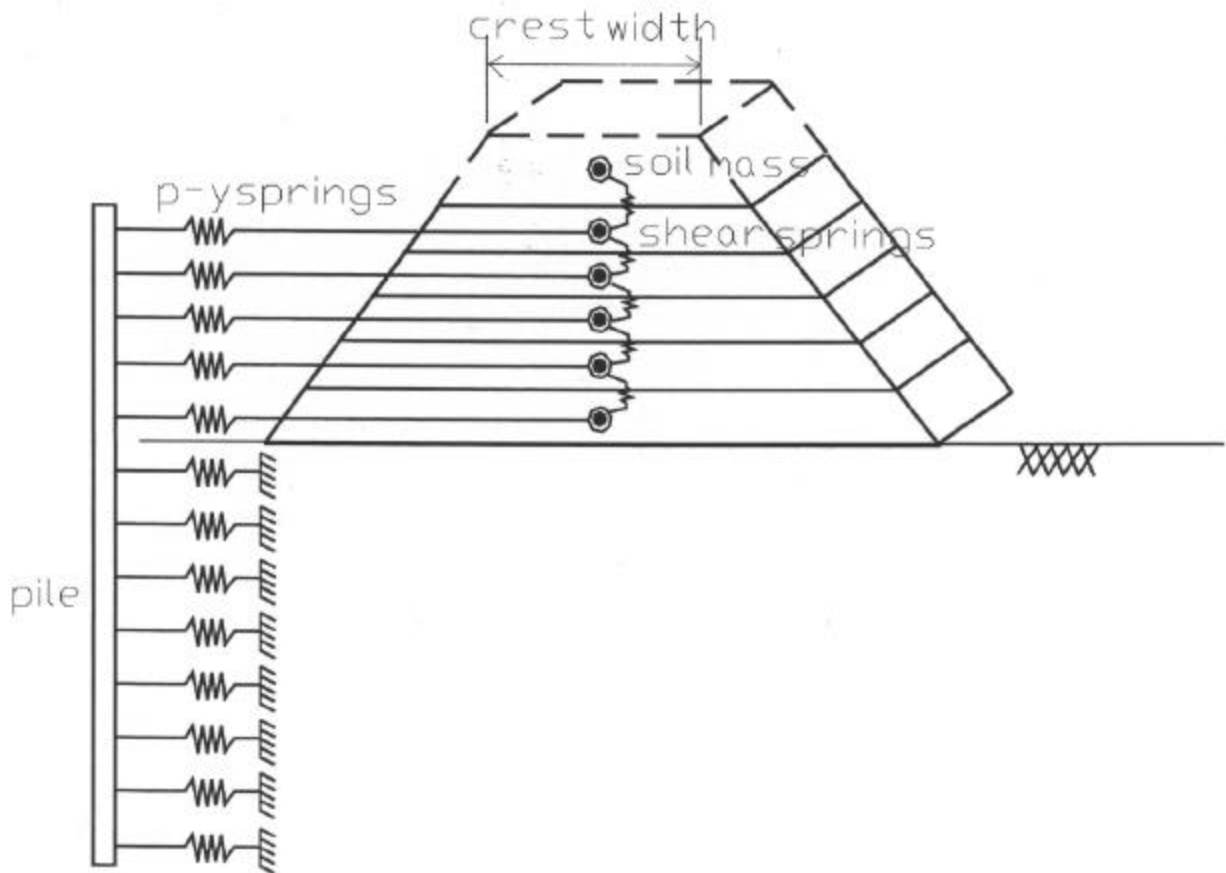


Figure 3.4 Illustration of Soil-Pile Model



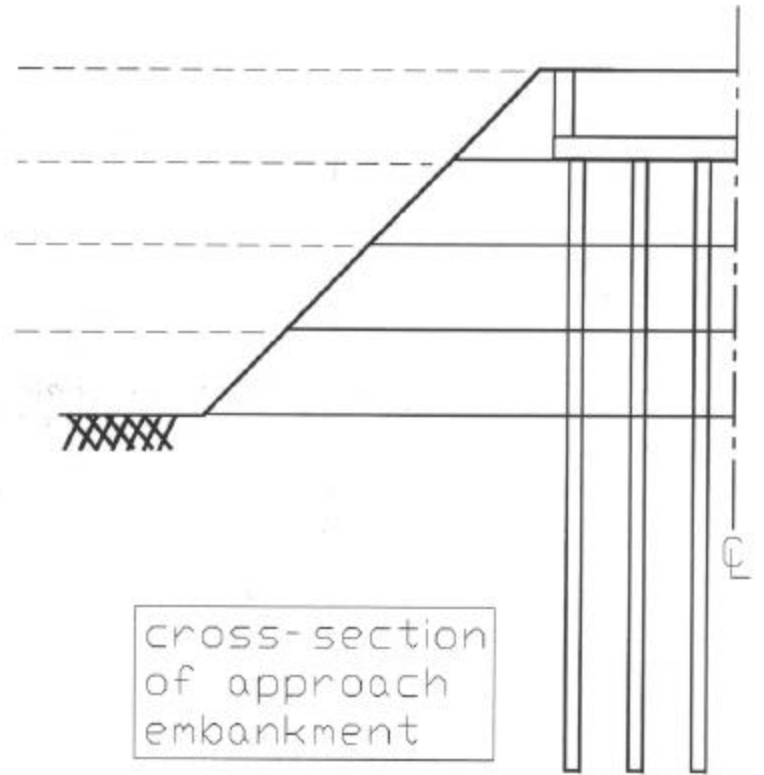
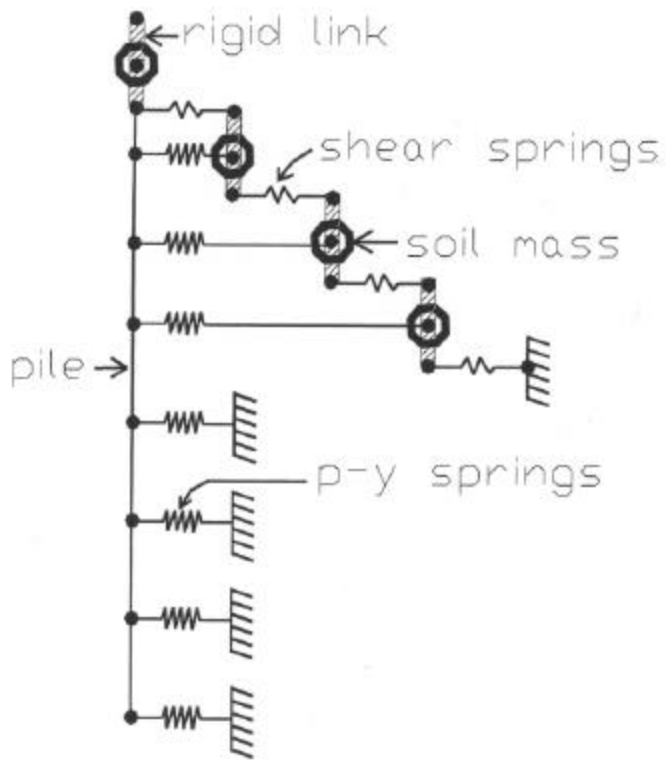


Figure 3.5 Implementation of Soil-Pile Model

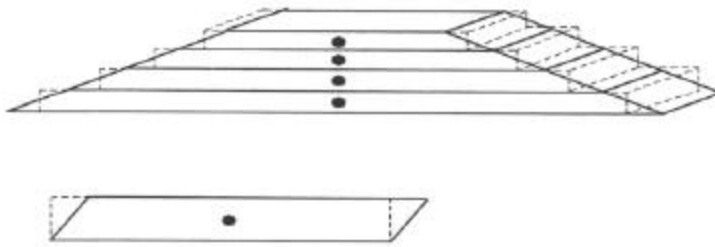


Figure 3.6a) Approach Embankment Wedge  
3.6b) Shear Deformation in Each Soil Layer

Iwan Model(1973)

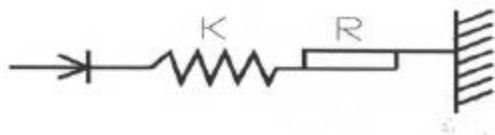


Figure 3.7a) Iwan Spring

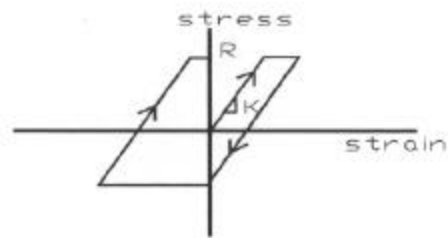


Figure 3.7b) Stress-strain Relationship of Iwan Spring

Taylor(1978)

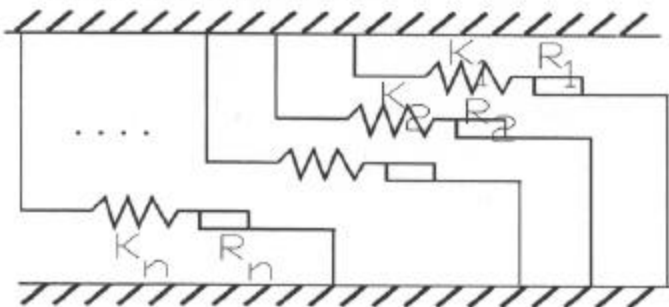


Figure 3.8a) Iwan Springs in Parallel

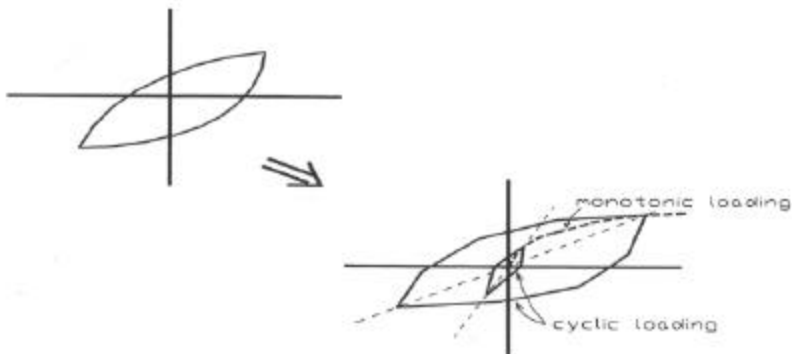


Figure 3.8b) Use of Iwan-type Springs to Represent Non-linear Hysteretic Behavior of Soils

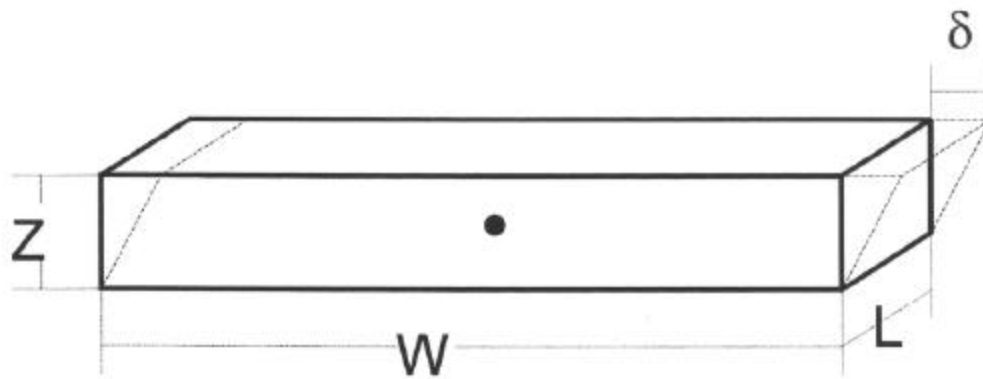


Figure 3.9a) Dimension of a Layer of an Approach Embankment

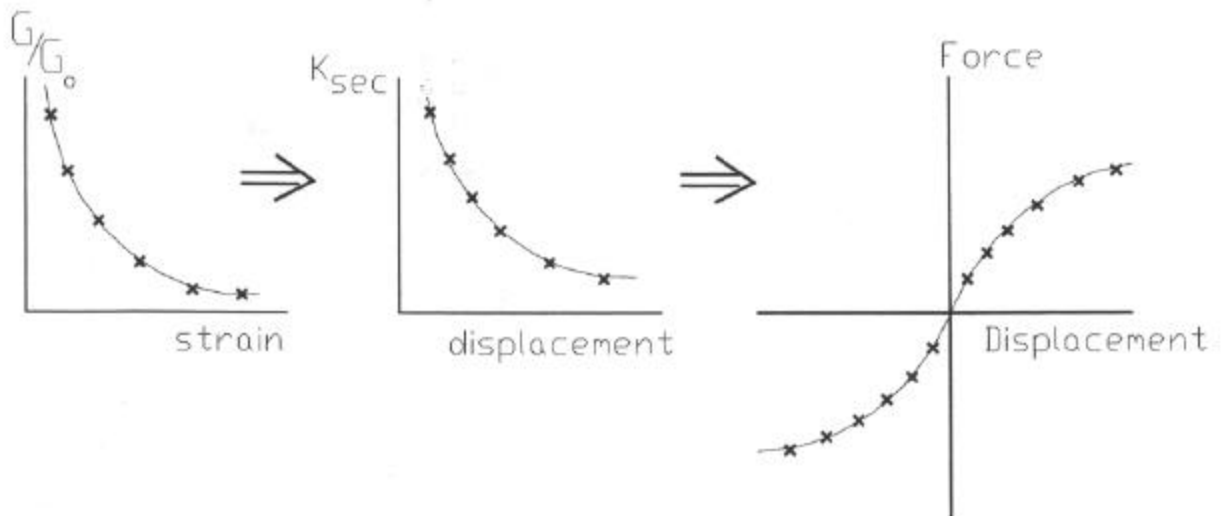


Figure 3.9b) Schematic View of the First Three Steps to Generate the Shear Springs

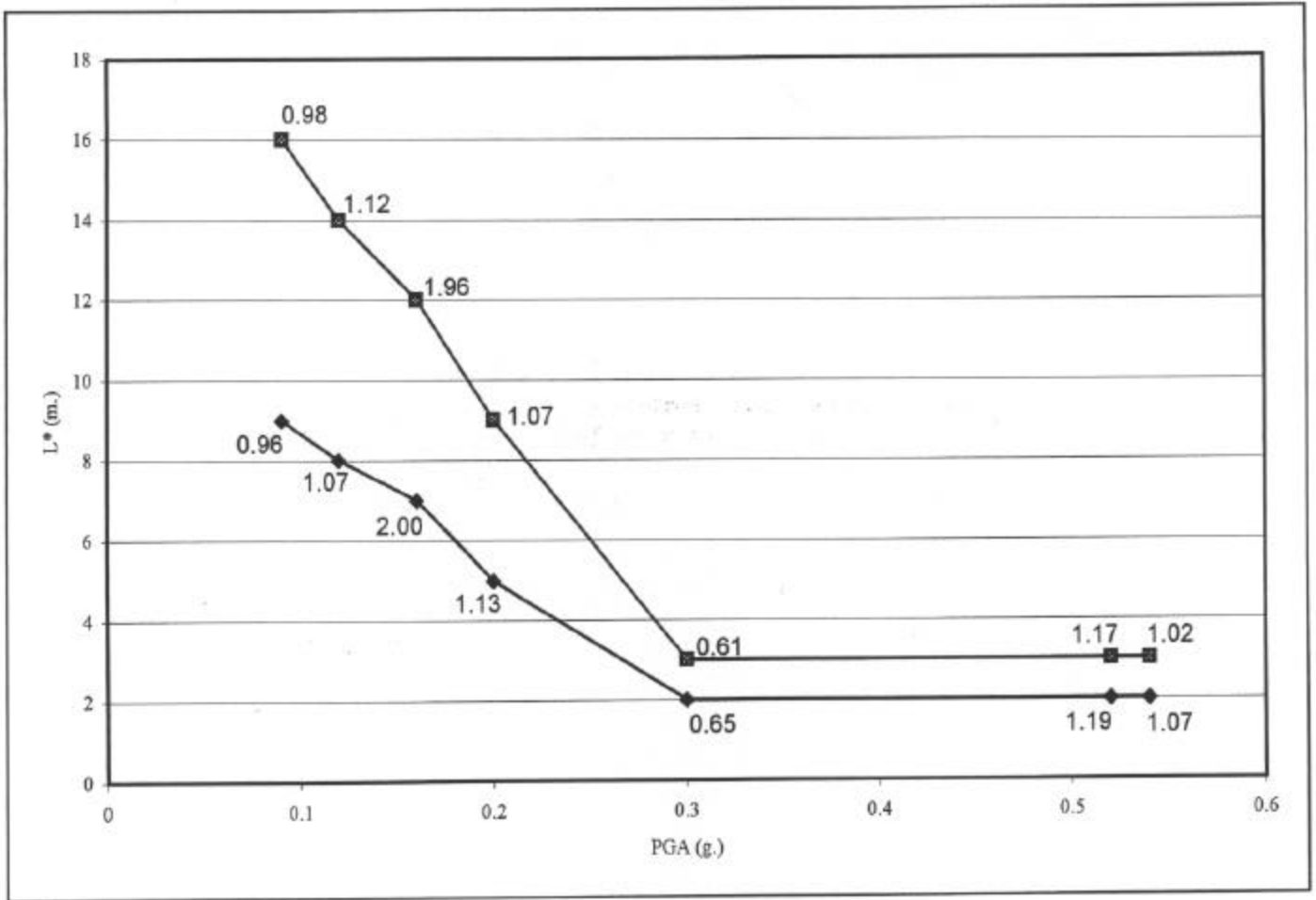


Figure 3.10 Ranges of Approach-Embankment Thickness ( $L^*$ ) for Soil-Pile Model Calibrated to MRO and PSO along with the Ratio Between the Calculated and the Recorded Peak Relative Displacement at Pier.

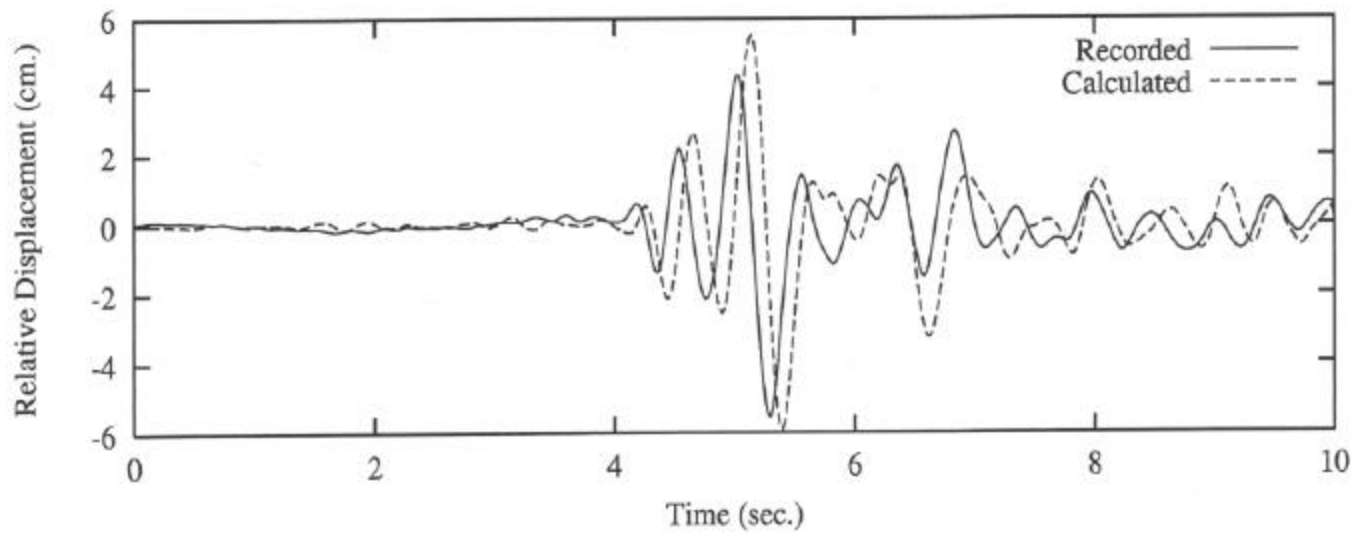
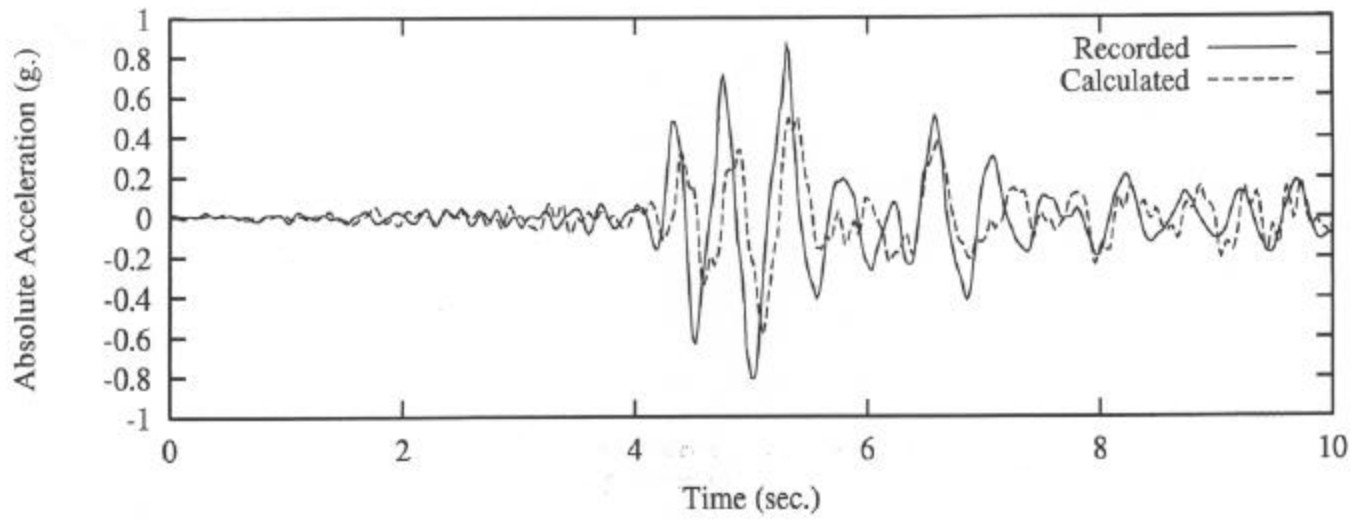


Figure 3.11 1992 Main Event on PSO (L= 2 m.), Soil-Pile Model

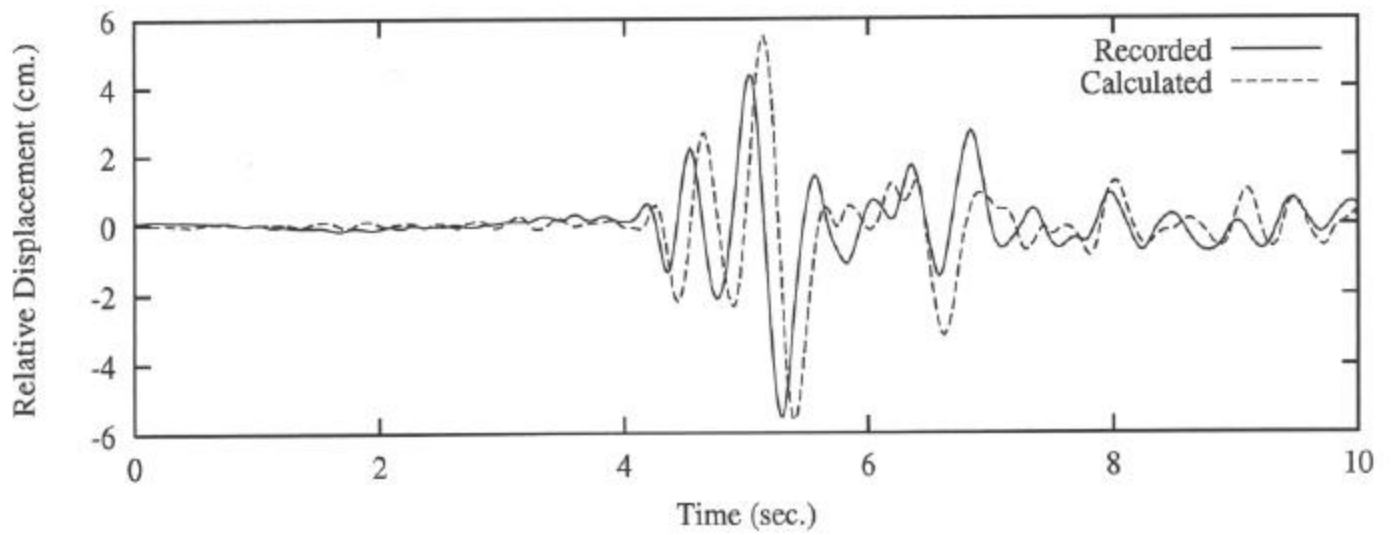
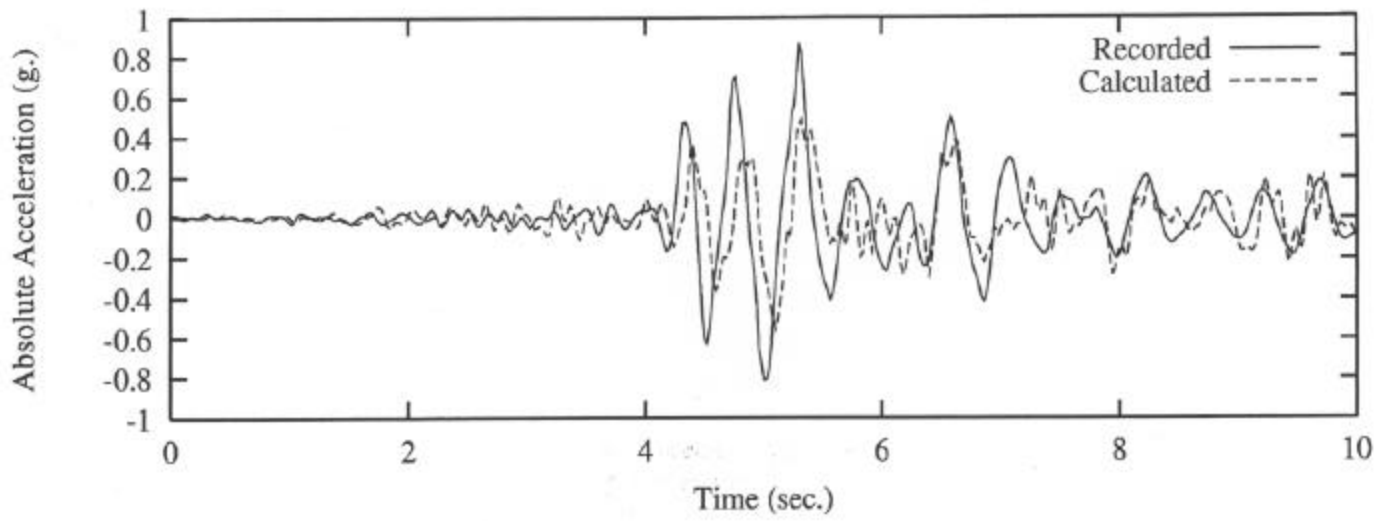


Figure 3.12 1992 Main Event on PSO ( $L=3$  m.), Soil-Pile Model

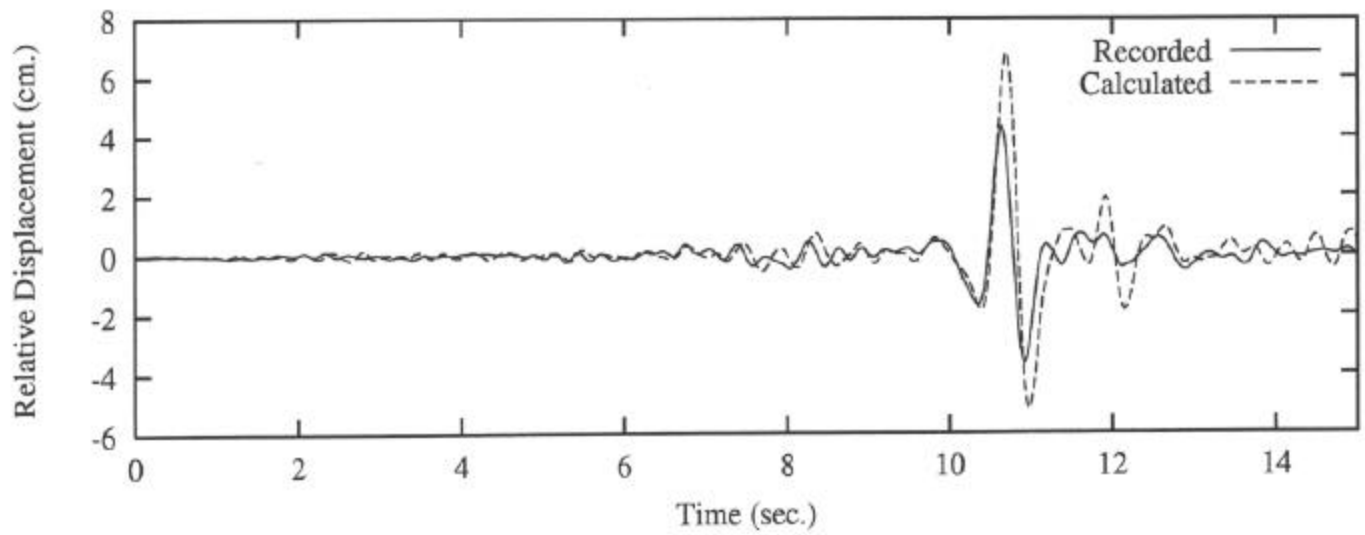
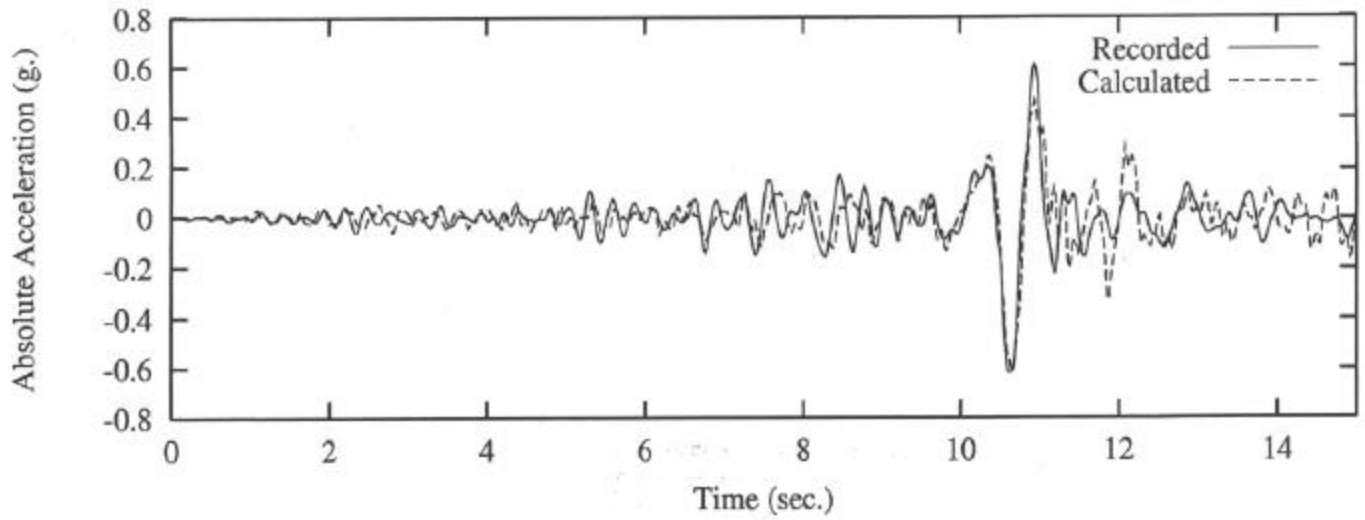


Figure 3.13 1992 Aftershock #1 on PSO (L= 2 m.), Soil-Pile Model

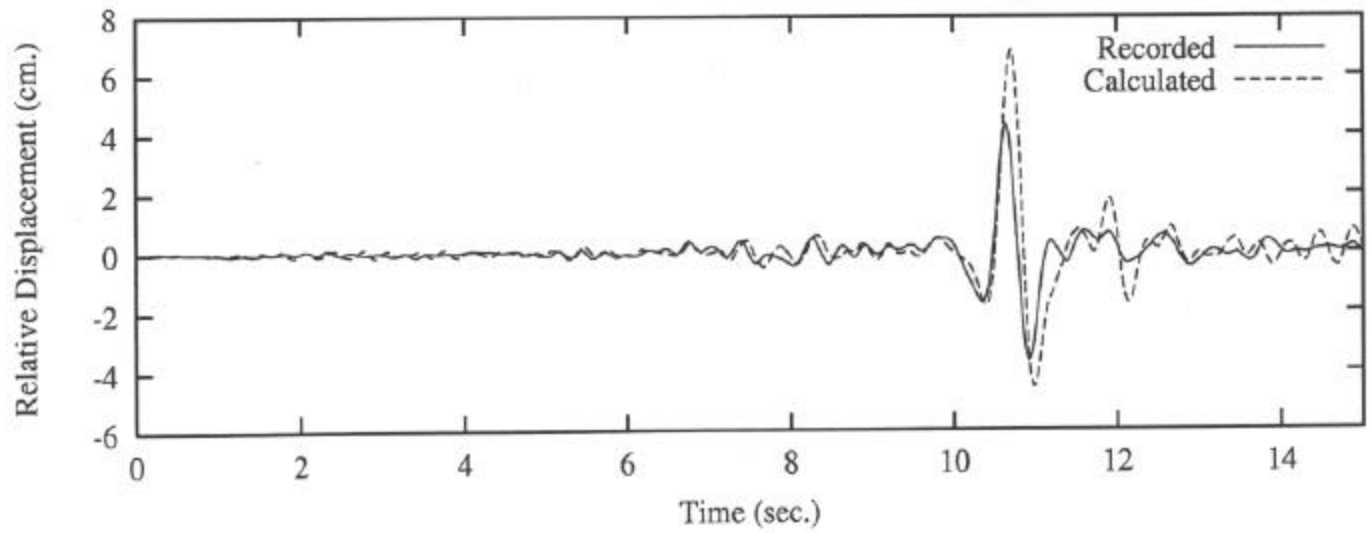
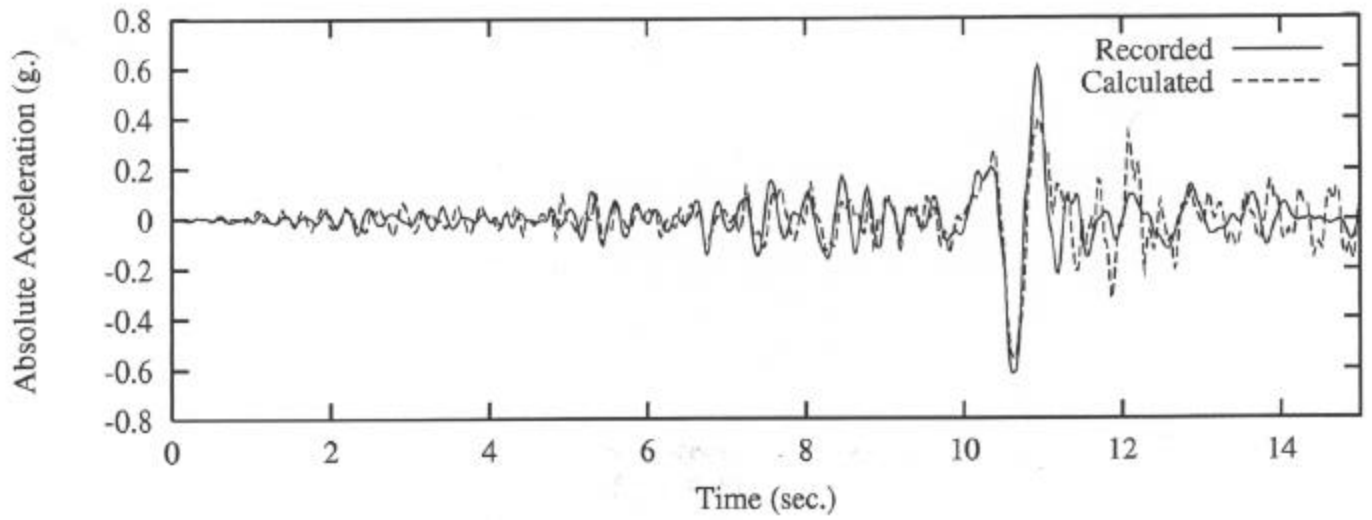


Figure 3.14 1992 Aftershock #1 on PSO (L= 3 m.), Soil-Pile Model



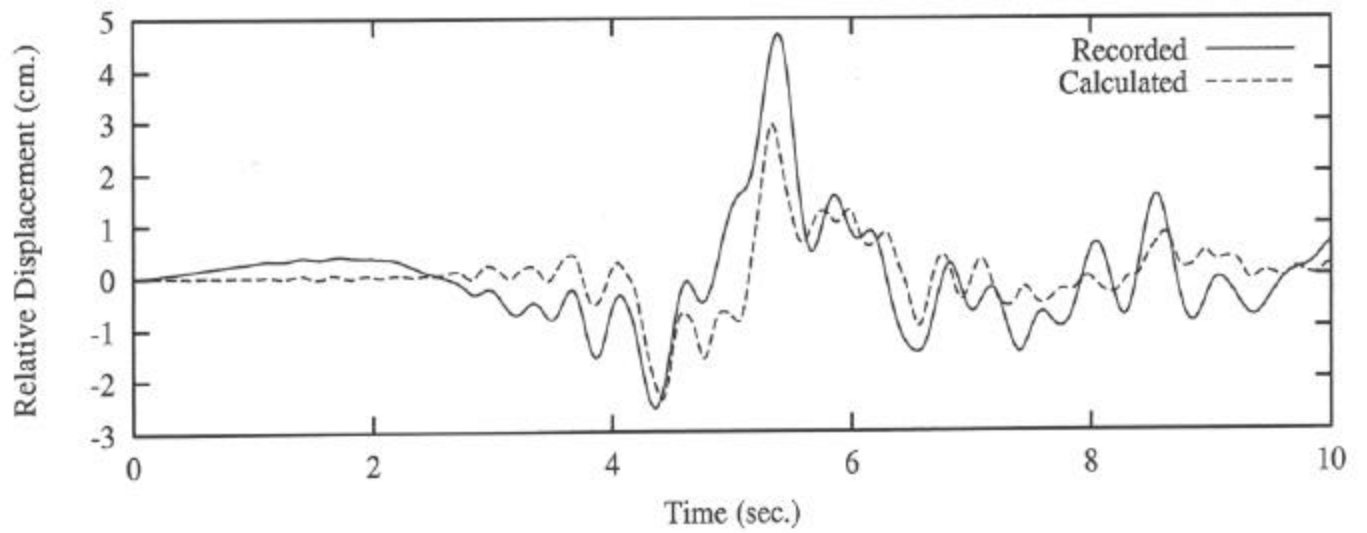
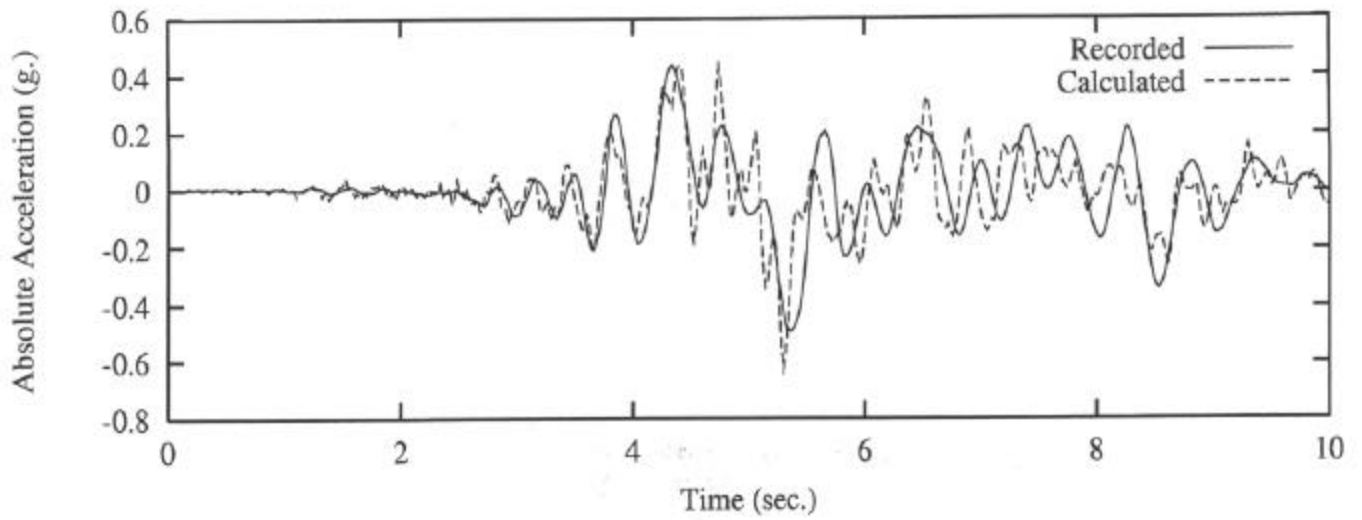


Figure 3.15 1979 Imperial Valley Earthquake on MRO (L= 2 m.), Soil-Pile Model

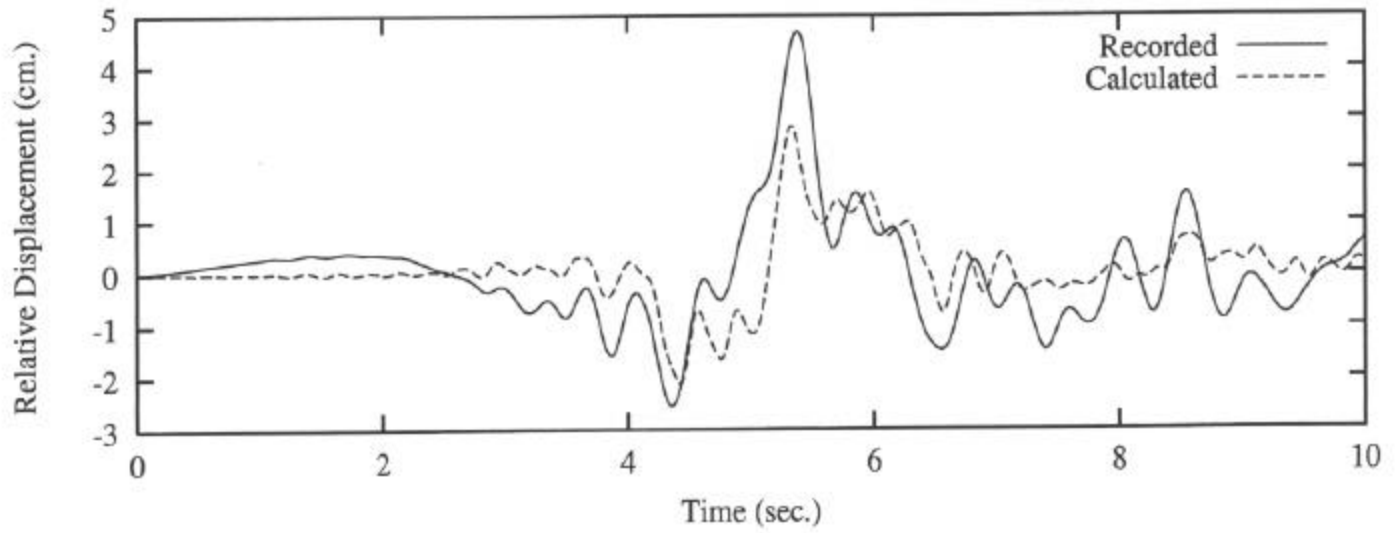
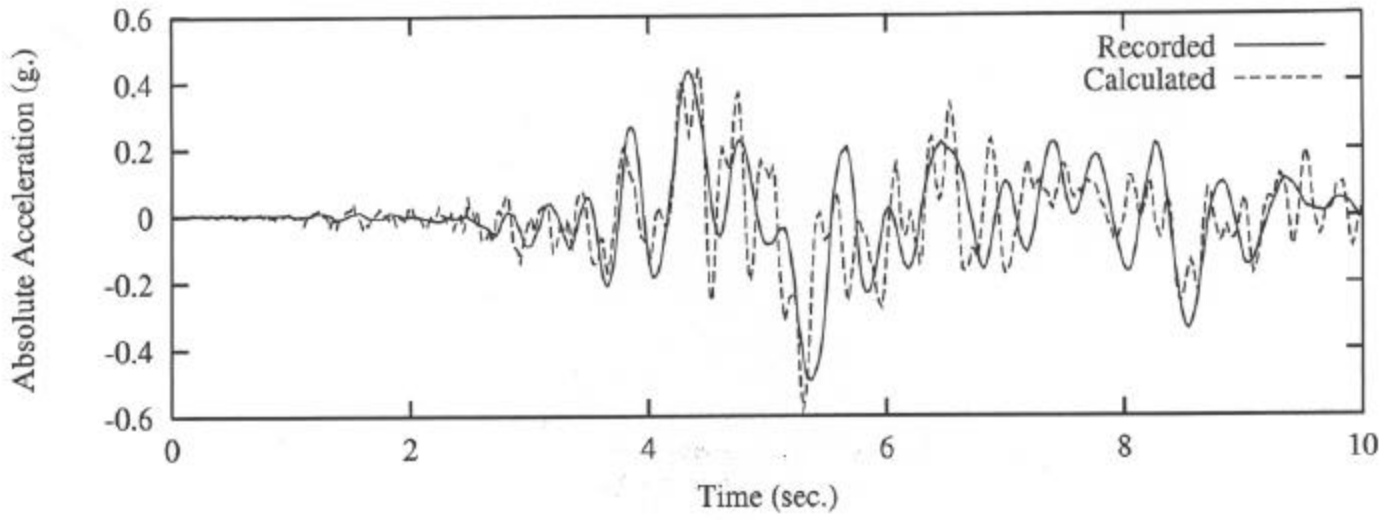


Figure 3.16 1979 Imperial Valley Earthquake on MRO (L= 3 m.), Soil-Pile Model

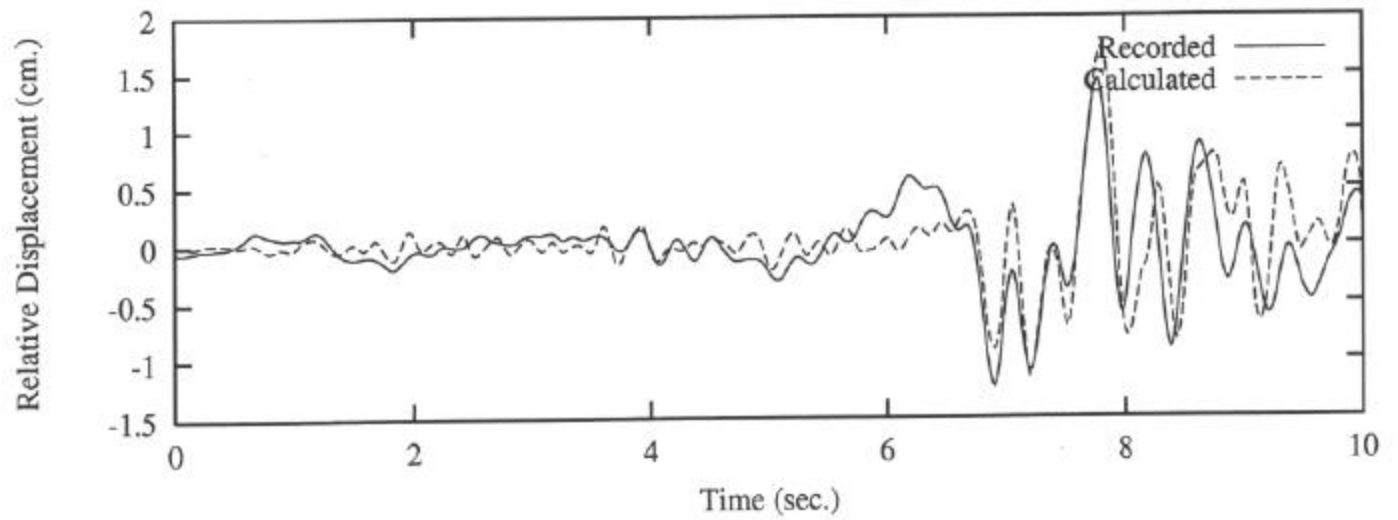
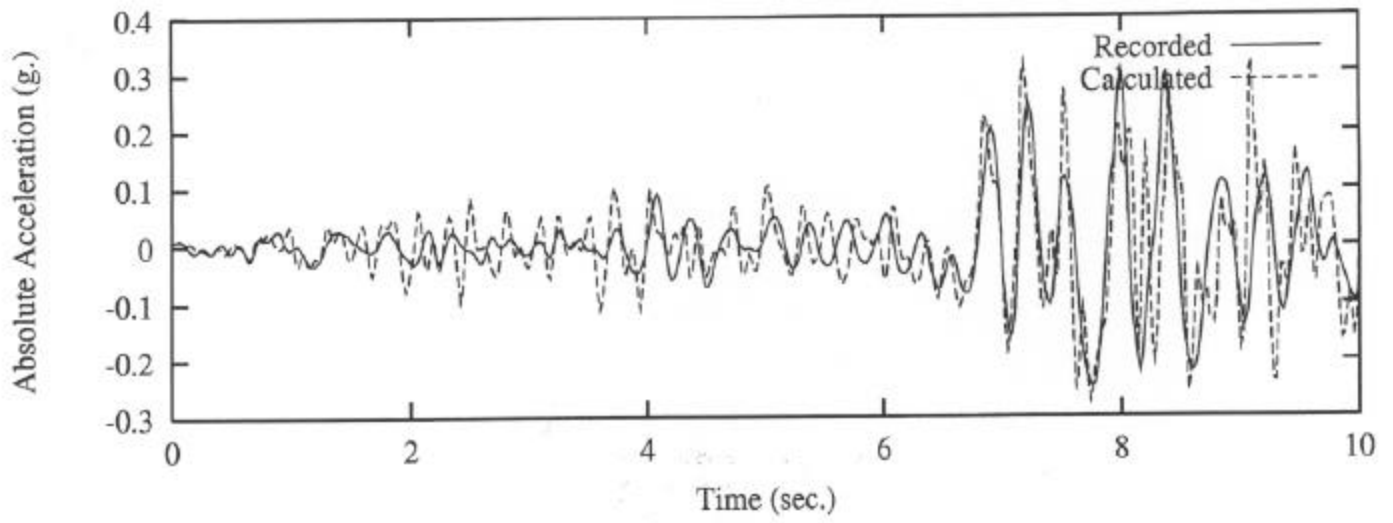


Figure 3.17 1992 Aftershock #2 on PSO (L= 5 m.), Soil-Pile Model

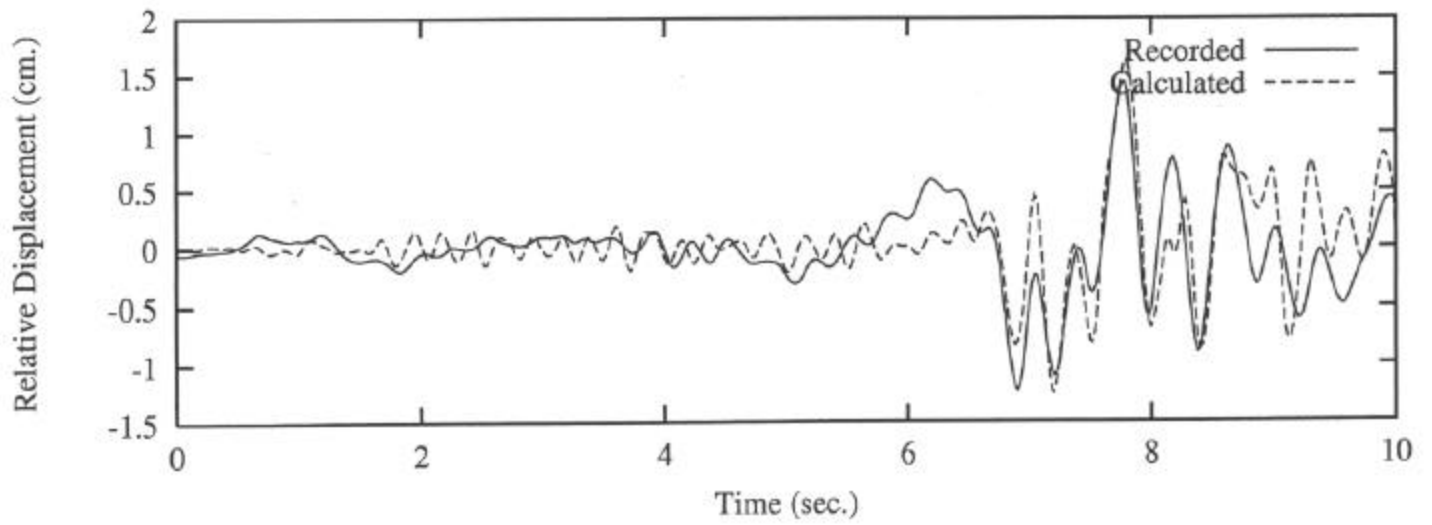
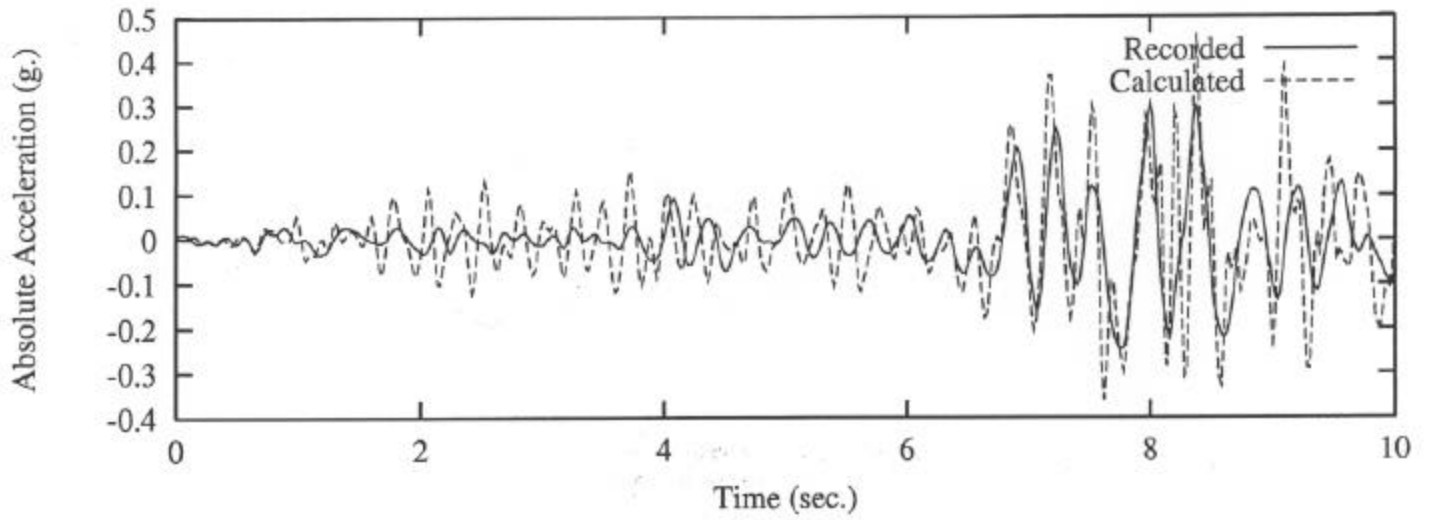


Figure 3.18 1992 Aftershock #2 on PSO (L= 9 m.), Soil-Pile Model

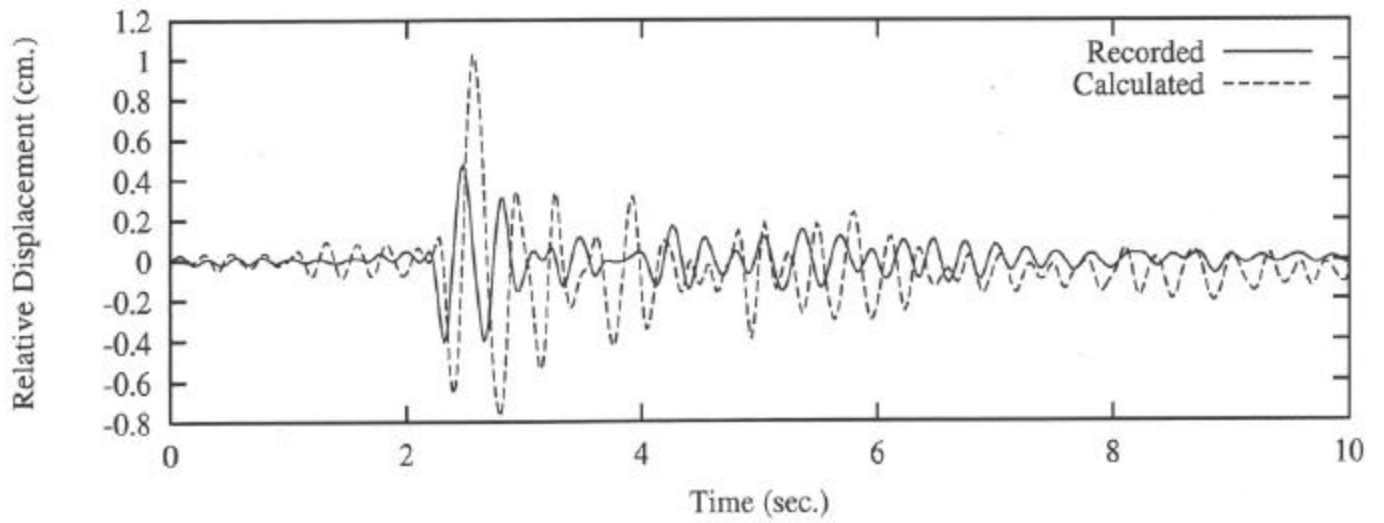
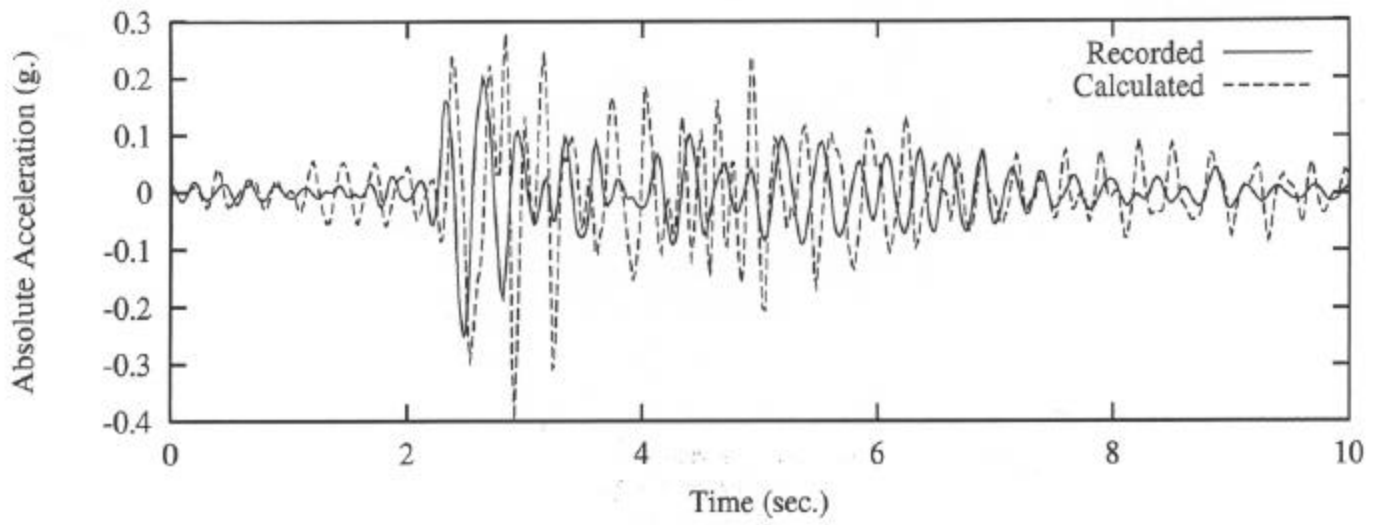


Figure 3.19 1986 Main Event on PSO (L= 7 m.), Soil-Pile Model

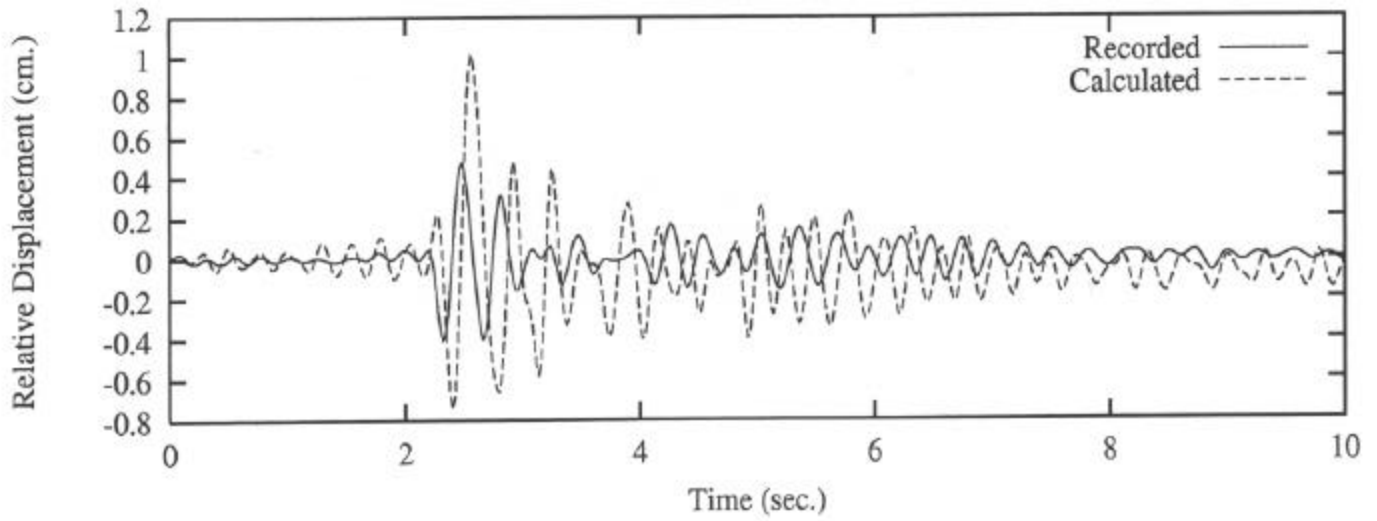
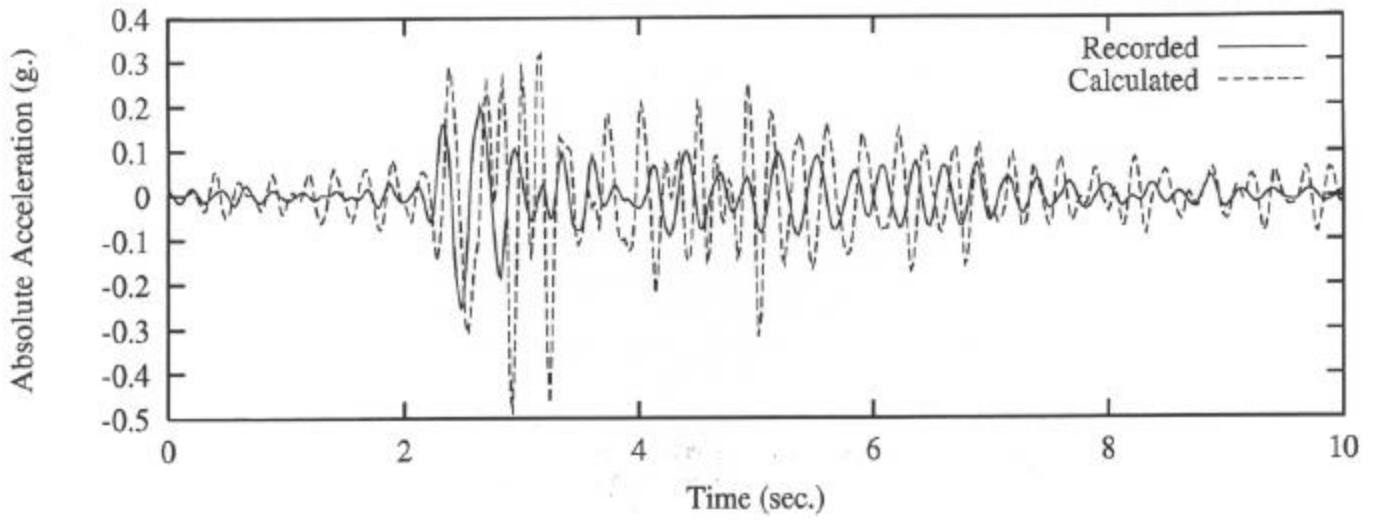


Figure 3.20 1986 Main Event on PSO (L= 12 m.), Soil-Pile Model

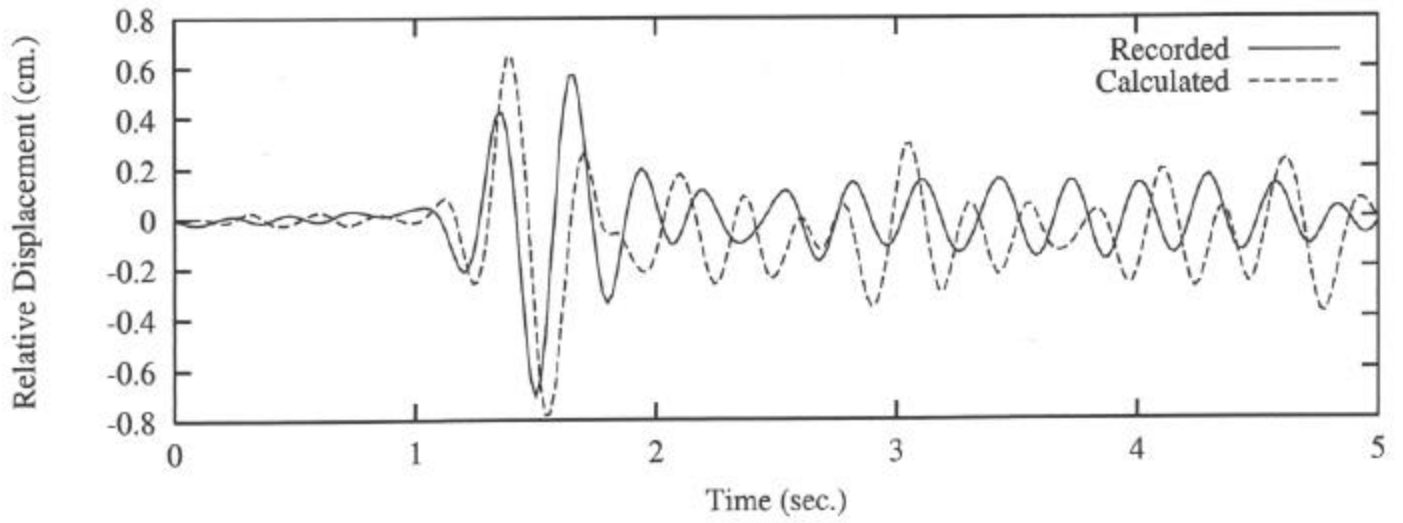
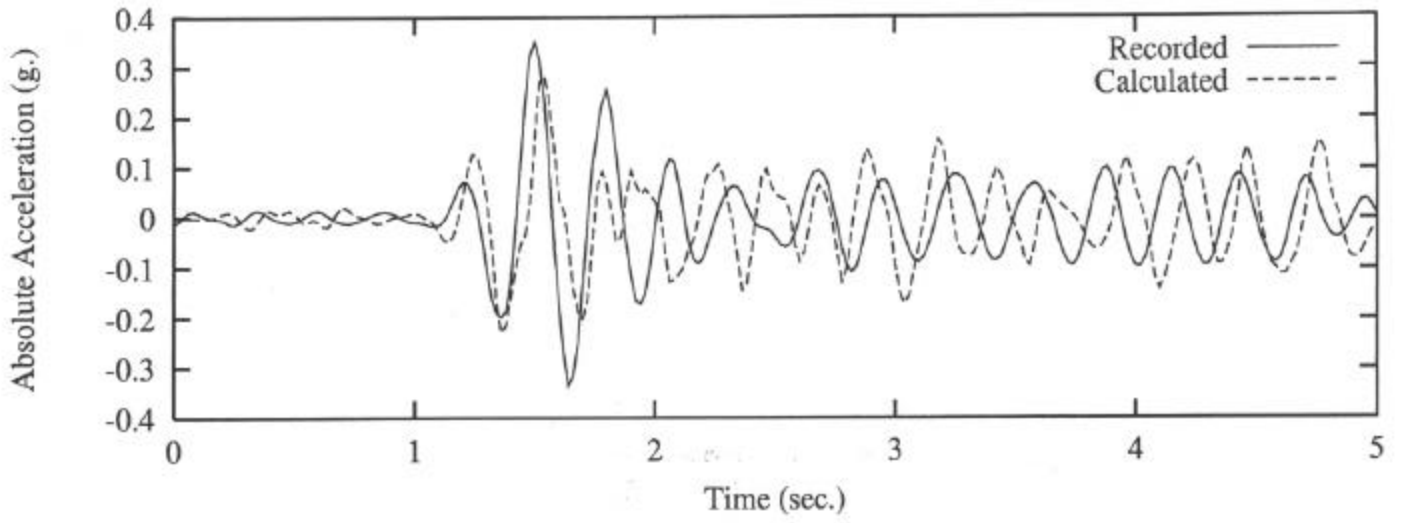


Figure 3.21 1986 Aftershock on PSO (L= 8 m.), Soil-Pile Model

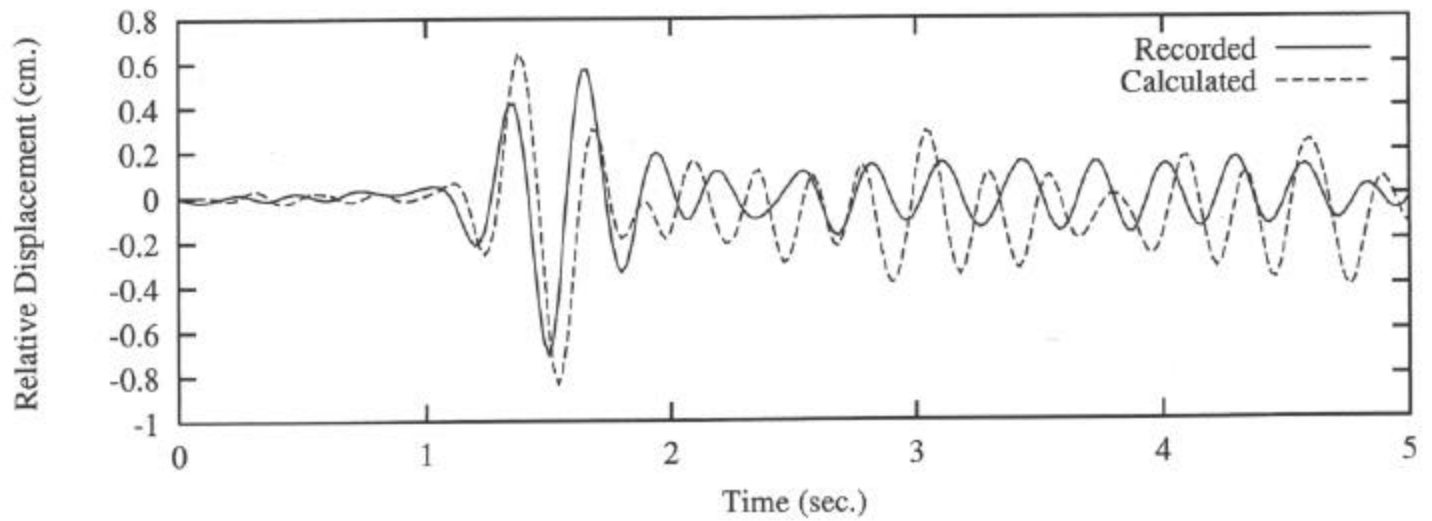
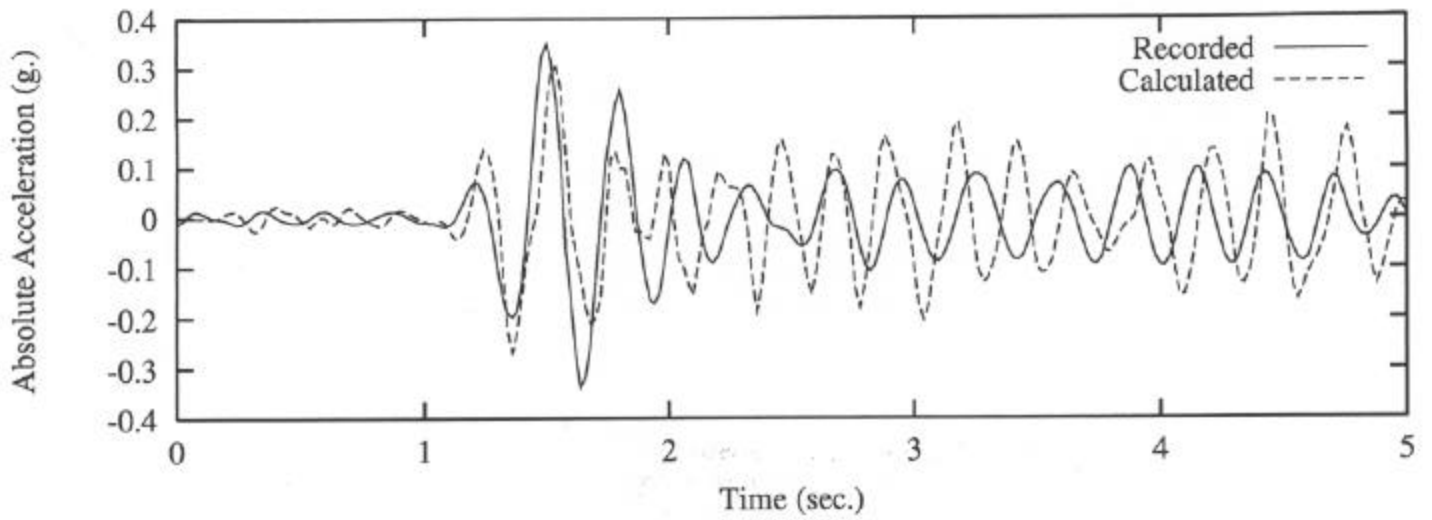


Figure 3.22 1986 Aftershock on PSO (L= 14 m.), Soil-Pile Model



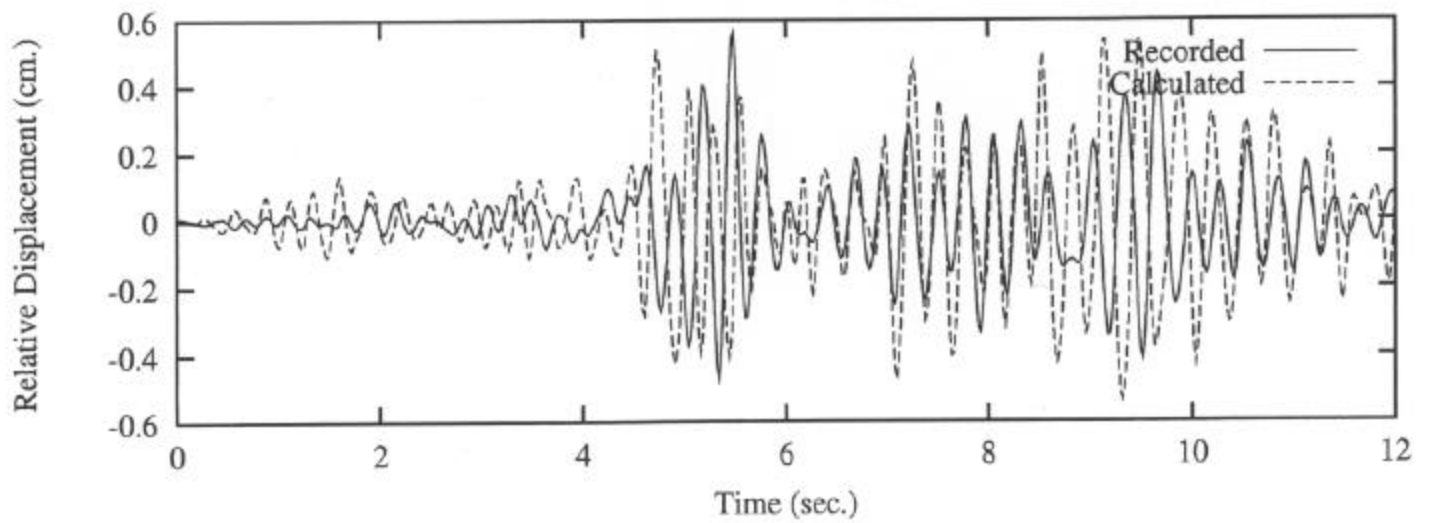
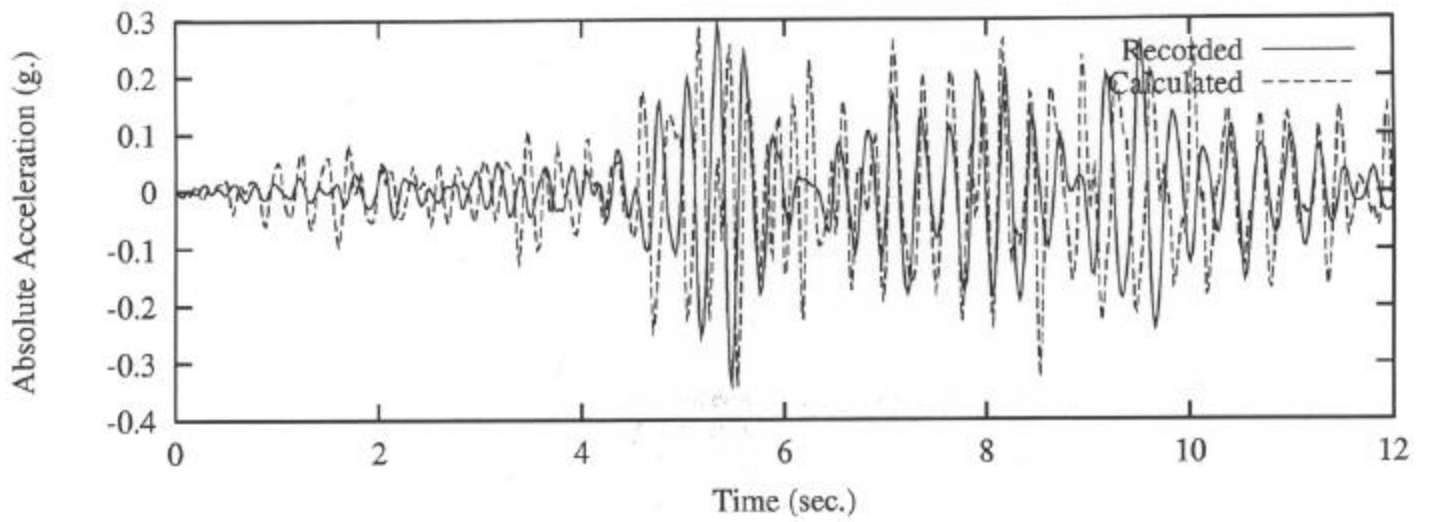


Figure 3.23 1987 Main Event on PSO (L= 9 m.), Soil-Pile Model

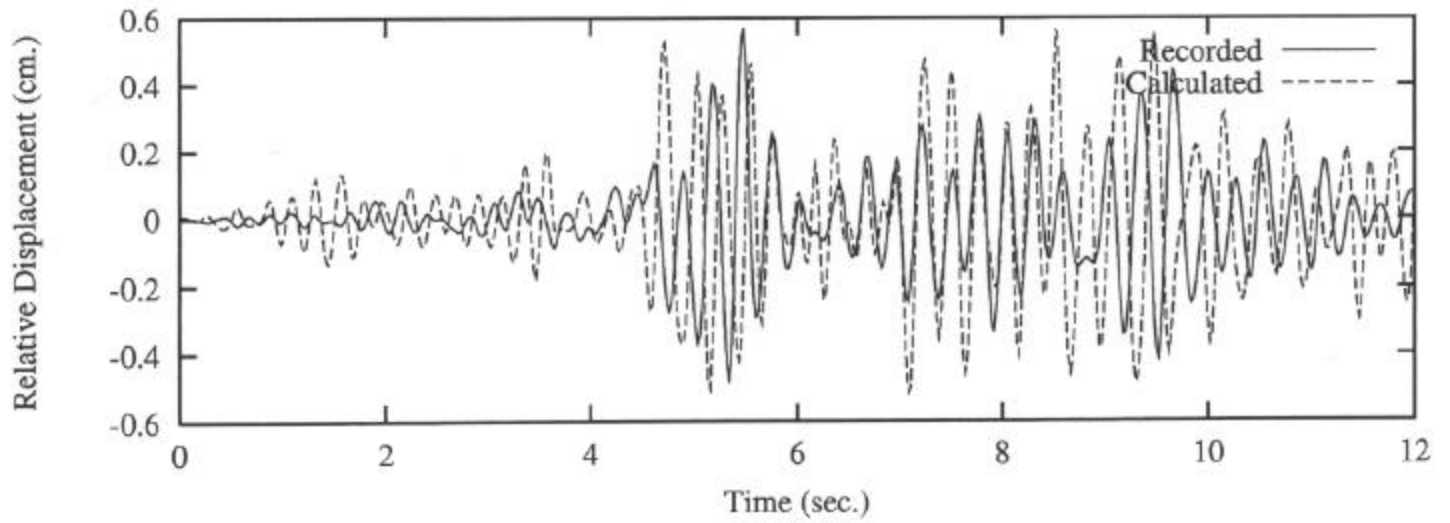
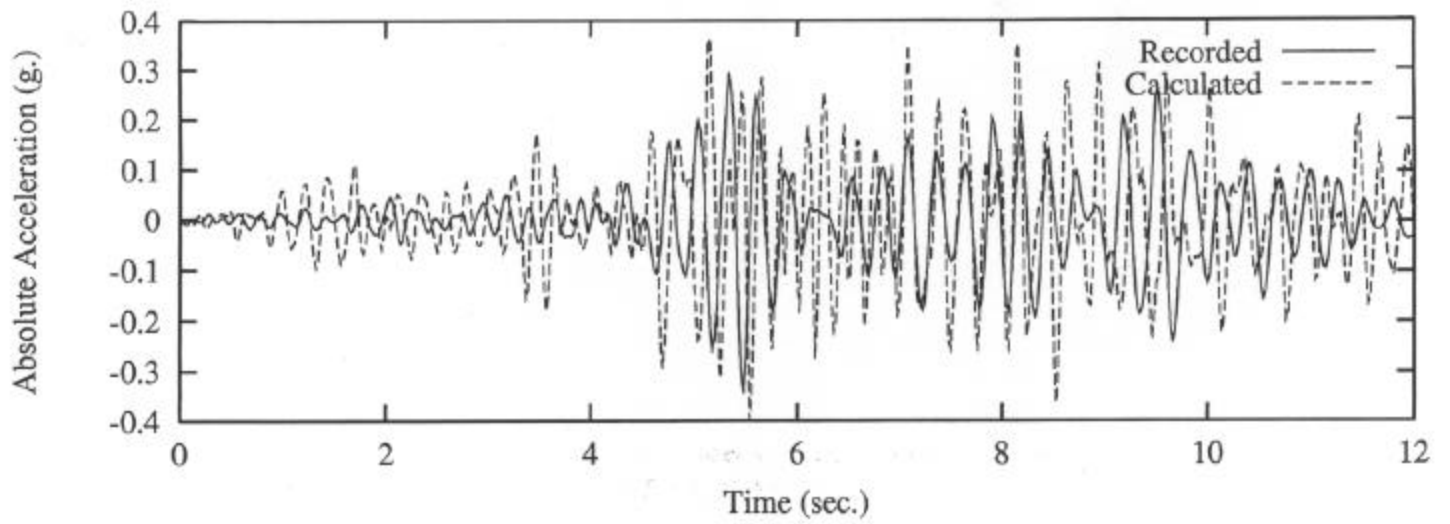
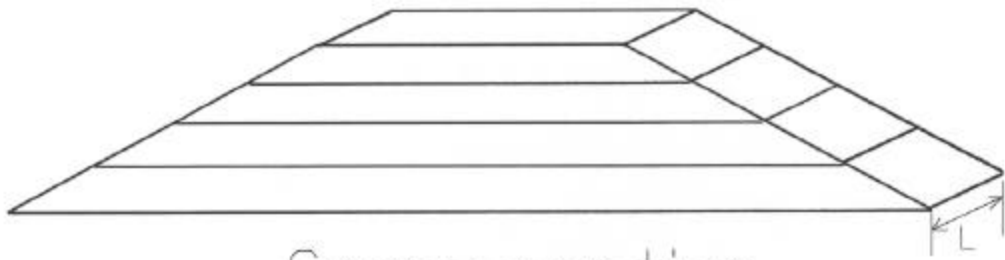


Figure 3.24 1987 Main Event on PSO (L= 16 m.), Soil-Pile Model



Cross-section

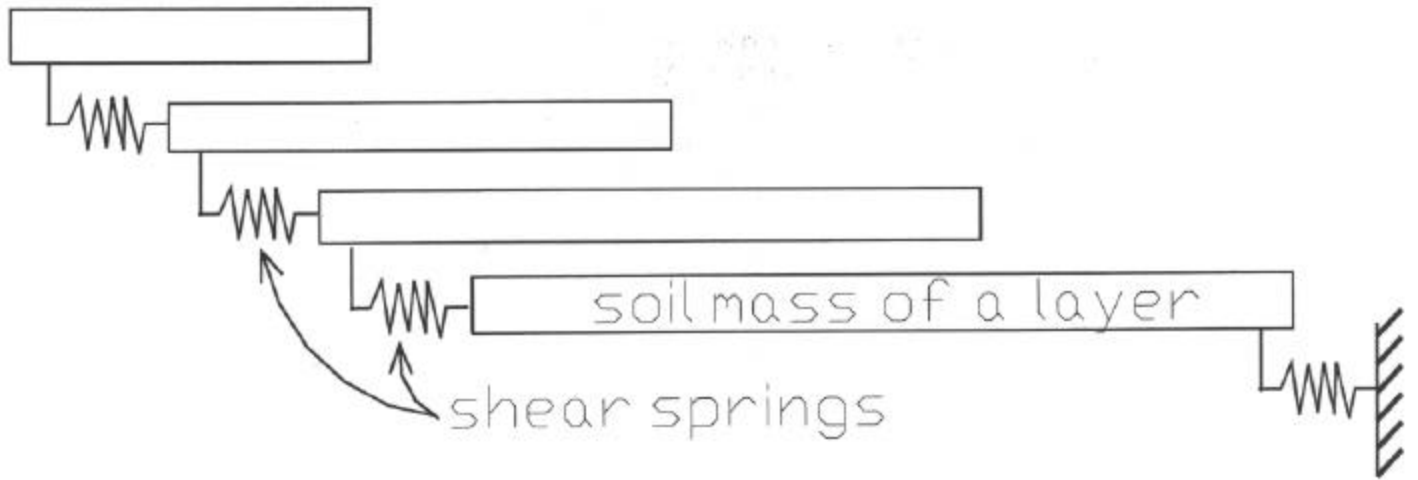


Figure 3.25 Soil-Slice Model

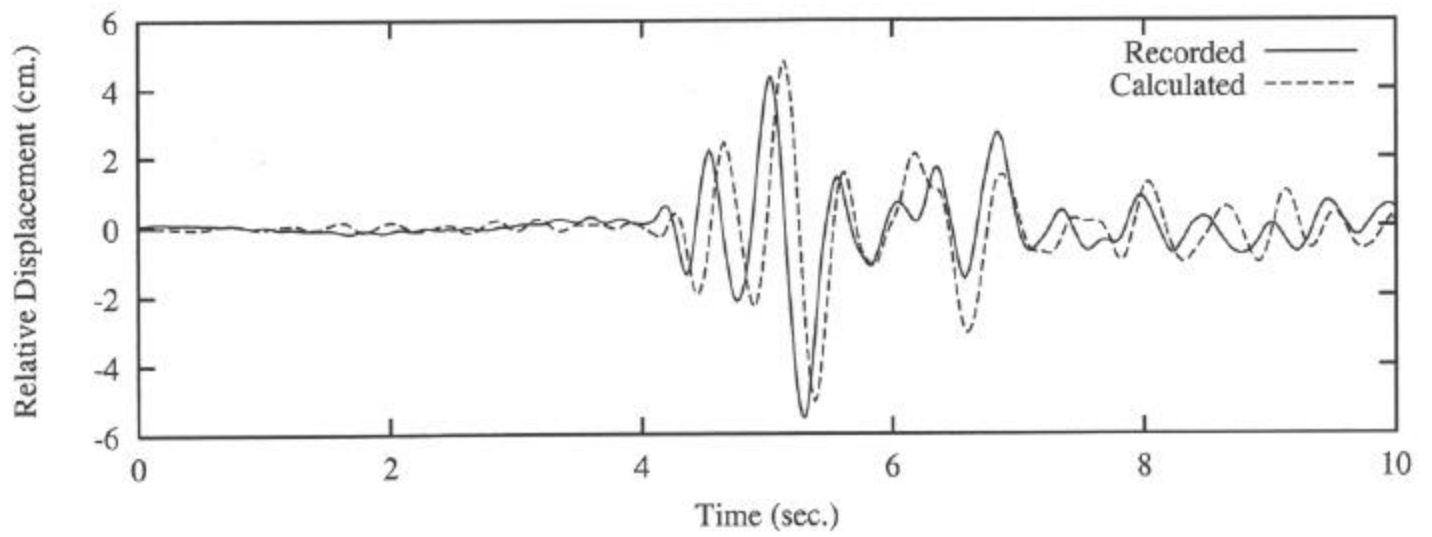
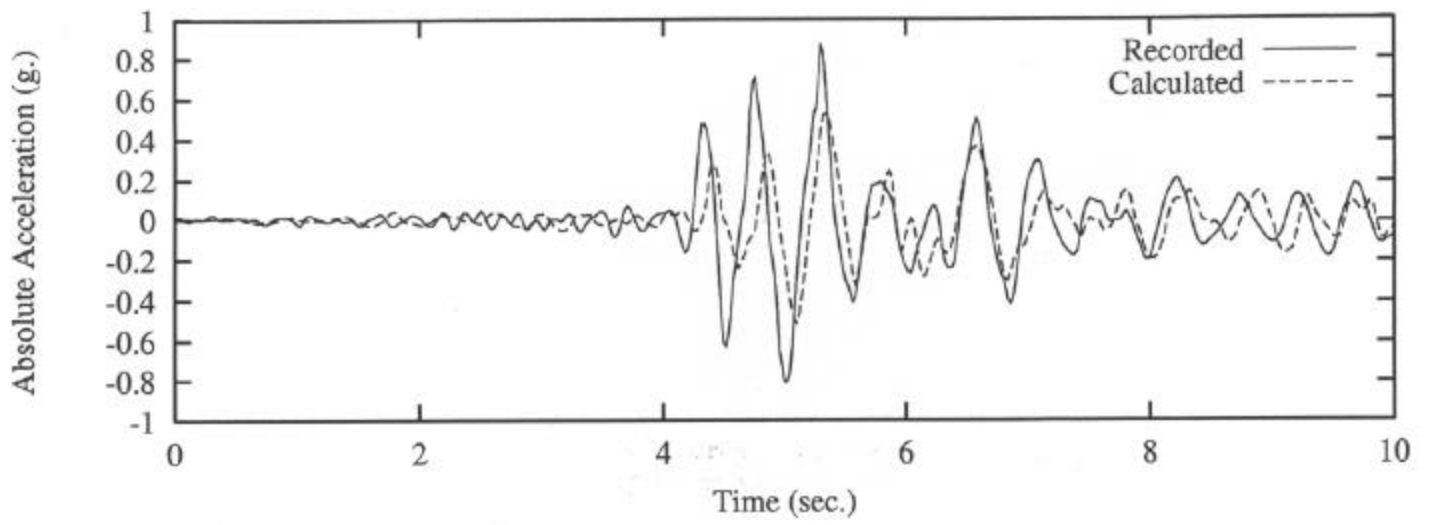


Figure 3.26 1992 Main Event on PSO (L= 1 m.), Soil-Slice Model

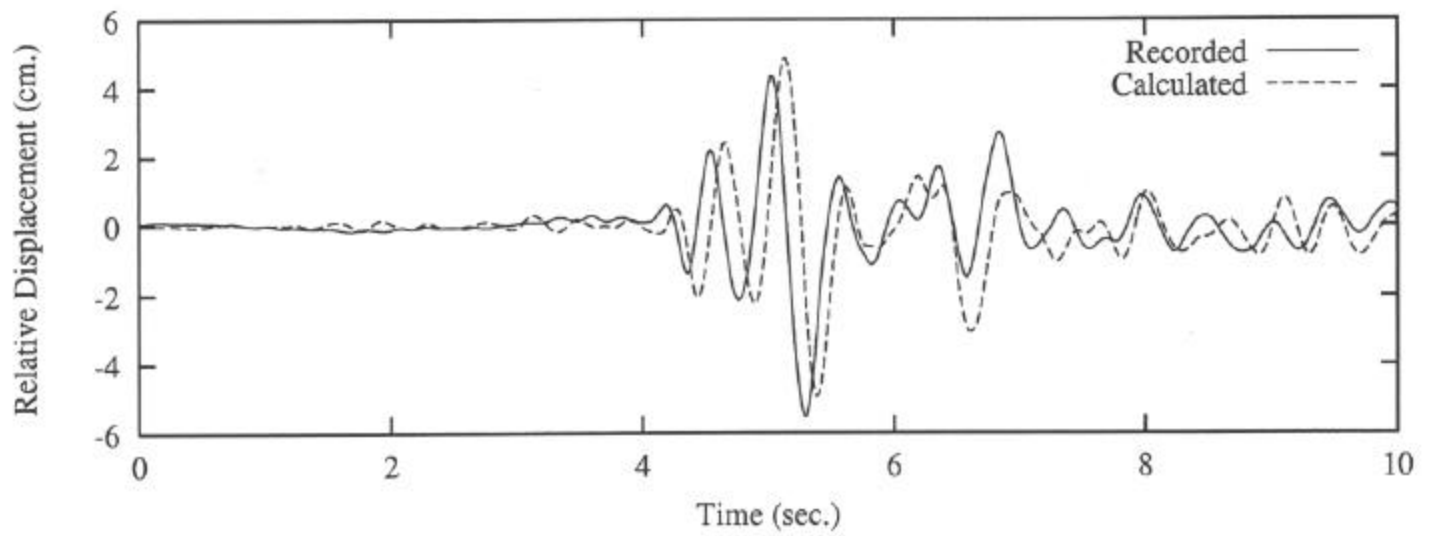
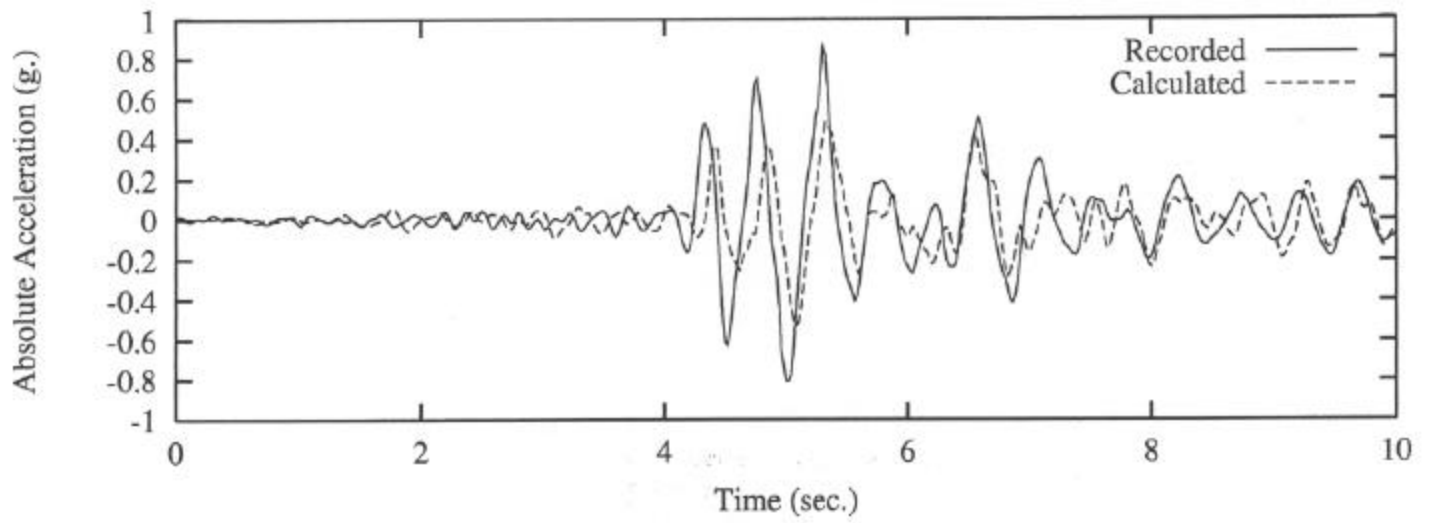


Figure 3.27 1992 Main Event on PSO (L= 2 m.), Soil-Slice Model

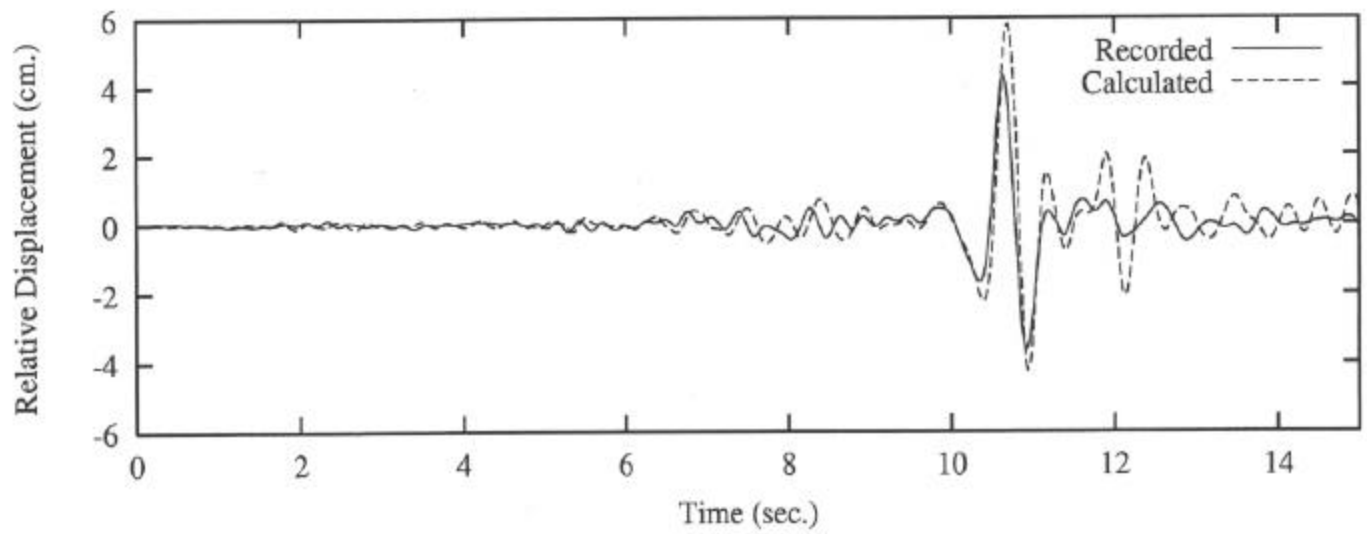
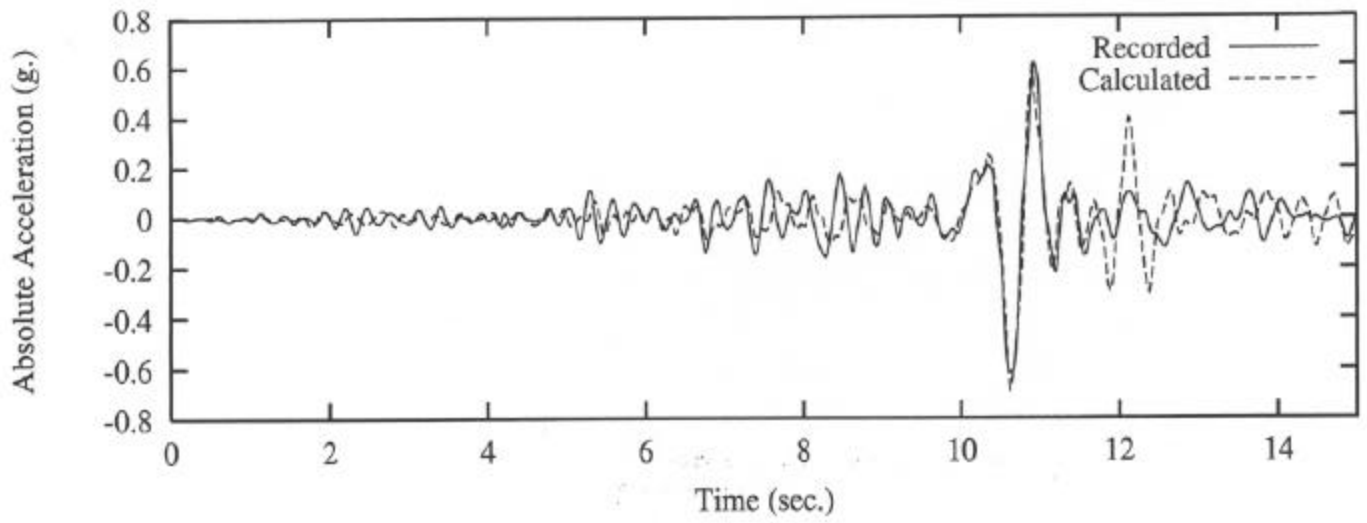


Figure 3.28 1992 Aftershock #1 on PSO (L= 1 m.), Soil-Slice Model

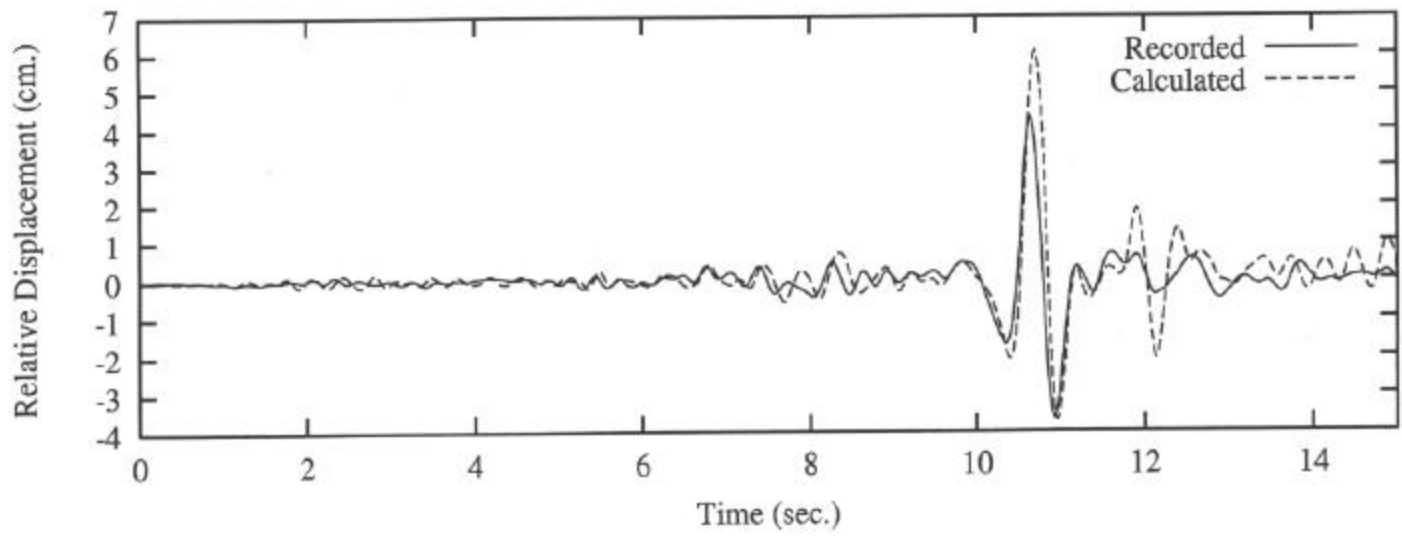
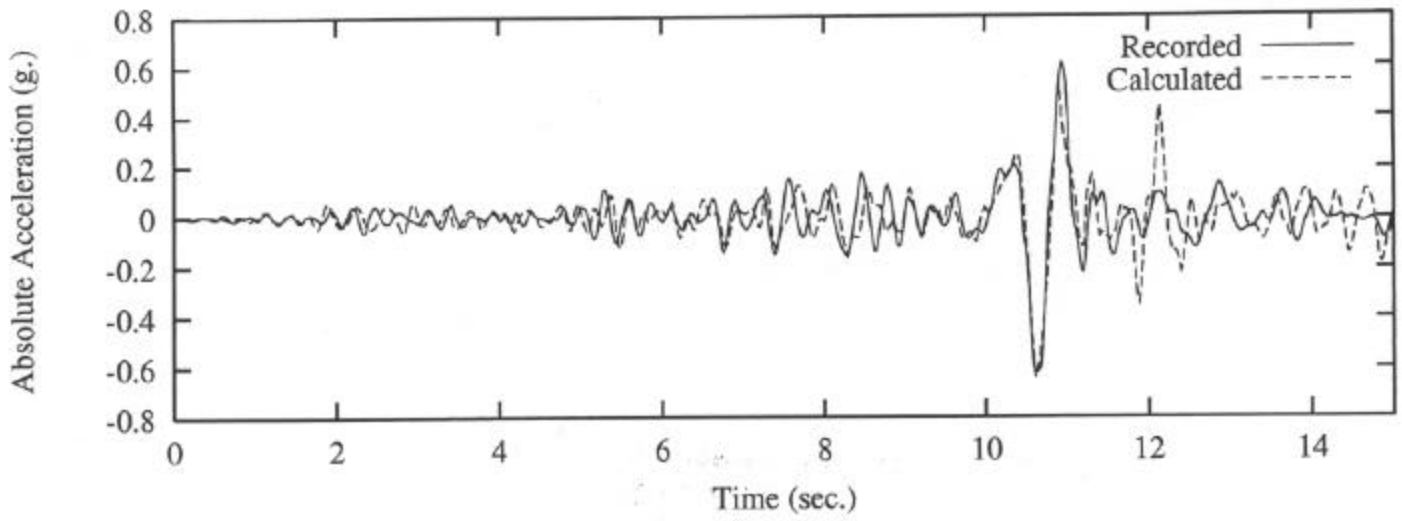


Figure 3.29 1992 Aftershock #1 on PSO (L= 2 m.), Soil-Slice Model

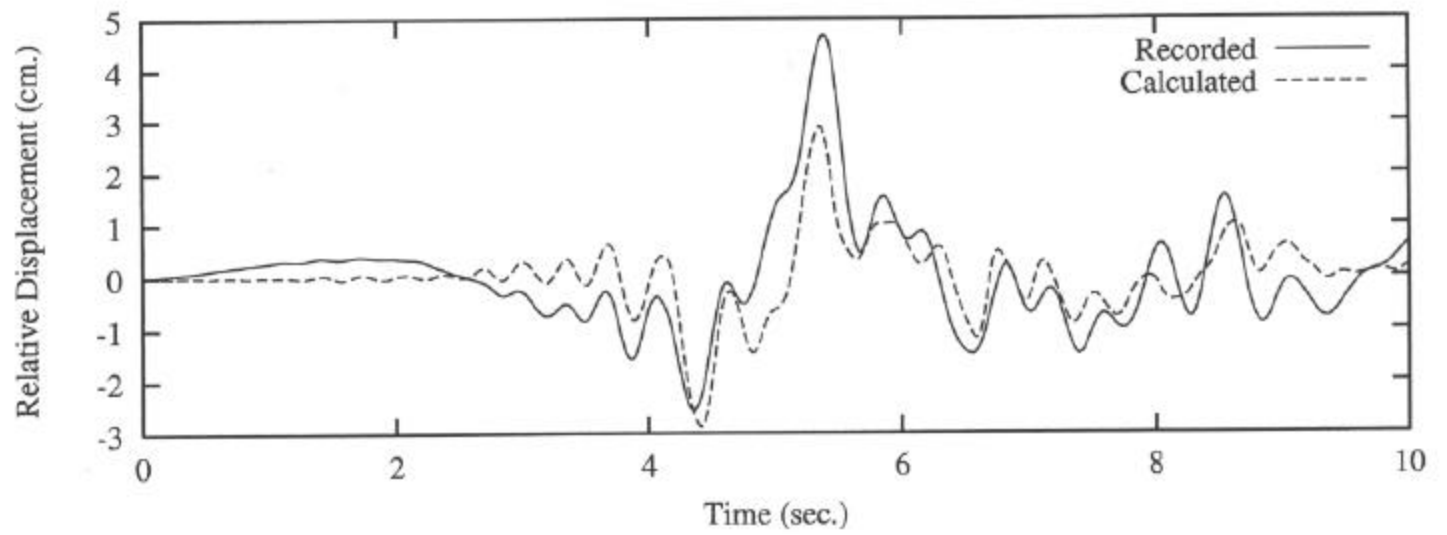
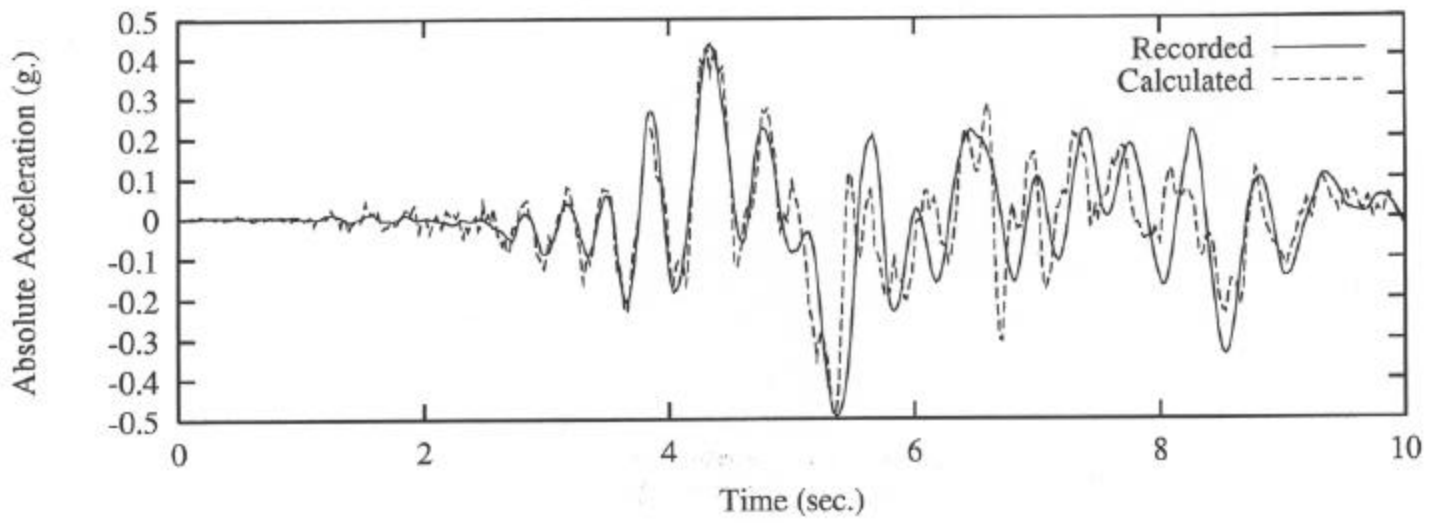


Figure 3.30 1979 Imperial Valley Earthquake on MRO (L= 1 m.), Soil-Slice Model



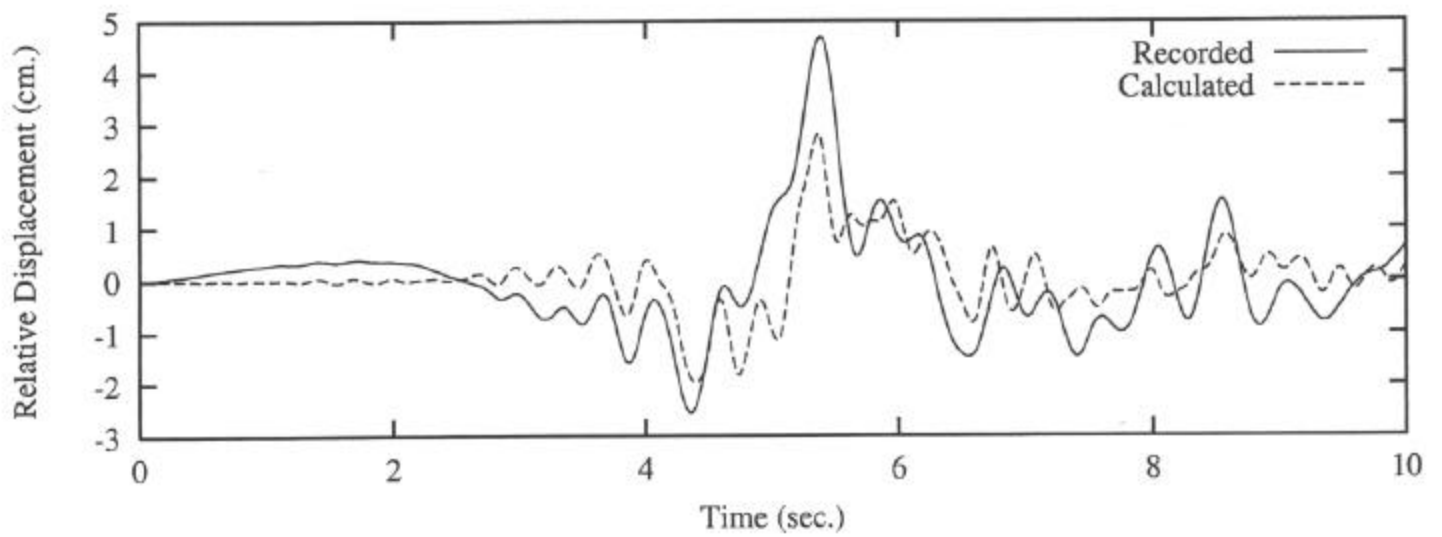
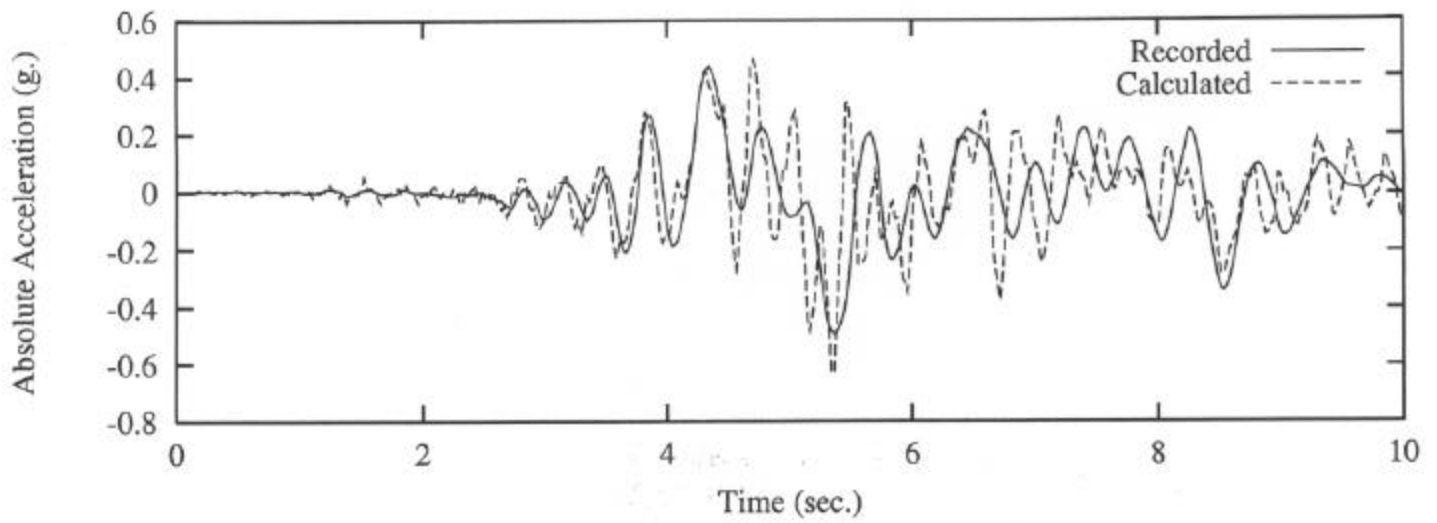


Figure 3.31 1979 Imperial Valley Earthquake on MRO (L= 2 m.), Soil-Slice Model

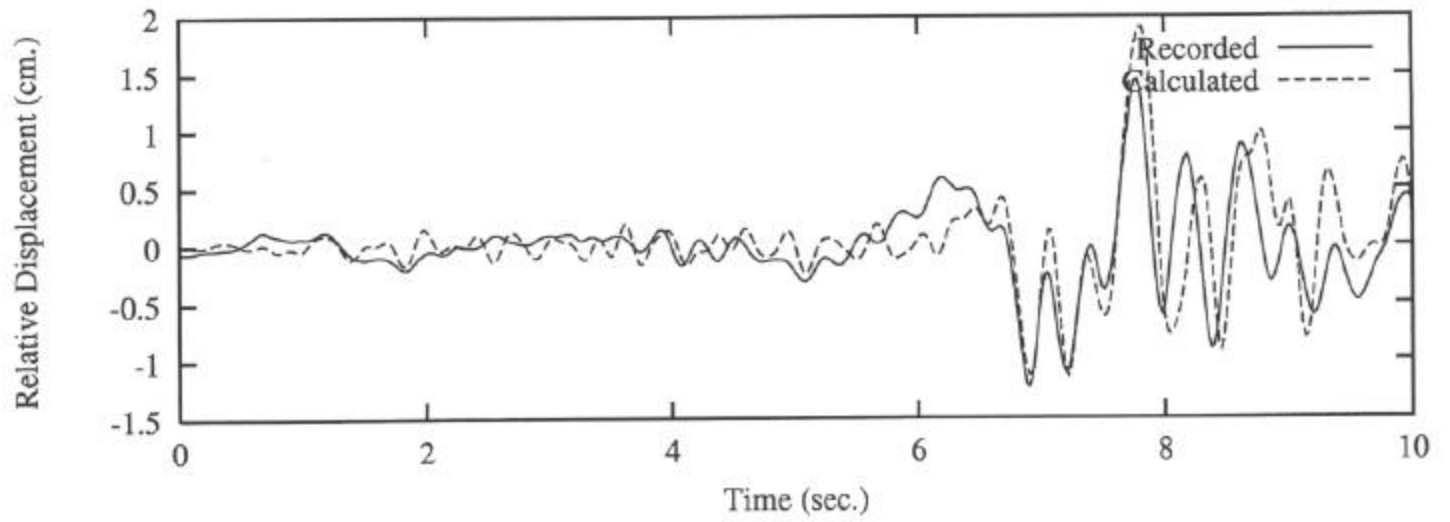
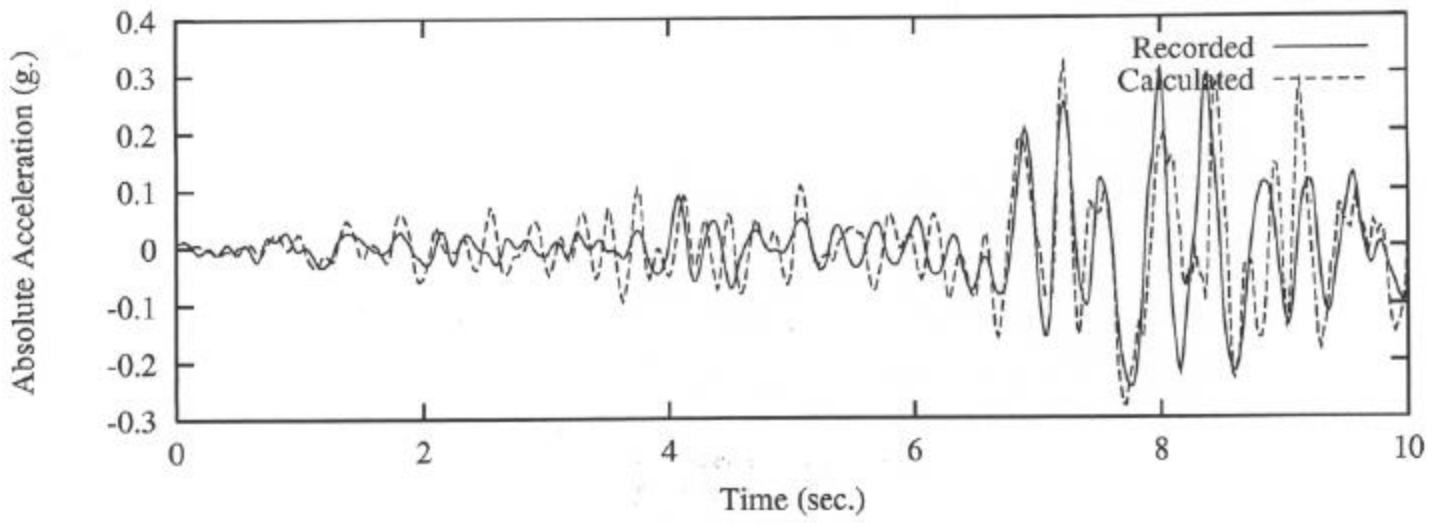


Figure 3.32 1992 Aftershock #2 on PSO (L= 3 m.), Soil-Slice Model

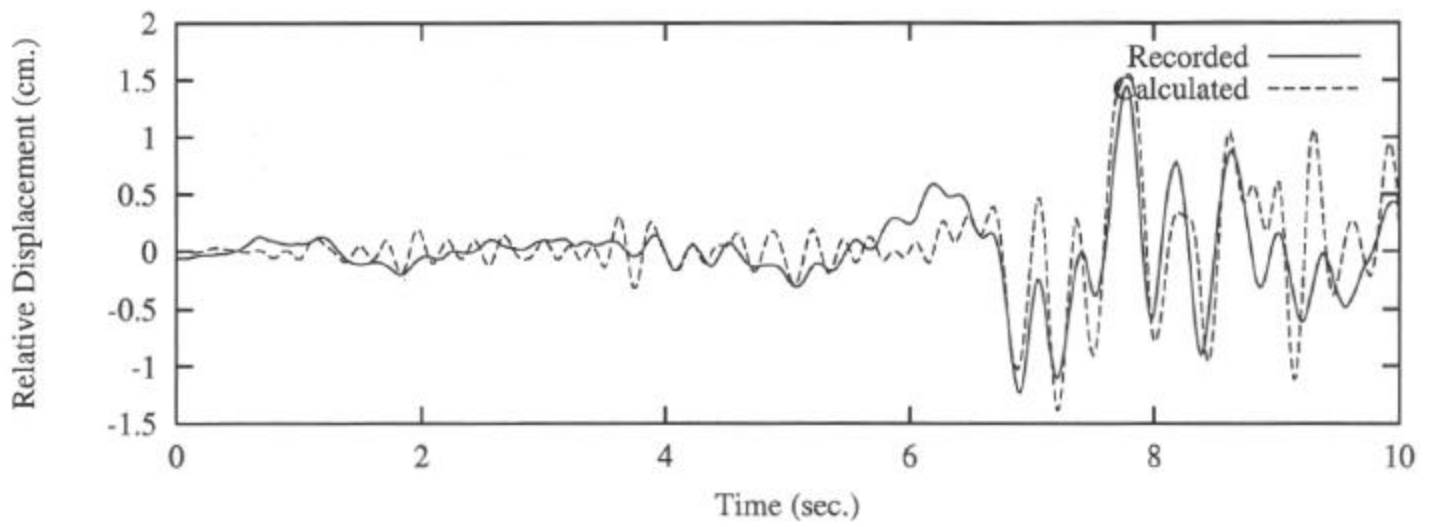
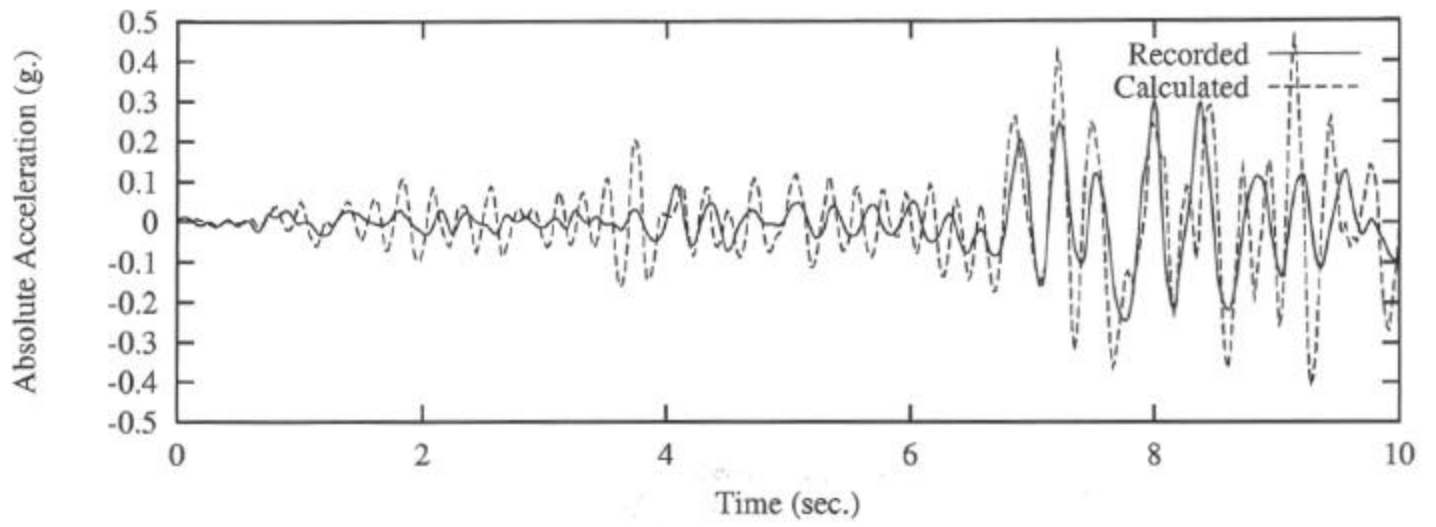


Figure 3.33 1992 Aftershock #2 on PSO (L= 7 m.), Soil-Slice Model

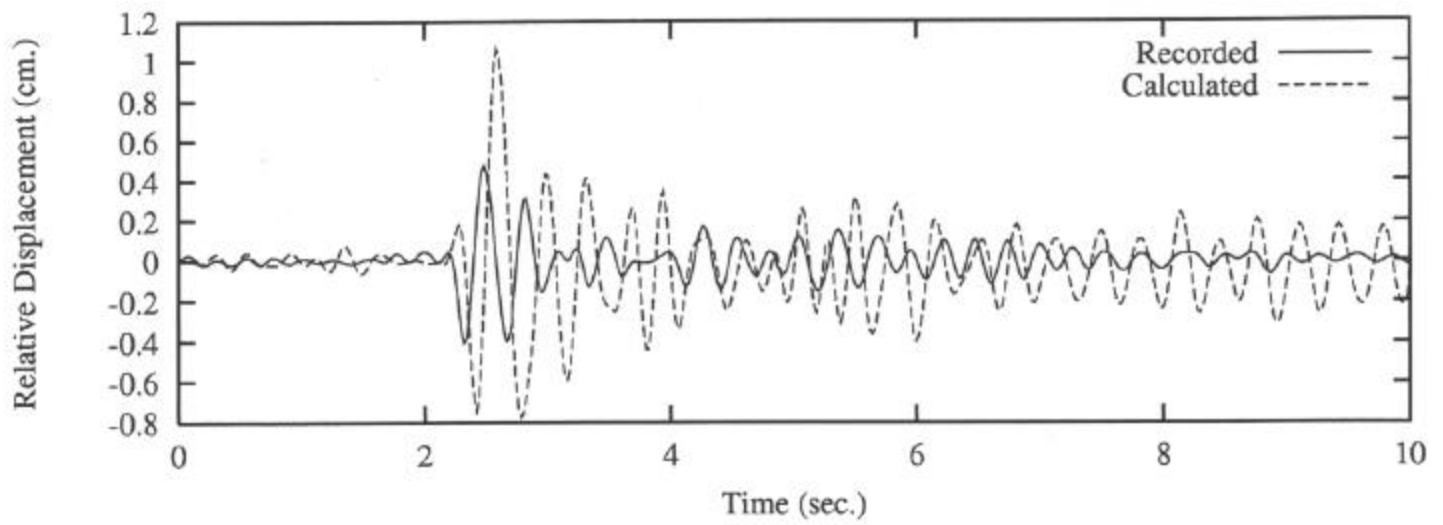
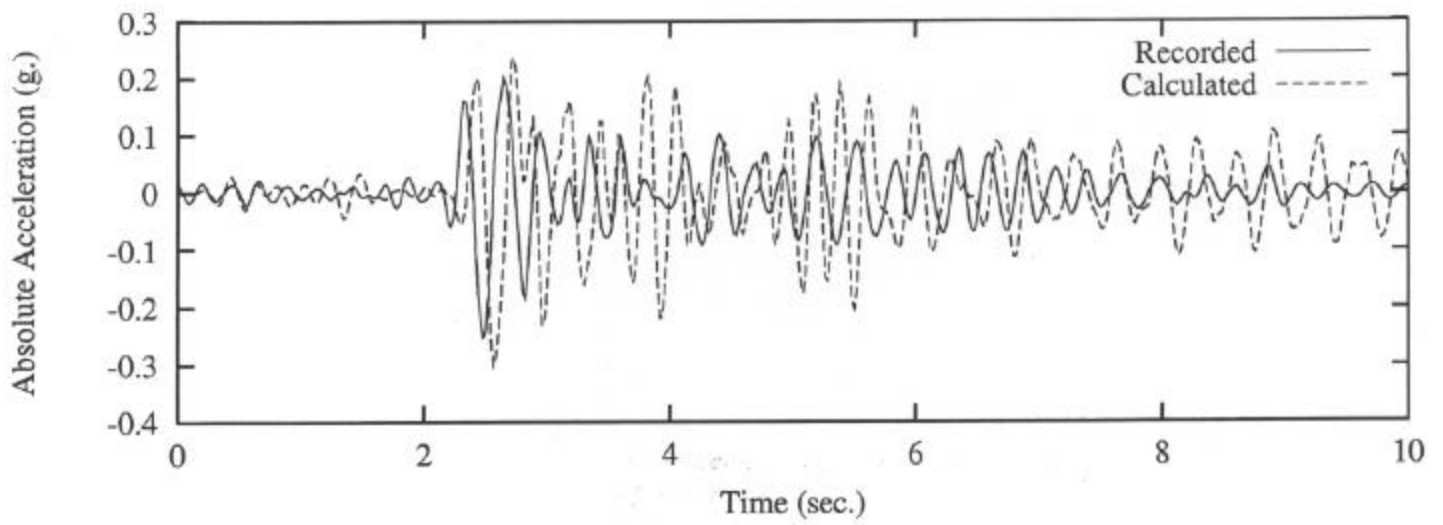


Figure 3.34 1986 Main Event on PSO (L= 4 m.), Soil-Slice Model

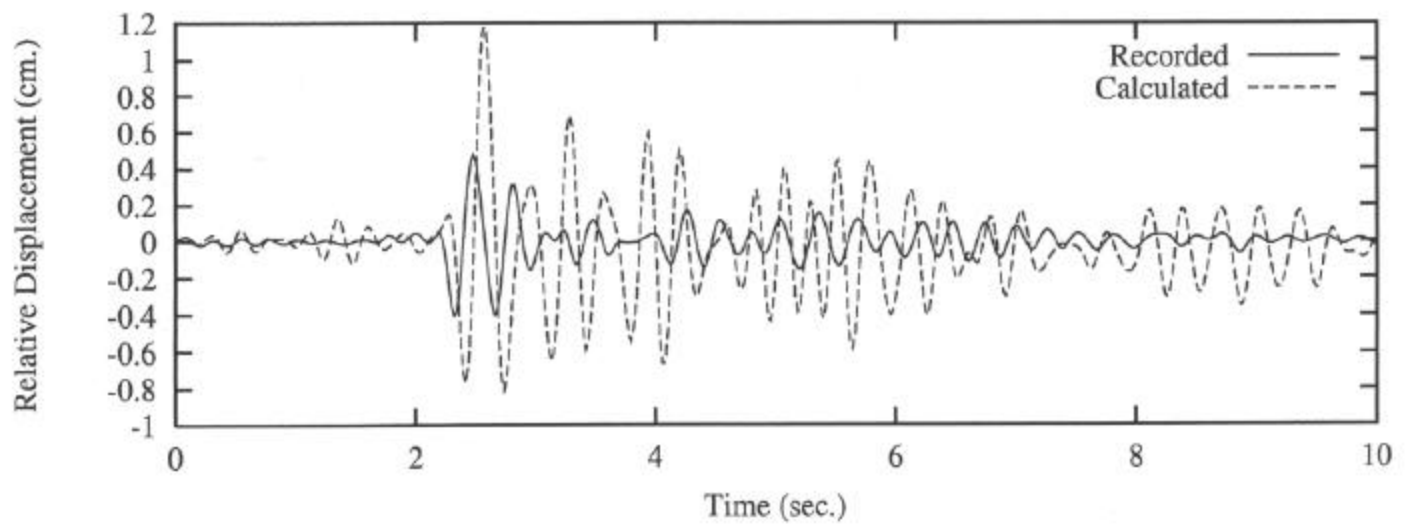
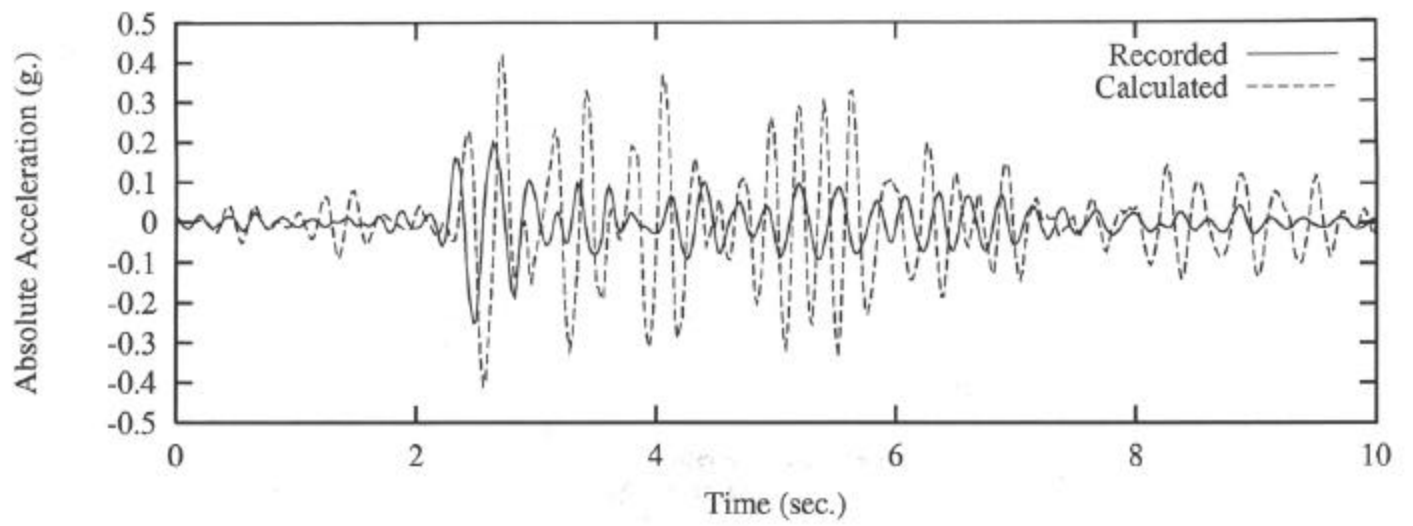


Figure 3.35 1986 Main Event on PSO (L= 9 m.), Soil-Slice Model

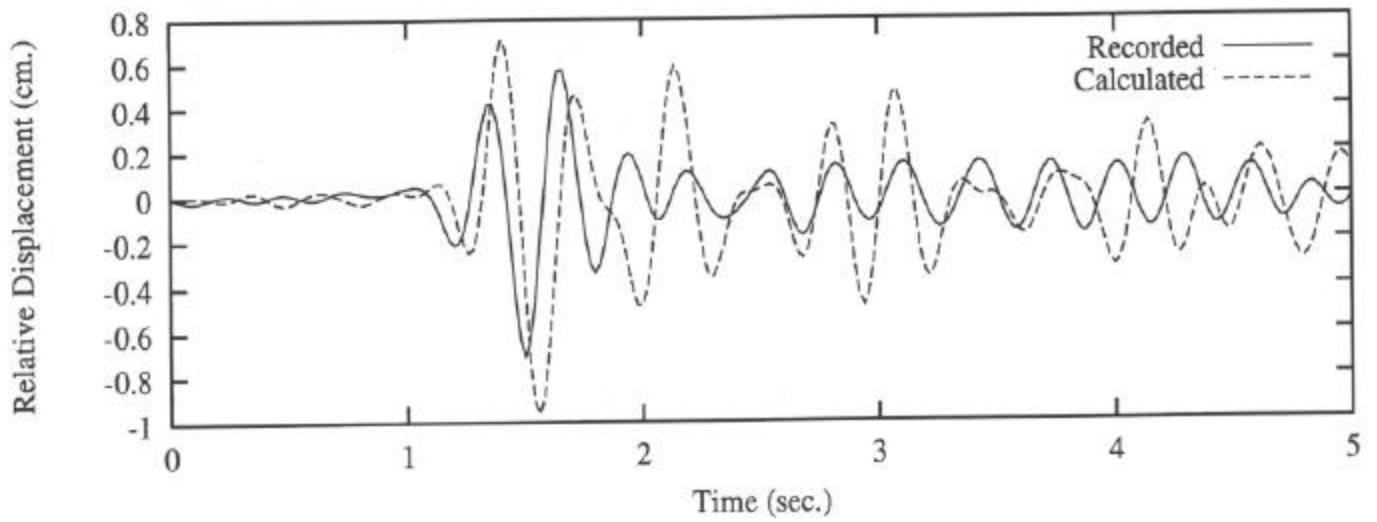
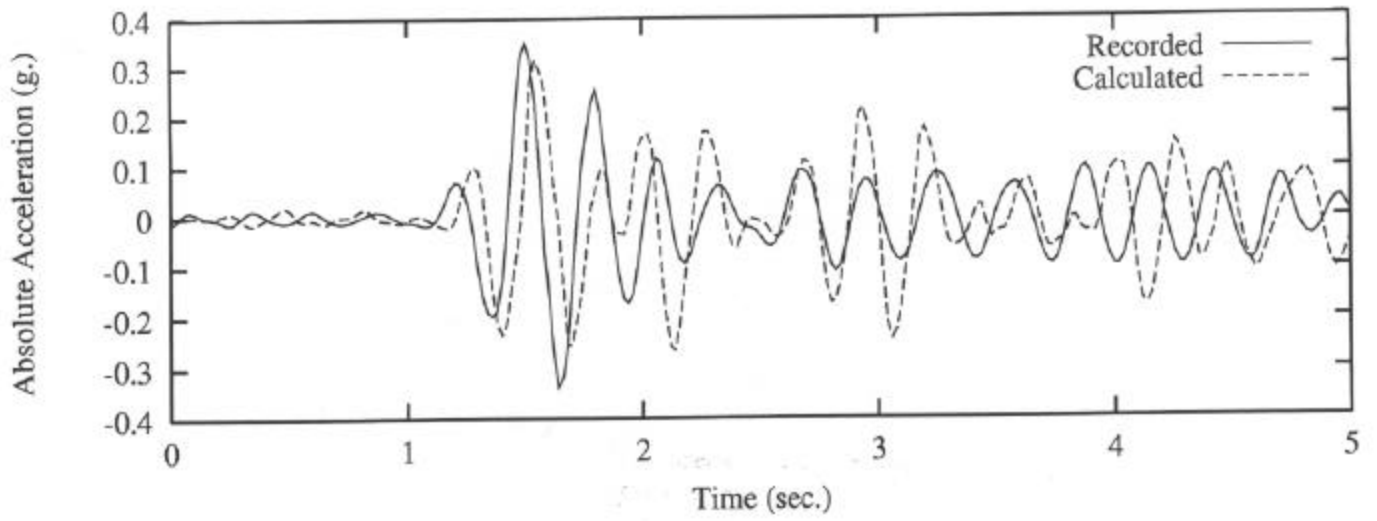


Figure 3.36 1986 Aftershock on PSO (L= 5 m.), Soil-Slice Model

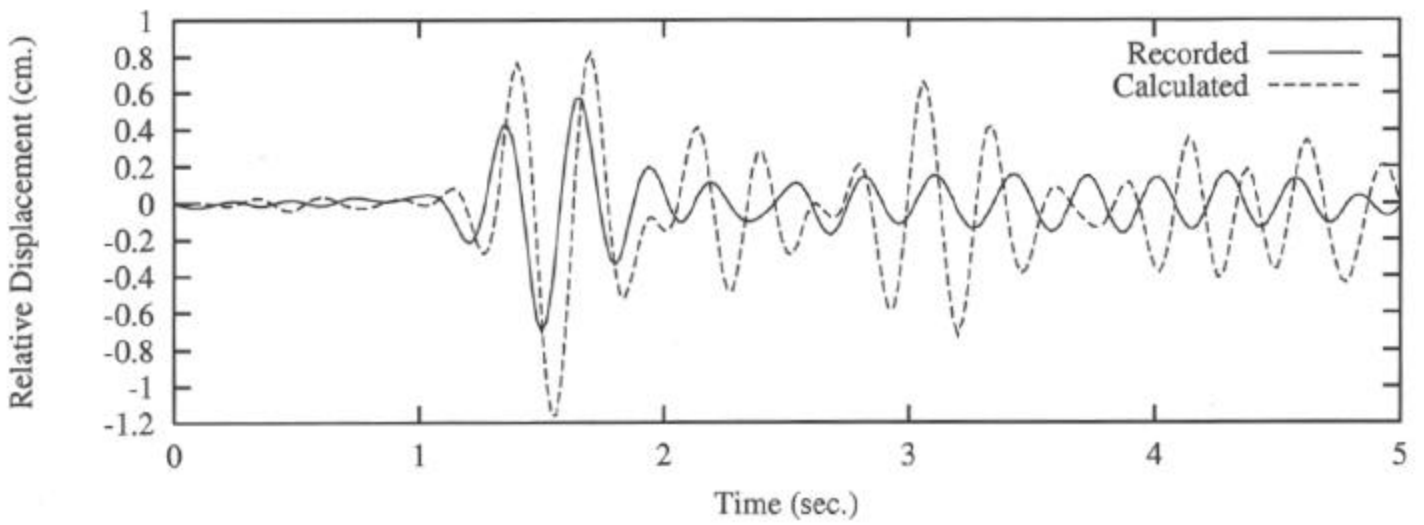
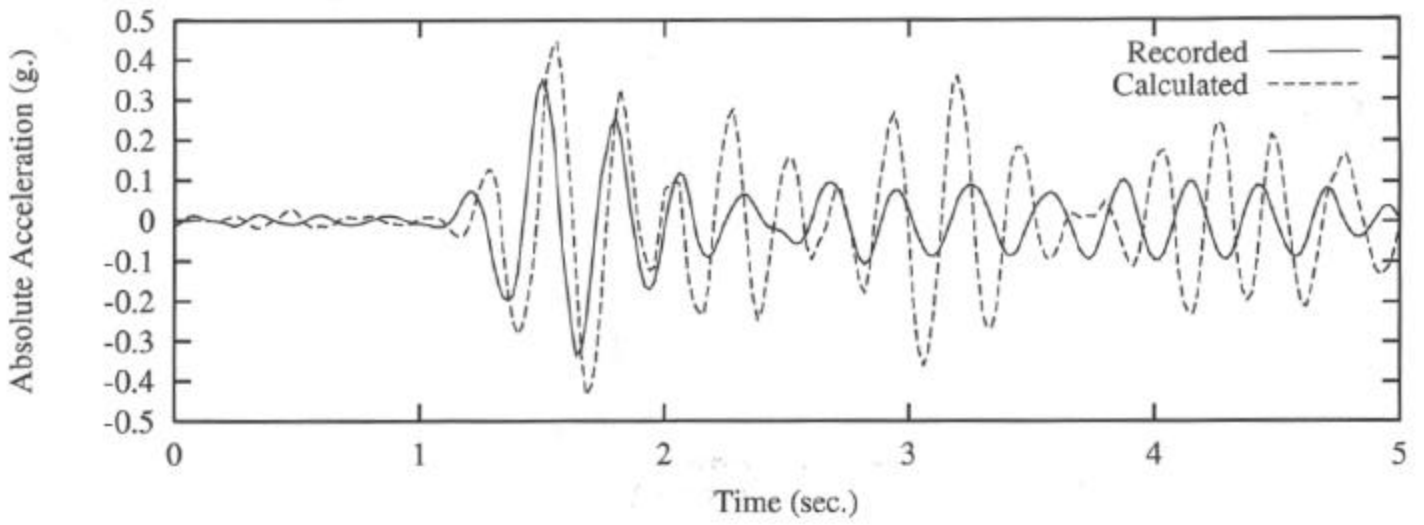


Figure 3.37 1986 Aftershock on PSO (L= 11 m.), Soil-Slice Model

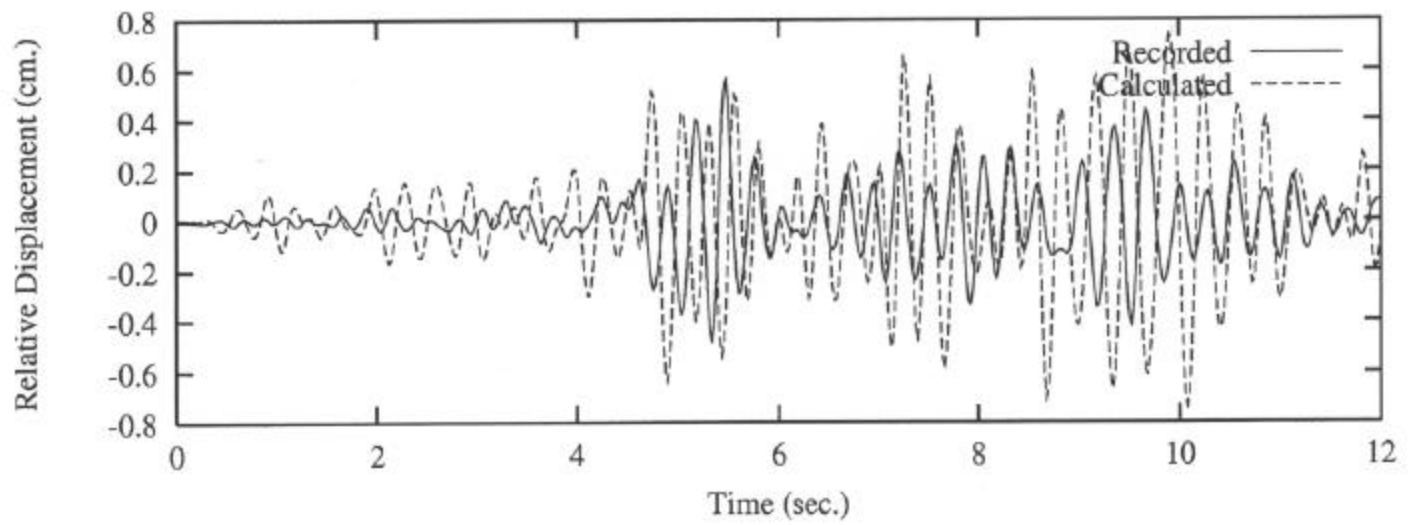
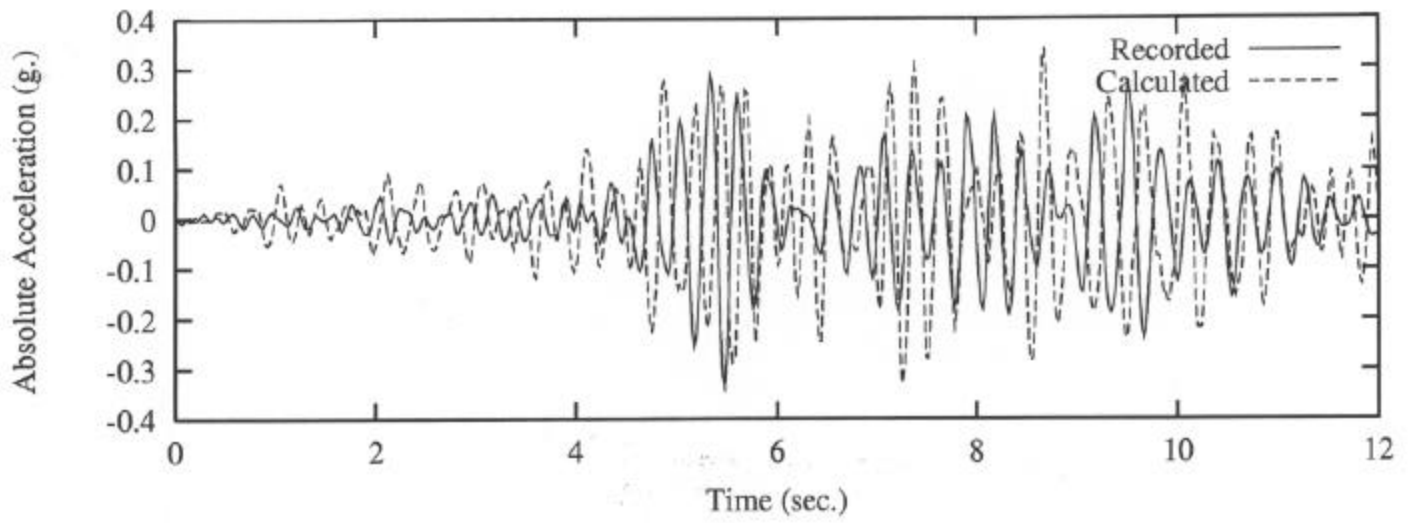


Figure 3.38 1987 Main Event on PSO (L= 6 m.), Soil-Slice Model



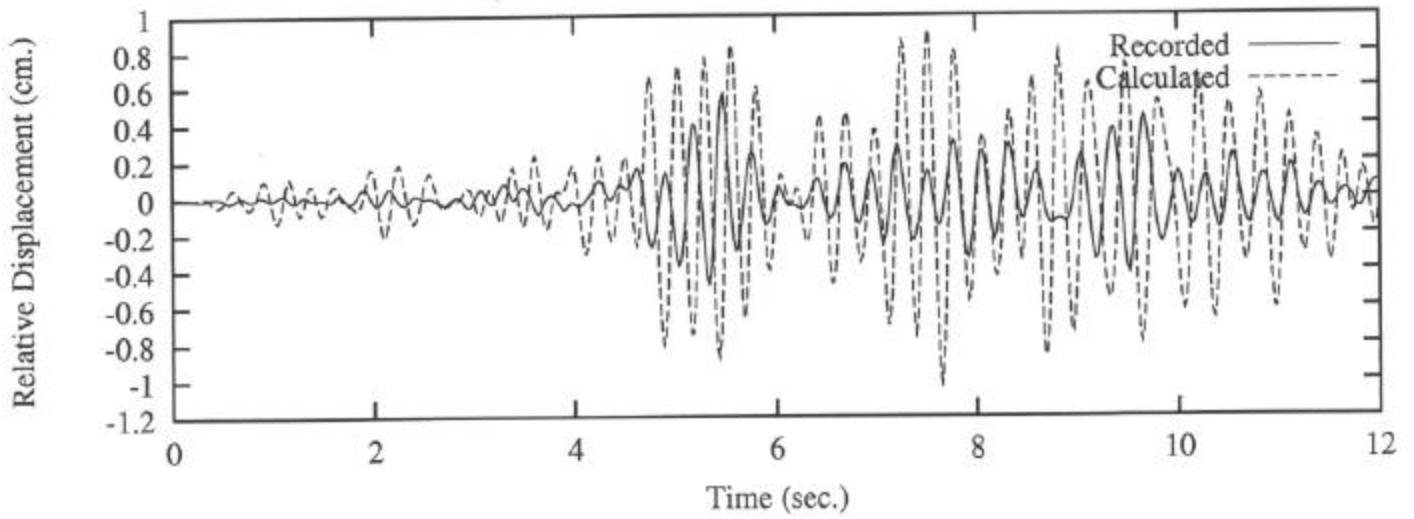
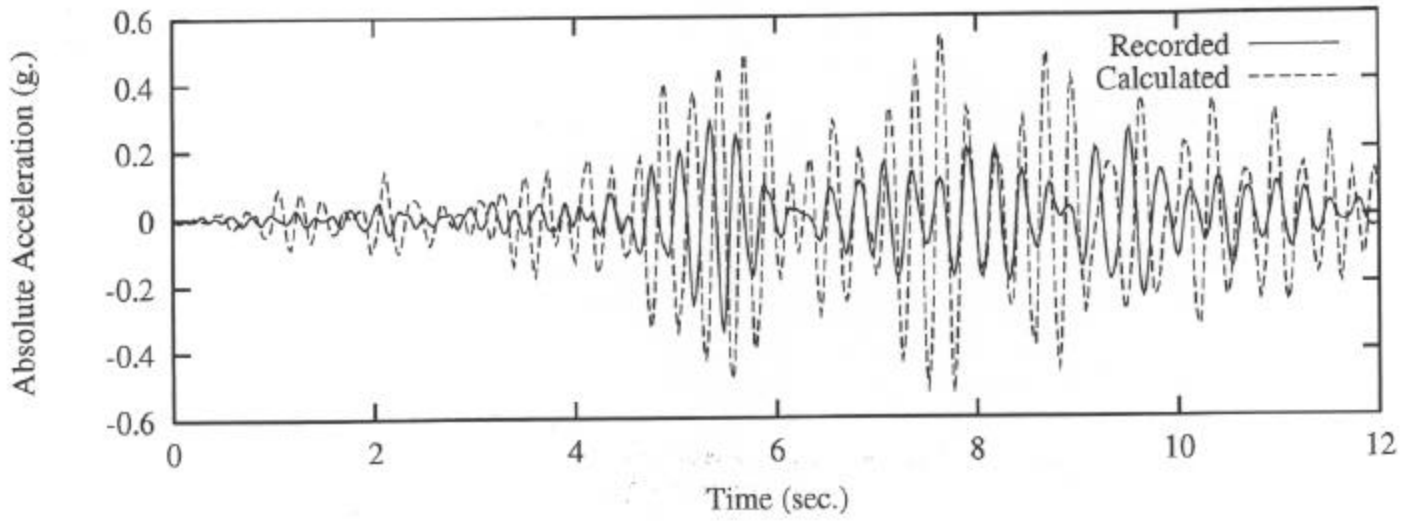


Figure 3.39 1987 Main Event on PSO (L= 13 m.), Soil-Slice Model

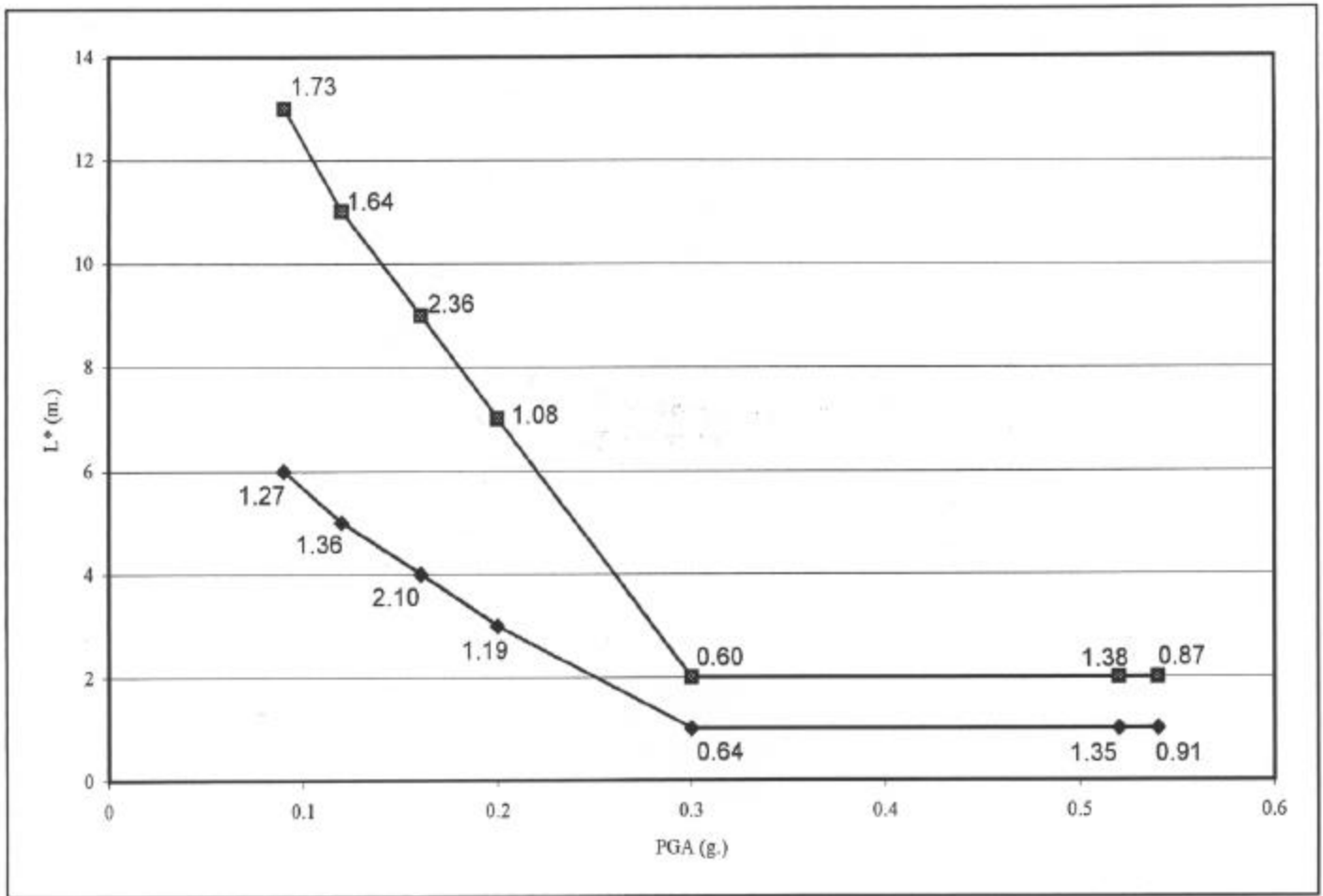


Figure 3.40 Ranges of Approach-Embankment Thickness ( $L^*$ ) for Soil-Slice Model Calibrated to MRO and PSO along with the Ratio Between the Calculated and the Recorded Peak Displacement at Pier.

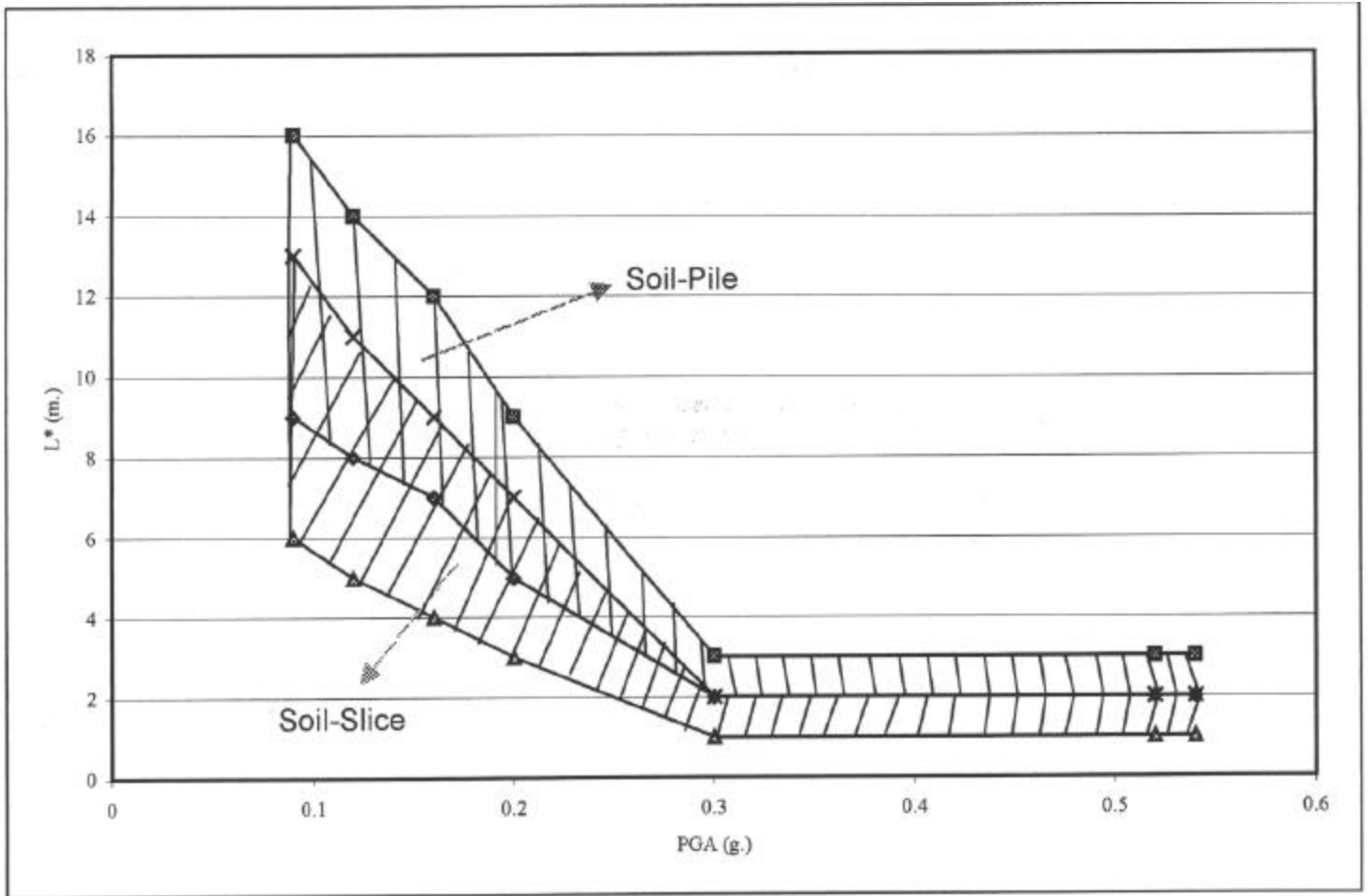


Figure 3.41 Ranges of Approach-Embankment Thickness ( $L^*$ ) for Soil-Pile and Soil-Slice Model Calibrated to MRO and PSO

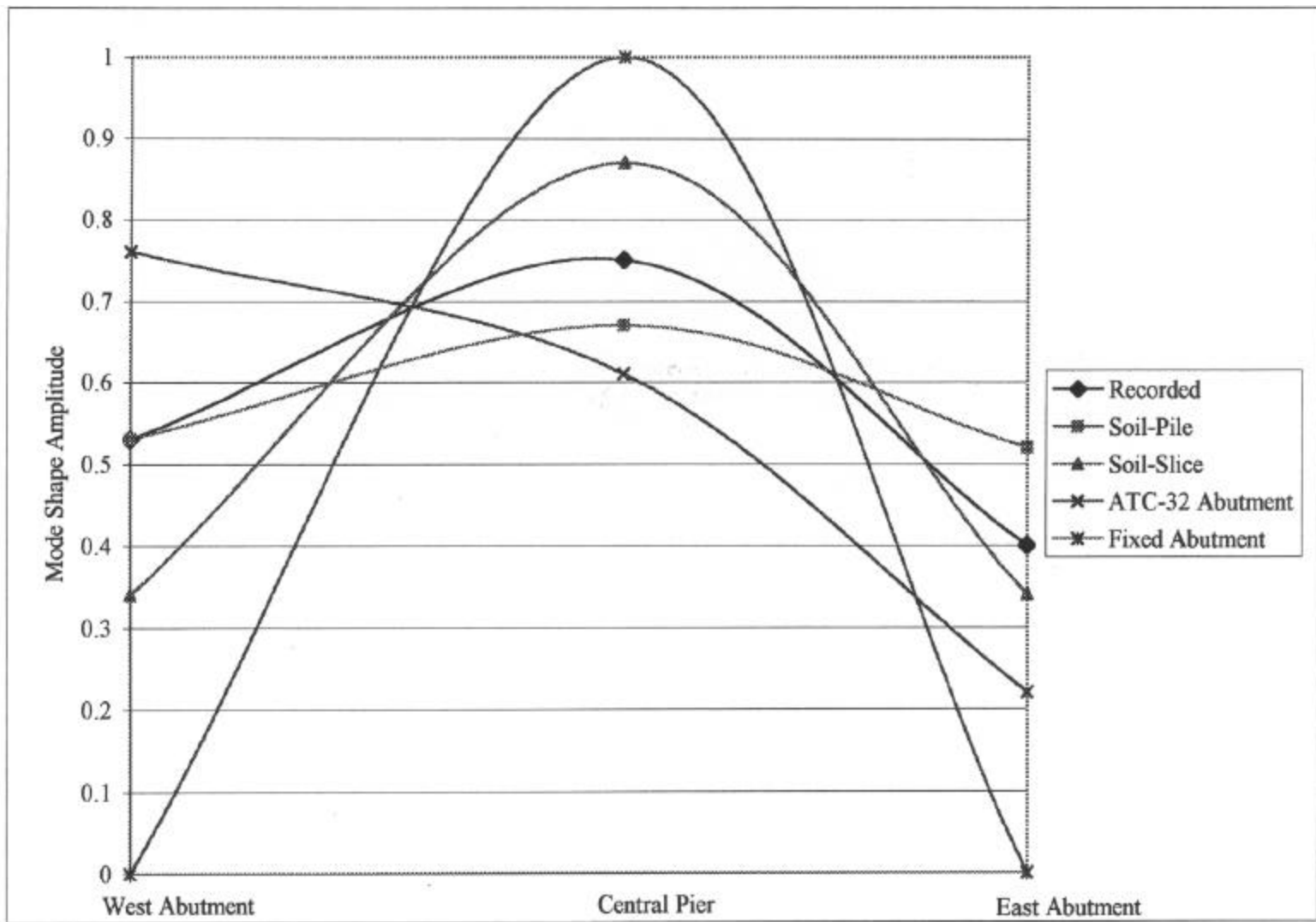


Figure 3.42 a) First PCA Mode Shape (PGA = 0.09 g.)

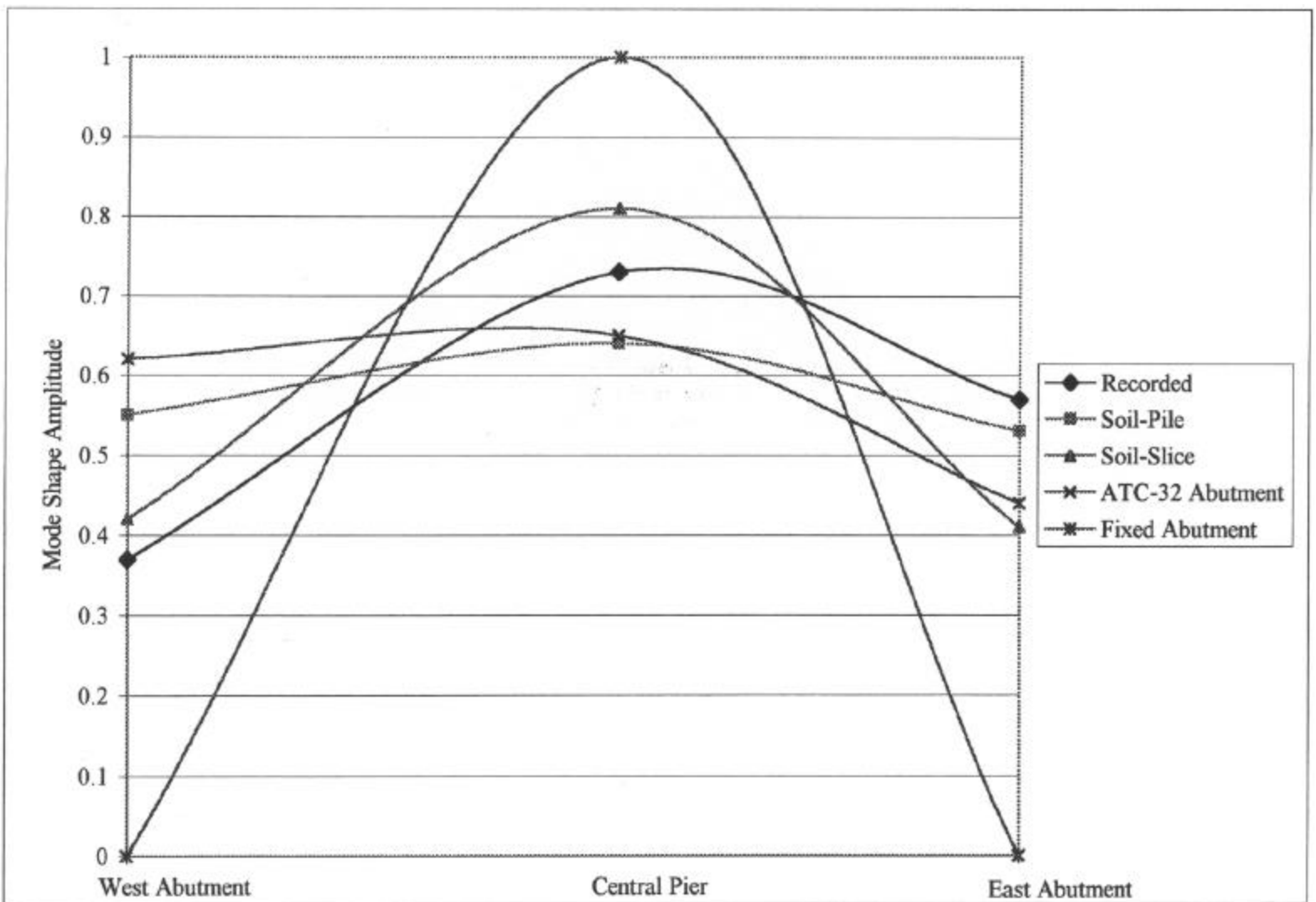


Figure 3.42 b) First PCA Mode Shape (PGA = 0.12 g.)

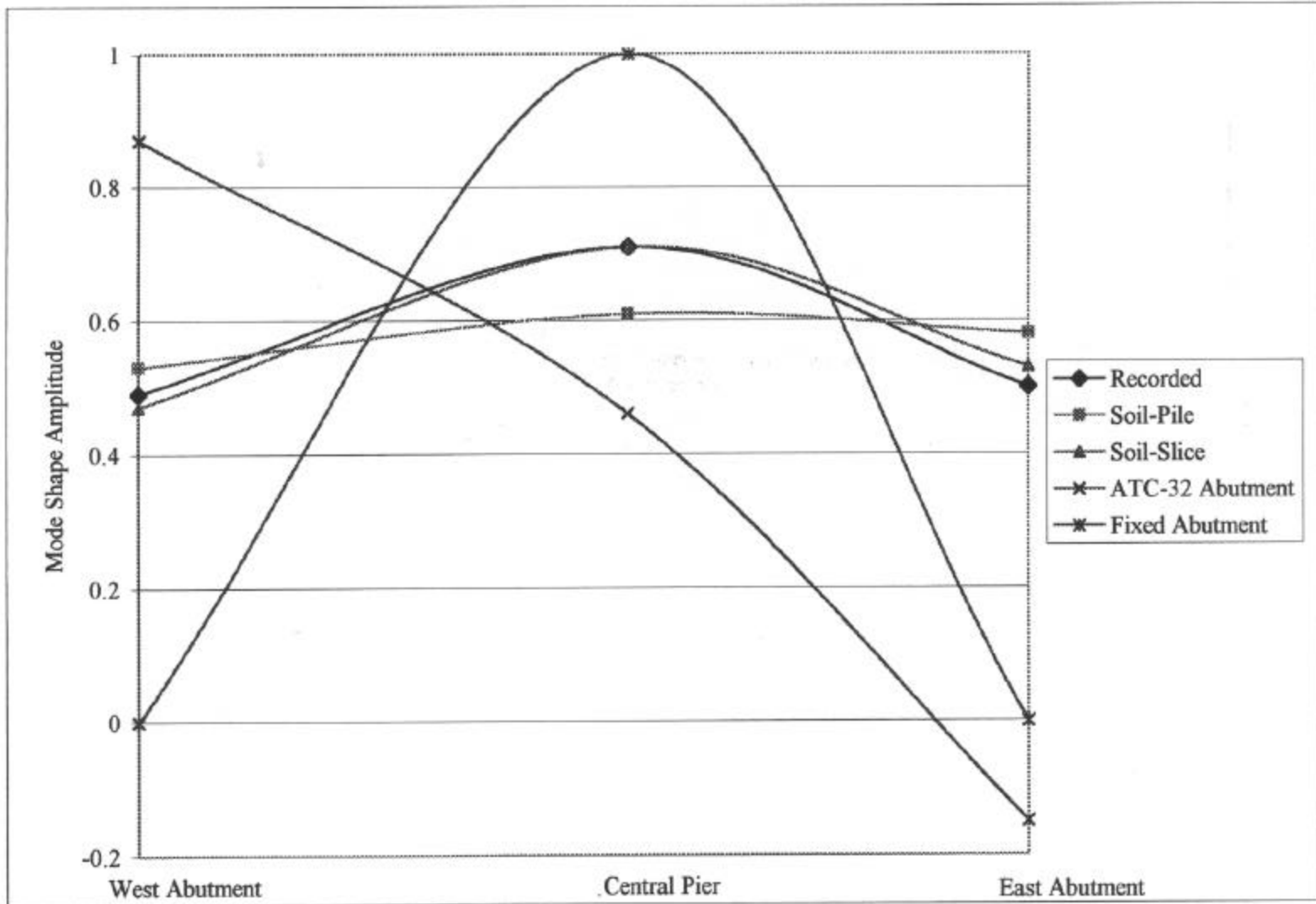


Figure 2.42 - First PCA Mode Shape (PCA = 0.16 %)

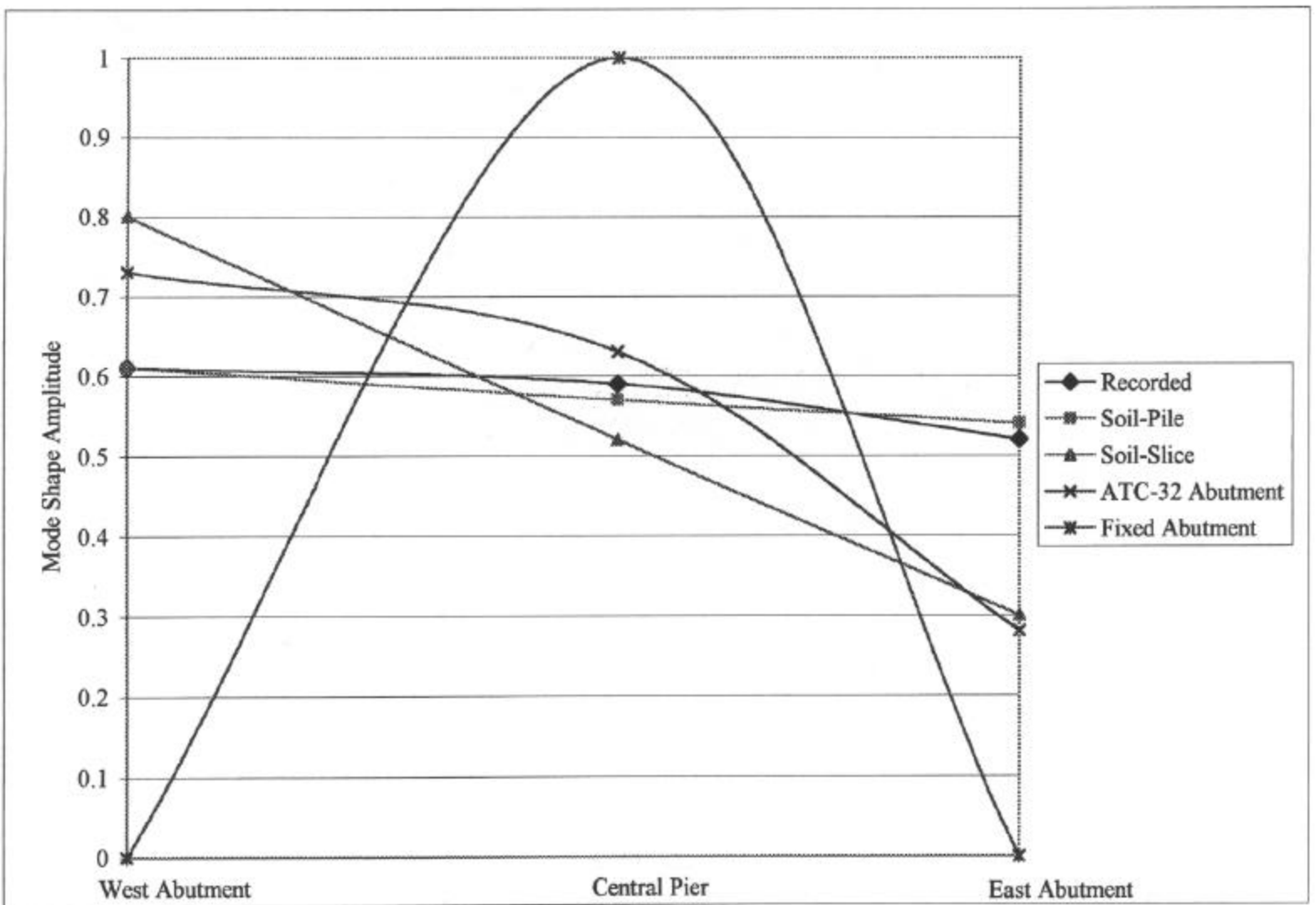


Figure 3.42 d) First PCA Mode Shape (PGA = 0.20 g.)

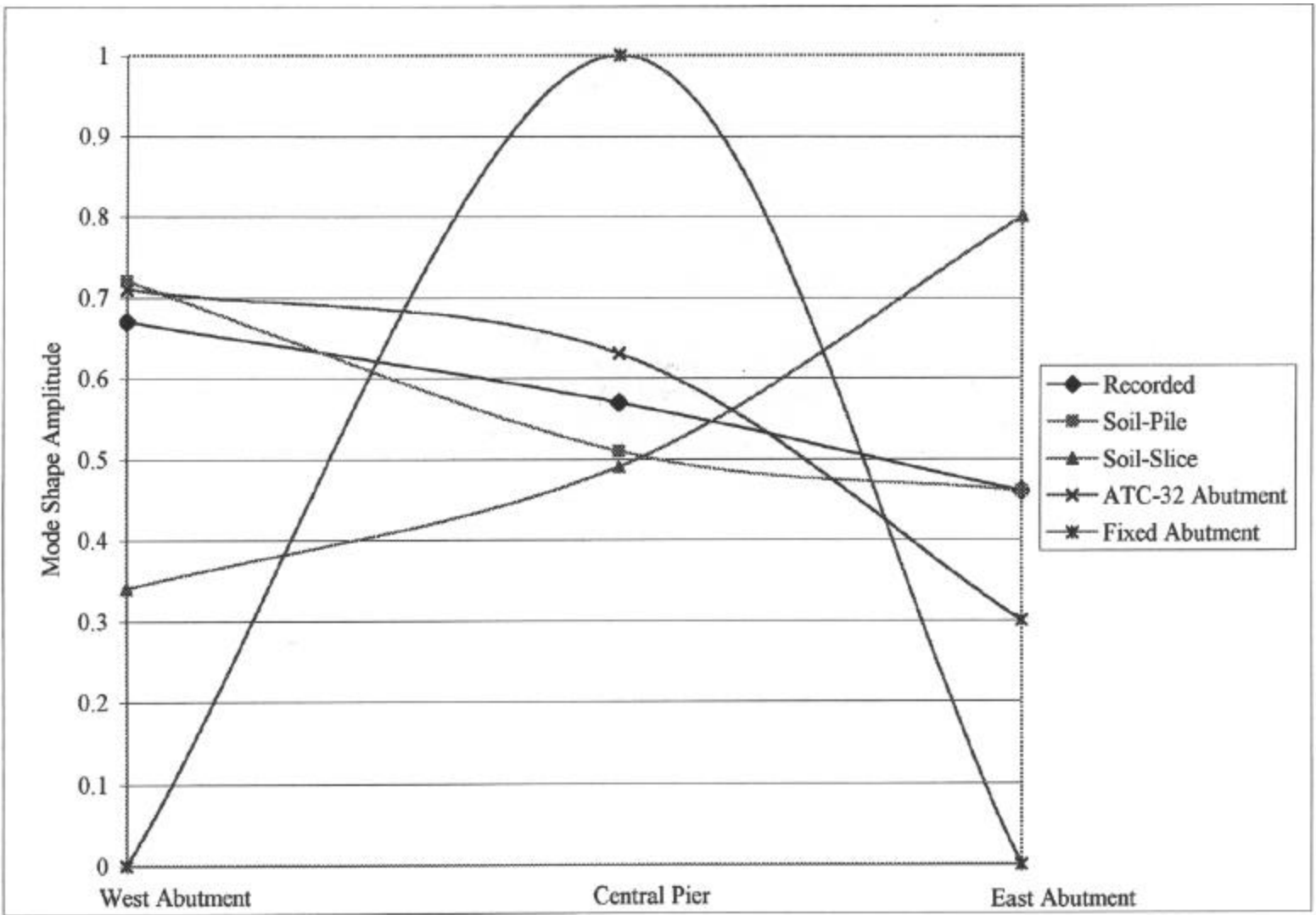


Figure 3.42 e) First PCA Mode Shape (PGA = 0.52 g.)



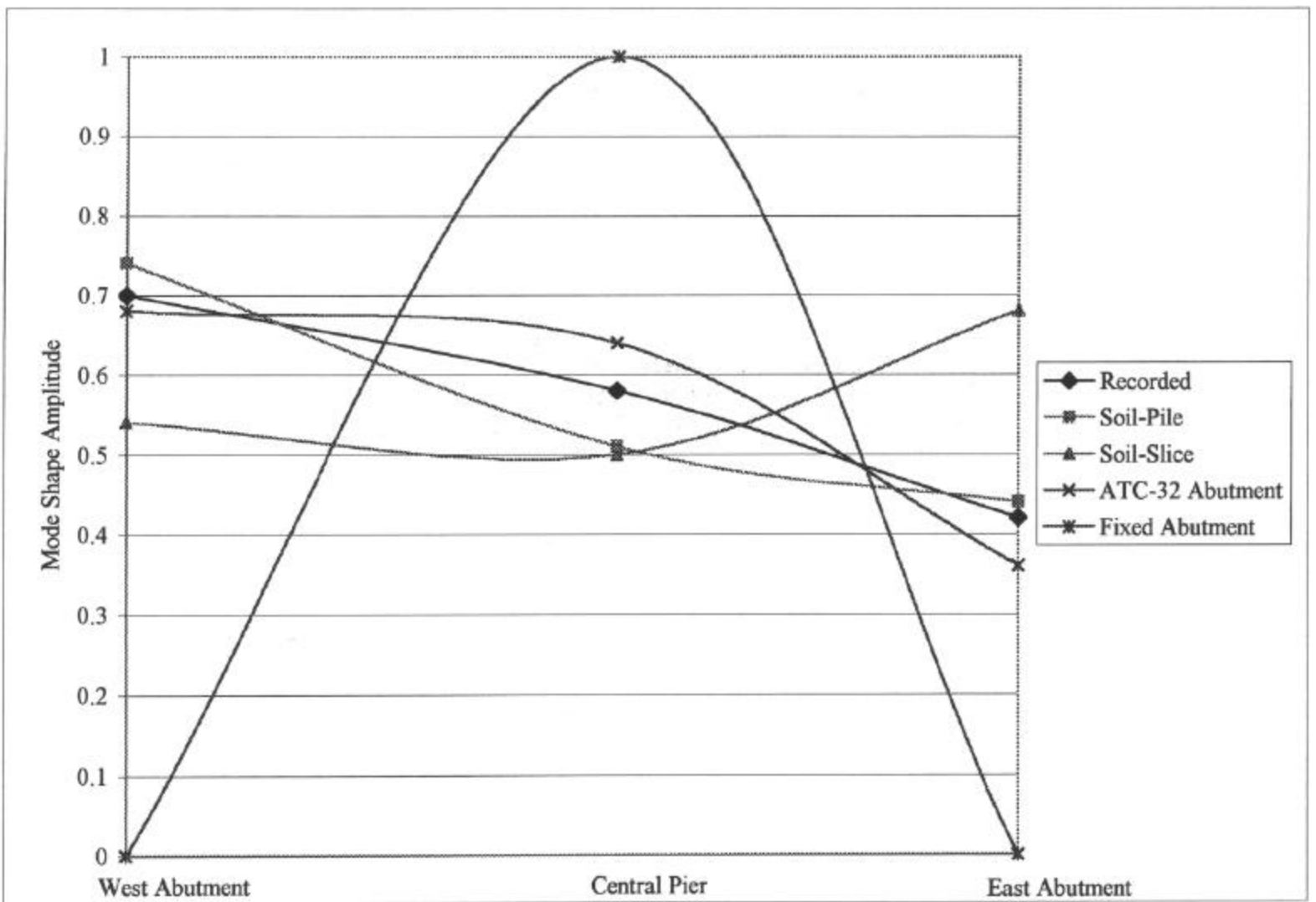


Figure 3.42 f) First PCA Mode Shape (PGA = 0.54 g.)

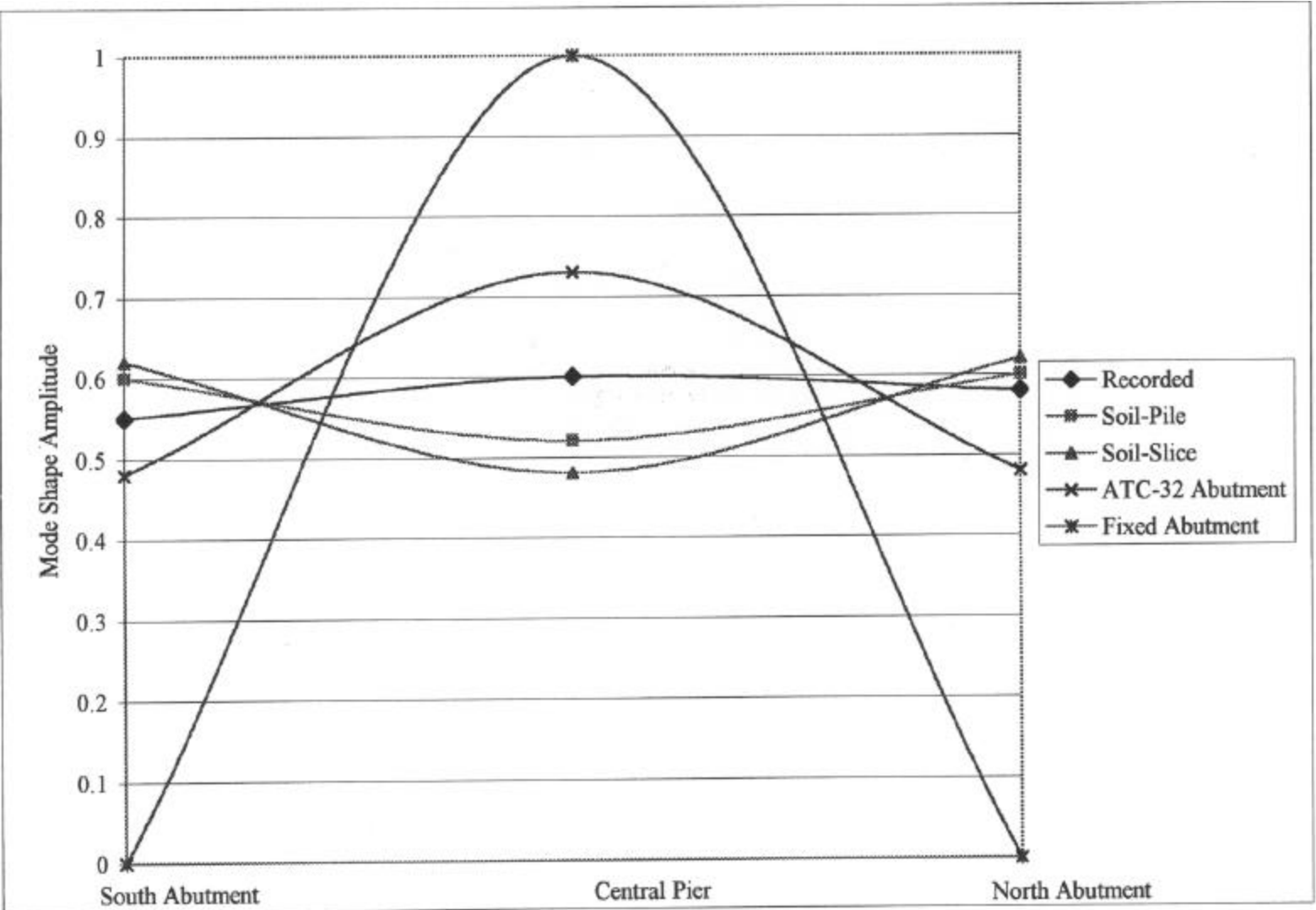


Figure 3.43 First PCA Mode Shape (PGA = 0.30 g.)

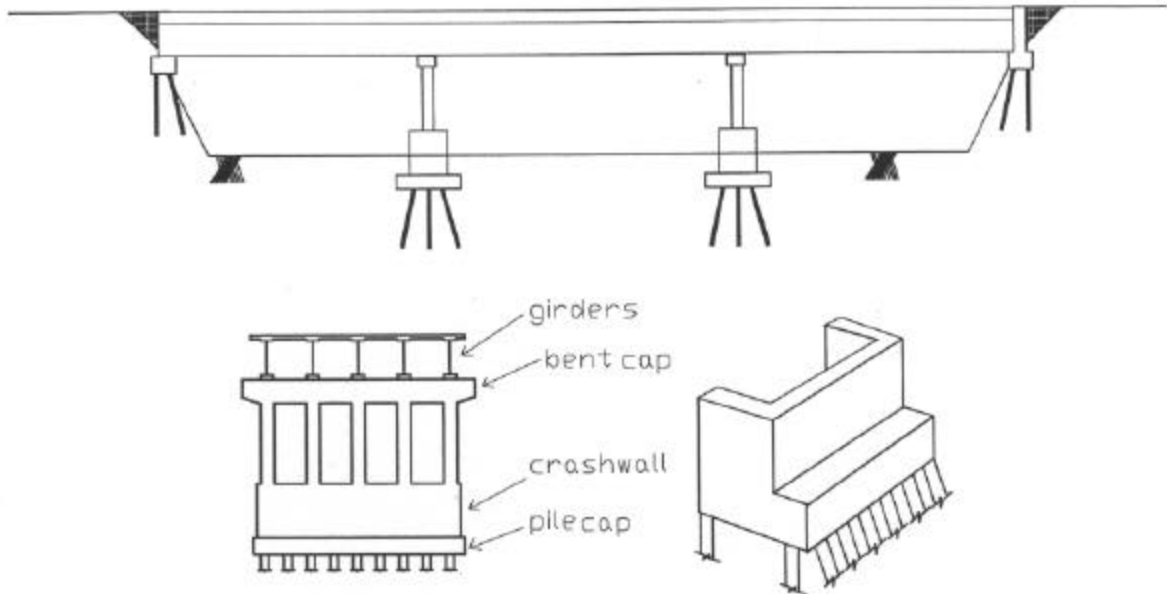


Figure 3.44 A Typical Illinois Bridge

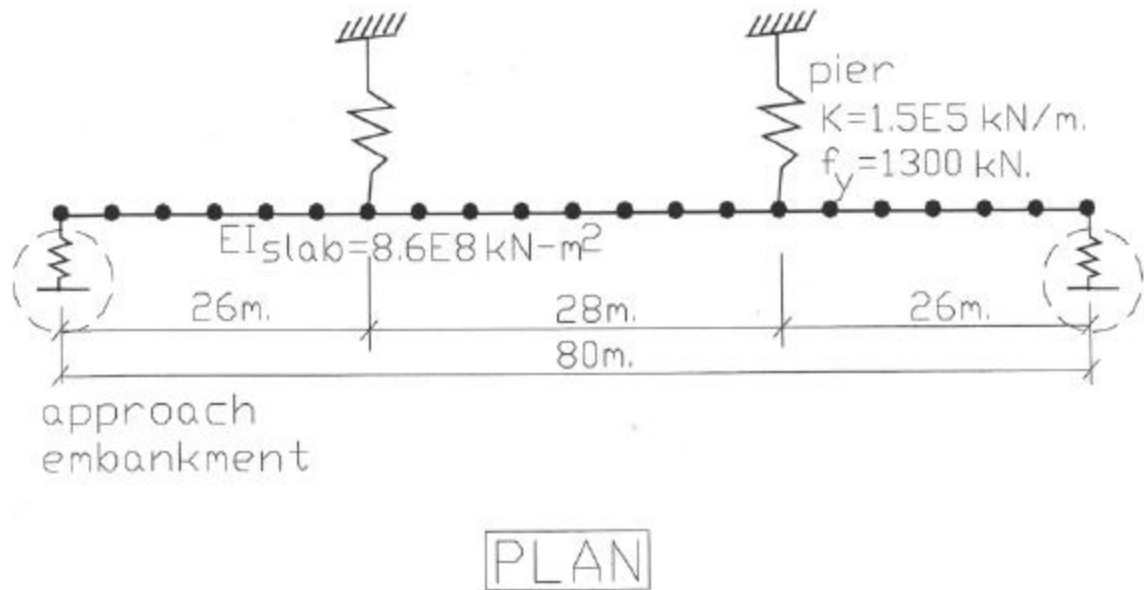


Figure 3.45 Analytical Model of an Illinois Bridge

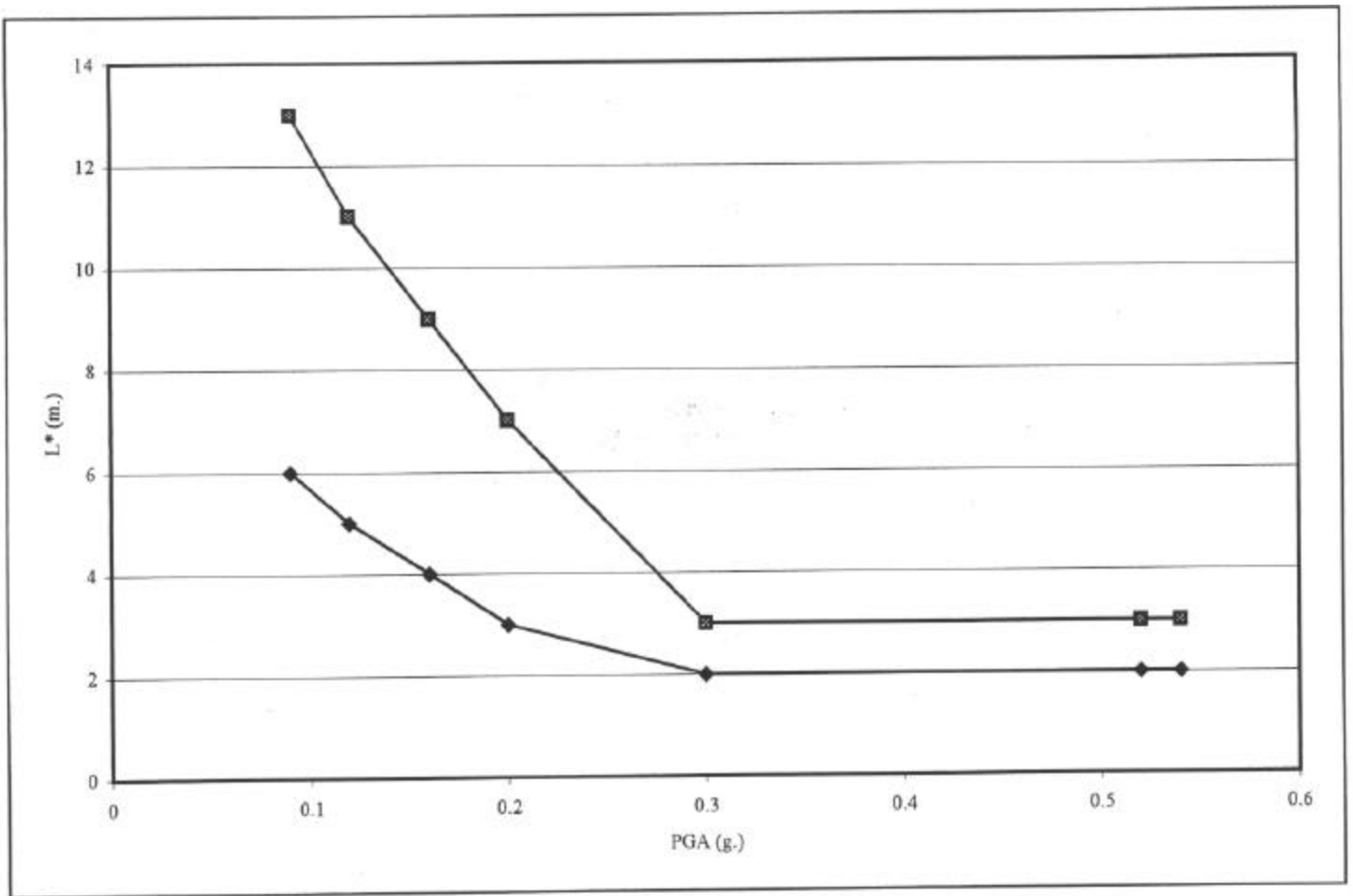


Figure 3.46 Ranges of Approach-Embankment Thickness ( $L^*$ ) for Soil-Slice Model for Illinois Bridges

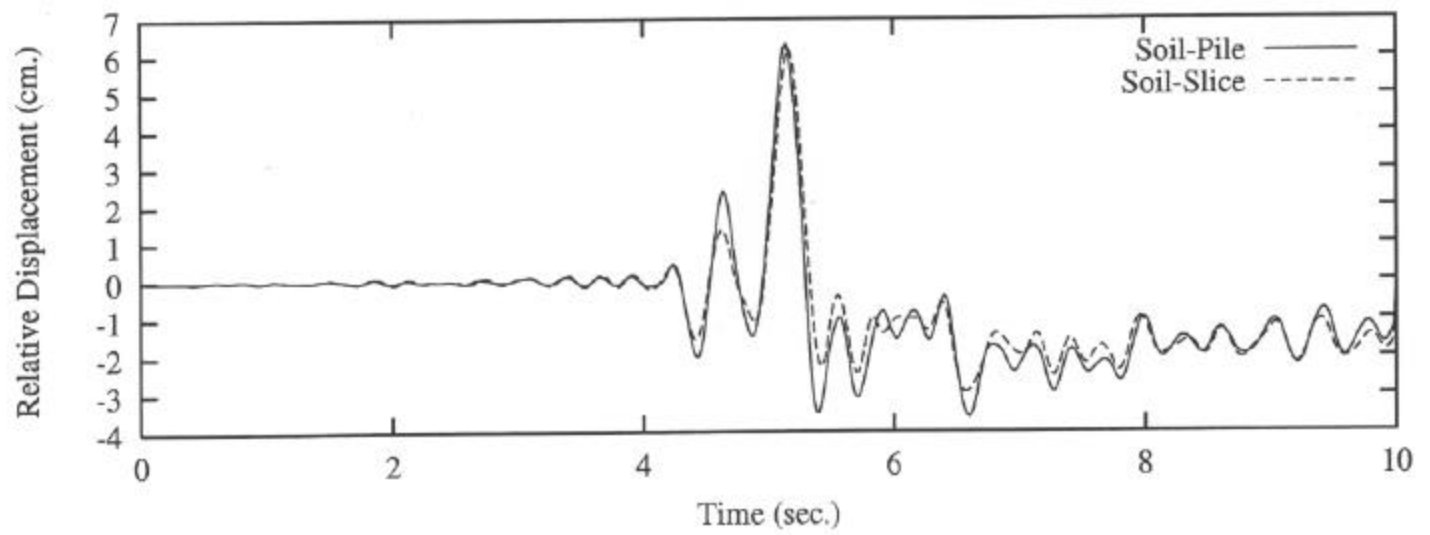
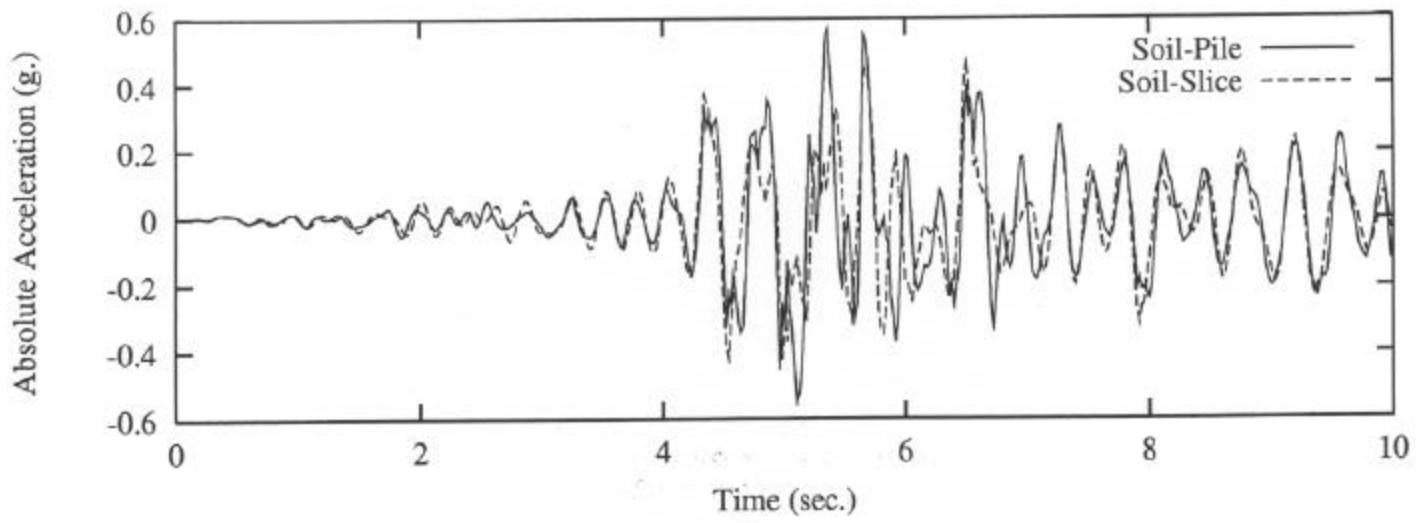


Figure 3.47 1992 Main Event on IL-1, L= 2 m. (Soil-Slice Model), L= 2 m. (Soil-Pile Model)

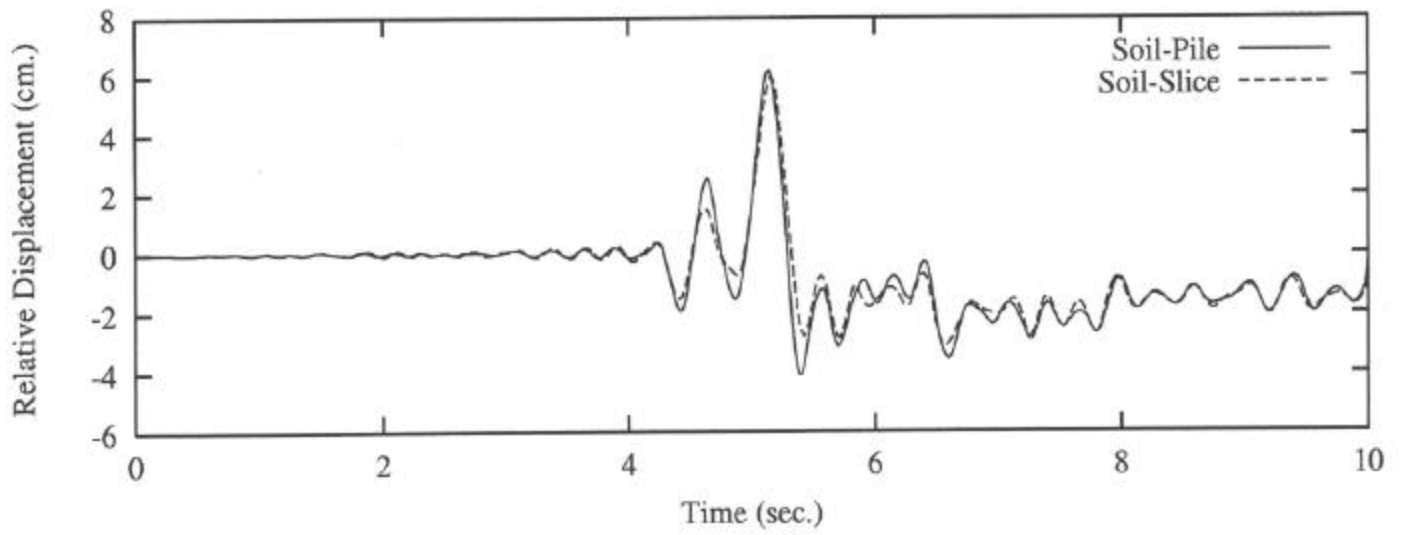
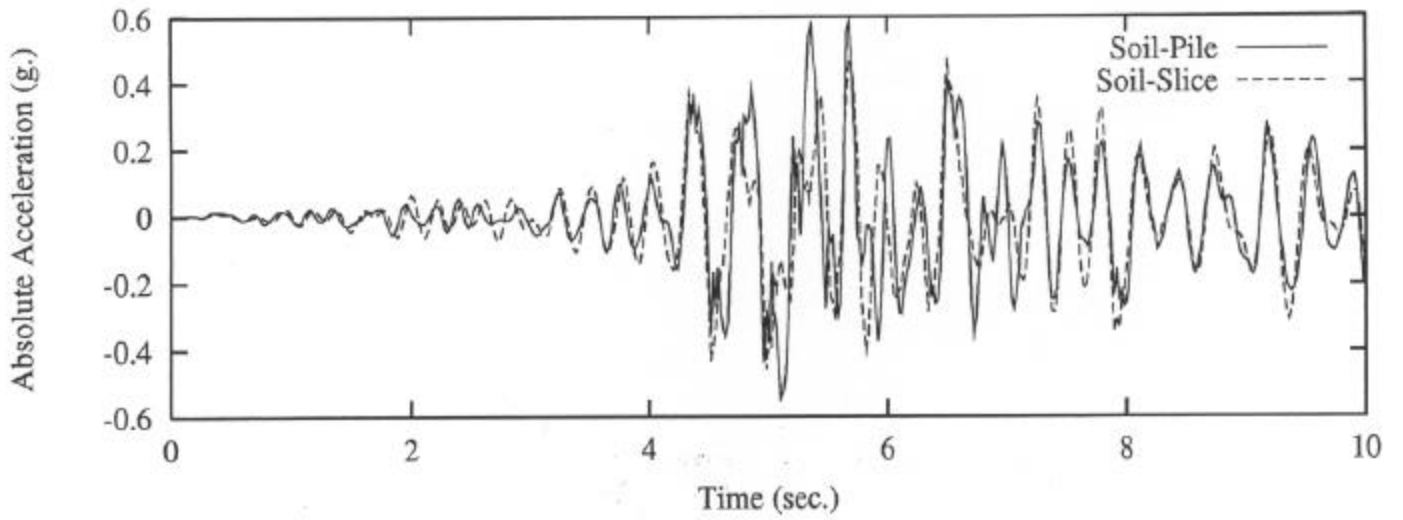


Figure 3.48 1992 Main Event on IL-1, L= 3 m. (Soil-Slice Model), L= 3 m. (Soil-Pile Model)

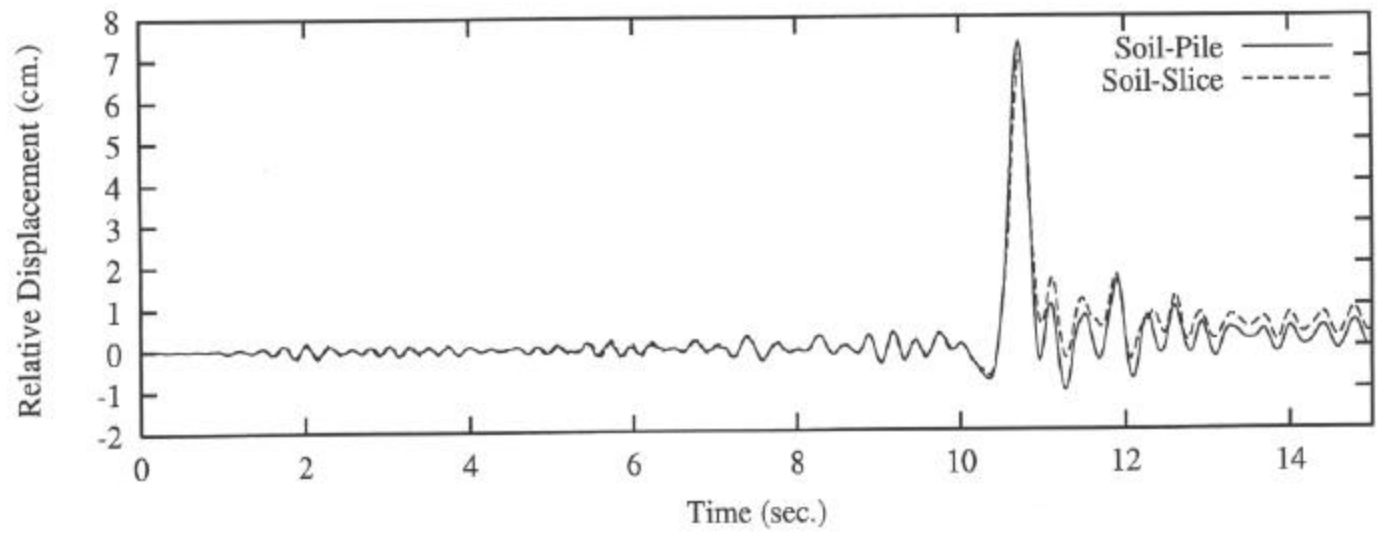
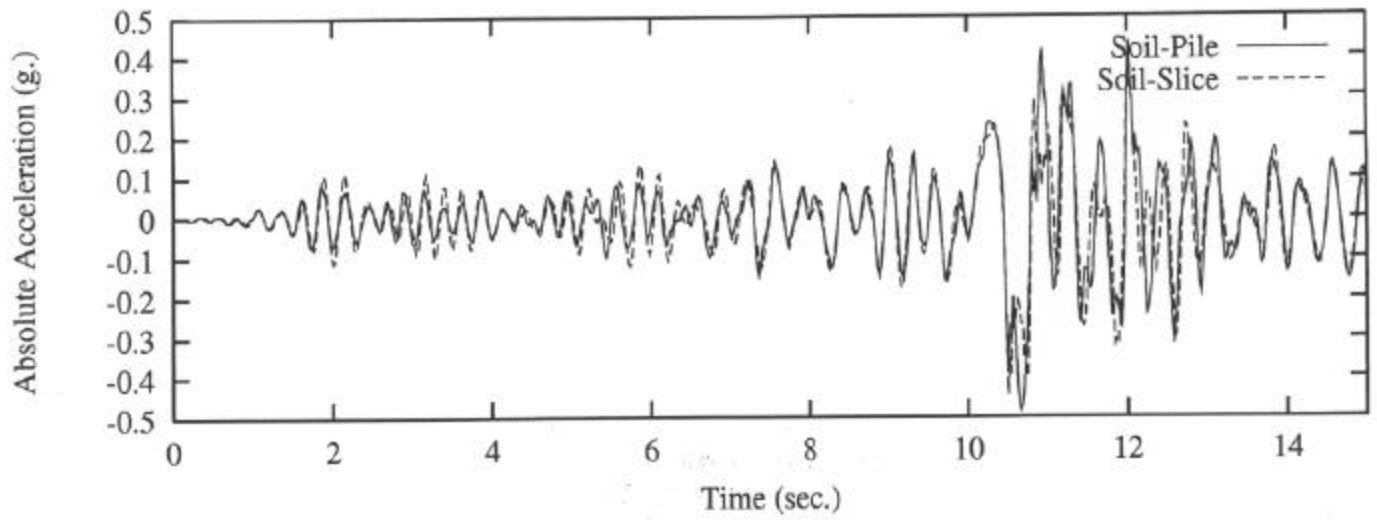


Figure 3.49 1992 Aftershock #1 on IL-1, L= 2 m. (Soil-Slice Model), L= 2 m. (Soil-Pile Model)

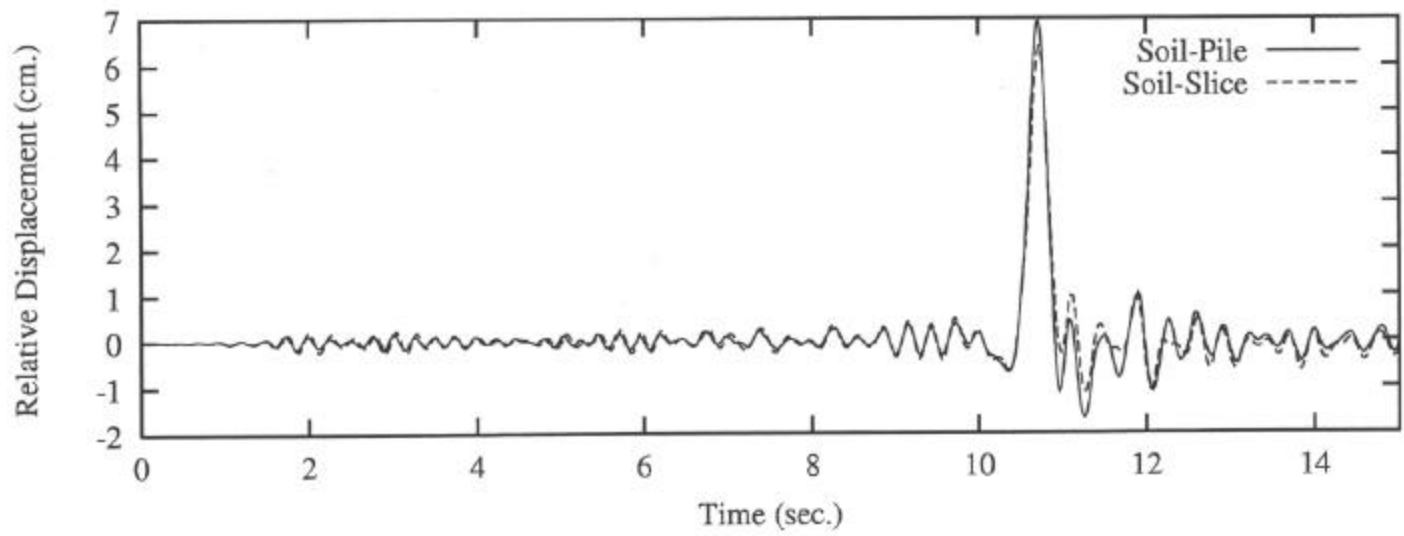
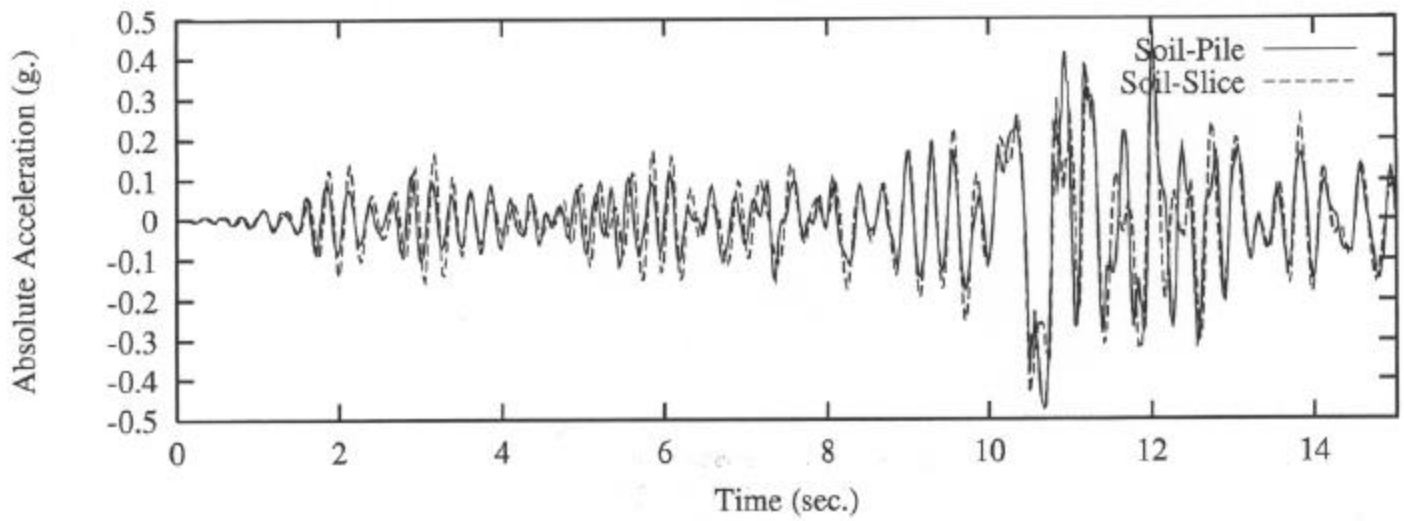


Figure 3.50 1992 Aftershock #1 on IL-1, L= 3 m. (Soil-Slice Model), L= 3 m. (Soil-Pile Model)



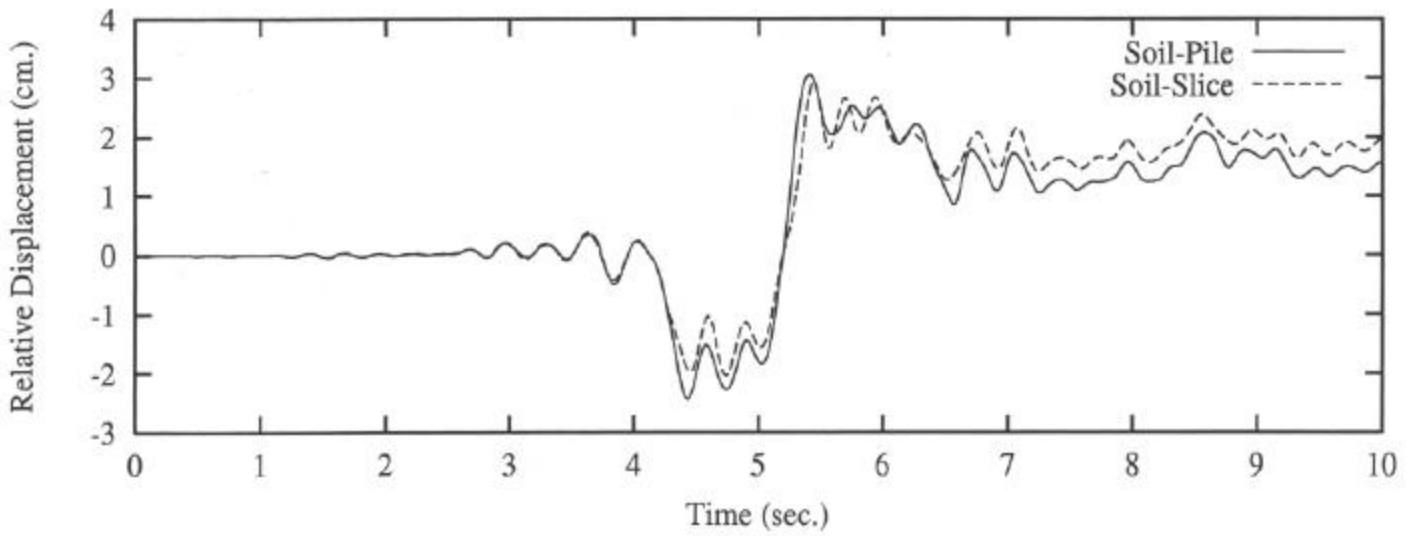
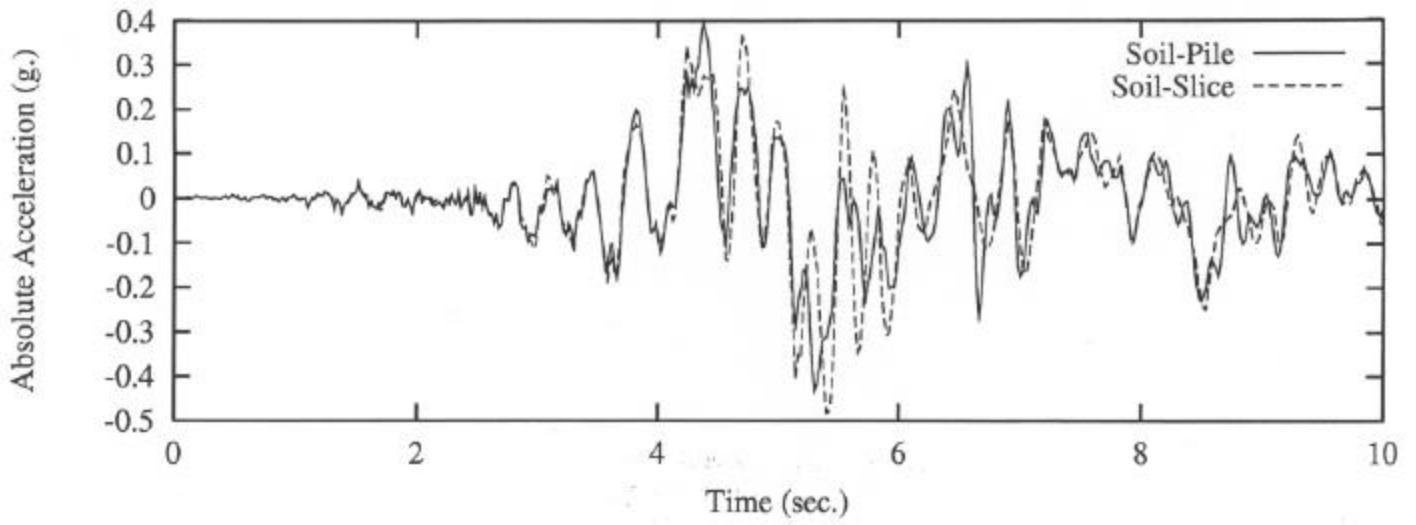


Figure 3.51 1979 Imperial Valley Earthquake on IL-1, L= 2 m. (Soil-Slice Model), L= 2 m. (Soil-Pile Model)

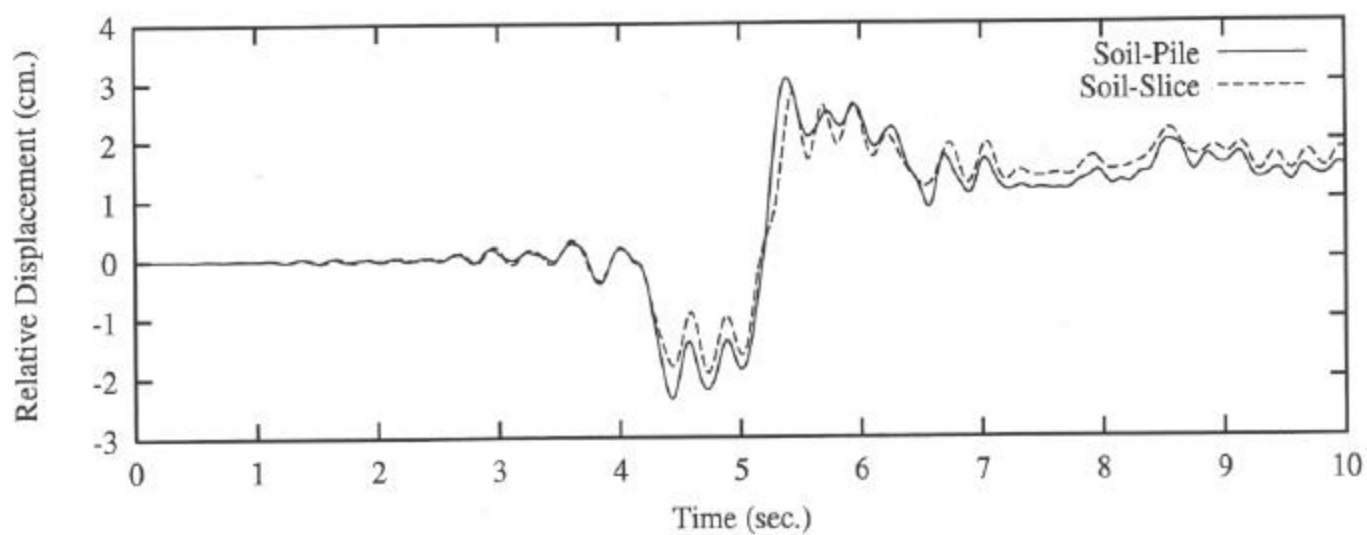
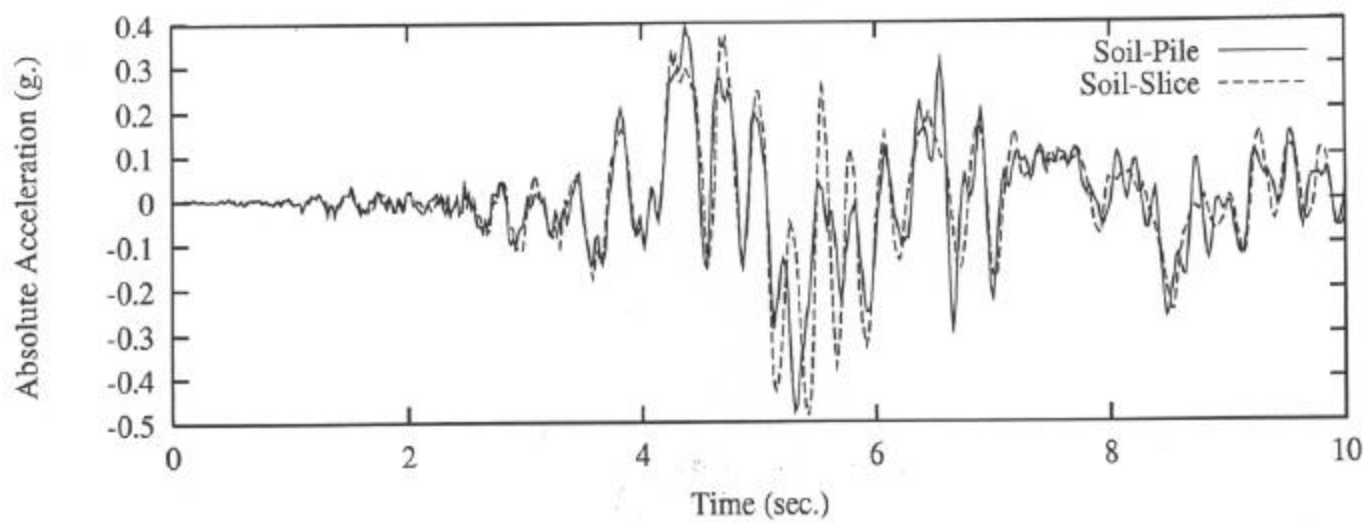


Figure 3.52 1979 Imperial Valley Earthquake on IL-1, L= 3 m. (Soil-Slice Model), L= 3 m. (Soil-Pile Model)

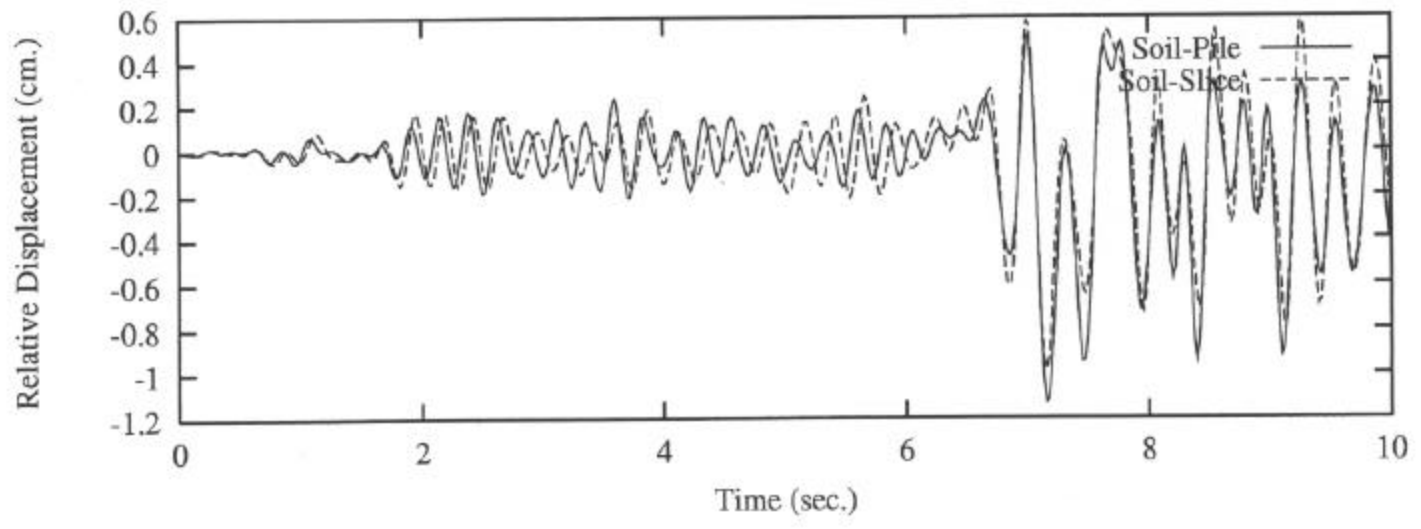
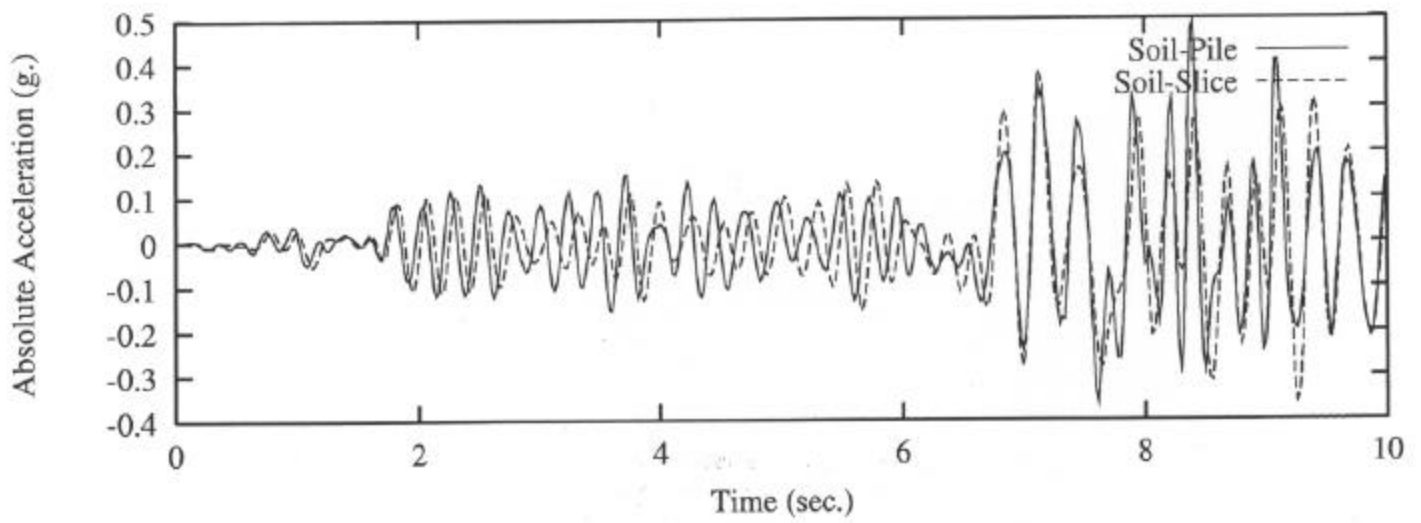


Figure 3.53 1992 Aftershock #2 on IL-1, L= 3 m. (Soil-Slice Model), L= 5 m. (Soil-Pile Model)

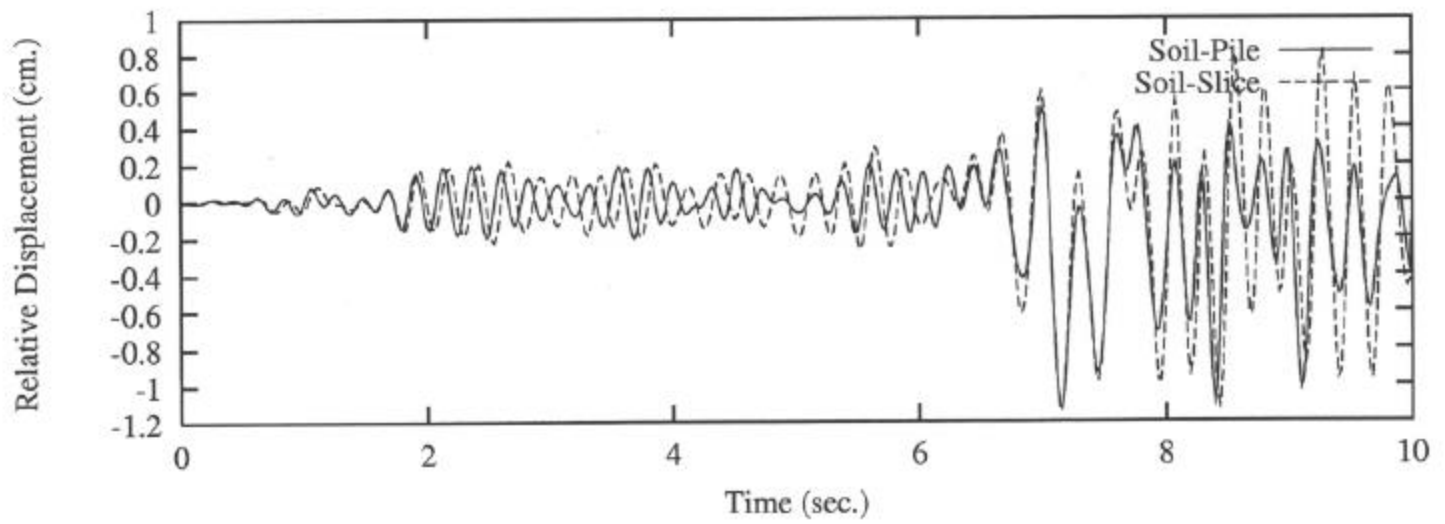
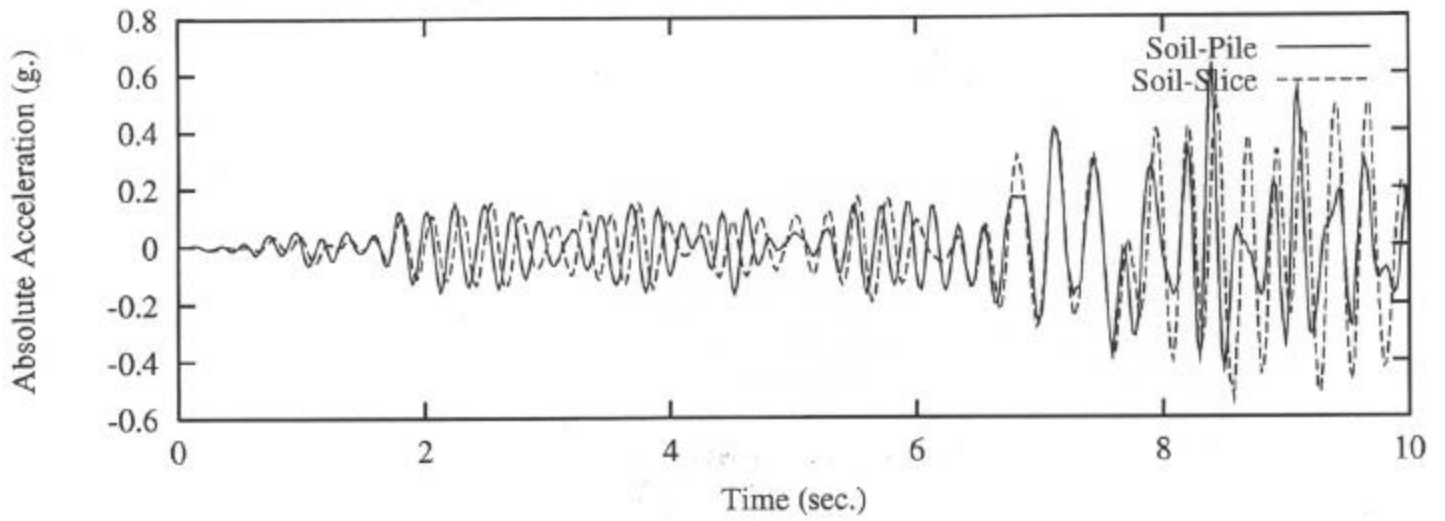


Figure 3.54 1992 Aftershock #2 on IL-1, L= 7 m. (Soil-Slice Model), L= 9 m. (Soil-Pile Model)

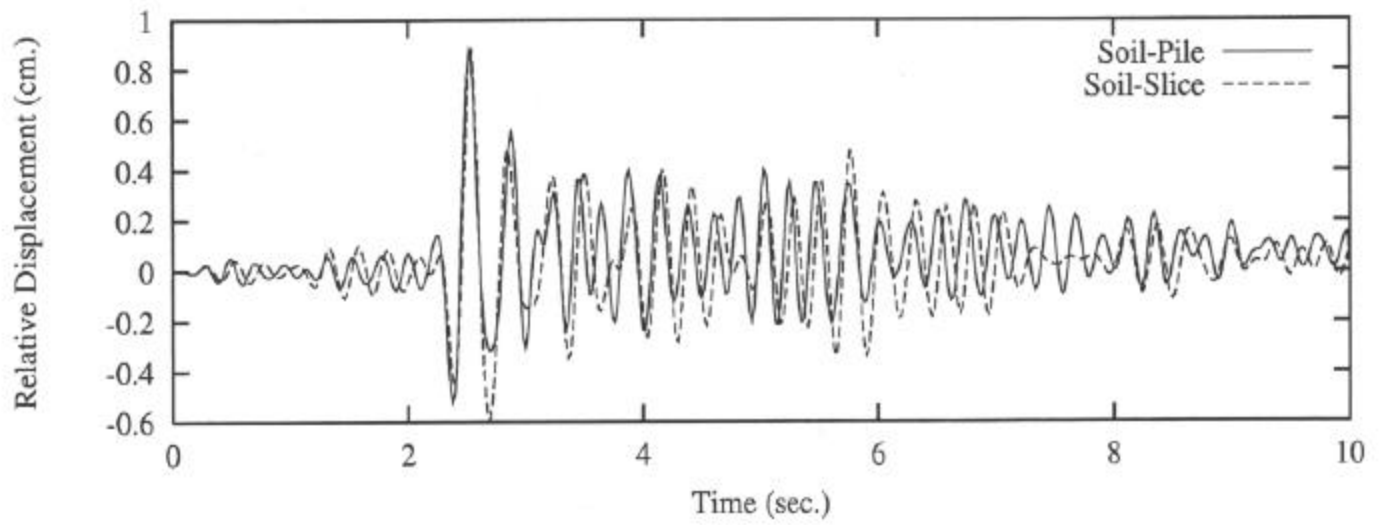
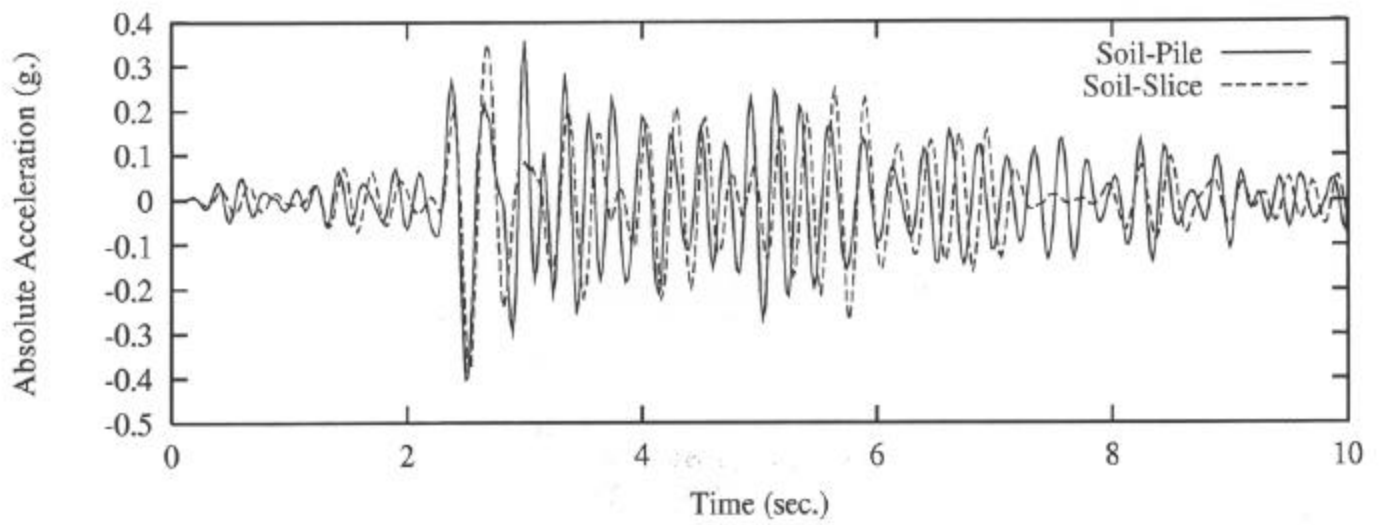


Figure 3.55 1986 Main Event on IL-1, L= 4 m. (Soil-Slice Model), L= 7 m. (Soil-Pile Model)

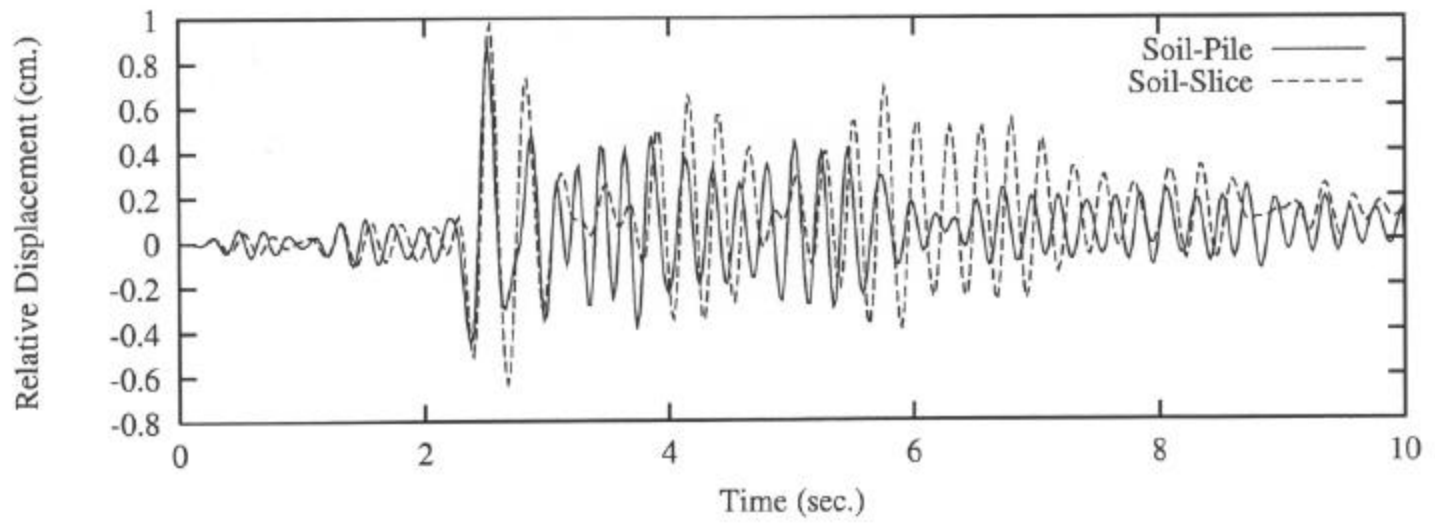
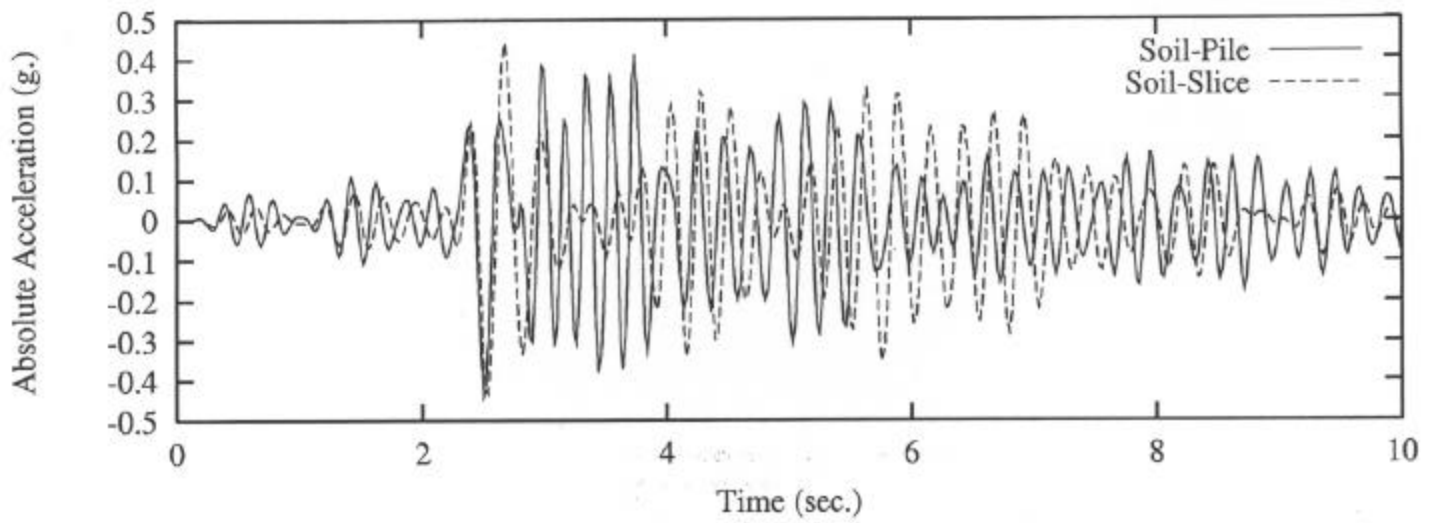


Figure 3.56 1986 Main Event on IL-1, L= 9 m. (Soil-Slice Model), L= 12 m. (Soil-Pile Model)

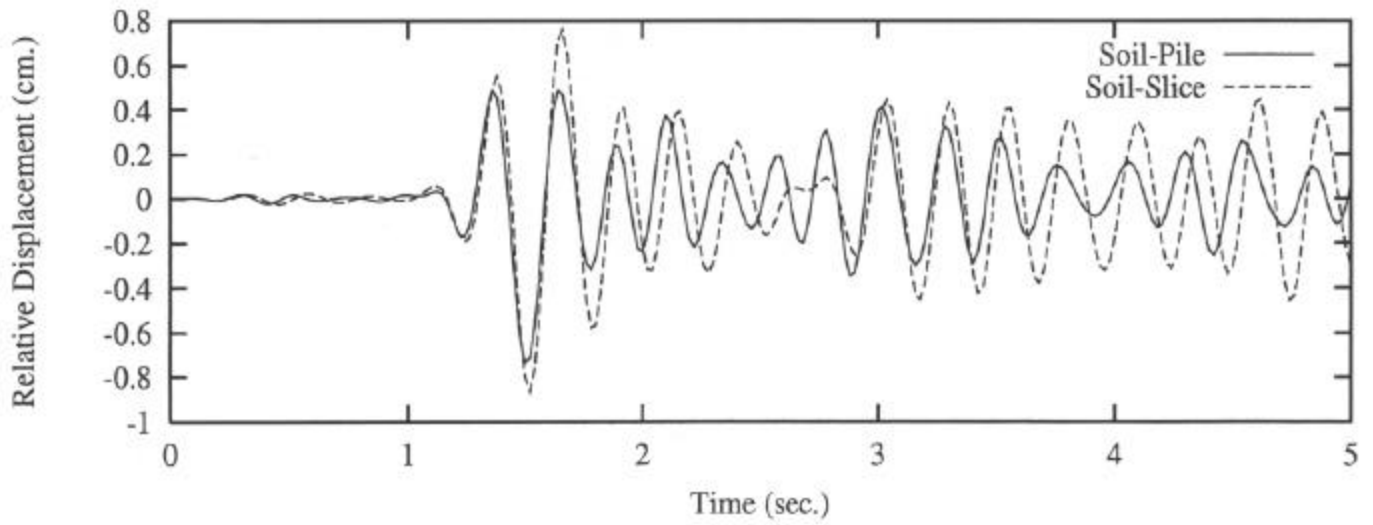
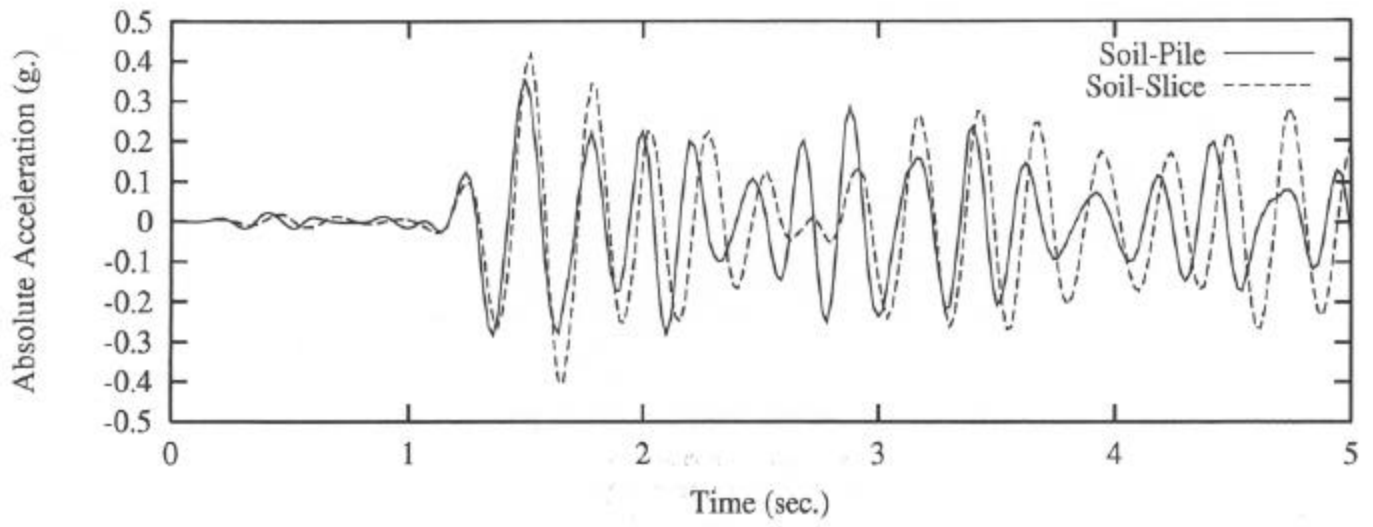


Figure 3.57 1986 Aftershock on IL-1, L= 5 m. (Soil-Slice Model), L= 8 m. (Soil-Pile Model)

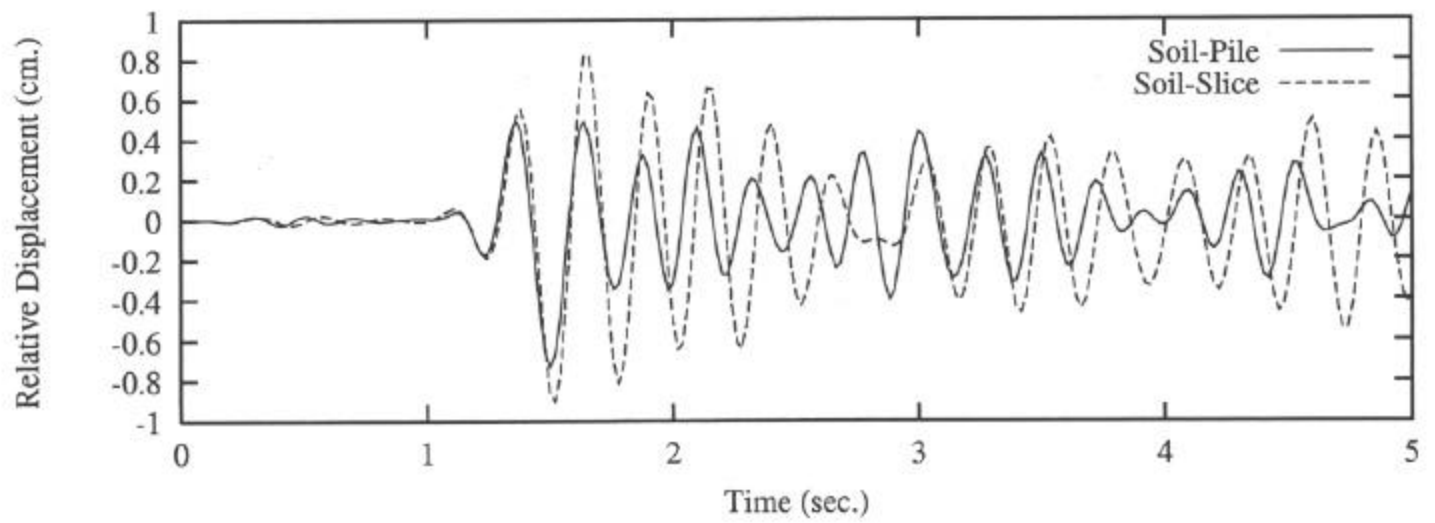
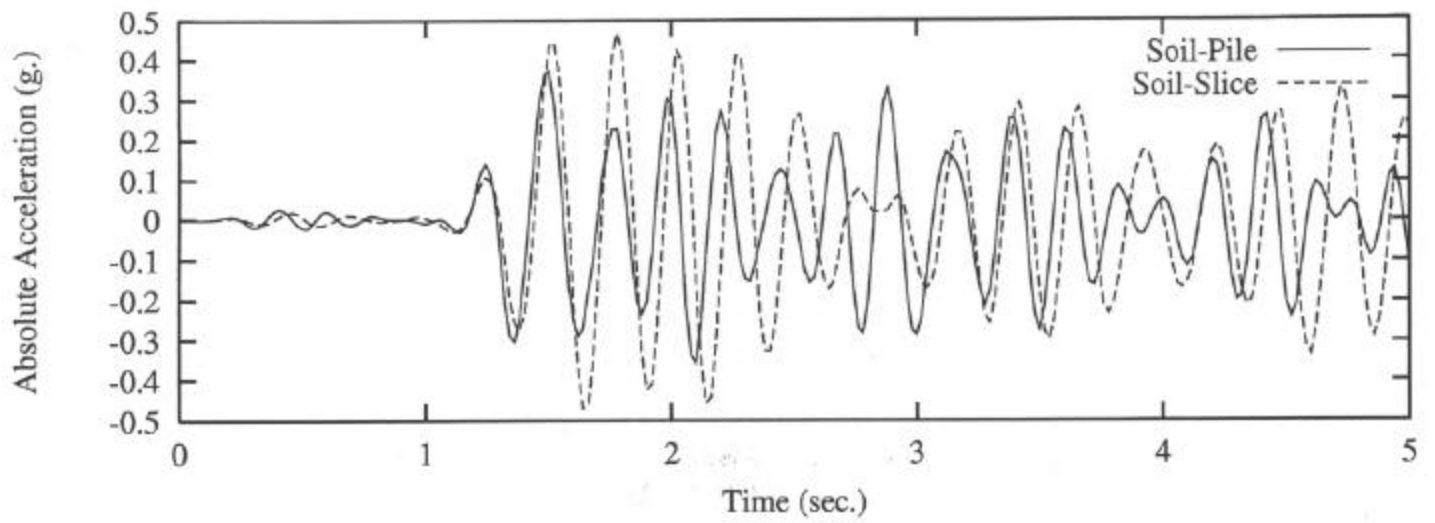


Figure 3.58 1986 Aftershock on IL-1, L= 11 m. (Soil-Slice Model), L= 14 m. (Soil-Pile Model)



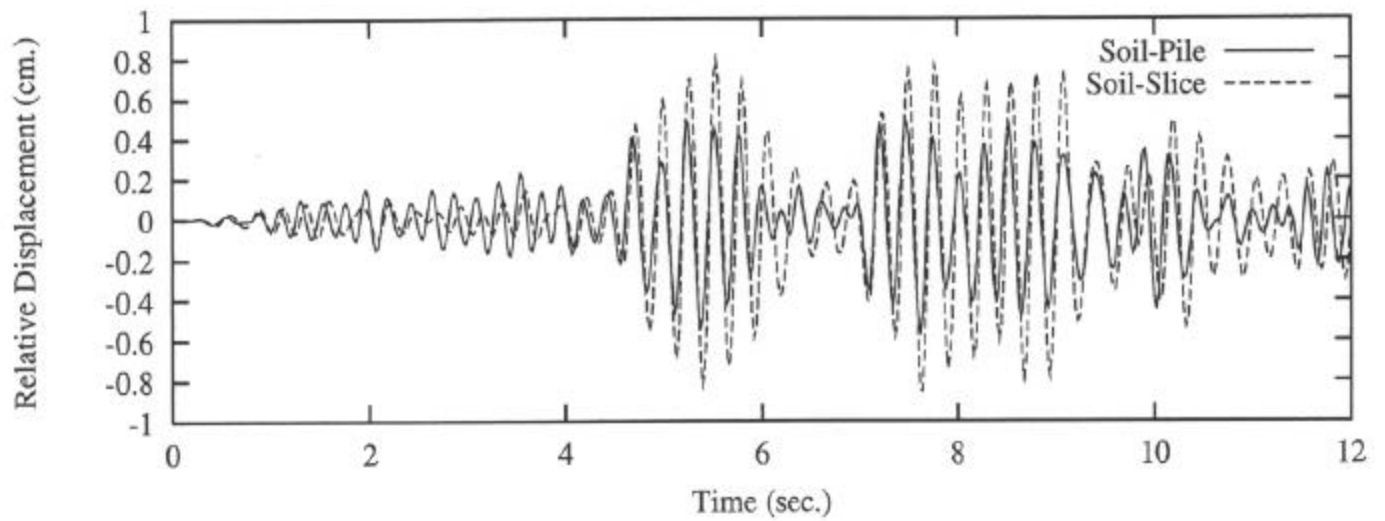
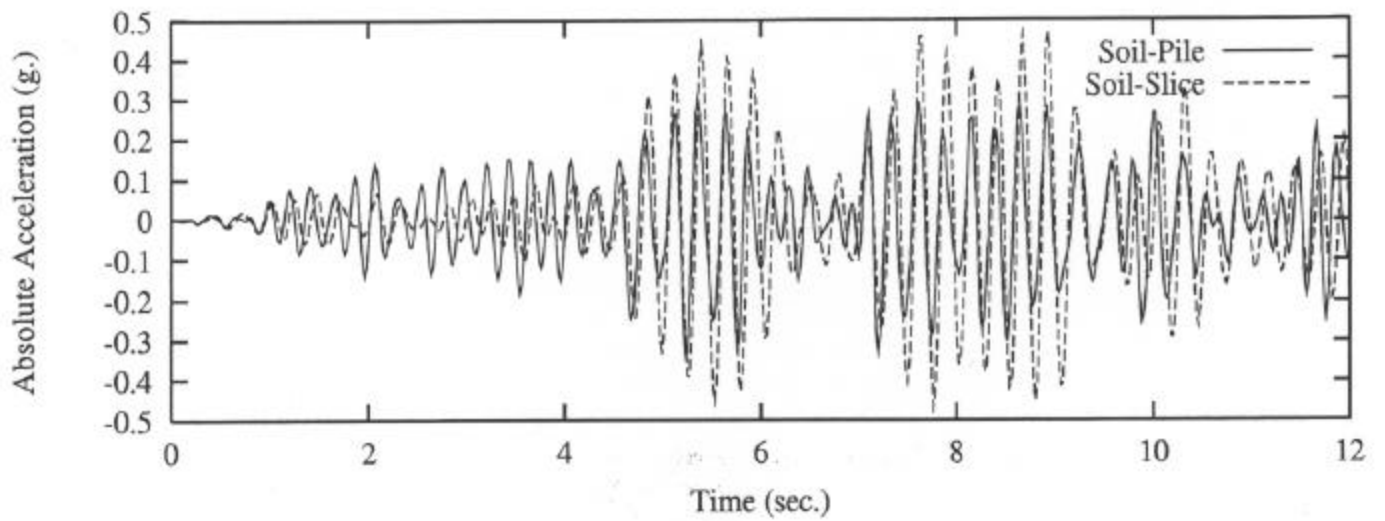


Figure 3.59 1987 Main Event on IL-1, L= 6 m. (Soil-Slice Model), L= 9 m. (Soil-Pile Model)

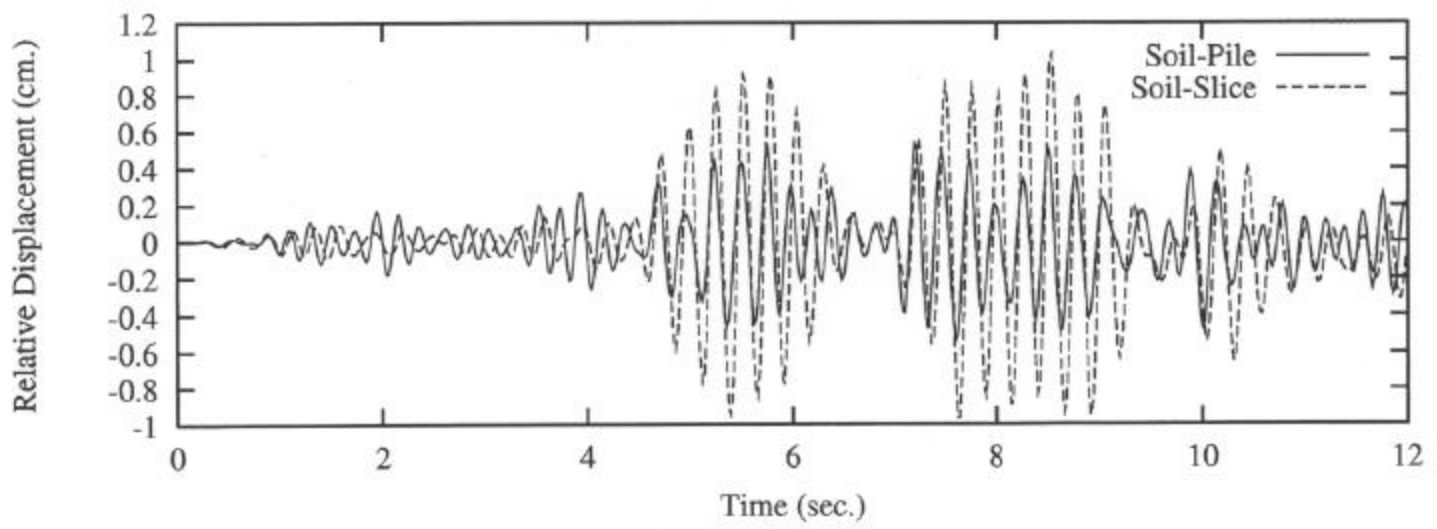
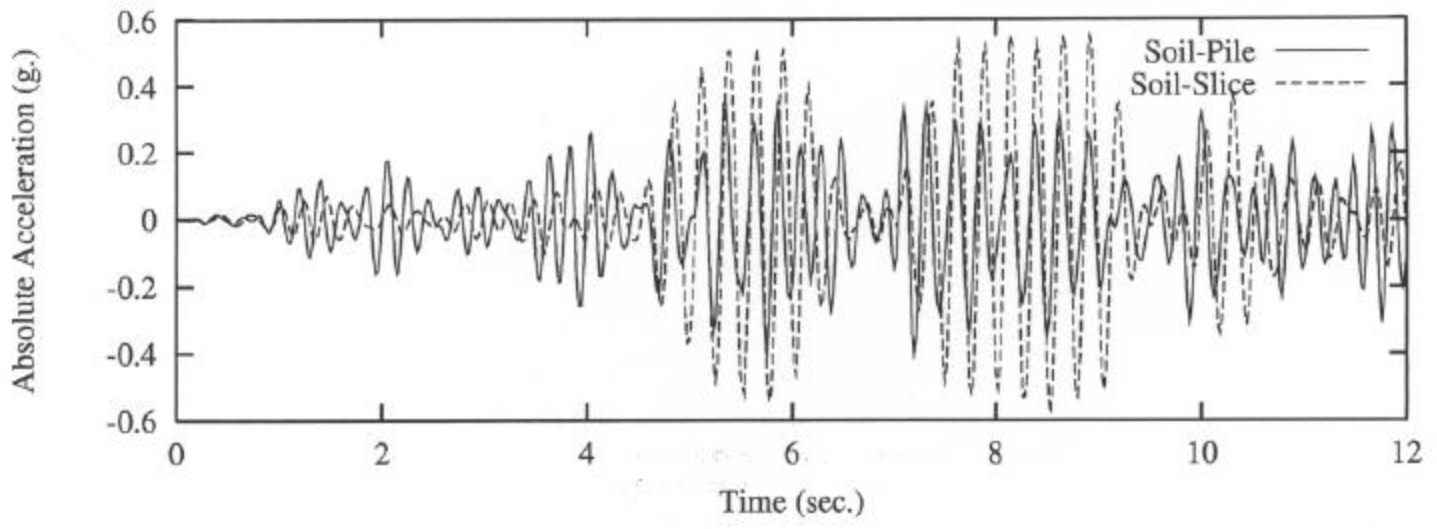


Figure 3.60 1987 Main Event on IL-1, L= 13 m. (Soil-Slice Model), L= 16 m. (Soil-Pile Model)

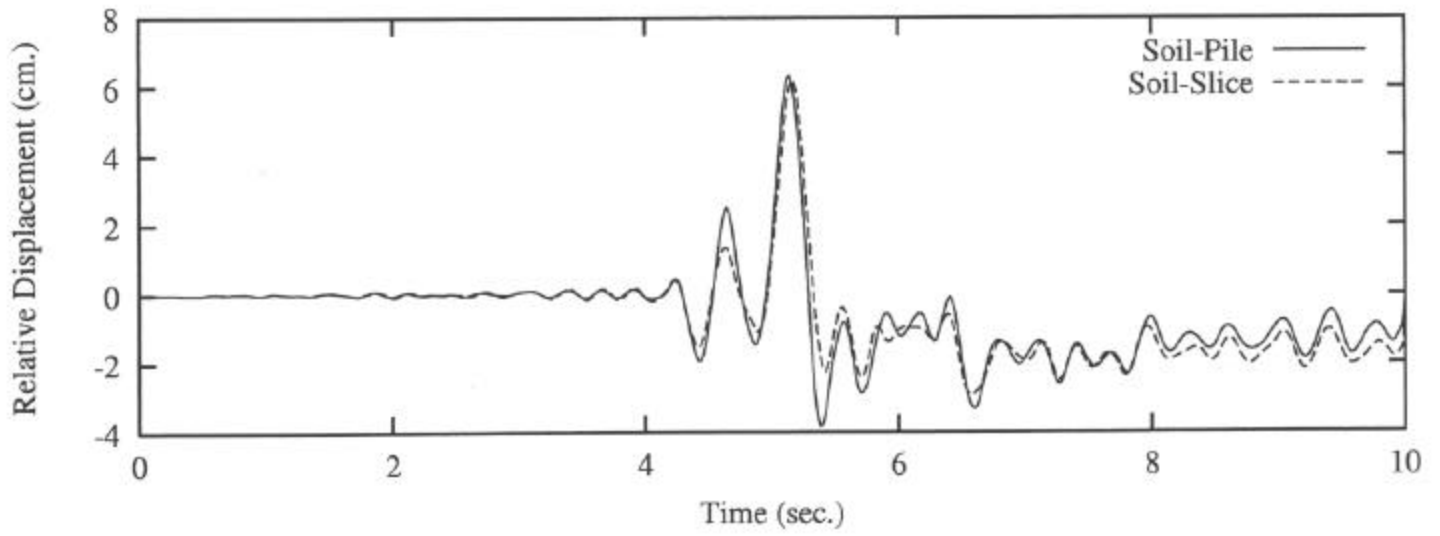
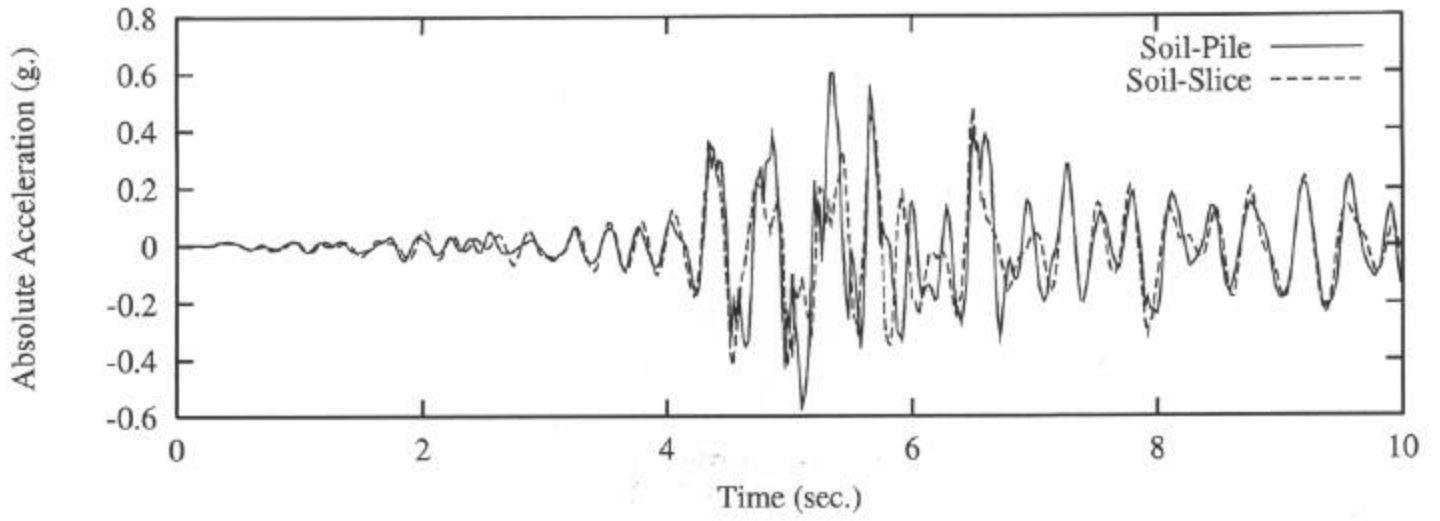


Figure 3.61 1992 Main Event on IL-2, L= 2 m. (Soil-Slice Model), L= 2 m. (Soil-Pile Model)

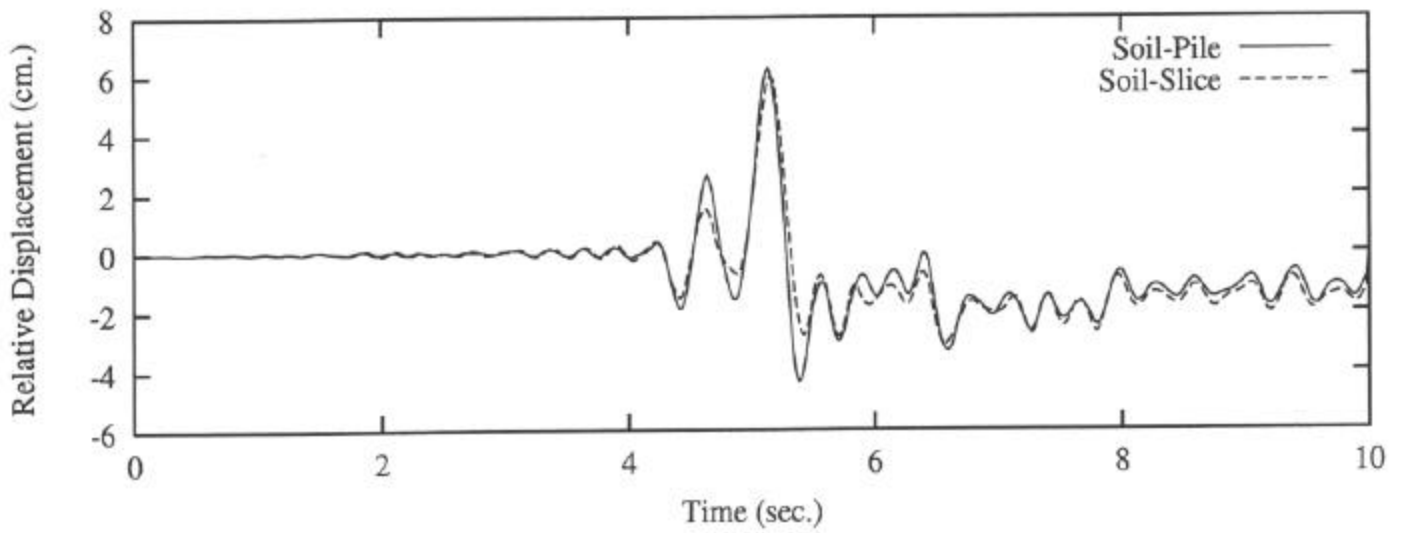
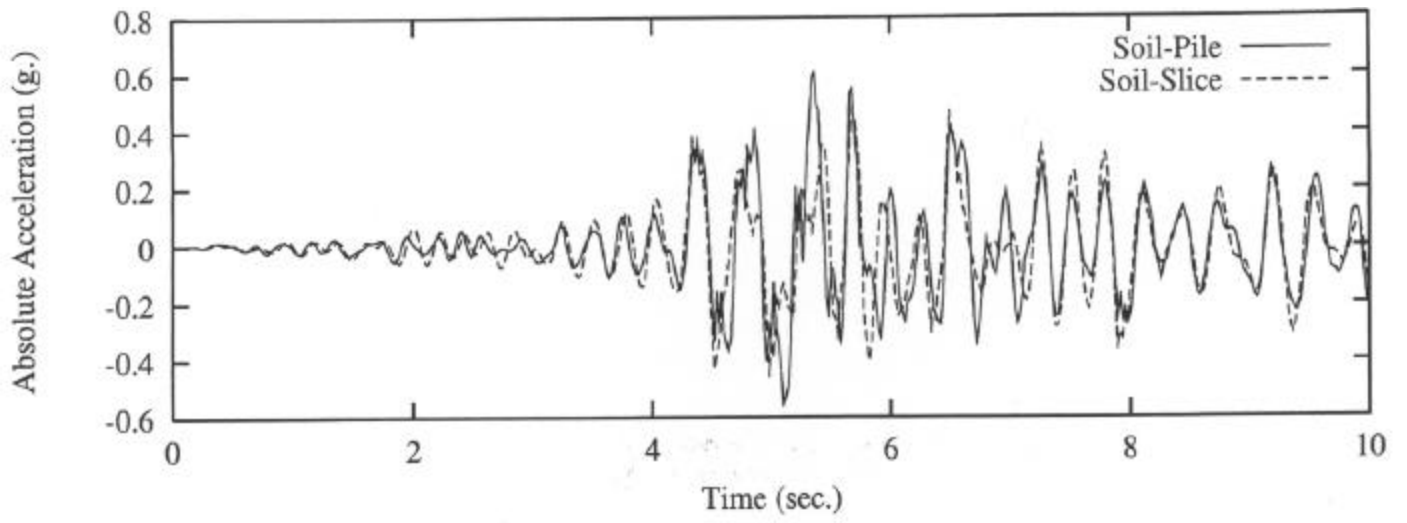


Figure 3.62 1992 Main Event on IL-2, L= 3 m. (Soil-Slice Model), L= 3 m. (Soil-Pile Model)

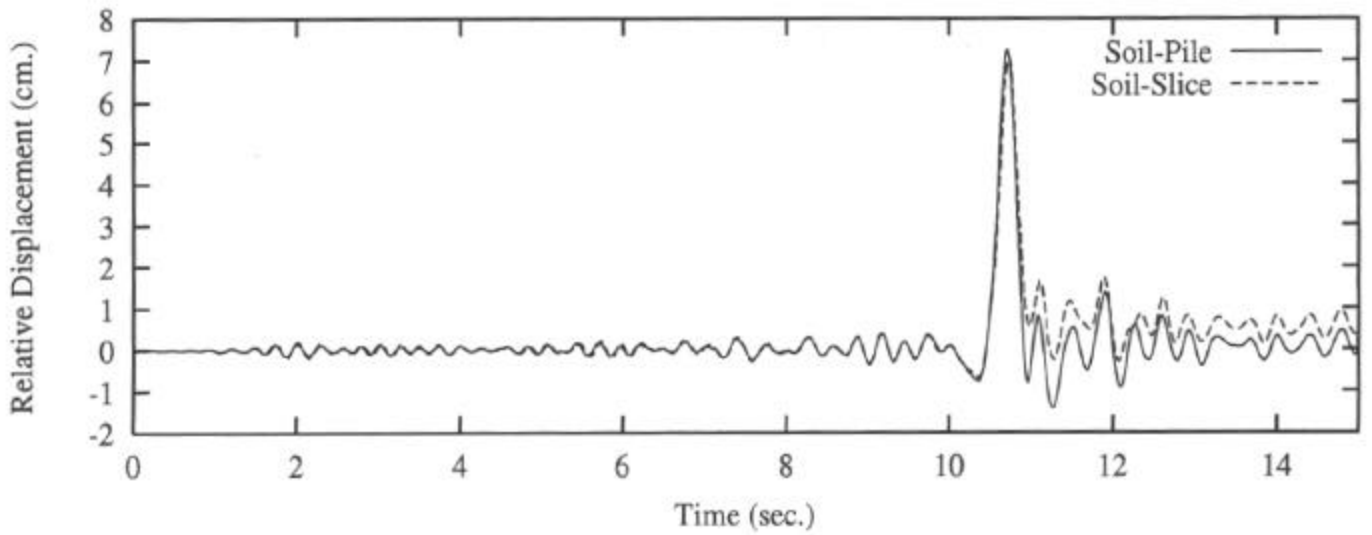
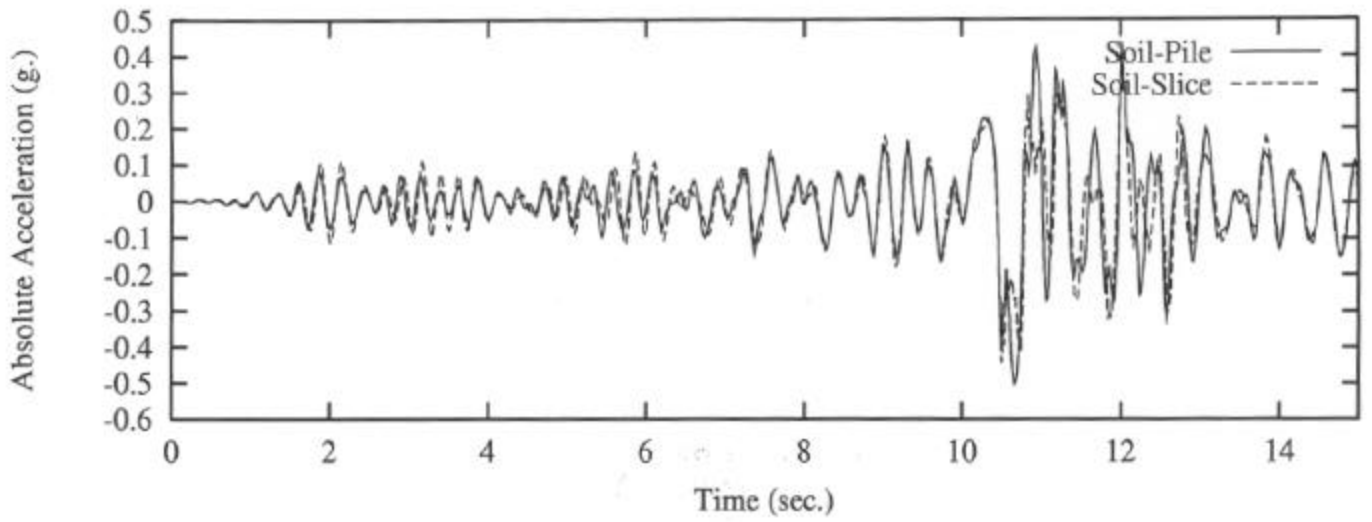


Figure 3.63 1992 Aftershock #1 on IL-2, L= 2 m. (Soil-Slice Model), L= 2 m. (Soil-Pile Model)

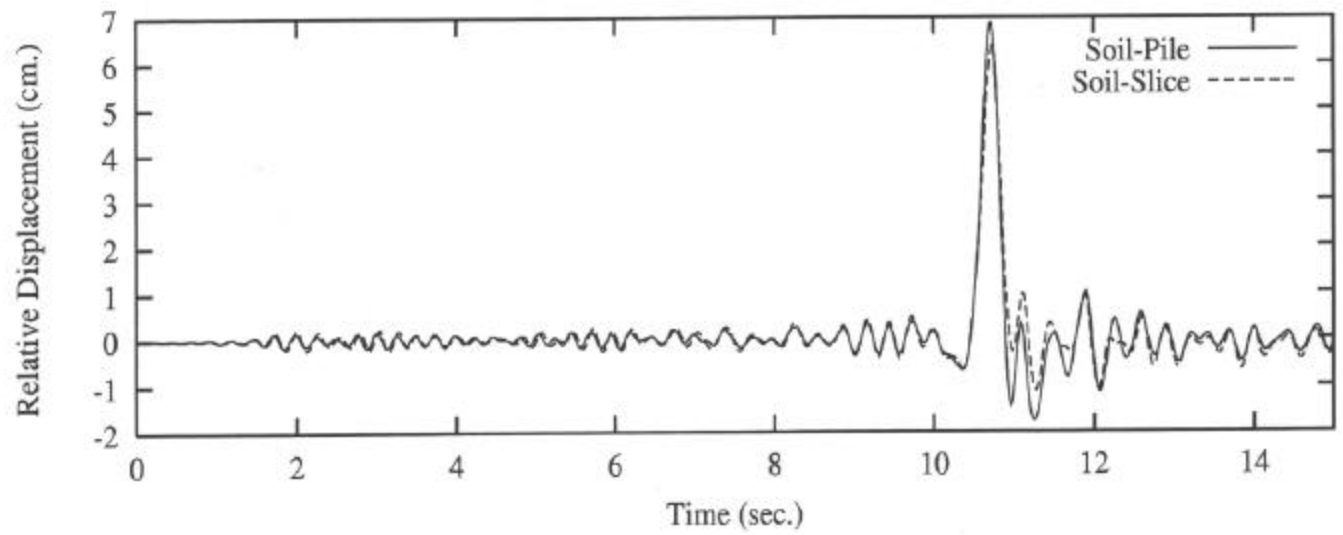
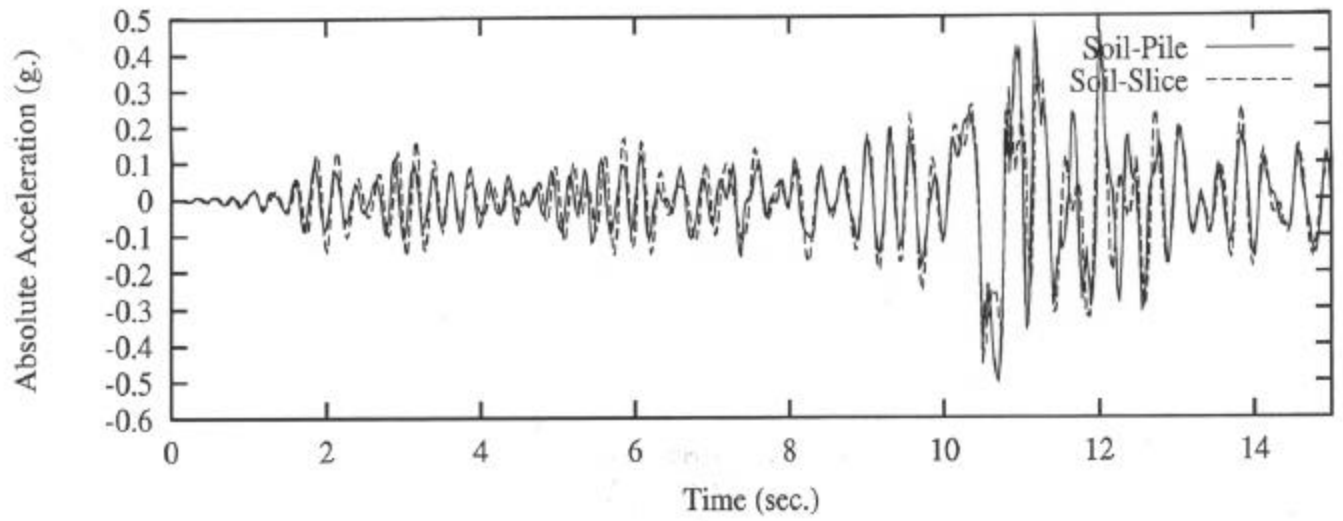


Figure 3.64 1992 Aftershock #1 on IL-2, L= 3 m. (Soil-Slice Model), L= 3 m. (Soil-Pile Model)

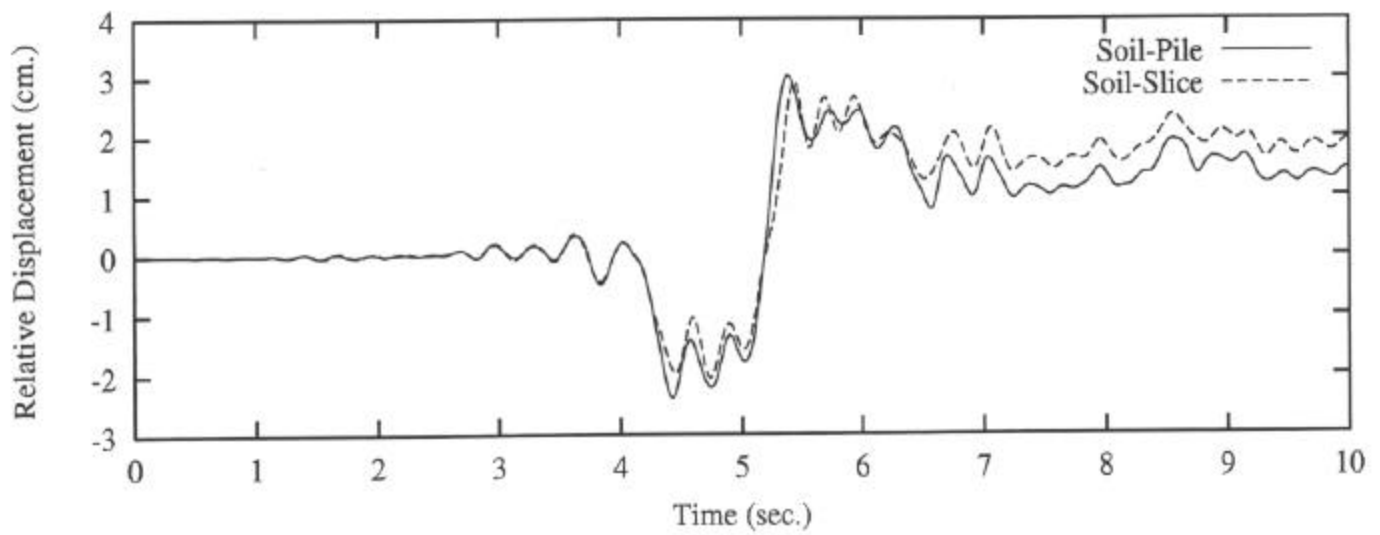
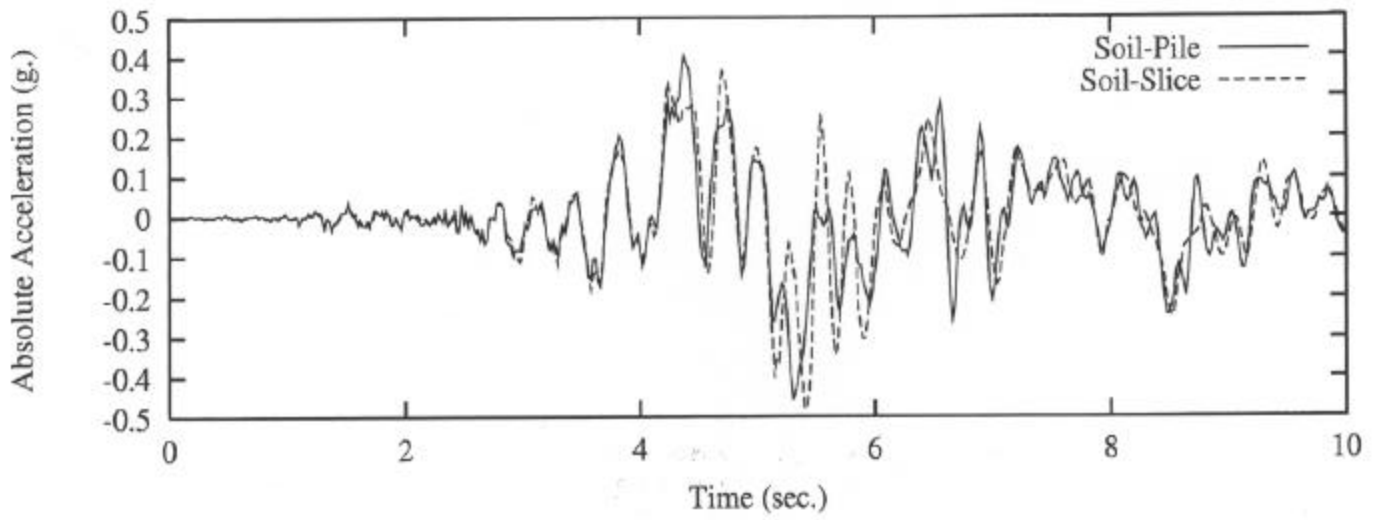


Figure 3.65 1979 Imperial Valley Earthquake on IL-2, L= 2 m. (Soil-Slice Model), L= 2 m. (Soil-Pile Model)

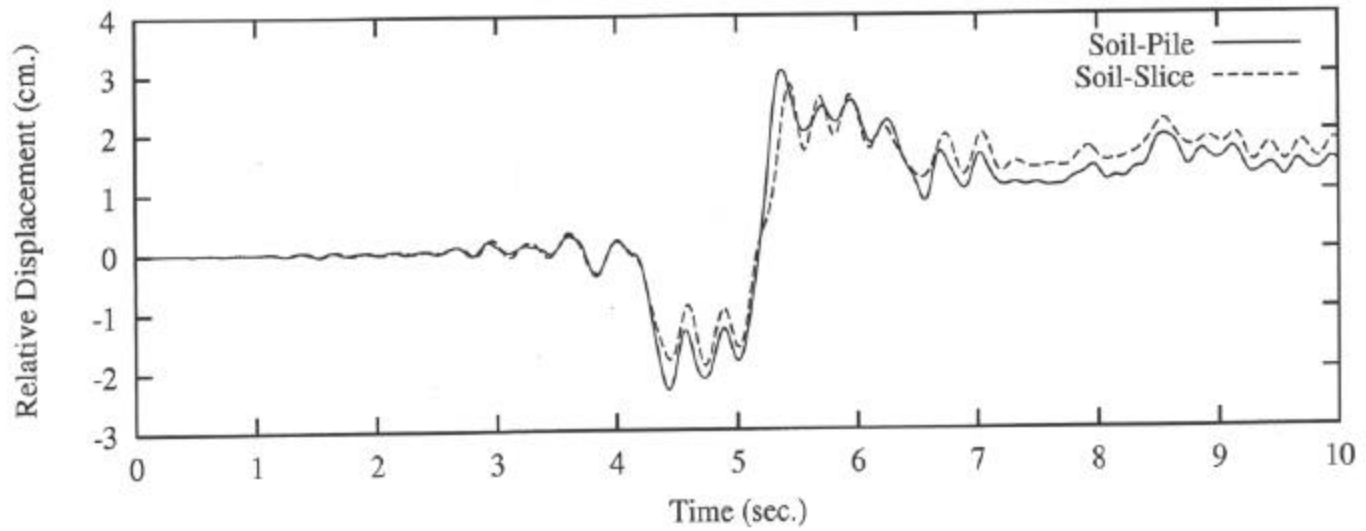
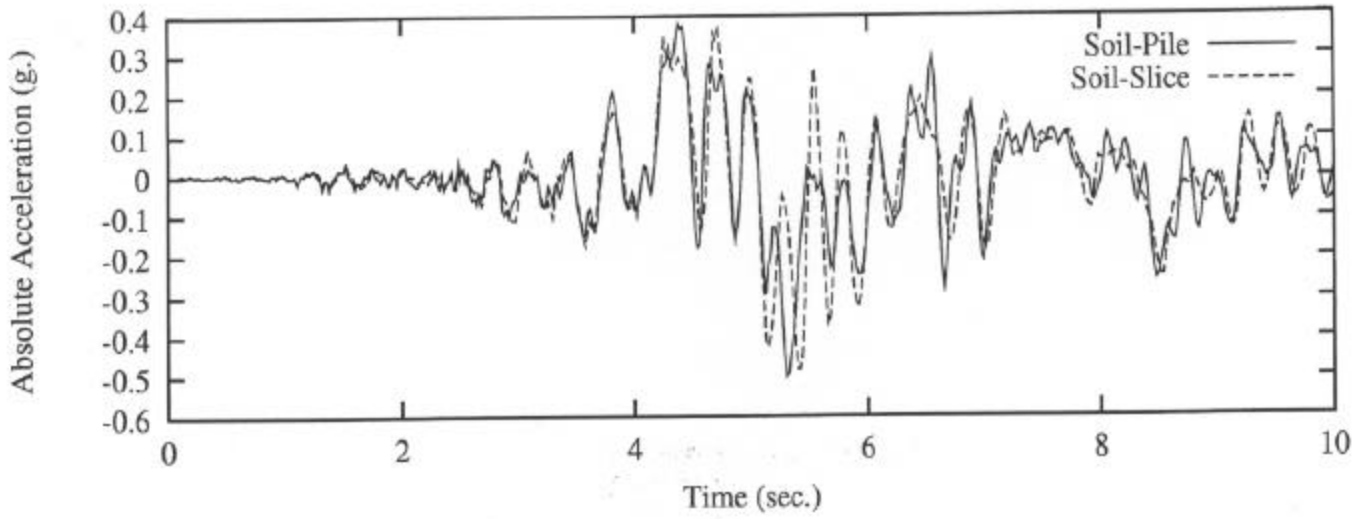


Figure 3.66 1979 Imperial Valley Earthquake on IL-2, L= 3 m. (Soil-Slice Model), L= 3 m. (Soil-Pile Model)



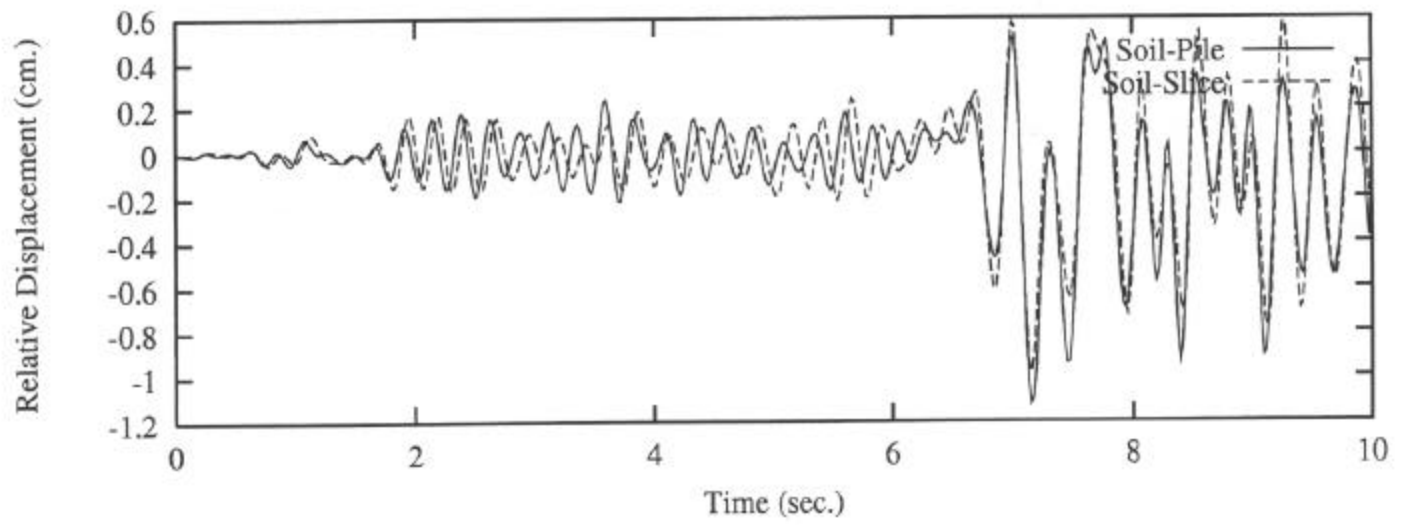
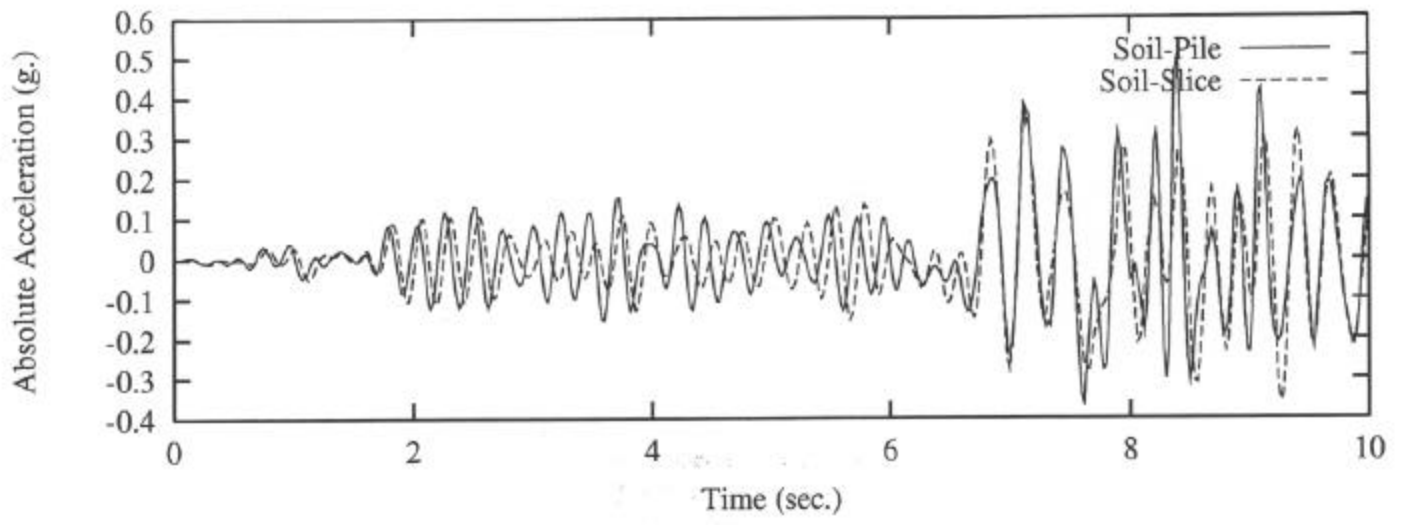


Figure 3.67 1992 Aftershock #2 on IL-2, L= 3 m. (Soil-Slice Model), L= 5 m. (Soil-Pile Model)

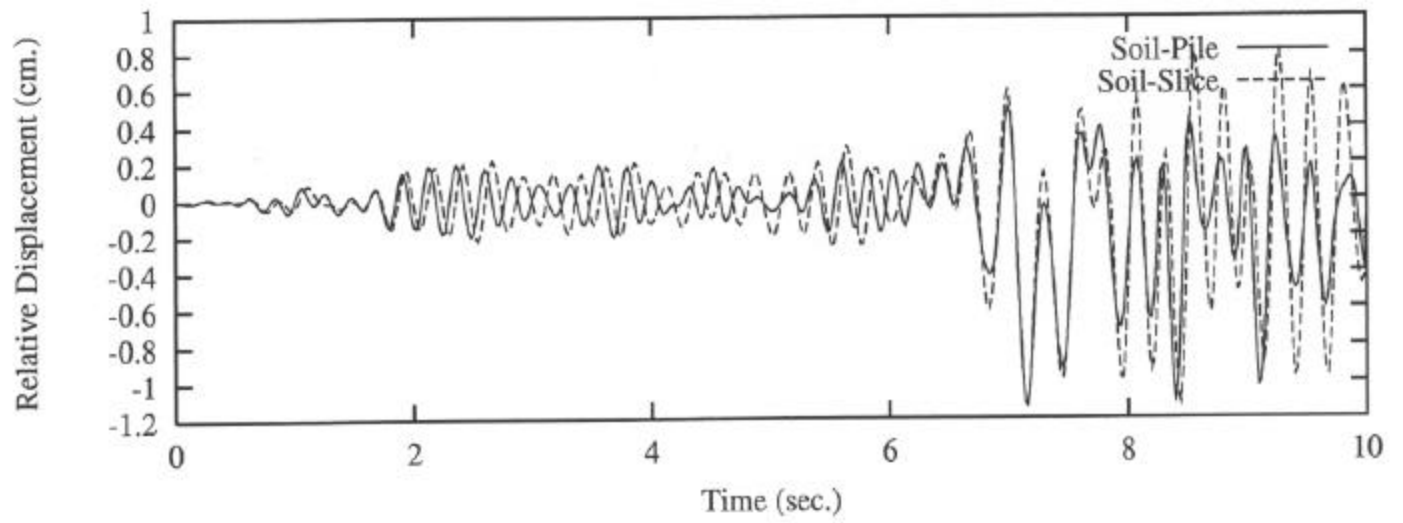
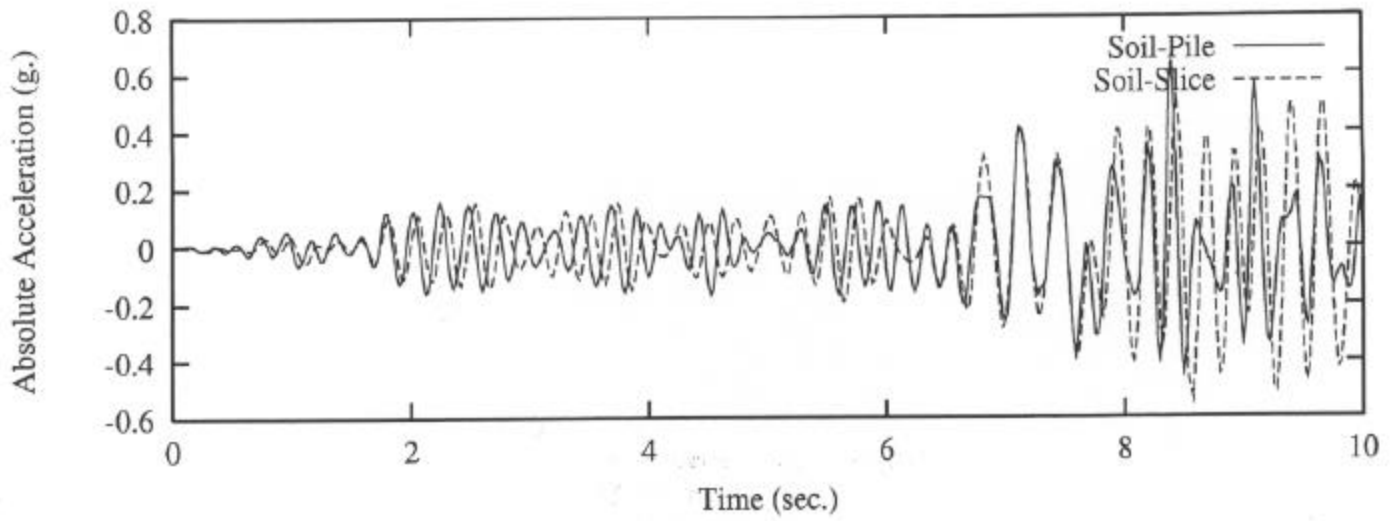


Figure 3.68 1992 Aftershock #2 on IL-2, L= 7 m. (Soil-Slice Model), L= 9 m. (Soil-Pile Model)

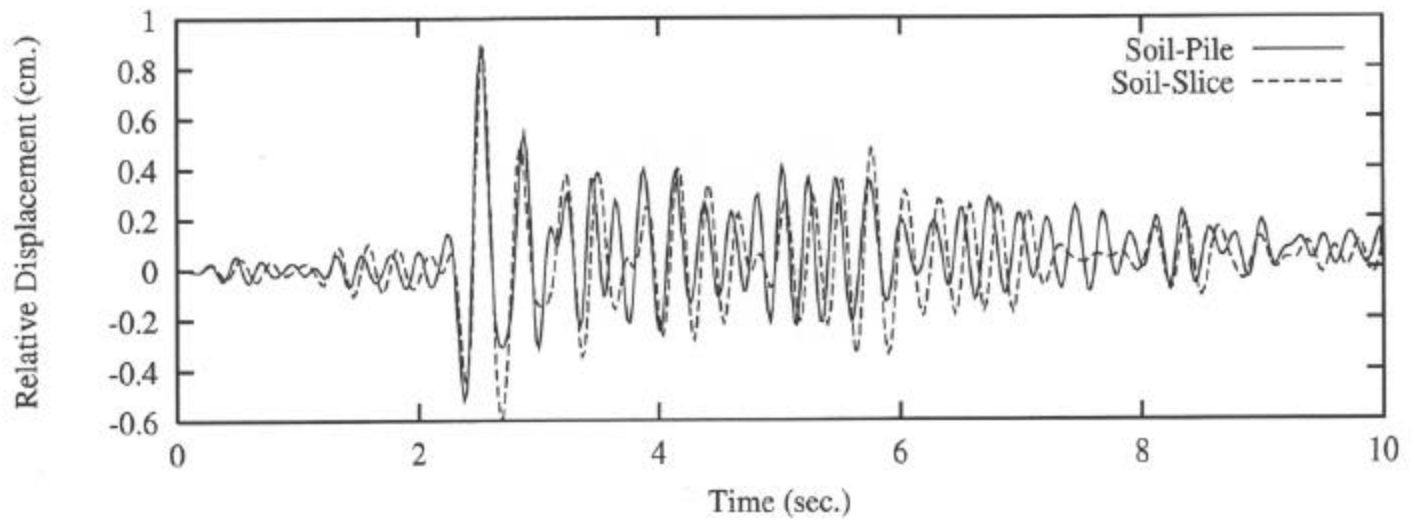
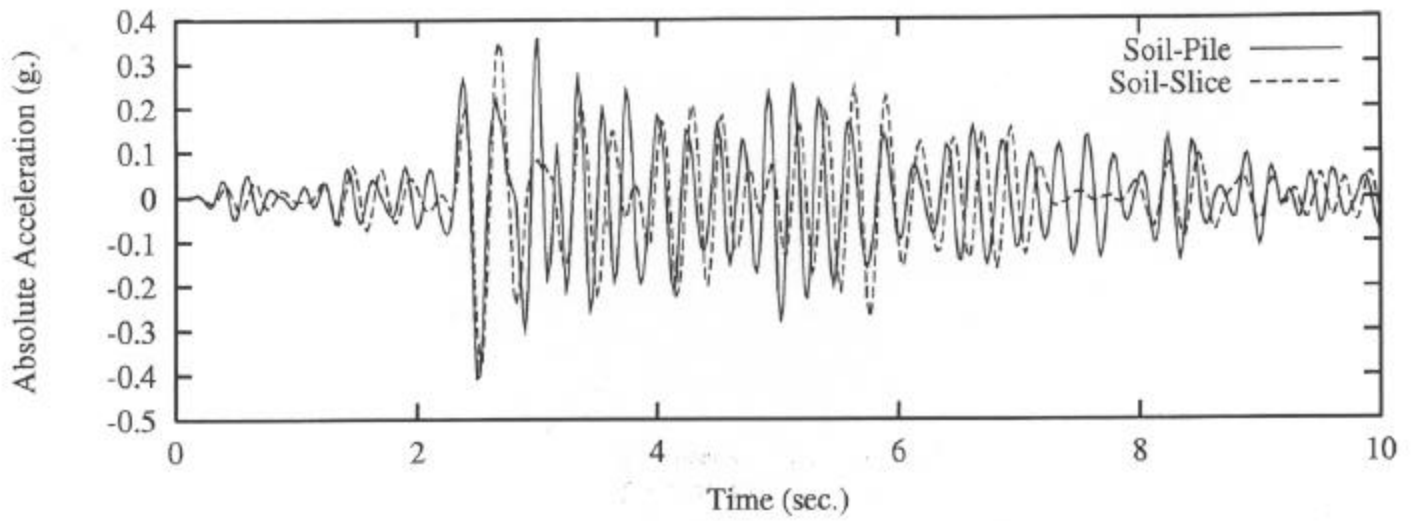


Figure 3.69 1986 Main Event on IL-2, L= 4 m. (Soil-Slice Model), L= 7 m. (Soil-Pile Model)

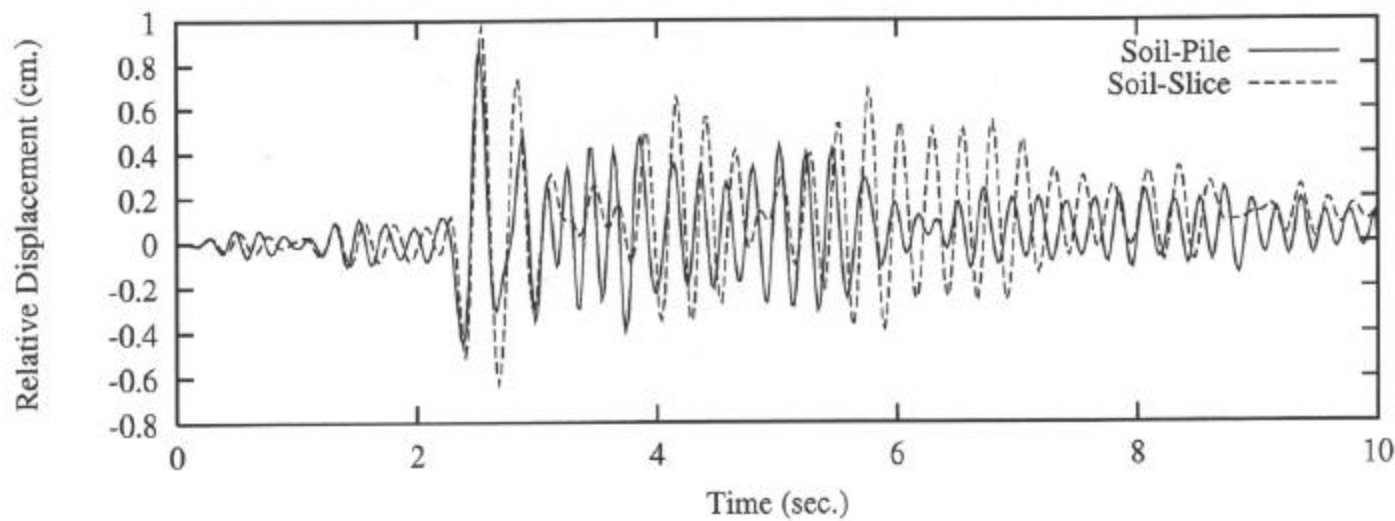
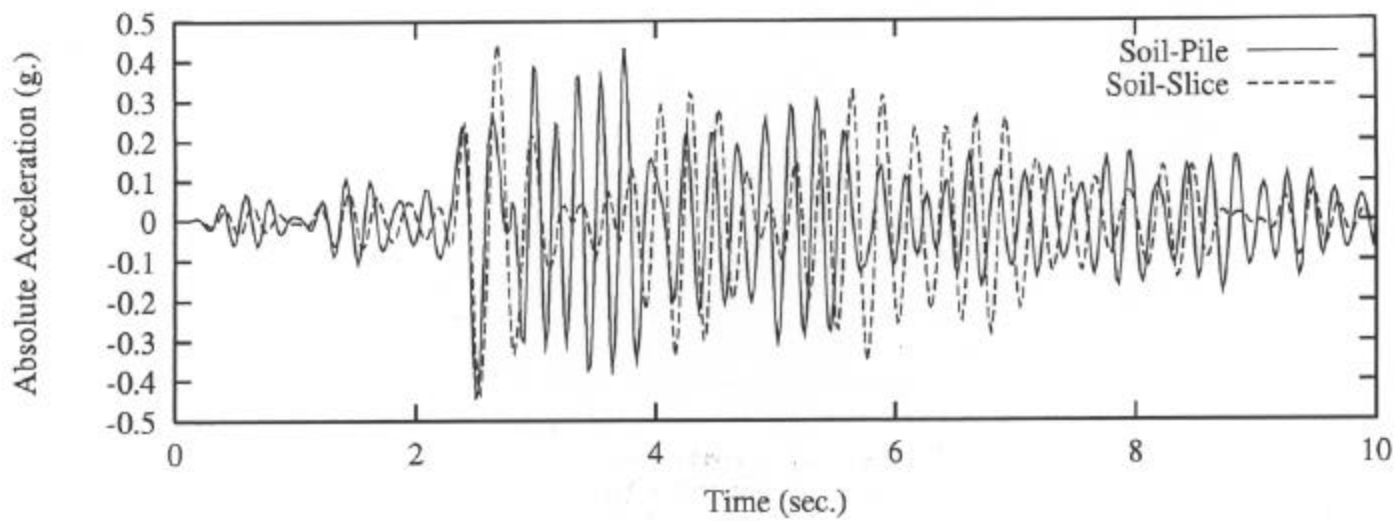


Figure 3.70 1986 Main Event on IL-2, L= 9 m. (Soil-Slice Model), L= 12 m. (Soil-Pile Model)

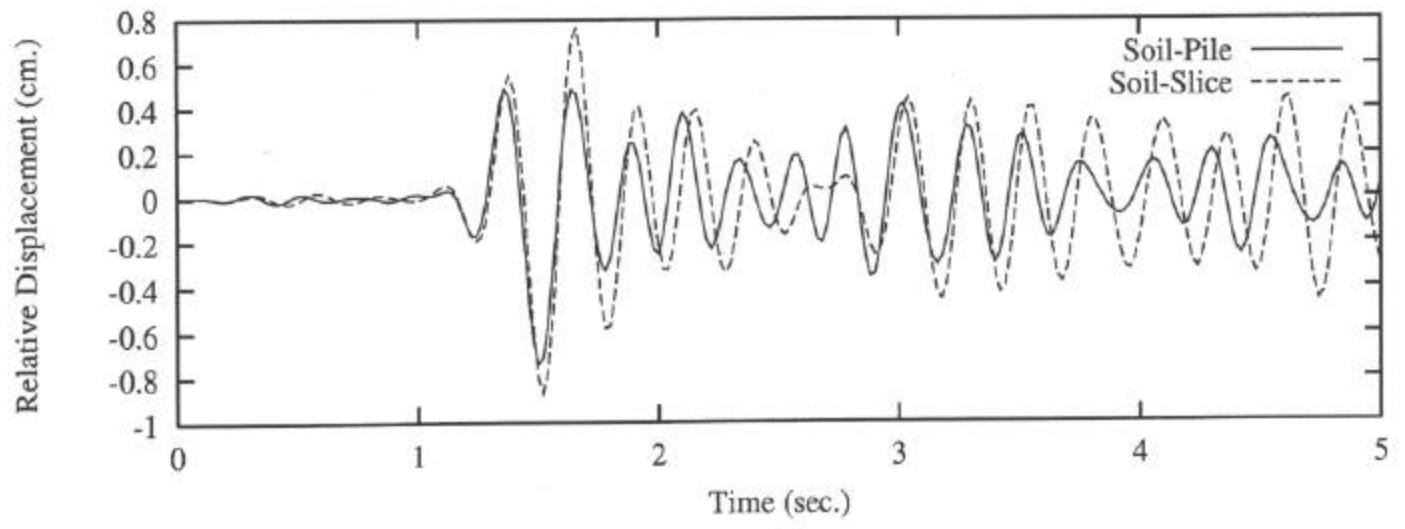
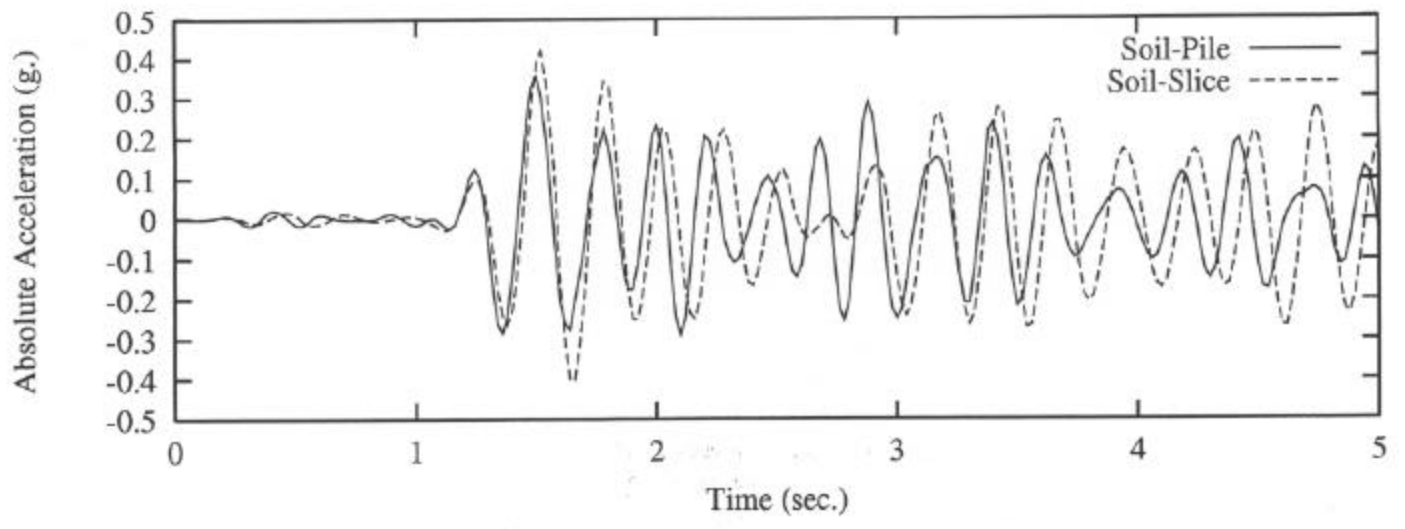


Figure 3.71 1986 Aftershock on IL-2, L= 5 m. (Soil-Slice Model), L= 8 m. (Soil-Pile Model)

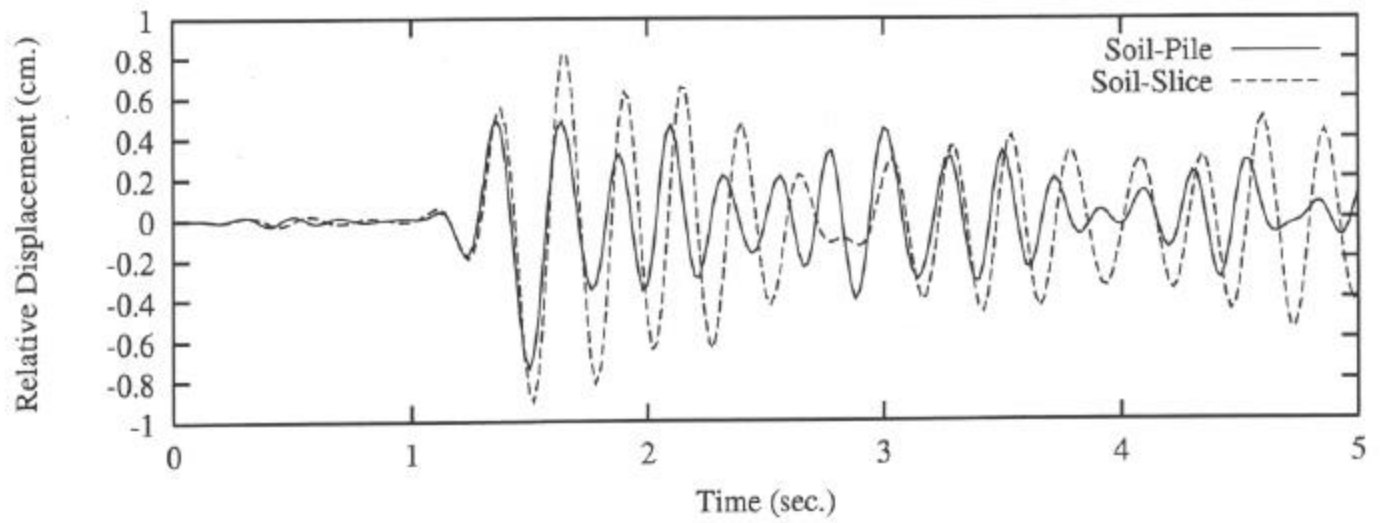
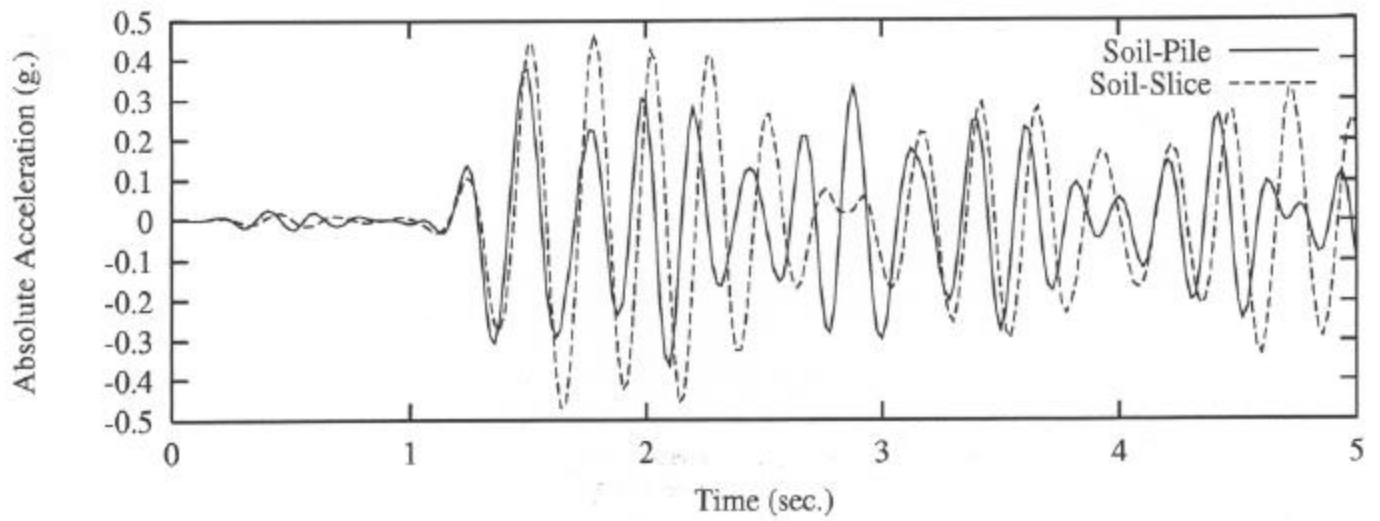


Figure 3.72 1986 Aftershock on IL-2, L= 11 m. (Soil-Slice Model), L= 14 m. (Soil-Pile Model)

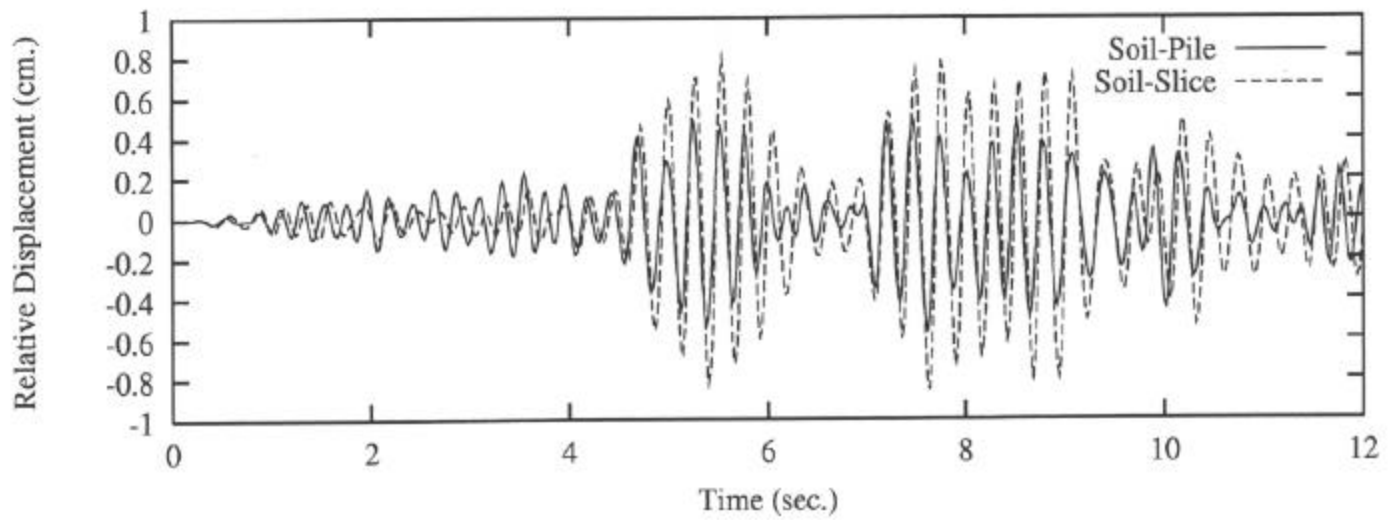
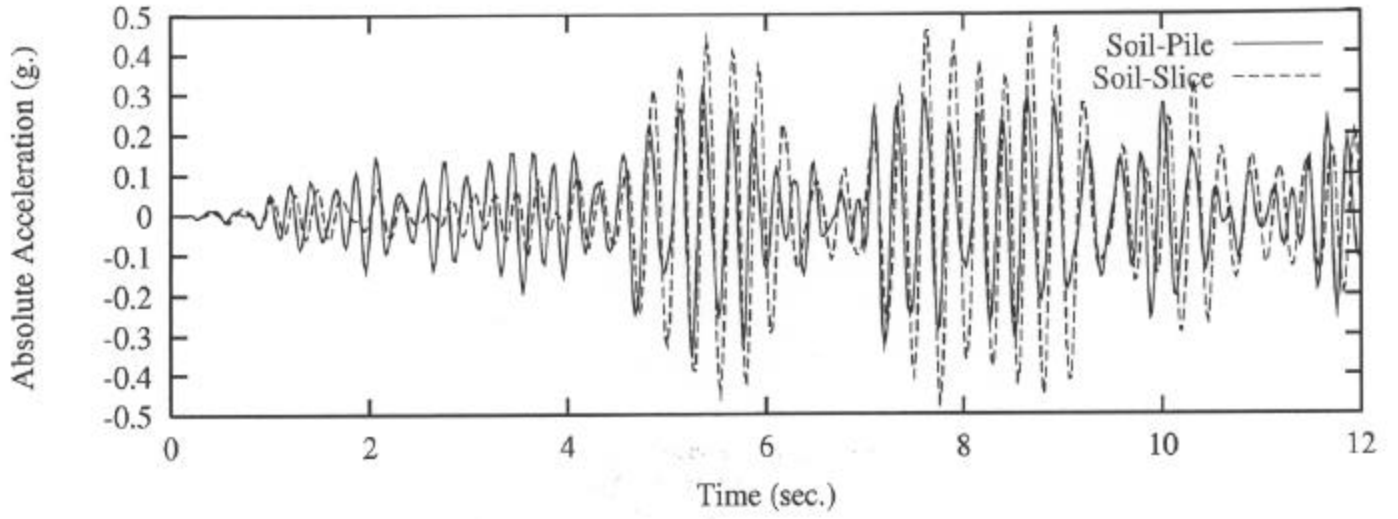


Figure 3.73 1987 Main Event on IL-2, L= 6 m. (Soil-Slice Model), L= 9 m. (Soil-Pile Model)

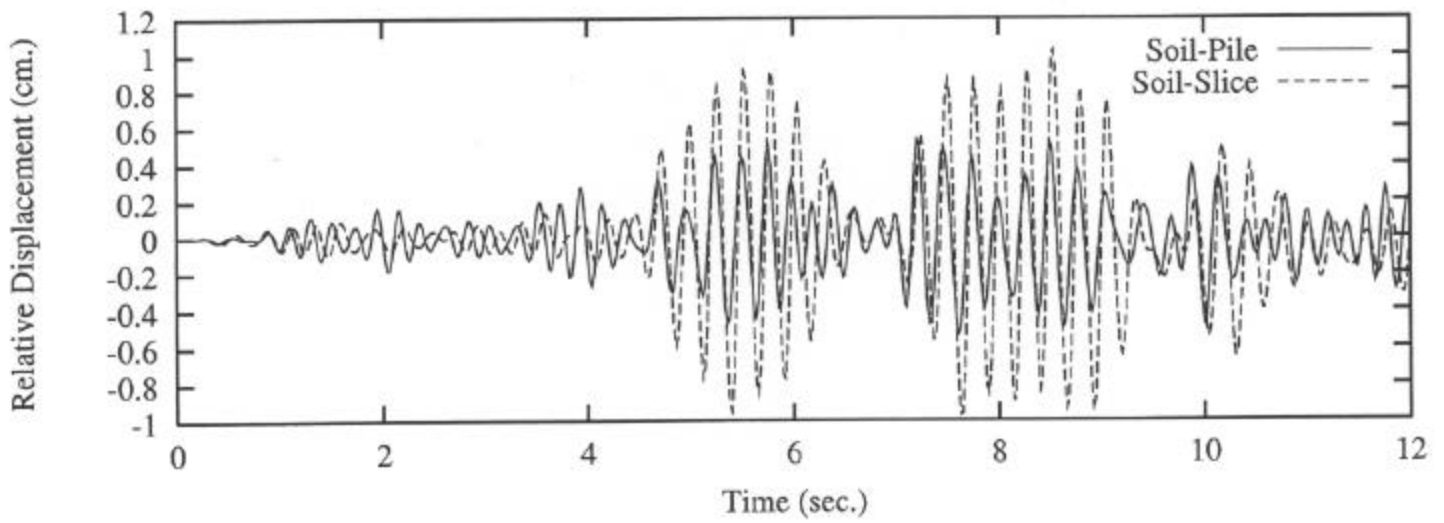
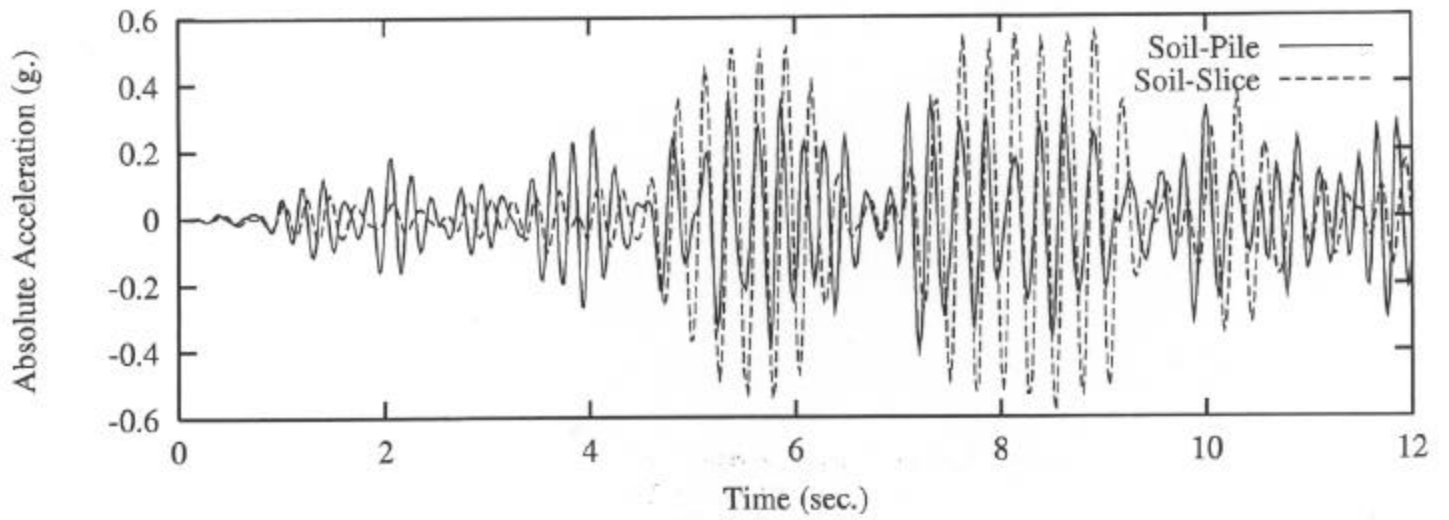


Figure 3.74 1987 Main Event on IL-2, L= 13 m. (Soil-Slice Model), L= 16 m. (Soil-Pile Model)



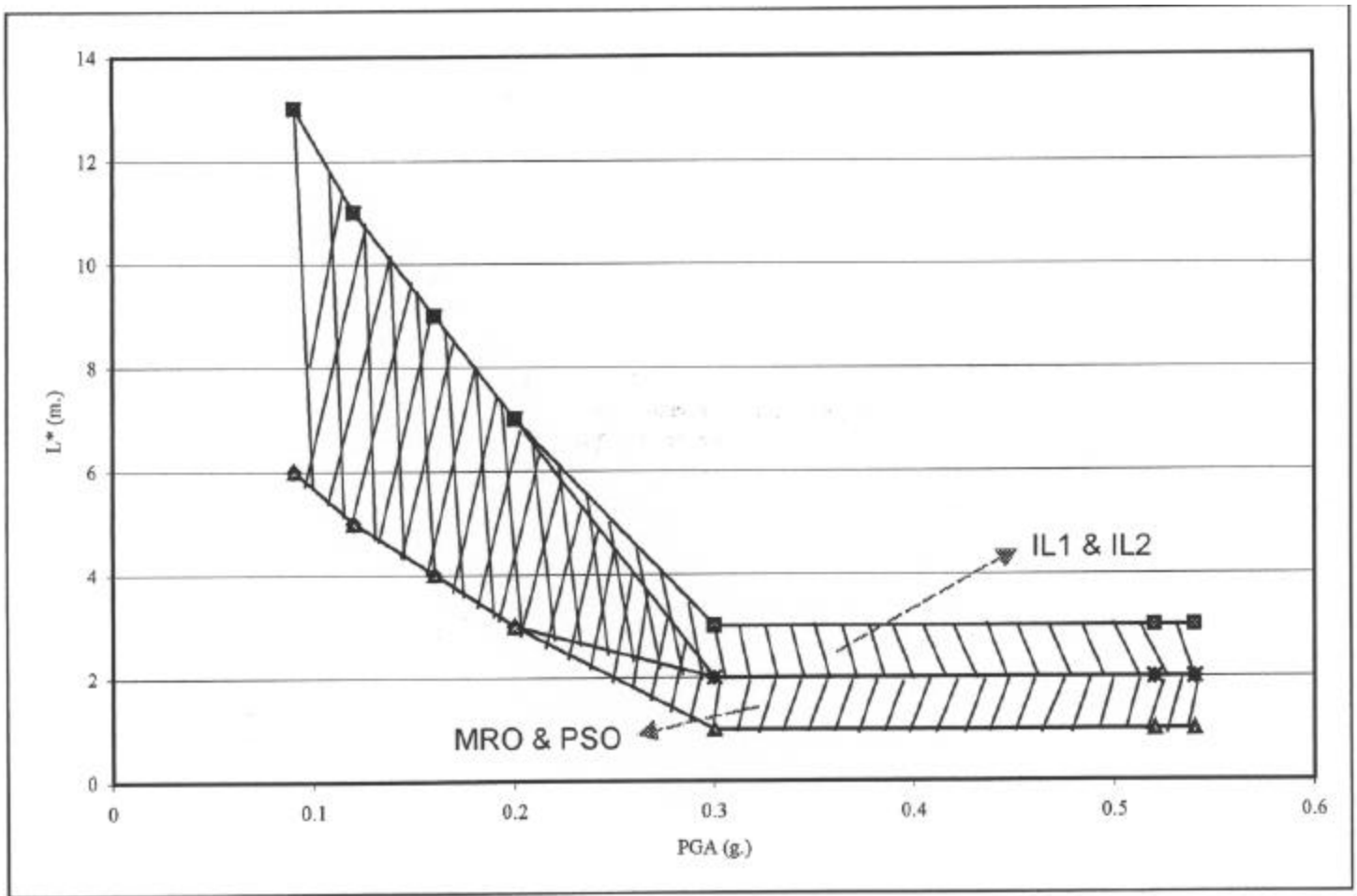


Figure 3.75 Ranges of Approach-Embankment Thickness ( $L^*$ ) for California vs. Illinois Bridges (Figure 3.40 vs. Figure 3.46)

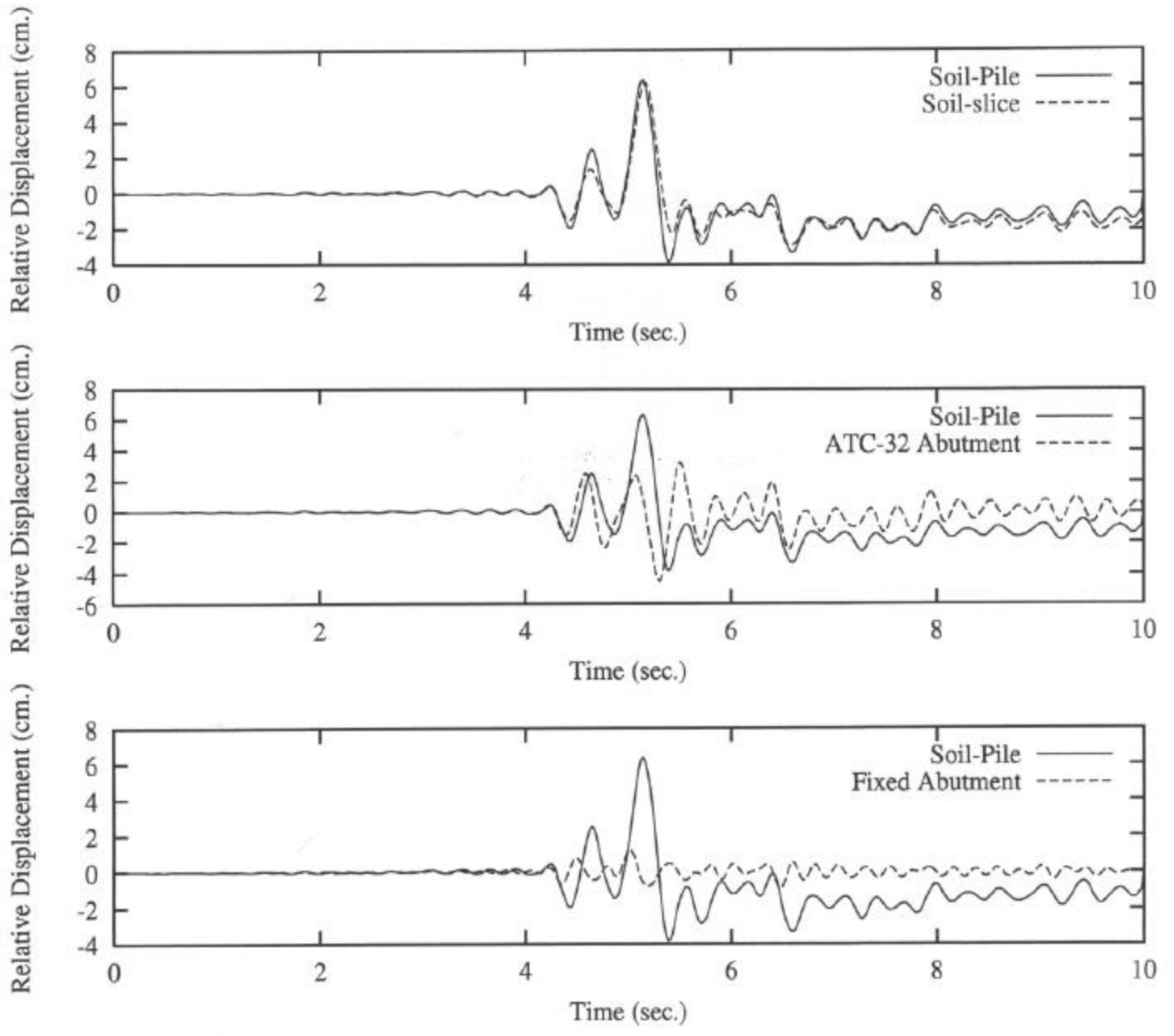
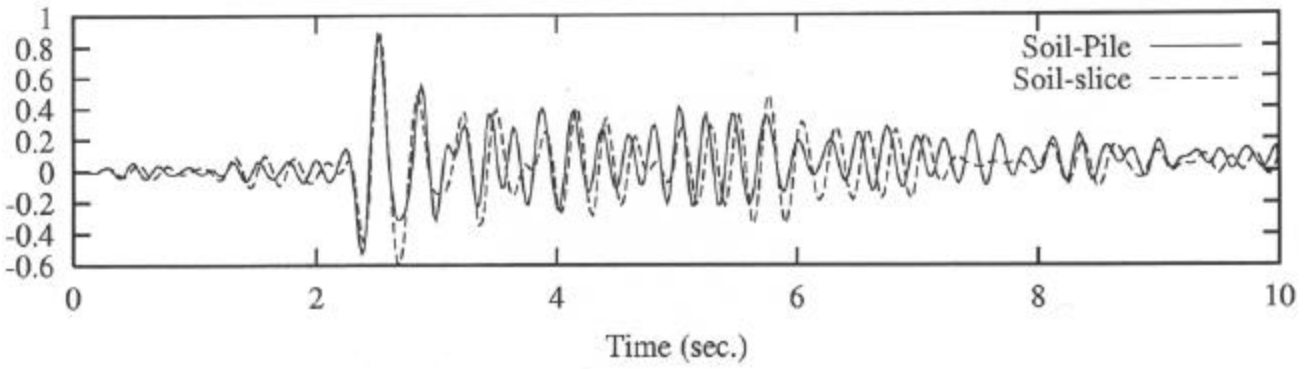
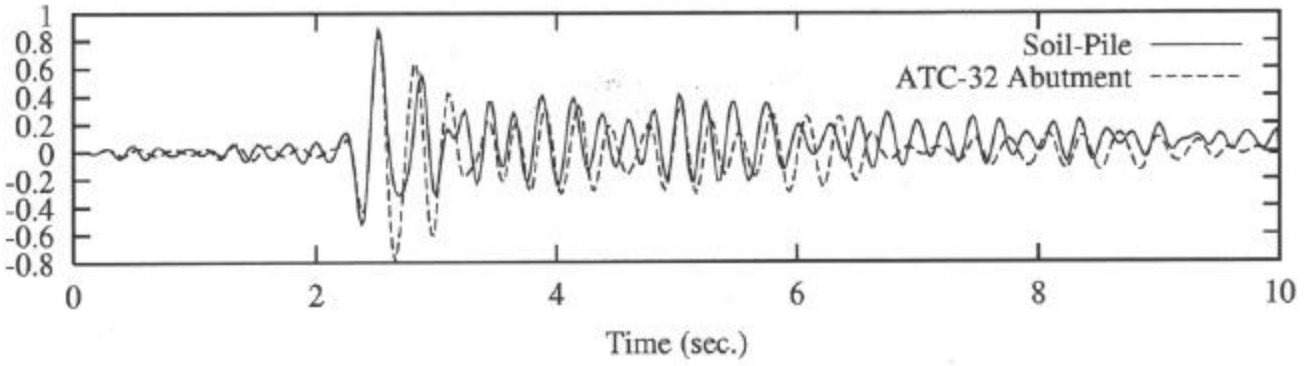


Figure 3.76 Response Comparison Between Different Models Subjected to 1992 Main Event on IL-2

Relative Displacement (cm.)



Relative Displacement (cm.)



Relative Displacement (cm.)

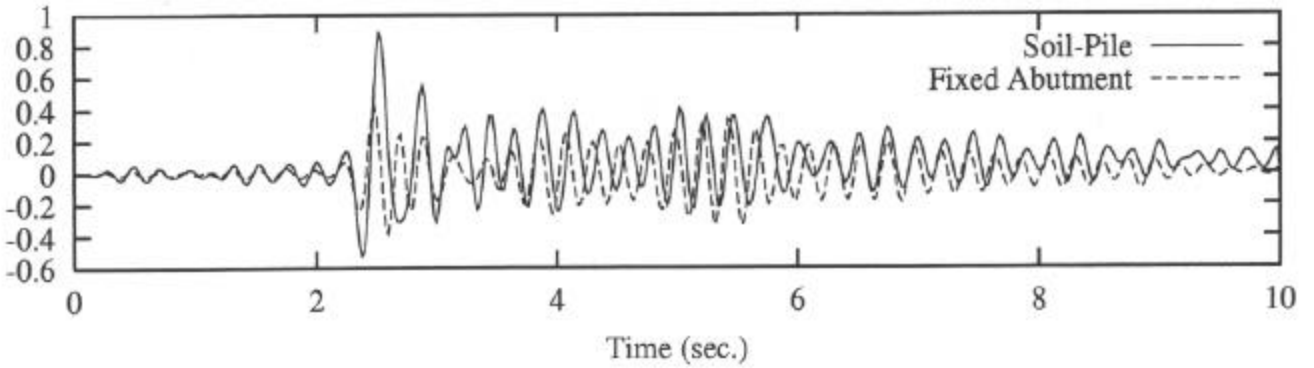


Figure 3.77 Response Comparison Between Different Models Subjected to 1986 Main Event on IL-2

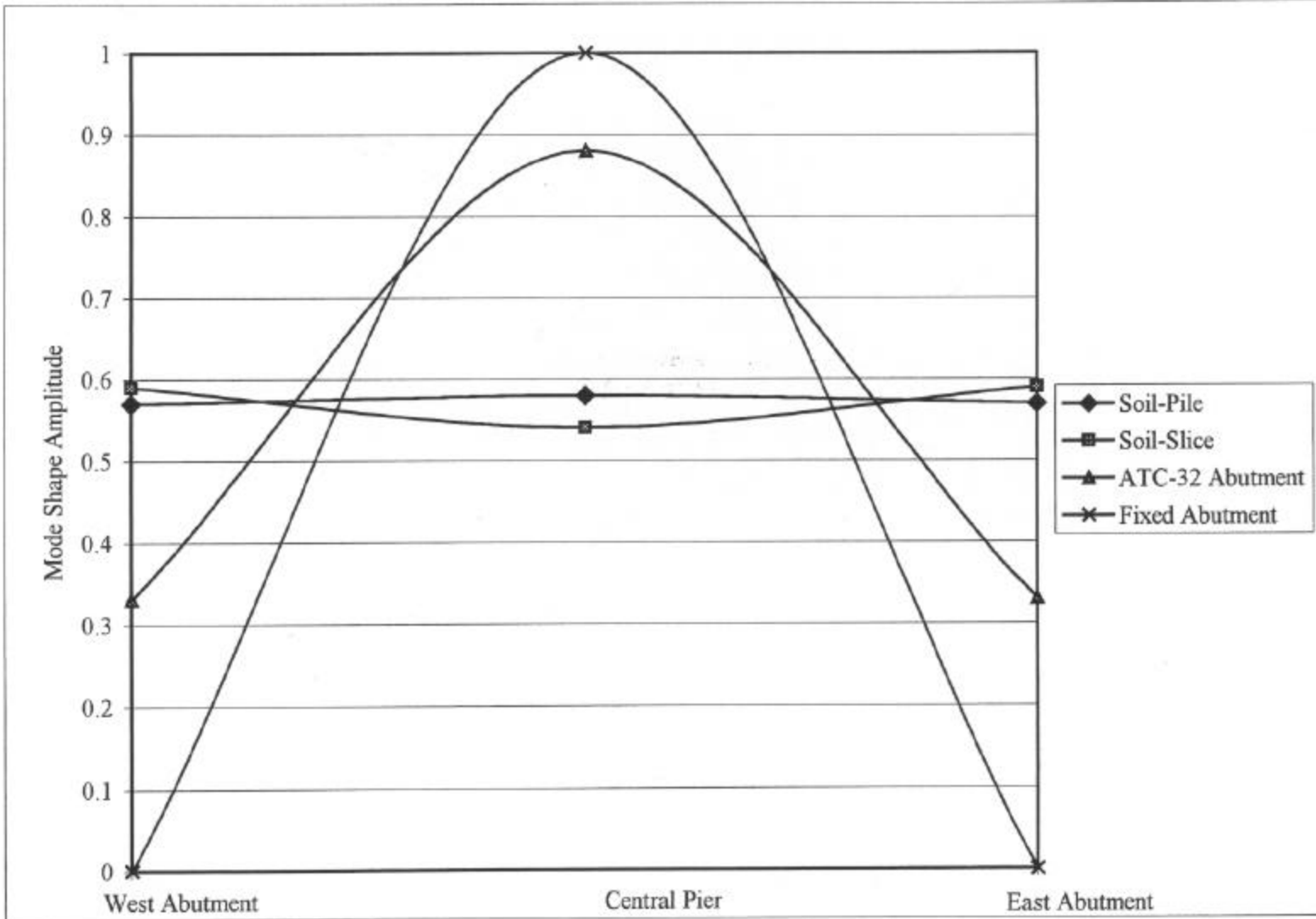


Figure 3.78 Comparison of First PCA Mode Shape for IL-2 Bridge Subjected to 1992 Main Event

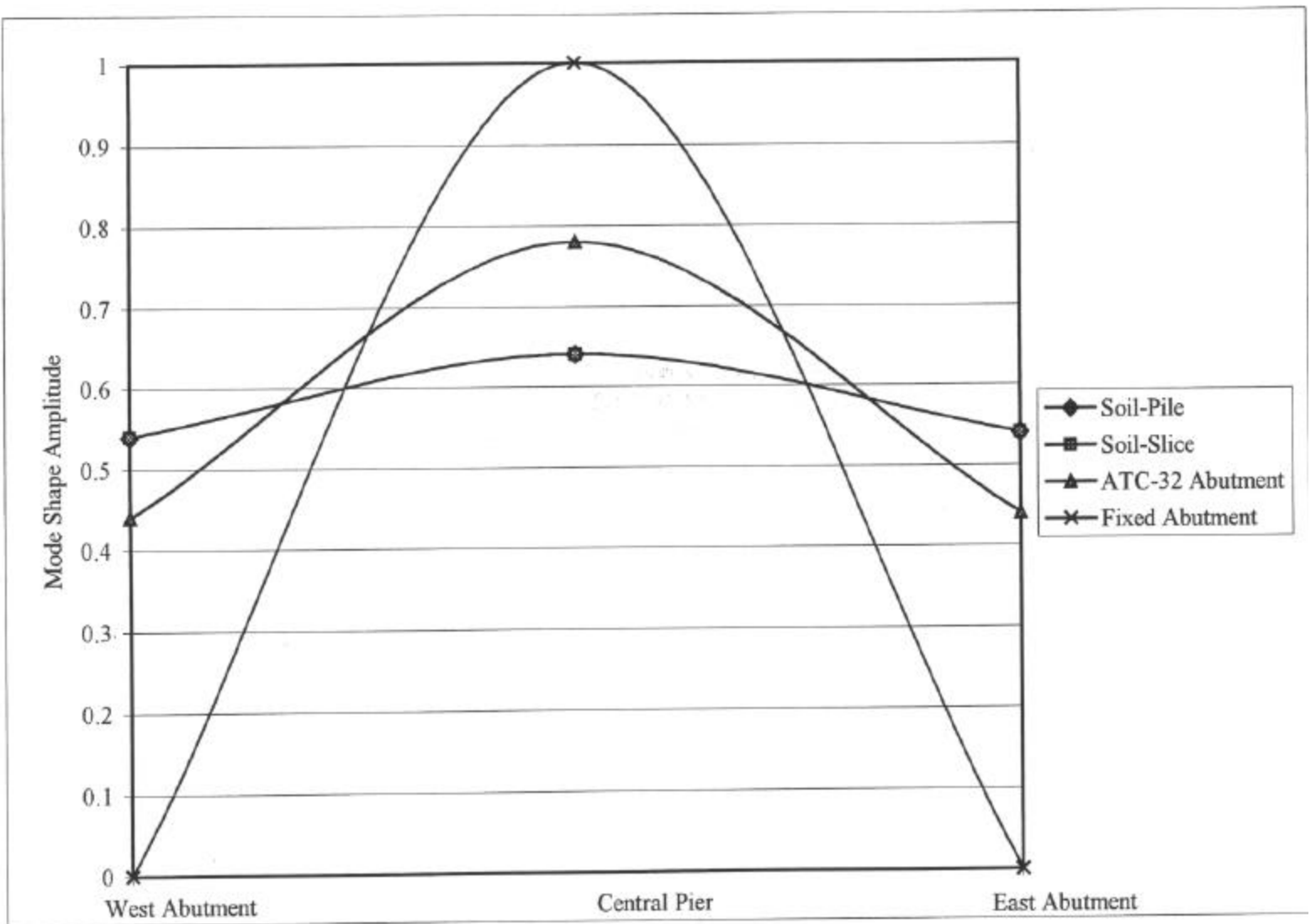


Figure 3.79 Comparison of First PCA Mode Shape for IL-2 Bridge Subjected to 1986 Main Event

## CHAPTER 4

## REVIEW OF ELASTOMERIC BEARING BEHAVIOR AND MODELING

4.1 Overview

Since the 1960s, elastomeric bearings have been used in structures such as bridges to accommodate thermally-induced displacement and rotation. The advantages of elastomeric bearings include low cost and low maintenance. Behavior of the elastomeric bearings is sensitive to the composition of the elastomers. Elastomers are nonlinear incompressible materials and may be natural or synthetic. They are flexible in shear but less flexible in uniaxial compression when used in thin layers sandwiched between stiff plates. Horizontal flexibility causes a period lengthening which can decrease the acceleration response in an earthquake, relative to cases in which fixed bearings are used. Since the 1980s, elastomeric bearings have been used in structures for seismic isolation.

Energy dissipation through hysteretic rubber deformation response also may decrease acceleration and displacement response in earthquakes. A lead core may be used to provide wind and braking resistance together with increased hysteretic energy dissipation through yielding of the lead core during seismic actions. In addition to an overview on elastomeric bearings, this chapter also describes the development of nonlinear models for three types of elastomeric bearings commonly used in Illinois to accommodate thermally-induced movement. These models are used in Chapter 6 to investigate bearing effectiveness for reducing column displacement demands during earthquakes.

## 4.2 General Characteristics

The mechanical behavior of elastomeric bearings is highly dependent on the material properties of the elastomer. Most elastomeric bearings are made of either natural rubber (NR) or synthetic rubber such as chloroprene (CR). The stress-strain behavior of both rubbers is highly nonlinear and is time, temperature, and frequency dependent. CR and NR stiffen at low temperatures. CR is more susceptible to low temperature stiffening than NR. The low temperature effect is discussed further in Section 4.3. NR is more susceptible to ozone cracking although this is usually controlled by adding an anti-ozonant chemical to the elastomer compound. Both NR and CR stiffen under dynamic loads. (Roeder and Stanton, 1983)

During manufacture, a raw rubber goes through a vulcanization process, which involves adding a cross-linking agent such as sulfur and applying heat and pressure. Fillers such as carbon black, processing oils, antioxidants and antiozonants are frequently added to the elastomer to aid the manufacturing process, to modify the hardness and adjust the stiffness, or to inhibit ozone cracking. High damping rubber may be created by adding a high percentage of carbon; Kelly (1991) reported 31 percent carbon filler in high damping Bridgestone test bearings.

Stanton and Roeder (1982) discussed several potential modes of failure as follows:

- (1) fatigue or endurance limits of the rubber;
- (2) internal rupture and tension cracking of the rubber;
- (3) reinforcement rupture or yield due to tensile stress;
- (4) delamination of reinforcement or bond failure;
- (5) serviceability failure due to excessive creep of the bearing; and,
- (6) buckling or instability of bearing.

These modes of failure are considered in the design of the bearings, particularly fatigue and tension cracking of the rubber. Fatigue cracks under compression are initiated at tensile stress concentrations at the edges of the bond interface between rubber and reinforcement. The tensile stress concentrations are normally caused by ozone cracking. For both causes, performance is improved when a protective rubber edge cover is provided. Vulcanization improves the bond between the steel reinforcement plates and rubber layers, and this can prevent delamination.

#### 4.3 Mechanical Characteristics

Elastomeric bearings have been used in a large number of experimental programs since the 1960s. Recent reports include those by Kelly et al. (1987), Kelly (1991), and Kelly, and Quiroz (1992), who determined the mechanical characteristics of bearings used for base isolation. They reported that the bearings are stiff at small shear strains. For intermediate strain levels (15-200 percent shear strain), the bearing secant stiffness is lower than at small strains. At larger shear strains, the secant stiffness increases, due to strain-induced crystallization. This behavior can be beneficial in seismic isolation, because the high stiffness at low strains provides stiffness for service conditions, while the reduced stiffness of the bearing at larger strains developed in seismic response causes a period lengthening in the structure. However, since physical gaps of specific sizes are provided around the isolated structure, some control over displacement response is helpful. The strain-induced crystallization at large strains ensures some degree of displacement control, though at the risk of increased strength demands in the structure above the isolation layer.



Elastomer stiffness increases at low temperatures. This increase in stiffness may occur during North American winter temperatures and can influence the effectiveness of the bearings as seismic isolators. Murray and Detenber (1961) conducted experiments to study the low temperature serviceability of elastomer products for Du Pont. They reported that the first order transition, neoprene crystallization causing a large increase in stiffness, is a completely reversible phenomenon and the rate of crystallization depends on temperature (Figure 4.1). Figure 4.1 also shows the dependency of the crystallization rate on the type of neoprene. The crystallization rate is retarded when the state of cure is more advanced and when compounding ingredients such as sulfur are used.

The second order transition temperature (glass transition temperature) is the temperature that turns the elastomer into a glasslike condition. This temperature is independent of the degree of crystallization. Figure 4.2 shows the variation in stiffness as a function of temperature for one sample of neoprene. For this sample, the stiffness increases by a factor of 10 when temperature was reduced below the second order transition temperature. Eyre and Stevenson (1991) also studied the low temperature behavior of elastomers. They tested sheet samples of elastomer layers taken from elastomeric bearing units. They found that the increase in stiffness depends not only on temperature but also on the duration of exposure to cold temperature and the formulation of the rubber. The first transition temperature was around -10 to -15 F. The increase in stiffness depended on the length of exposure to a low temperature. After approximately

-40 F, the rubber reached the second order transition (glass transition) temperature and became brittle. The increase in stiffness of different rubber compounds with respect to temperature is shown in Figure 4.3.

Seasonal temperature cycling effects on low temperature stiffening was investigated by Eyre and Stevenson (1991). A test specimen was subjected to temperature cycling between +25 C and -25 C. The “winter” period was represented by reducing the temperature to -25 C within 1 hour; shear modulus tests were then performed until 20 hours elapsed under the same temperature. The bearing was then exposed to a “summer” period, represented by raising the temperature to +25 C within 1 hour and held at that value for 1 hour. Winter-Summer cycles were repeated six times; results are shown in Figure 4.4. In general, the stiffness increases with exposure time. Subsequent winters caused a similar increase in stiffness, greater than the increase during the first winter. However, a lack of cumulative effect after the first winter suggests that a maximum stiffness increase can be reached after a single winter period.

In 1994, the Highway Innovative Technology Evaluation Center (HITEC) in collaboration with the California Department of Transportation (CALTRANS) and Federal Highway Administration (FHWA) developed an evaluation program for seismic isolation and energy dissipating devices. Several major bearing manufacturers participated in the program. Full scale dynamic tests were performed; results are summarized in Table 4.1.

Kelly (1996) studied the effect of age on seismic isolation bearings obtained from the Foothill Communities Law and Justice Center in San Bernardino County, CA. After ten years of use in the building, bearings were removed and tested. The bearings showed a 15 percent decrease in shear stiffnesses and virtually identical compression stiffnesses to values obtained for

the same bearings prior to original installations. Prior to Kelly's study in 1996 where there was no published data on the tests of aged rubber bearings, Martin (1991) commented that there should not be much difference due to aging between seismic and non-seismic isolation bearings. This is because the materials and manufacturing processes are basically the same. The only major difference is the performance requirements; the seismic isolation bearings are designed to withstand larger earthquake-induced deformations.

#### 4.4 DIS Lead-Rubber Isolators

A commonly-used isolation bearing is manufactured by Dynamic Isolation Systems, Inc. (DIS). In the DIS lead-rubber bearing, a lead core is located at the center of the bearing. The yield stress in shear of the lead core is very low (~ 1.5 ksi.) (Kelly et al. 1986); the core is intended to yield during an earthquake but remain elastic under service loading. The force-displacement relationship of the bearing may be represented by a bilinear hysteretic model as shown in Figure 4.5. (Dynamic Isolation Systems 1993) It is stated in FEMA 274 (1996) that the characteristic strength,  $Q_d$ , is related to the area of the lead plug,  $A_p$ , and the shear yield stress of lead,  $\sigma_{YL}$ . According to FEMA,  $Q_d$  is written as

$$Q_d = A_p \sigma_{YL} \quad (4.1)$$

The post-yield stiffness,  $K_d$ , is higher than the shear stiffness of the bearing without the lead core since the lead core helps resist the force after it reaches yield.

$$K_d = \frac{A_r G_r f_L}{\sum t_r} \quad (4.2)$$

where  $A_r$  = bonded rubber area

$\sum t_r$  = total rubber thickness

$G_r$  = shear modulus of rubber (typically the secant modulus computed at 50 percent shear strain)

$f_L$  = a factor larger than 1, typically = 1.15

For typical bearings, the post-yield stiffness is approximately increased by 15 percent above the bearings without lead. The elastic stiffness,  $K_u$  ranges between 6.5-10 times the post-yield stiffness,  $K_d$  depending on the lead core. The equivalent viscous damping,  $\beta$ , can be approximated as

$$\mathbf{b} = \frac{W_D}{2\mathbf{p}K_{eff}\Delta_m^2} \quad (4.3)$$

where  $W_D$  = the total area under the hysteresis loops

$K_{eff}$  = the effective stiffness as shown in Figure 4.5

$\Delta_m$  = the maximum displacement as shown in Figure 4.5

The equivalent viscous damping above is based on modeling the bearing as an elastic and linear viscous element. It is derived from assuming a single degree of freedom is subjected to sinusoidal displacement cycles.

#### 4.5 Sliding Bearing

Kelly and Chalhoub (1990) carried out an experiment to investigate a combined sliding bearing, and rubber bearing isolation system. The sliding bearing consisted of a layer of teflon in contact with a stainless steel plate, as shown in Figure 4.6. The teflon layer was 1/25 inch thick, and the stainless steel was 1/32 inch thick. Their areas were 10x7 and 10.5x7.5 inches square, respectively. The sliding bearings only allowed movement at the teflon-steel interface; the rubber bearings did not provide a sliding surface. Thus, the structure is supported on the isolation system, which consists of sliders in parallel with the rubber bearings.

The investigators found a reduction in relative displacement under earthquake excitations when the sliding bearings were used, attributed to energy dissipation provided mostly by friction on the teflon sliding surfaces. The rubber bearings provided additional stiffness, both prior to and during sliding. The coefficient of friction of the teflon-stainless steel interface can vary from 5-17 percent. Kelly and Chalhoub (1990) found the coefficient of friction increases with sliding velocity but decreases with increasing normal pressure.

#### 4.6 Illinois Bearings

Elastomeric bearings have been widely used in Illinois bridges since the 1970s. The elastomeric bearing assemblies used in Illinois consist of three types (see Figure 4.7), each able to accommodate different degrees of thermal expansion. The bearings were not designed for seismic isolation, though they may be suitable for this purpose. Type I bearing is a conventional steel-laminated elastomeric pad in which all movement is taken by rubber distortion. Type II has a teflon sliding surface that provides initial slippage shortly after the bearing is installed. This allows the bearings to be installed at any time of the year, regardless of temperature.

Temperature induced movements cause the bridge to center itself over the bearings, and once centered, no additional slip is intended. Type III bearings are used for spans longer than about 45 m. The Type III assembly is the same as for Type II, but a shear restrictor pin is added to prevent overstress in the rubber in shear. For this bearing assembly, any further movement is accommodated by slip on the teflon surface after the shear restrictor pin locks up against the elastomer.

Unlike the lead in a lead-rubber bearing commonly used in base isolation, the yield strength of a shear restrictor pin in Type III bearings is very high. Wieser (1980) reported a tensile yield stress of 210 ksi for the AISI 4340 quenched and tempered low alloy steel used for restrictor pins. Assuming a coefficient of friction of 7 percent and a Type III bearing size of 12in. x 18in., the vertical bearing pressure would need to be 15 ksi to induce enough force to yield the shear restrictor pin. It is evident that the shear restrictor pins are unlikely to yield in an earthquake event. Its intended role is to limit the shear strain in rubber and force additional displacement to occur at the teflon sliding surface.

Jacobsen (1977) tested the three types of elastomeric bearings used in Illinois. He found that the coefficient of friction at the teflon sliding surface decreases with increasing pressure, and it ranges between 7 to 20 percent. These compare well with the range of 5 to 17 percent reported later by Kelly and Chalhoub (1990). Figure 4.8 shows that the coefficient of friction increases after several thousand cycles, observed in repetitive tests of the Type III bearings.

#### 4.6.1 Modeling of Type I Bearings

Type I bearings are comprised of only steel-reinforced elastomer layers. An approximate bilinear curve (Figure 4.9) was used to model the nonlinear response of steel-reinforced elastomeric bearings based on test results reported by Kelly and Quiroz (1992). The curve is fit to approximately match the initial stiffness of the bearing and its energy dissipation characteristics. Such a curve may be implemented in simple nonlinear analysis programs that use bilinear elements. Iteration is required to determine the force at which “yielding” occurs. A post yield stiffness of about 50 percent of the initial stiffness was a reasonable approximation to the Kelly and Quiroz test results over a range of shear strains up to 200 percent.

In this model, it is assumed that the shear stresses are uniform over the width of the bearing. Assuming simple shear deformation in the elastomer layers,

$$K_1 = \frac{G_r A_r}{\sum t_r} \quad (4.4)$$

where  $G_r$  = low strain shear modulus of rubber

$A_r$  = total rubber area

$\sum t_r$  = total rubber thickness, summed over the individual layer thicknesses

The iterative nonlinear model in Figure 4.9 is adjusted as follows: (1) the yield force,  $F_y$ , is assumed; (2) the post-yielding stiffness,  $K_2$ , is assumed to be one-half of the initial stiffness,  $K_1$ ; (3) the nonlinear analysis is performed; (4) the value of yield force,  $F_y$ , is revised, is taken as one-half the maximum force,  $F_{\max}$ , developed in the previous analysis. This process is repeated until  $F_y$  converges.

This calibration is intended to give a good match for initial stiffness and a good result for peak displacement response, since peak displacement response is usually governed by just a

few high amplitude cycles. It is for these high amplitude cycles that the energy dissipated by the bearing is approximately matched; intermediate responses will be poorly estimated because softening may not be captured for these cycles. The models are based upon tests of low shape factor bearings under vertical pressures of less than 1000 psi and a maximum strain less than 200 percent. Elastomeric bearings used in many bridge applications meet the above limitations.

#### 4.6.2 Modeling of Type II Bearings

A Type II bearing consists of steel-reinforced elastomer layers together with a teflon sliding surface. The bearing system can be modeled using a Coulomb unit connected in series with a Type I rubber bearing, modeled as shown in Figure 4.10. The force in rubber,  $F_{\max}$ , is limited to the frictional force required to cause sliding on the teflon surface. Gravity load usually is assumed constant, representing an assumption that vertical acceleration can be neglected. If the maximum force in rubber,  $F_{\max}$ , is below the frictional force, the bearing works like a Type I bearing.

#### 4.6.3 Modeling of Type III Bearings

A Type III bearing differs from a Type II bearing in that it has a steel alloy pin inserted in the bearing. This pin will not yield in the event of an earthquake if the slip force is less than the yield force of the pin. To model the bearing-pin contact that occurs when bearing deformations are large enough, tension and compression gap elements are connected in series with a stiff pin. The rubber unit is connected in parallel with the gap and pin. The rubber, pin, and gap are then connected to the slider in series. This can be seen schematically in Figure 4.11. In this type of



Table 4.1 HITEC Results for Temperature Effects on Bearings.

Bearing Manufacturer	Increase in Shear Stiffness, as percent of Initial Stiffness
Dynamic Isolation Systems -15 F (-26 C) for 2 days	23 %
Skellerup -20 F (-29 C) for 2 days	56 %
Tekton -20 F (-29 C) for 2 days	88 %
Scougal -40 F (-40 C) for 4 days	>3000 %

\* Bearings were stored in a cold chamber for the time specified. Then they were removed and tested under reversed cyclic sinusoidal loading at 0.5 Hz. No more than 75 minutes elapsed between removal and the start of testing; each test lasted about 5 minutes.

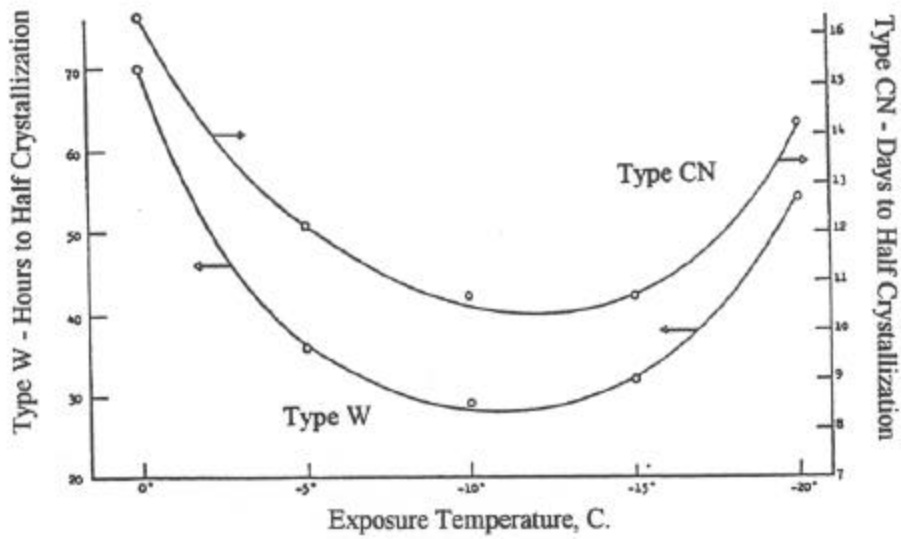


Figure 4.1 Effect of Temperature on Crystallization Rate (Murray and Detenber 1961)

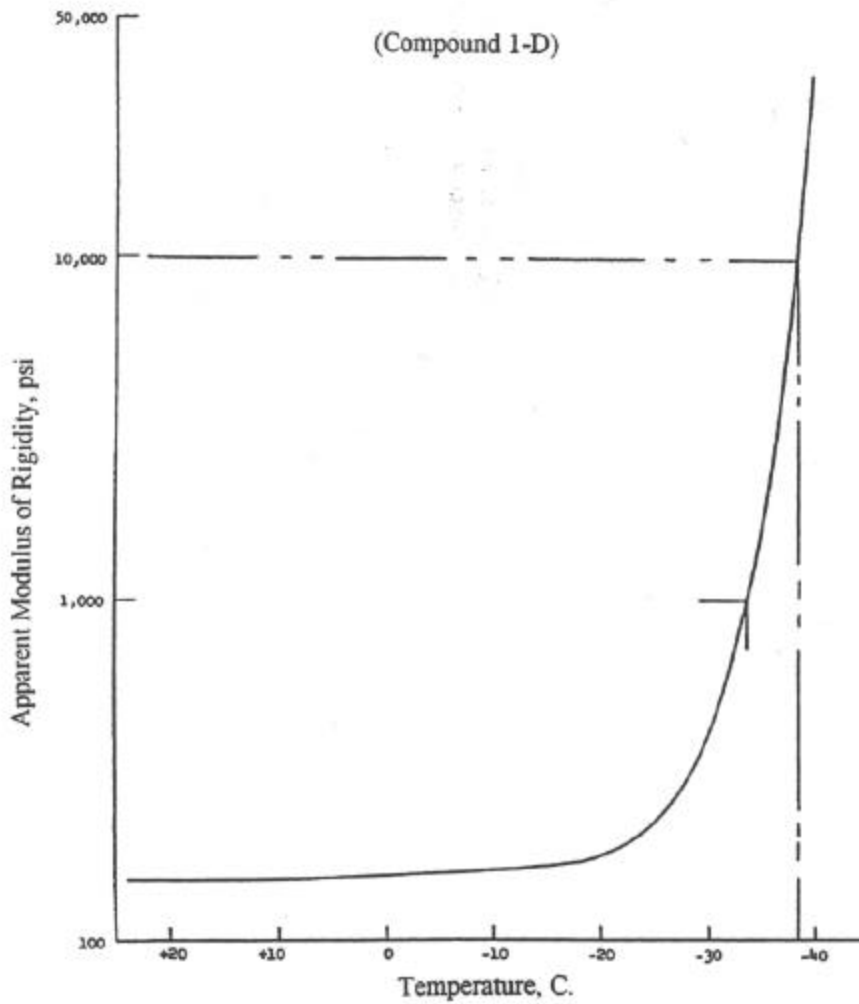


Figure 4.2 Effect of Temperature on Stiffness (Murray and Detenber 1961)

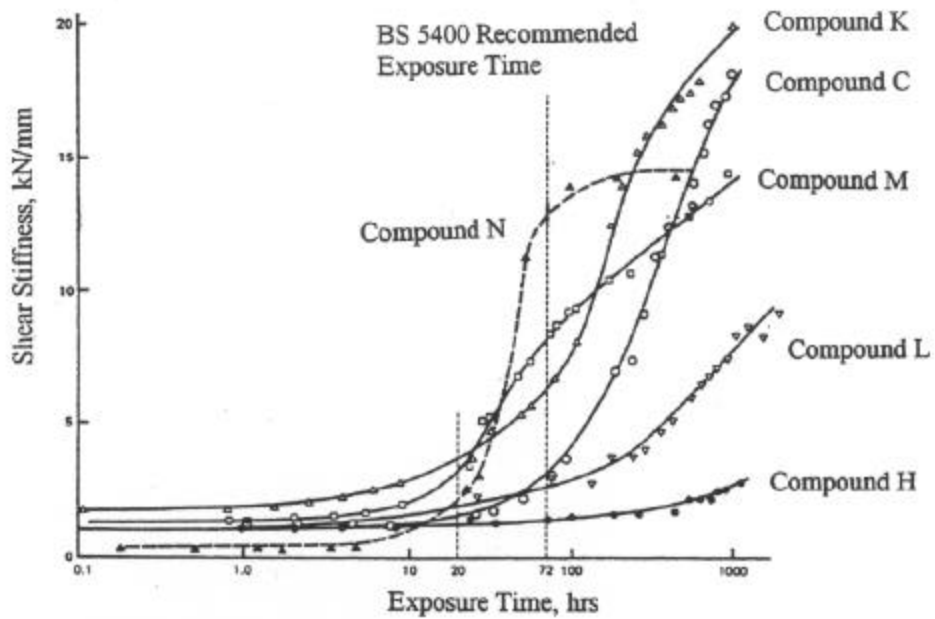


Figure 4.3 Increase in Shear Stiffness with Exposure time (Hours) to -13 F (-25 C) (Eyre and Stevenson 1991)

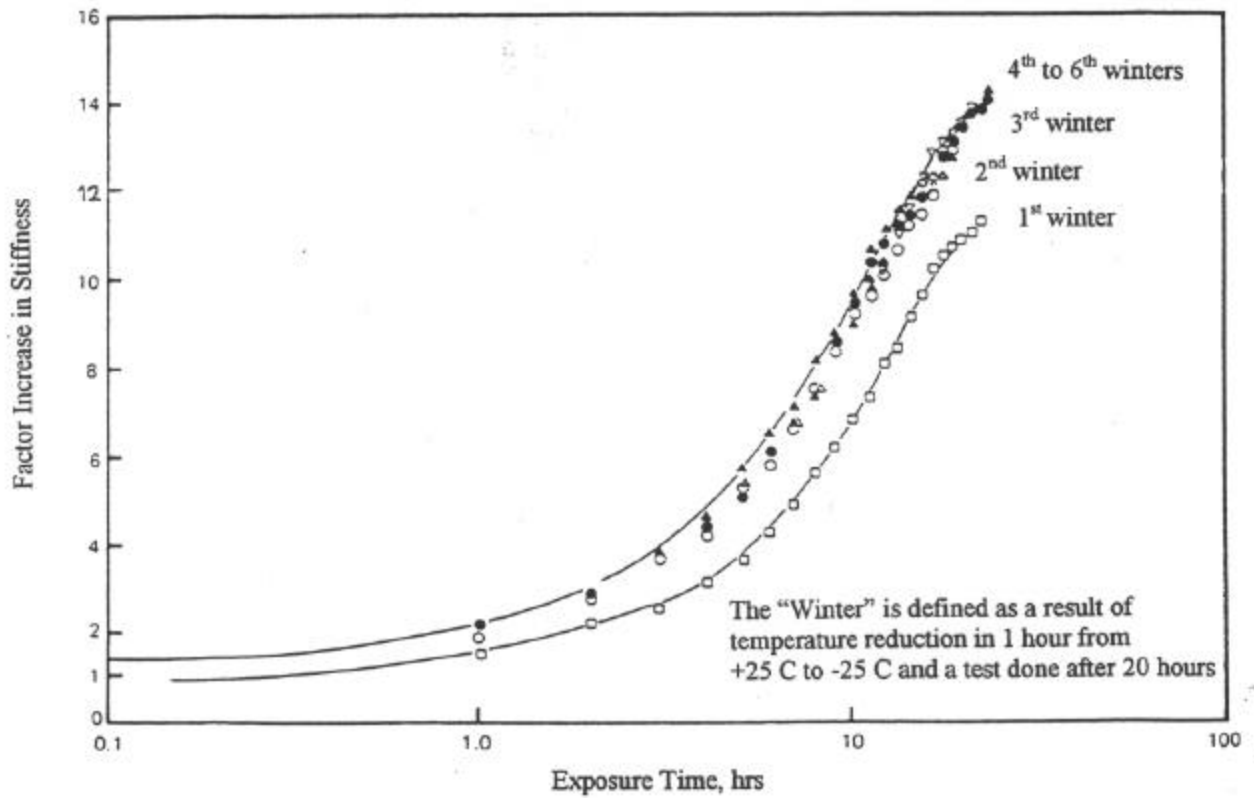


Figure 4.4 Effect of Freeze-Thaw Cycles on Low Temperature Stiffening (Eyre and Stevenson 1991)

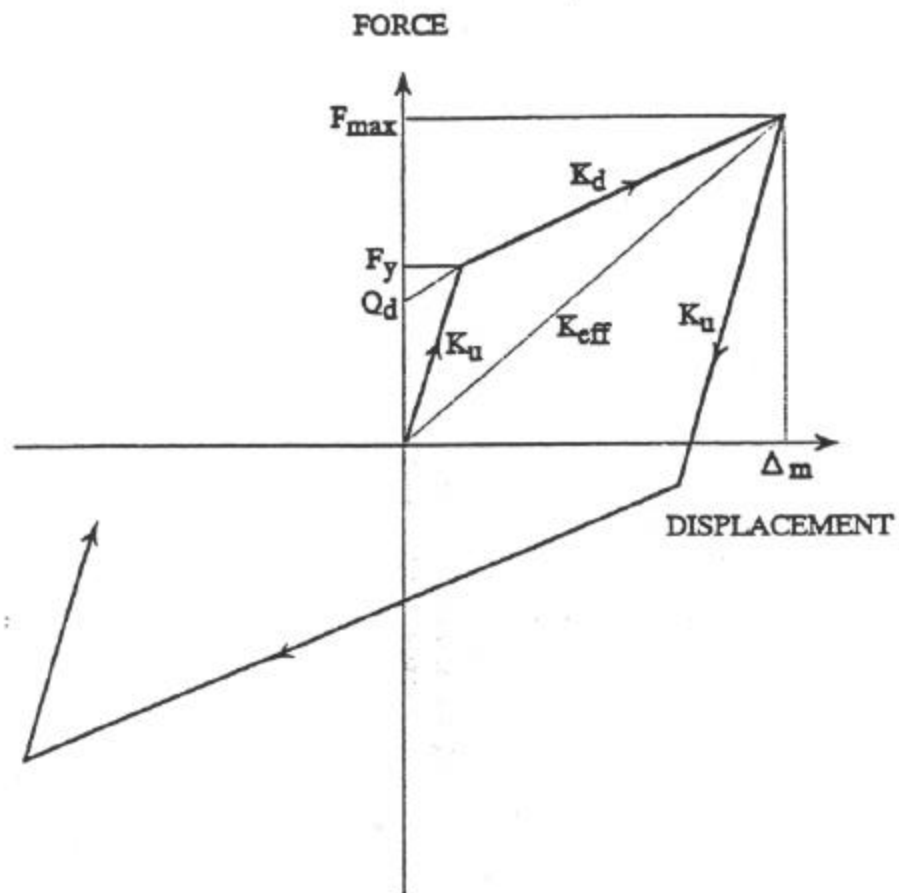


Figure 4.5 Force Displacement Relationship for DIS Lead-Rubber Isolators (Dynamic Isolation System 1993)

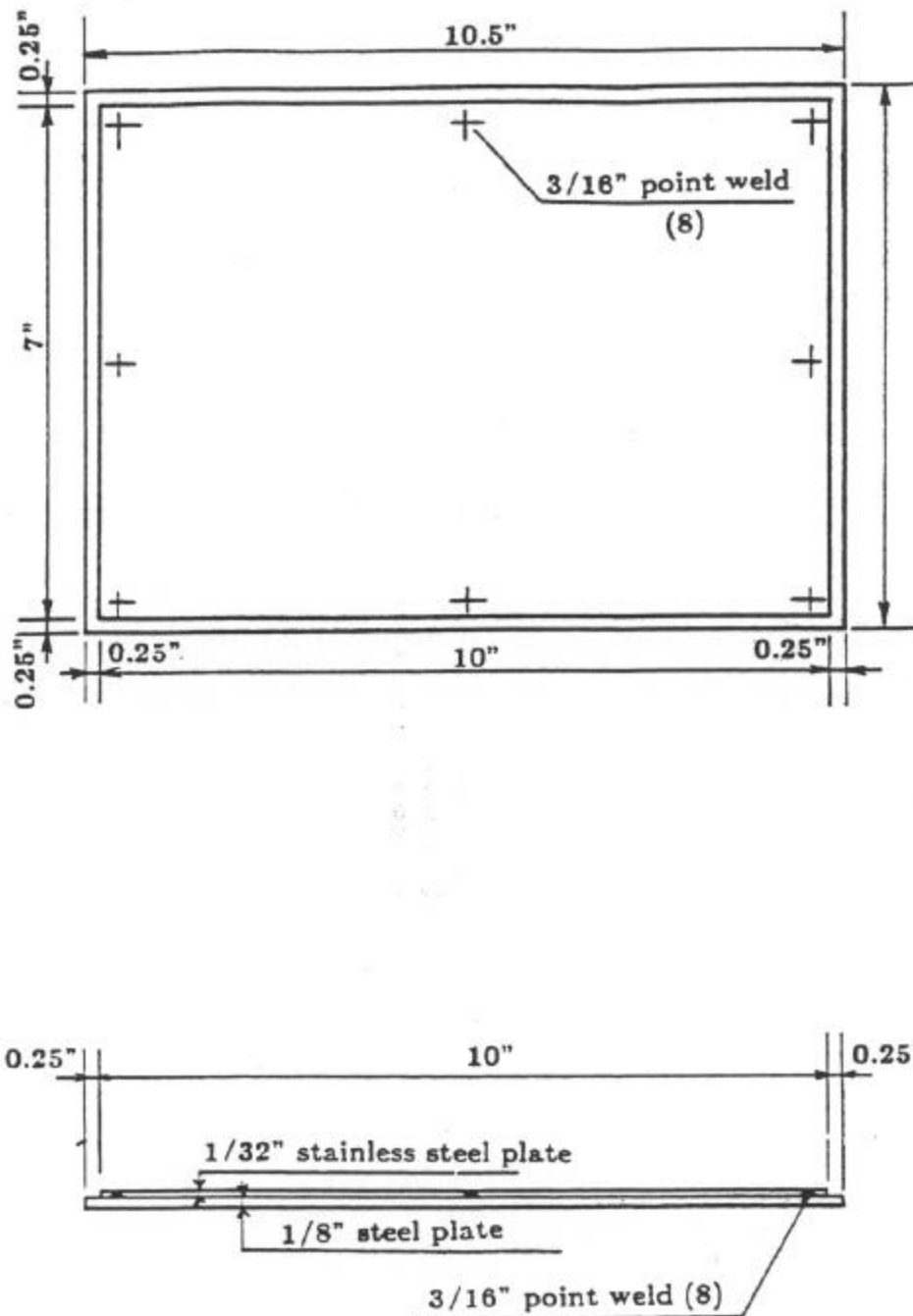


Figure 4.6 Teflon-Stainless Steel Slider Showing Dimensions (Kelly and Chalhoub 1990)

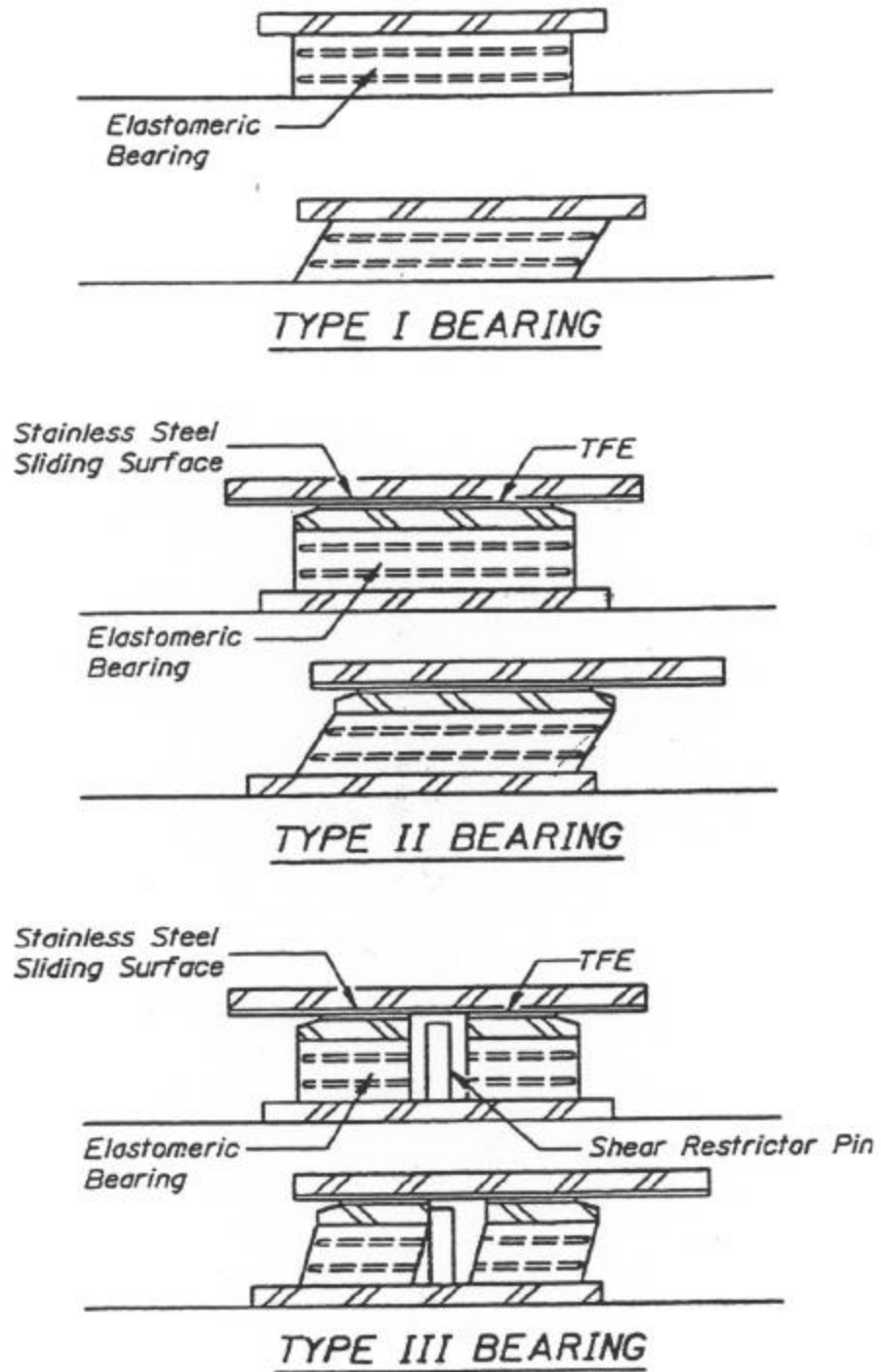


Figure 4.7 Elastomeric and TFE Elastomeric Expansion Bearings used in Illinois (Jacobsen 1977)

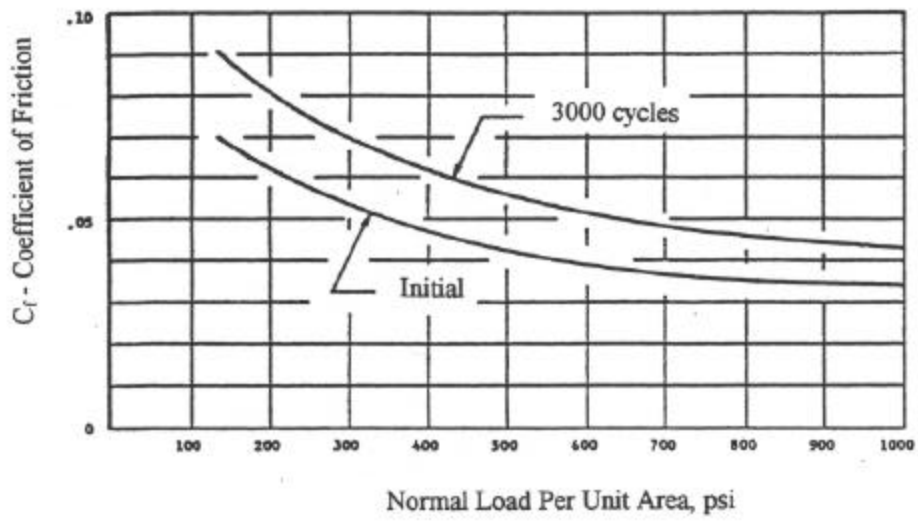


Figure 4.8 Coefficient of Friction vs. Vertical Pressure for Laminated Elastomeric - TFE Sliding Bearing (Jacobsen 1977)

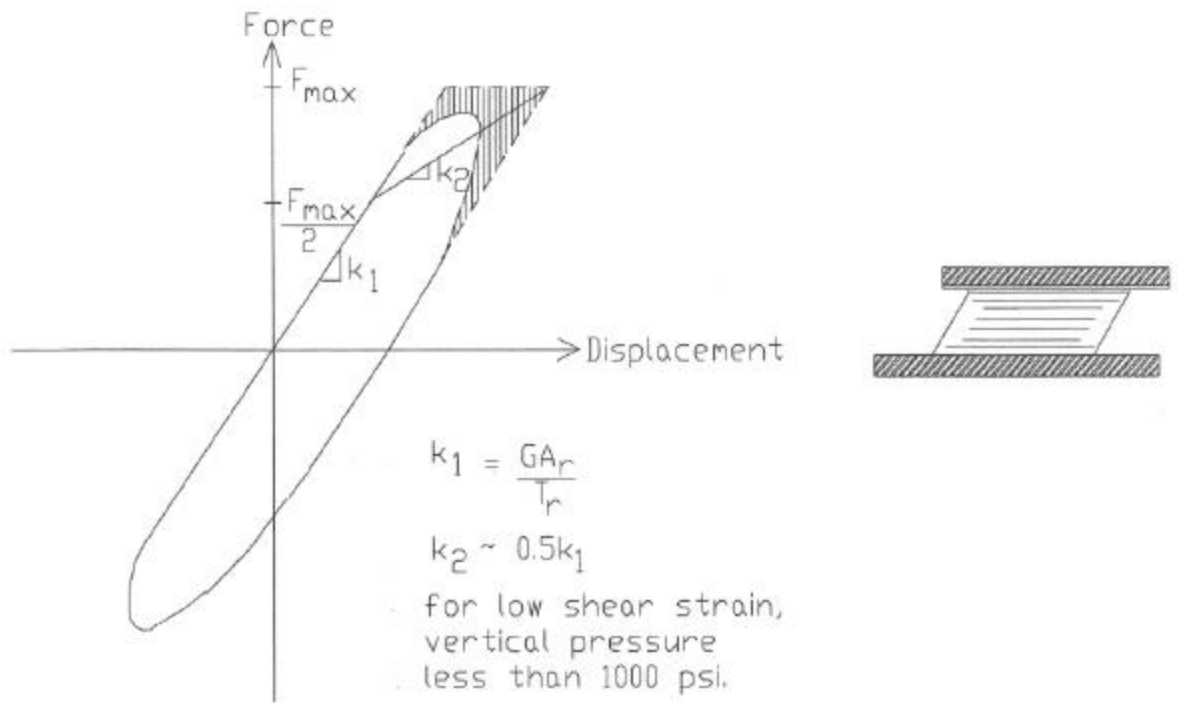


Figure 4.9 Modeling of Type I Bearing (Without Teflon Sliding Surface)

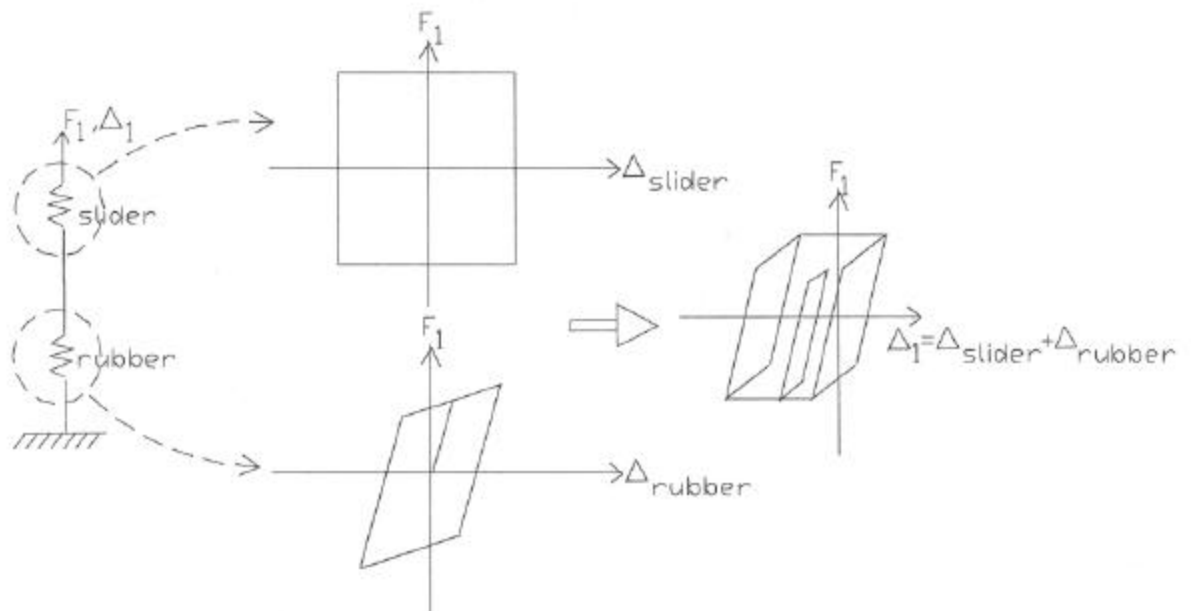


Figure 4.10 Modeling of Type II Bearing (With Teflon Sliding Surface)



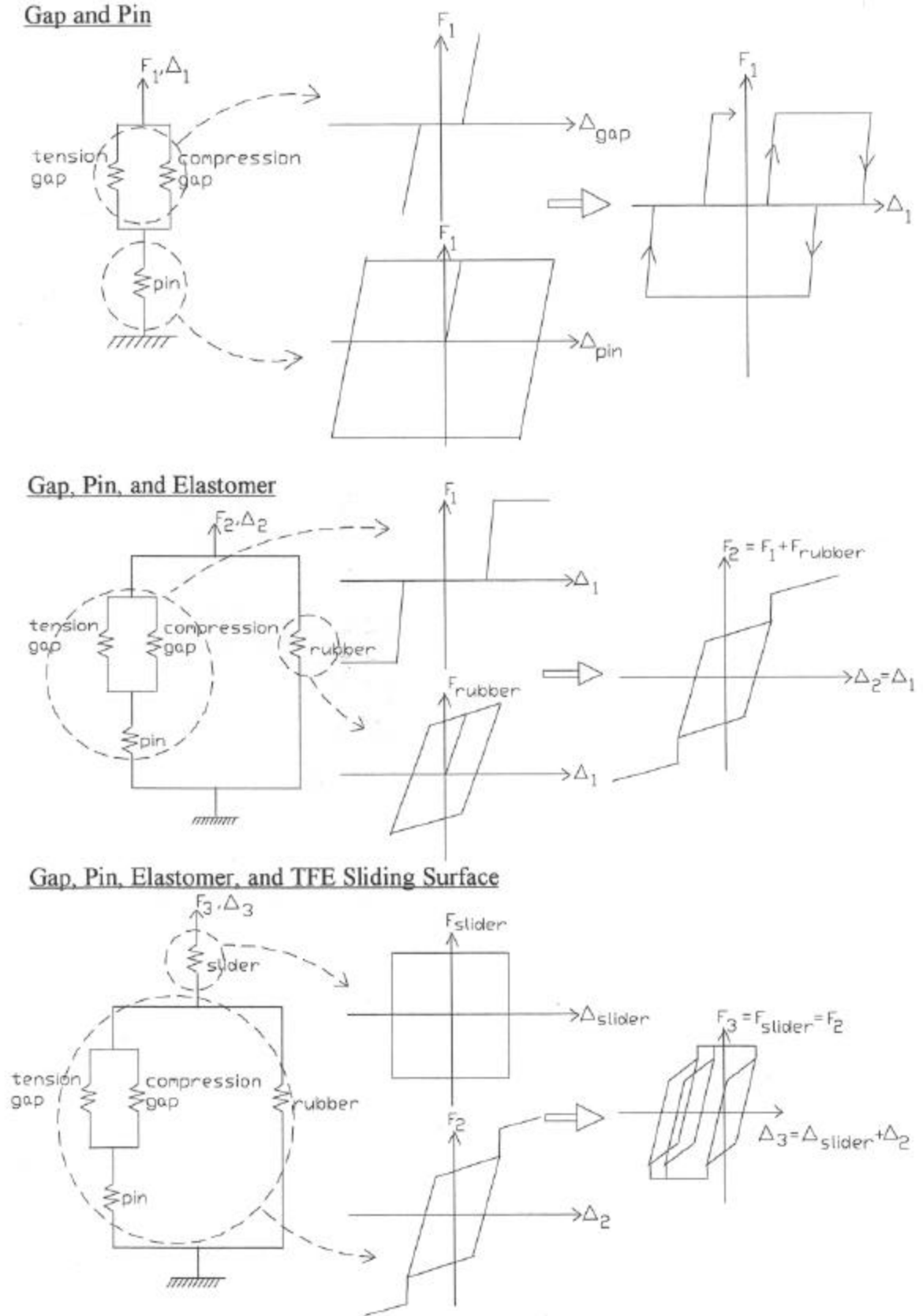


Figure 4.11 Modeling of Type III Bearing with Sequence of Model Construction

## CHAPTER 5

### MODELING OF BRIDGE COMPONENTS

#### 5.1 Introduction

Elastomeric bearings such as the three types commonly used in Illinois to accommodate thermal movement may reduce bridge damage during earthquakes. Analytical models for these bearings were presented in Chapter Four; these models are used in Chapter Six to investigate the effectiveness of these bearings for reducing column displacement demands in earthquakes. Chapter Three discussed the modeling of approach-embankments; Chapter Four discussed the modeling of the bearings; and this chapter presents conventional modeling guidelines for other bridge components.

Short- and medium-span bridges in Illinois often are composed of a concrete deck on multiple-steel-girders, with multiple-column piers supported on pile foundations. In past earthquakes, older reinforced concrete pier columns have been shown to be one of the most vulnerable bridge components. Concrete columns designed prior to the 1970s are likely to have low confinement, which may lead to a loss of flexural capacity or shear failure if displacement demands are large. The analytical study of Chapter Six focuses on the transverse response of concrete pier columns. For bridges with little or no skew, a two-dimensional bridge model is adequate for the purpose of identifying performance improvements that may result from the use of elastomeric bearings.

This chapter describes the modeling of a bridge representative of central U.S. slab-on-girder construction. Bridges in the central U.S. often have a concrete deck supported on multiple-steel-girders, in turn supported on multiple-column piers, founded on piles as shown in

Figure 5.1. For bridges with little or no skew, a two-dimensional bridge model is considered to be adequate. The bridge deck was modeled as a stick beam element. Transverse resistance from the piers and pile foundations at piers were modeled using bilinear springs in the horizontal plane of the bridge. The properties of these springs were determined by separate analyses of the piers and pile foundations.

## 5.2 Modeling of Bridge Deck

A bridge deck which is a concrete slab on multiple-steel-girders is modeled as a stick beam. Deck mass is lumped at the nodes which are distributed along the bridge. Enough nodes must be provided between supports to admit higher modes, should they be significant. Different recommendations have been given for modeling of the moment of inertia of the deck, ranging from a non-composite cracked slab to a fully composite gross section slab, as described below and shown in Figure 5.2.

*1. Fully-Composite (Upperbound).* Fully composite action between concrete slab and steel girders is assumed. This is the upper bound value of deck moment of inertia. This is calculated as the sum of the gross moment of inertia of the slab and the moment of inertia of the steel sections.

*2. ATC-32 Recommendation.* This is calculated as the sum of 75 percent of the gross moment of inertia of the slab and 75 percent of the moment of inertia of the steel section.

3. *Shear Lag in Girders.* The gross moment of inertia of a concrete slab is used. However, only half the area of the steel girders is used in calculating moment of inertia of the composite steel-concrete section. (Foutch et al. 1997). The reduction in steel area is intended to account for shear lag effects in the steel girders. These effects would be expected to be greater in section with deep, slender webs and for longer spans.

4. *Uncracked Slab, Non-Composite.* Only the gross moment of inertia of concrete slab is considered.

5. *Cracked Slab, Non-Composite (Lowerbound).* Only the cracked moment of inertia of concrete slab is considered.

The numerical values for the bridge deck moment of inertia are 6.89, 5.16, 5.22, 3.55, 1.21 m<sup>4</sup> respectively for the above assumptions. A preliminary analysis showed the overall response of the bridge is not very sensitive to variation in the deck moment of inertia over these ranges. Rather, it is the approach-embankment flexibility that has the most significant influence.

### 5.3 Modeling of Bridge Bents

#### 5.3.1 Nonlinear Static Push-Over Analysis

Transverse resistance from the pier-columns are approximated by bilinear springs. The springs are attached to the deck nodes in the horizontal plane of the bridge at deck level. One approach is to perform a nonlinear static push-over analysis as shown in Figure 5.3 to determine

load-deflection relationship for use in DRAIN-2DX model. Rigid end offsets in the cap beam were used, assumed equal to one hundred percent of the physical column-cap joint dimensions. Fifty percent of gross moment of inertia was used in columns, while one hundred percent of gross moment of inertia was used in the bent cap. The plastic hinge beam-column element of DRAIN-2DX (Element 02) is used in the nonlinear static push-over analysis, and the computed force-displacement response is then approximated by a bilinear model (pier spring). In the analyses of the entire bridge system, a control spring is added in series with the pier spring; both the control spring and the pier spring utilize the simple connection element of DRAIN-2DX (Element 04). The purpose of the added spring is to model the load-deformation relationship as tri-linear. This represents a cap in the strain hardening obtained from the bilinear spring in the bridge system.

### 5.3.2 Displacement Capacity

This displacement capacity is compared with the displacement demands computed in Chapter Six. The method proposed by Pujol (1997) is adopted for calculating the yield and ultimate displacement capacity of reinforced concrete columns. The data that Pujol considered included both ductile and non-ductile columns.

According to Pujol, the yield displacement ( $\Delta_y$ ) is composed of displacement due to flexure ( $\Delta_{flexure}$ ), shear deformation ( $\Delta_{shear}$ ), and reinforcement slip ( $\Delta_{slip}$ ):

$$\Delta_y = \Delta_{flexure} + \Delta_{shear} + \Delta_{slip} \quad (5.1)$$

Pujol's derivation was based on the displacement of a cantilever column. However, the displacement equations can be derived for other boundary conditions such as the one shown in Figure 5.4. In this case, the column is fixed at the bottom but free to translate at the top without any rotations. For this condition, the displacement equations are as follows:

$$\Delta_{flexure} = \mathbf{f}_o \frac{\left(\frac{L}{2} - d\right)^2}{3} + \mathbf{f}_y \frac{\left(\frac{L}{2}\right)^2}{3} \quad (5.2)$$

$$\mathbf{f}_o = \mathbf{f}_y \left(\frac{L}{2} - d\right) \left(\frac{2}{L}\right) \quad (5.3)$$

$$\Delta_{shear} = \frac{6V_y L}{5G_c A_g} \quad (5.4)$$

where  $L$  = the column length (in.),  $d$  = the effective depth of the section (in.),  $\phi_y$  = the curvature at yield (rad/in.),  $V_y$  = the lateral load at yield (lbs.),  $G_c$  = the concrete shear modulus (psi) (approximately equal to Young's modulus/2.4), and  $A_g$  = the gross area of the cross section (in<sup>2</sup>).

$$\Delta_{slip} = \frac{(\epsilon_y + \epsilon'_c)d + slip}{2d - h} L \quad (5.5)$$

$$slip = \frac{\epsilon_y d_b f'_y}{8\mu_b} \quad (5.6)$$

where  $\epsilon_y$  = the longitudinal reinforcement yield strain,  $\epsilon'_c$  = the unit strain corresponding to the compressive strength of the concrete,  $h$  = the total depth of the section (in.),  $d_b$  = the bar diameter (in.),  $f'_y$  = the yield stress of the longitudinal reinforcement (psi.), and  $\mu_b$  = a bond stress of  $15\sqrt{f'_c}$  in psi units.

The ultimate displacement or the drift capacity of the column suggested by Pujol (1997) is

$$[\mathbf{q}_{\text{limit}}]_{\%} = \left[ \frac{V_s}{V_p} \right] \frac{a}{d} \leq \min \begin{cases} \frac{a}{d} \\ 4 \end{cases} \quad (5.7)$$

$$V_s = \frac{A_v f_y d}{s} \quad (5.8)$$

$$V_c = 2 \left[ 1 + \frac{N}{2000 A_g} \right] \sqrt{f'_c} b_w d \quad (5.9)$$

$$V_p \leq V_n = V_c + V_s \quad (5.10)$$

and  $\theta_{\text{limit}}$  = the drift capacity of the column (percent),  $V_s$  and  $V_c$  are estimated using Equations 5.8 and 5.9,  $a/d$  = the column aspect ratio, where  $a$  = the shear span and  $d$  has been previously defined,  $A_v$  = the area of transverse steel (in<sup>2</sup>),  $f_y$  = the yield stress of transverse steel (psi.),  $s$  = the spacing between transverse steel (in.),  $N$  = the axial load in the column (lbs.),  $f'_c$  = the compressive strength of concrete (psi.), and  $b_w$  = the width of the section (in.).

#### 5.4 Modeling of Bridge Pier Foundation

The pier foundation stiffness is represented by a translational spring. Nonlinear p-y analysis was performed, using COM624 computer program (Sullivan et al. 1980) as shown in Figure 5.5. Site-specific soil properties such as effective unit weight, undrained shear strength, and the angle of internal friction are entered into the program. P-y curves are generated in the

program, based on the following p-y criteria depending on the soil type: soft clay (Matlock 1970); stiff clay below the water table (Reese et al. 1975); stiff clay above the water surface (Reese and Welch 1975); sand (Reese et al. 1974); and uniform criteria for clay (Sullivan et al. 1977).

### 5.5 Modeling of Bridge Abutment

In the next chapter, the approach embankment model developed in Chapter 3 will be compared with the ATC-32 recommendation for abutment modeling. In the ATC-32 recommendation, the abutment wingwall stiffness can be calculated based on a passive earth pressure of 7.7 ksf. The wall is assumed to be effective up to the depth of 8 feet. The effective width for a cantilever wall is limited to 5 feet. One wingwall is assumed to be fully effective and another is only 1/3 effective. The ultimate passive pressure is mobilized at 0.01 times the wall height. An assumed pile stiffness of 40 kips/in per pile is used.



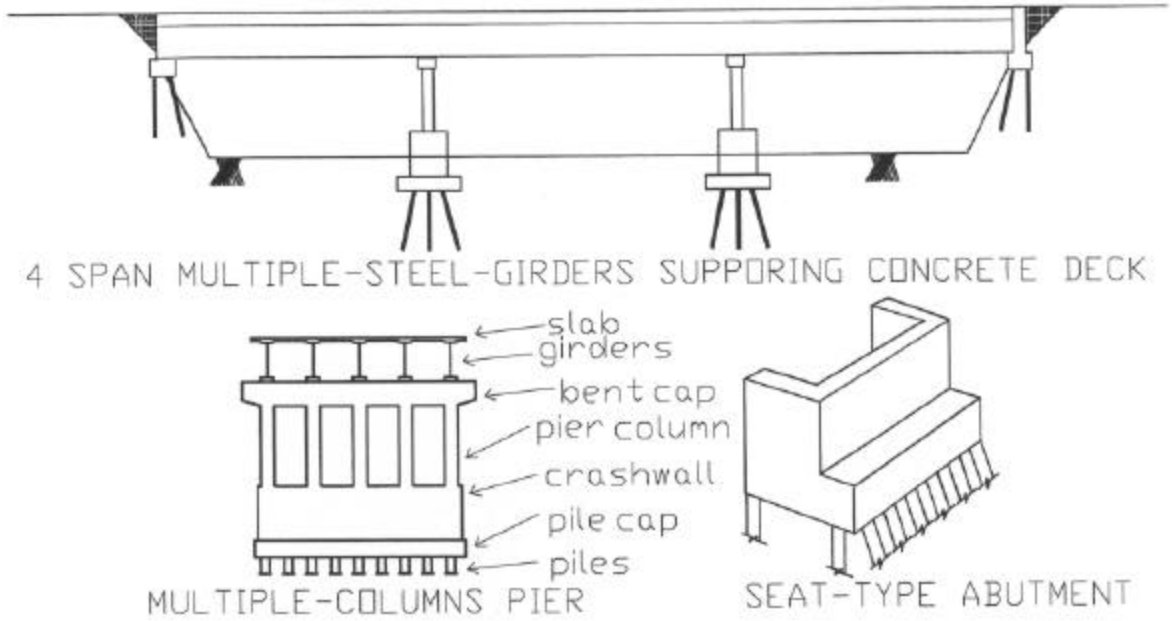


Figure 5.1 A Representative Four-Span Bridge Commonly in Illinois

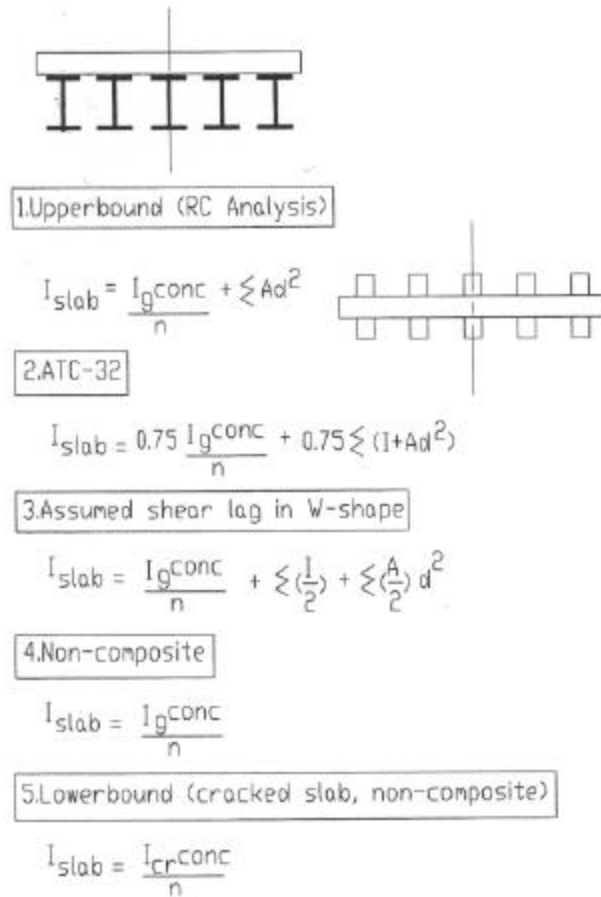


Figure 5.2 Ranges of Deck Moment of Inertia Used in the Model

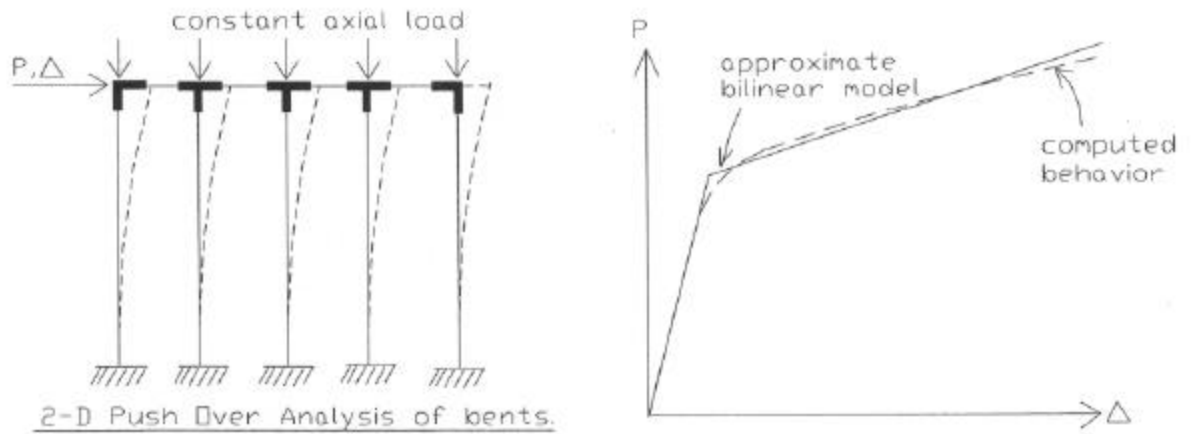


Figure 5.3 Nonlinear Static-Pushover Analysis for Multiple Pier-Columns

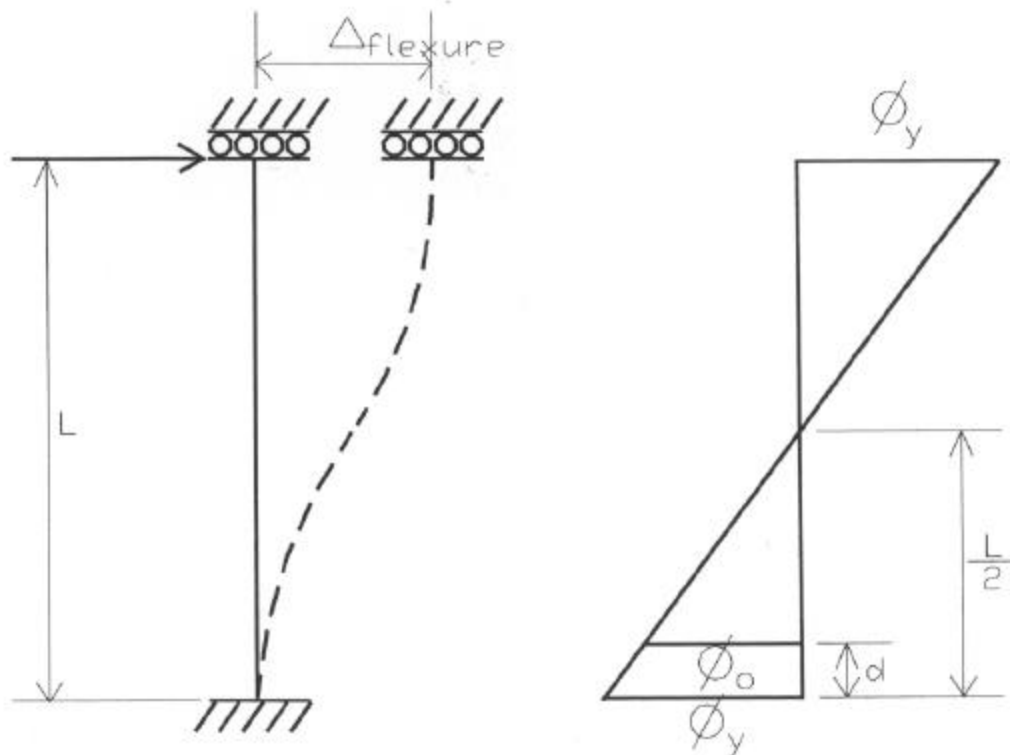


Figure 5.4 Flexure Contributions to Column Yield Displacement

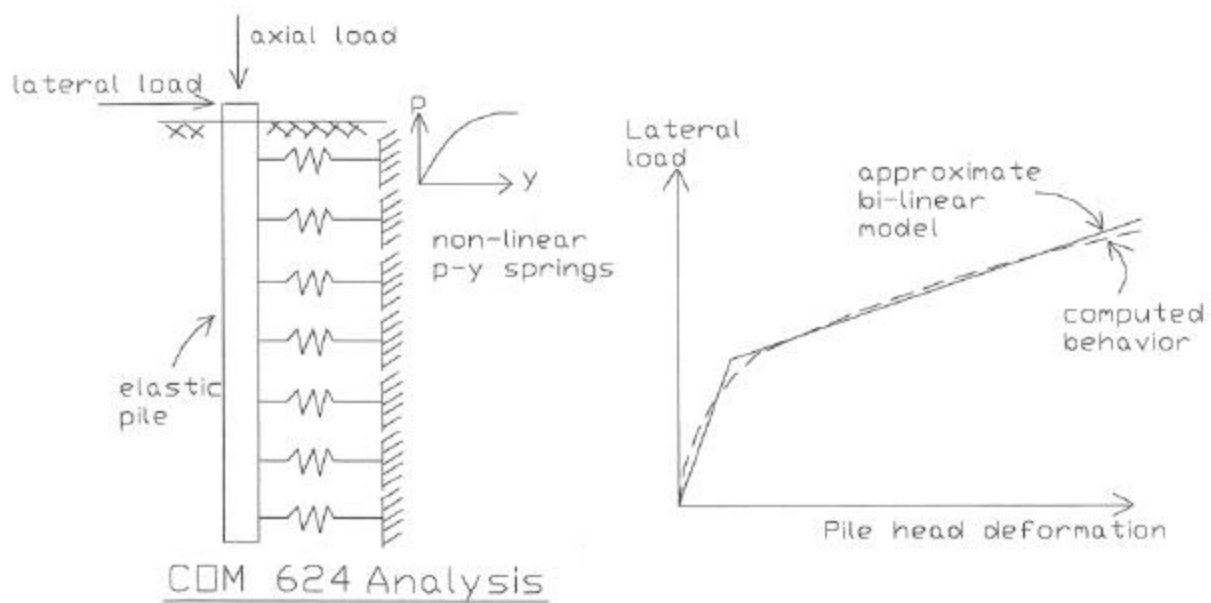


Figure 5.5 Pier Foundation Spring p-y Analysis

## CHAPTER 6

EFFECTIVENESS OF ELASTOMERIC BEARING FOR REDUCING ILLINOIS  
BRIDGE COLUMN DISPLACEMENT DEMANDS6.1 Introduction

The potential for earthquakes in the Mid-American region has received attention only recently. This is largely due to the absence of strong shaking in the twentieth century. Historical accounts, however, indicate the strongest earthquakes to ever occur in North America occurred in the New Madrid area in 1811-1812. The New Madrid seismic area is at the southern tip of Illinois, and Illinois is one of six states in the immediate New Madrid Seismic Zone. Many existing bridges in Illinois may have deficiencies because most were not explicitly designed for seismic motions. Many of these bridges already employ elastomeric bearings for accommodating temperature-induced movements.

The transverse response of bridge column bents often is critical to the seismic performance of the bridge. Collapse may occur if the displacement demand at the bents exceeds the displacement capacity. In many cases, column displacement demands can be reduced if the superstructure response is isolated by using elastomeric bearings. In this chapter, the effectiveness of elastomeric bearing for reducing column displacement demands is investigated for a slab-on-girder bridge representative of Illinois construction, using the bearing models and bridge model described in Chapters Four and Five. The bridge model was analyzed under various ground motions having varied intensities. Transverse displacement response histories were compared for the bridge model with and without elastomeric bearings. Results obtained using the soil-slice approach-embankment model of Chapter Three are compared with

those obtained using the ATC-32 recommendation for abutment modeling for fully-isolated bridges.

## 6.2 Bridge Description

A single bridge considered to be representative of Illinois bridge construction was modeled. The bridge is a four-span concrete slab deck supported on steel girders, extending 240 m. between abutments as shown in Figure 6.1a. The bridge was assumed to be located in Knox County, Marion County, and Massac County, about 470, 180, and 50 km., respectively, from the New Madrid Seismic Zone, as shown in Figure 6.1b. The bridge has multiple column bents supported on a crash wall, and the crash wall is monolithically integrated with the pile cap. The bridge is symmetric and has no skew.

Elastomeric and steel bearings are widely used in bridges in the mid-America region. In the “as-built” bridge model, elastomeric bearings are located beneath the steel girders at Abutment 1, Pier 2, Pier 4, and Abutment 5. Steel rocker bearings with pintles are used at Pier 3, restricting movement in both transverse and longitudinal directions. This configuration, in which rocker or bolster bearings are placed at the central pier to restrain the longitudinal movement of the superstructure, is typical. At other locations, elastomeric bearings are used to accommodate temperature-induced movement. These steel bearings are stiff and will transmit large forces between the deck and substructure in strong shaking unless and until they fail.

### 6.3 Ground Motions

A summary of the ground motions used in the analyses is shown in Table 6.1. The recorded ground motions were chosen to match, approximately, the smooth design spectrum corresponding to the 1997 NEHRP provisions for 2 percent probability of exceedance in 50 years. The ground motions were chosen considering peak ground acceleration (PGA), characteristic period ( $T_g$ ), and epicentral distance. The NEHRP design spectra for all three sites are shown in Figure 6.2. The chosen earthquake records were scaled uniformly so that the spectral ordinates ( $S_d$ ,  $P_{sv}$ ,  $P_{sa}$ ) approximately matched the design spectrum in the period range between 0.6 and 0.9 seconds. This period range is the upper and lower bound of the bridge period under the all fixed and as-built cases, at different seasonal temperatures. The scaled records were used for all analyses, including the fully-isolated bridge cases. Scaling of the earthquake is shown in Figure 6.3-6.10. The original and scaled accelerograms are shown in Figure 6.11 and 6.12 respectively. The ground motions used are varied in intensity according to distance from the New Madrid Seismic Zone according to the NEHRP (1997) maps, and are considered to be adequate to investigate the effectiveness of elastomeric bearing for reducing bridge column displacement demands.

### 6.4 Analytical Model

As mentioned previously, this research focused primarily on the transverse response of the bridge. The bridge was modeled using DRAIN-2DX with plastic hinge beam-column elements to represent the deck and girder system as shown in Figure 6.13 for the “as-built”

case and Figure 6.14 for the “fixed bearing” case. Bilinear force-displacement relationships were used in the horizontal plane of the bridge to represent the transverse resistance provided by the abutments, piers, and pile foundations as described in Chapter 5. Because of lack of skew and lack of curvature, a two-dimensional model was considered to be adequate for this bridge. The properties of each bilinear spring were determined by separate analyses as described in Chapter 5. Thus, they could be represented by simple nonlinear elements in the two-dimensional model, located at the superstructure level. The bridge was excited by ground motion in the transverse direction. The gravity load was not considered explicitly in the dynamic analysis, but it was considered explicitly when determining the pier and pile springs as described in Chapter 5. The analysis did not consider the possibility of steel bearing failures due to reversed cyclic loading. Test results for steel bridge bearings subjected to reversed cyclic loading are described in a report by Mander et al (1996).

The analysis were conducted in three parts. The first focused on the effectiveness of elastomeric bearings for reducing displacement demands in the bridge piers. The second part focused on the effects of low-temperatures on the effectiveness of the elastomeric bearings for isolating the superstructure. In the third part, results using the ATC-32 recommendation for modeling abutments are compared with those obtained with the approach-embankment model (soil-slice) for isolated Illinois bridges.

#### 6.4.1 Displacement Demands in Conventional Bridges

Two scenarios were chosen for this study. The first scenario is called the “as-built” bridge. The as-built bridge has Type III elastomeric bearings at Abutment 1 and Abutment 5, Type II elastomeric bearings at Pier 2 and Pier 4, and steel rocker bearings with pintles at the central pier (Pier 3). The second scenario or the “fixed bearing” bridge has rocker bearings at all abutments and piers, allowing no transverse movement at the deck support locations. It is impractical to have fixed bearing at all supports. However, the fixed bearing bridge is used as a base line model used for comparison to the as-built bridge in the first scenario. The analytical model of the bridge for the first and second scenarios is shown in Figures 6.13 and 6.14 respectively. The derivation of each spring is discussed earlier in Chapter Five.

In determining the drift capacity of a pier column to compare with analytically determined drift demands, the yield displacement and the ultimate drift capacity were estimated based on the method proposed by Pujol (1997), as described in Chapter 5. Two cases of column confinement were considered. One was the modern (ductile) details, consisting of #5 spiral @ 3.3 inches spacing. Another one was the older (non-ductile) details, consisting of #4 spiral @ 12 inches. Table 6.2 summarizes the estimated column drift capacities. It should be noted that length of lap splices at the column to foundation connection may be critical, especially for Illinois bridges. Based on the bar cover, bar lap separation, and bar spacing, the as-built bridge was considered to have adequate column lap splices according to Lin (1996).

Elastic mode shapes of the bridge model are shown in Figures 6.15 and 6.16. Since the embankment mass at the abutment is large, elastic mode shapes having large amplitude at the abutment will also have high effective modal mass. Computed force-displacement response at



all abutments and piers is shown in Figures 6.17-6.24 for the as-built bridge and in Figures 6.25-6.32 for the fixed bearing bridge. Results are summarized in Table 6.3 and 6.4.

For the as-built bridge, it is evident that sliding is taking place at the TFE-stainless steel interface when the force reaches the sliding force. Correspondingly at Abutment 1, the slip begins when the rubber undergoes 16 percent shear strain, while at Pier 2, the maximum deformation in rubber does not exceed 19 percent shear strain. Both are lower than the 50 percent shear strain used in design of elastomeric bearings for service-level temperature induced deformations. Also, the maximum force in the steel pin is about 10 kN. This is about 4 percent of the yield force, estimated to be 244 kN. The maximum drift at Pier 2 is about 2.49 percent (10.7 cm) for Massac County, soil type D. Columns at Pier 3 (Central Pier) with steel bearings also undergo large inelastic deformation. The maximum drift at Pier 3 for Massac County, soil type D is about 2.26 percent (9.7 cm). This drift demand is less than the ultimate drift capacity for columns with ductile details (3.56 percent or 15.3 cm) but greater than that of the non-ductile columns (1.22 percent or 5.2 cm). The force transmitted to substructures is limited to the sliding force where bearing Type II or III is used. Energy is dissipated through friction at the sliding surface as well as through deformation of the elastomer. At the pier with steel bearings, energy is dissipated through cyclic deformation of the columns.

For the fixed bearing bridge, all piers experienced large inelastic deformation in moderate to strong ground motions. This is different from the as-built bridge where only Pier 3 was subject to large deformation. Maximum column drift demands of 2.44 percent (10.5 cm) at Pier 2, and 2.47 percent (10.6 cm) at Pier 3 exceeded the estimated yield displacement and would have caused failure if the column had older, non-ductile details.

#### 6.4.2 Effectiveness of Elastomeric Bearing at Reducing Column Displacement Demands at Normal and Low Temperatures

This section evaluates the effectiveness of elastomeric bearings when used to fully isolate the superstructure. Type I bearings were modeled at all superstructure supports; other elements were identical to those used in the analyses reported in Section 6.4.1. Figure 6.33 shows the model with ATC-32 recommendation for abutment stiffness and Figure 6.34 shows the model using the soil-slice approach-embankment. Eight cases were chosen as shown in Table 6.5. Type I bearings were used throughout since the stiffness increase of the bearing due to low temperature effect can be significant and this would be masked if the sliders of Type II and III bearings were also modeled. The bridge was assumed to be located in Massac County, Illinois, with soil type B. In each of the eight cases, there were differences in the support conditions between the bent cap and the steel girders, temperature, and the abutment modeling. The increase in shear stiffness of rubber with temperature can vary greatly from less than 2 to a factor greater than 30, as discussed in Chapter Four. For the purpose of this analysis, a four times increase in rubber shear stiffness was chosen for the “cold” temperature.

Peak displacement responses (envelope values of each component) are plotted in Figure 6.35 for ATC-32 recommendation (Cases 1-4) and Figure 6.36 for the approach embankment model (Cases 5-8). Table 6.6 summarizes the peak displacement from Figures 6.35-6.36. It is evident in both models that cold temperature causes an increase in pier drift demand (Case 3 vs. 4 and Case 7 vs. 8). By comparing Case 2 vs. 4 and Case 6 vs. 8, it is seen that the elastomeric bearing under cold temperature may cause column drift demands to be similar to the case with all fixed bearings. Replacement of fixed steel bearing with elastomeric

bearings at the central pier can reduce the drift demand at the central pier to less than the drift capacity (Case 1 vs. 3 and Case 5 vs. 7). If the elastomeric bearings are used at all supports, adequate stiffness should be provided to resist service loadings such as wind or braking force.

#### 6.4.3 Response Comparison between ATC-32 Recommendation for Abutment Modeling vs. Improved Approach-Embankment (Soil-Slice) Model

Although the ATC-32 abutment model and the soil-slice model show similar trends as far as low-temperature effect is concerned, the analysis results are different. To illustrate the model difference qualitatively, the “inelastic” mode shapes obtained from principal component analysis (PCA) are described here. Cases 3 and 7 from Table 6.5 were chosen, for which Type I bearings are used between the bent cap and the steel girders at all piers and abutments, with the only difference being the modeling of the abutment. The models for each case were subjected to “low” and “high” level of shakings, given by  $1.4 * (\text{norhntn.v2}(\text{CH } 1))$  and  $0.75 * (\text{ch85lleo.010})$  (Table 6.1), having PGA approximately 0.1 g and 0.5 g respectively. The comparisons of PCA mode shapes for “low” and “high” level of shakings are shown in Figures 6.37 and 6.38 respectively. The PCA mode shapes from the ATC-32 and soil-slice models are almost identical for low PGA shaking, but are quite different for high PGA shaking; the soil-slice model has larger mode shape amplitude at the abutments.

#### 6.5 Summary

This chapter has illustrated that the elastomeric bearings normally used in Illinois can help reduce the bridge column displacement demands. Type II and Type III bearings which utilize the teflon sliding surface are able to limit the force to bridge substructure to the sliding force. Additionally, the bearing stiffness at cold temperature is critical and must be evaluated especially in the older columns which may have inadequate displacement capacity because of low level of confinement.

Table 6.1 Description of Earthquakes Used in the Analysis.

Location	Distance from NMSZ**	Soil Profile Type	Identifier	Earthquake	Scale Factor
Knox County	470 km.	Type B	norhntn.v2(CH 1)	Northridge'94	1.4
Knox County	470 km.	Type D	norhntn.v2(CH 3)	Northridge'94	2.3
Knox County	470 km.	Type E	norhntn.v2(CH 3)	Northridge'94	3.4
Marion County	180 km.	Type B	ch85lleo.100	Central Chile'85	0.42
Marion County	180 km.	Type D	ch85lleo.100	Central Chile'85	0.7
Marion County	180 km.	Type E	iv40elcn.180	Imperial Valley'40	1.15
Massac County	50 km.	Type B	ch85lleo.010	Central Chile'85	0.75
Massac County	50 km.	Type D	ch85lleo.010	Central Chile'85	1.15

\*\* NMSZ = The New Madrid Seismic Zone

Table 6.2 Drift Capacity of Pier Column.

	Yield Drift	Ultimate Drift
Modern (Ductile) Details (#5 Spiral @ 3.3 inches)	3.2 cm (0.74 %)	15.3 cm (3.56 %)
Older (Non-Ductile) Details (#4 Spiral @ 12 inches)	3.2 cm (0.74 %)	5.2 cm (1.22 %)

Table 6.3 Maximum Relative Displacement for the "As-Built" Bridge.

Case	Bearing at Abut 1 (cm)	Bearing at Pier 2 (cm)	Central Pier (cm)
Knox County (Soil Type B)	2.5	1.1	1.0
Knox County (Soil Type D)	5.2	2.8	2.6
Knox County (Soil Type E)	6.3	4.8	4.4
Marion County (Soil Type B)	4.3	1.5	2.1
Marion County (Soil Type D)	6.9	5.9	6.6*
Marion County (Soil Type E)	11.3	7.4	5.5*
Massac County (Soil Type B)	16.0	7.7	7.9*
Massac County (Soil Type D)	20.0	10.7	9.7*

\* Maximum pier displacement exceeds estimated drift capacity for "non-ductile" column. Pier drift is calculated based on pier height of 4.3 m.

Table 6.4 Maximum Relative Displacement for the "Fixed Bearing" Bridge.

Case	Abut 1 (cm)	Pier 2 (cm)	Central Pier (cm)
Knox County (Soil Type B)	0.2	1.1	1.3
Knox County (Soil Type D)	0.4	3.0	3.5
Knox County (Soil Type E)	0.6	4.6	5.4*
Marion County (Soil Type B)	0.3	2.0	2.2
Marion County (Soil Type D)	0.6	4.1	4.6
Marion County (Soil Type E)	1.1	5.4*	7.2*
Massac County (Soil Type B)	0.9	6.1*	6.7*
Massac County (Soil Type D)	3.0	10.5*	10.6*

\* Maximum pier displacement exceeds estimated drift capacity for "non-ductile" column.

Table 6.5 Case Study of Low Temperature Effect on Bearings. \*\*\*

Case #	Abut 1	Pier 2	Pier 3	Pier 4	Abut 5	Temp.	Abutment/ Embankment
1 As-Built	I	I	F	I	I	WARM	ATC-32
2 All-Fixed	F	F	F	F	F	WARM	ATC-32
3 (warm) All Elastomeric	I	I	I	I	I	WARM	ATC-32
4 (cold) All Elastomeric	I	I	I	I	I	COLD	ATC-32
5 As-Built	I	I	F	I	I	WARM	Soil-Slice Model
6 All-Fixed	F	F	F	F	F	WARM	Soil-Slice Model
7 (warm) All Elastomeric	I	I	I	I	I	WARM	Soil-Slice Model
8 (cold) All Elastomeric	I	I	I	I	I	COLD	Soil-Slice Model

\*\*\* F = Steel bearings are used between the bent cap and the steel girders.  
 I = Type I bearings are used between the bent cap and the steel girders.  
 WARM = No increase in rubber stiffness.  
 COLD = Four times increase in shear stiffness of the rubber.

Table 6.6 Summary of Peak Displacement Response in All Eight Cases (Table 6.5)

Case #	Abut 1 (cm)	Pier 2 (cm)	Pier 3 (cm)	Pier 4 (cm)	Abut 5 (cm)	Temp.	Abutment/ Embankment
1 As-Built	4.8	7.1	8.3	7.1	4.8	WARM	ATC-32
2 All-Fixed	1.7	4.9	10.0	4.9	1.7	WARM	ATC-32
3 (warm) All Elastomeric	6.7	7.8	10.5	7.8	6.7	WARM	ATC-32
4 (cold) All Elastomeric	3.7	5.8	9.9	5.8	3.7	COLD	ATC-32
5 As-Built	8.7	7.7	6.8	7.7	8.7	WARM	Soil-Slice Model
6 All-Fixed	5.5	6.7	7.9	6.7	5.5	WARM	Soil-Slice Model
7 (warm) All Elastomeric	7.6	8.0	9.0	8.0	7.6	WARM	Soil-Slice Model
8 (cold) All Elastomeric	5.3	6.4	7.8	6.4	5.3	COLD	Soil-Slice Model

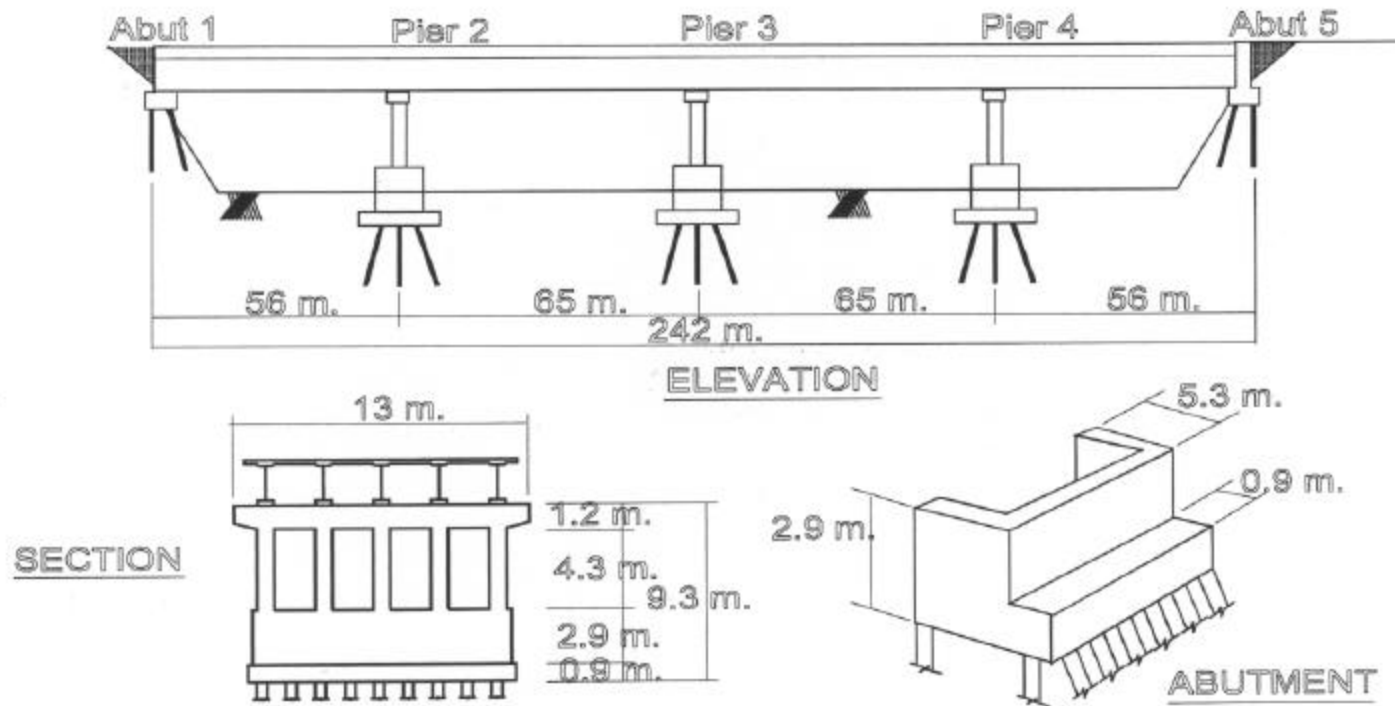


Figure 6.1 a) A Model Bridge





Figure 6.1 b) Map of Illinois Showing Three Bridge Sites:  
 1 = Knox County, 2 = Marion County, 3 = Massac County

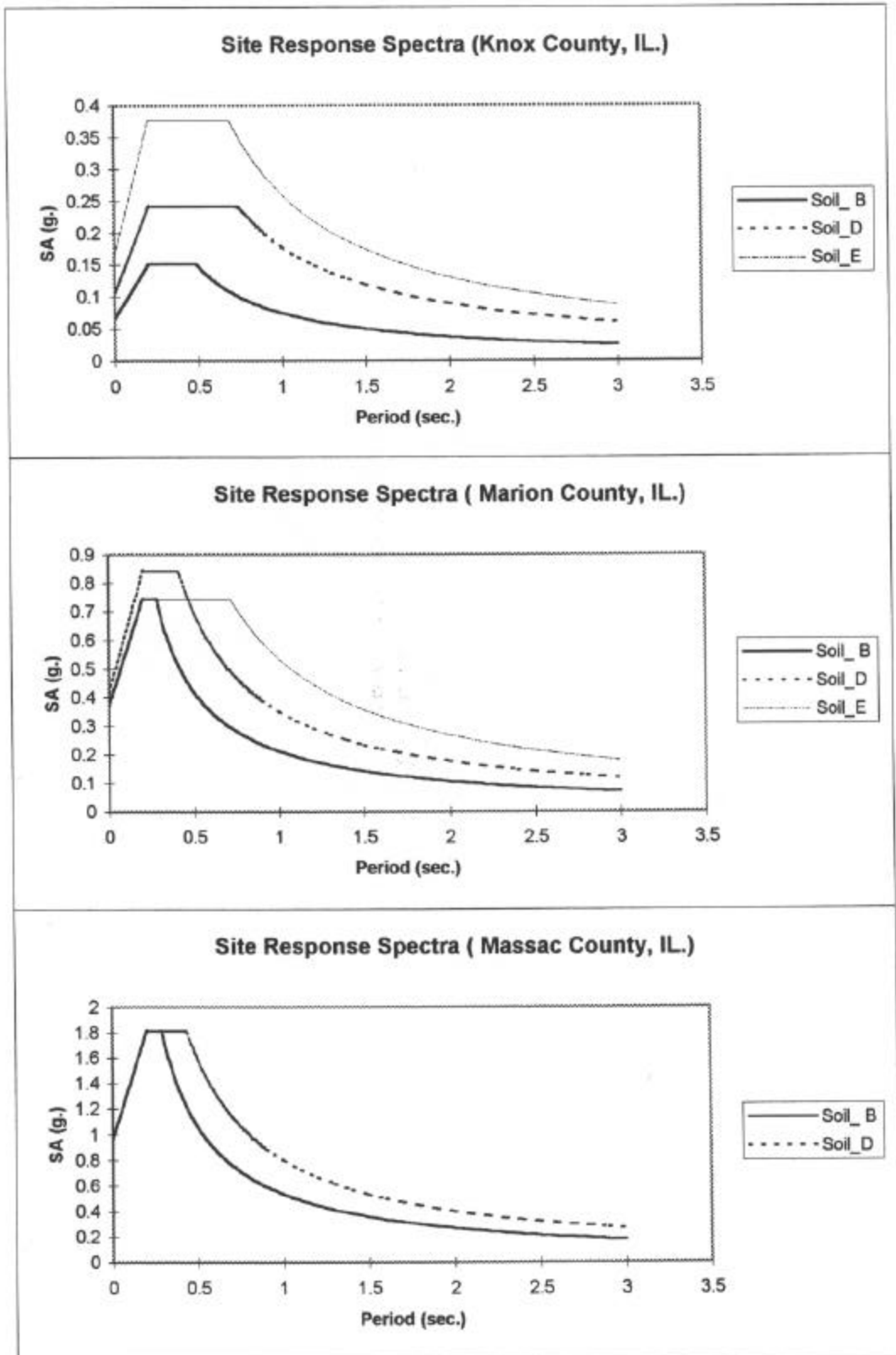


Figure 6.2 Design Spectra for the Three Bridge Sites.

NORHNTN.V2 CHANNEL1 Northridge Earthquake 1994

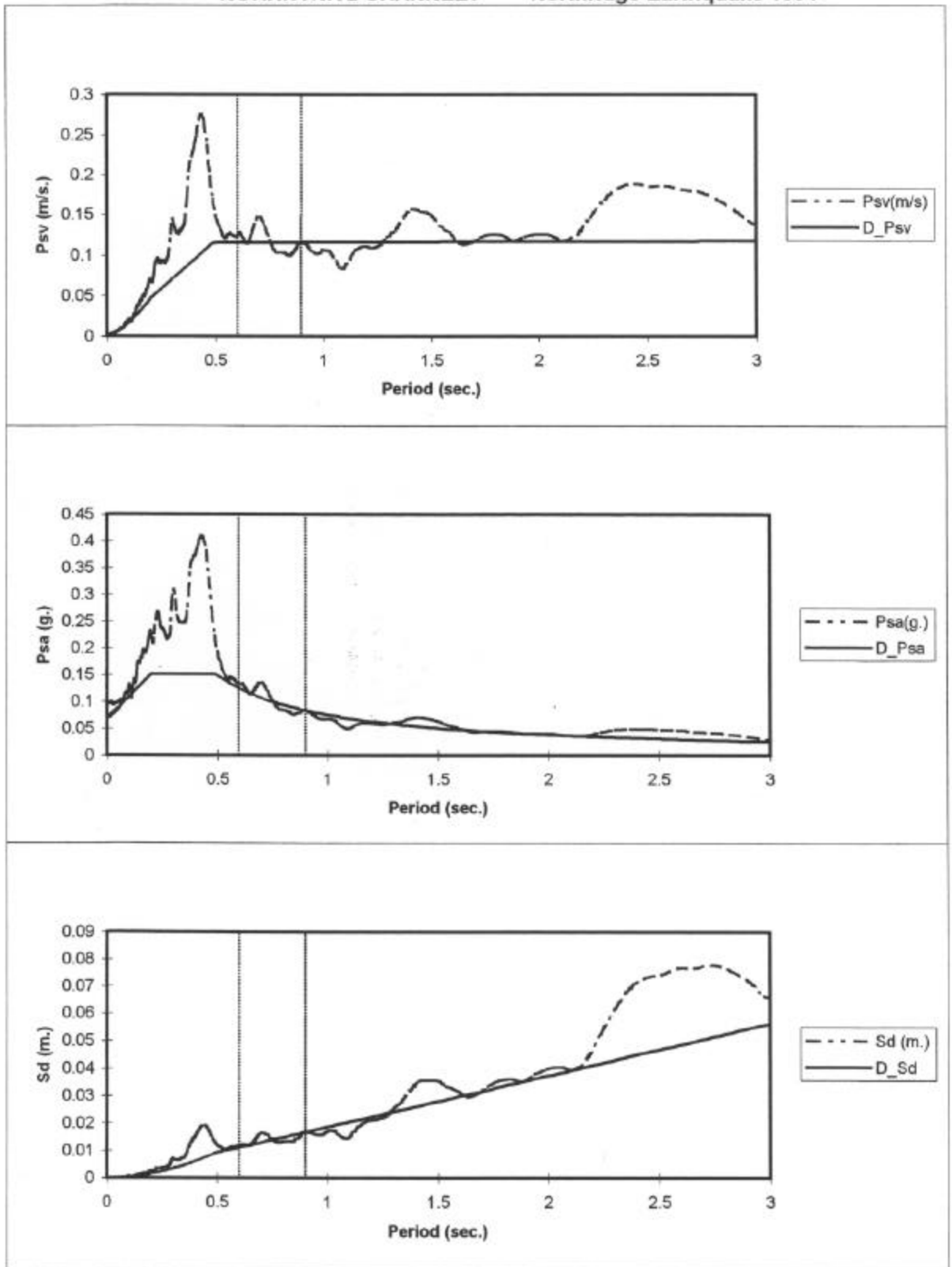


Figure 6.3 Scaling of the Earthquake Spectra for Knox County, Soil Type B.

NORHNTN.V2 CHANNEL3 Northridge Earthquake 1994

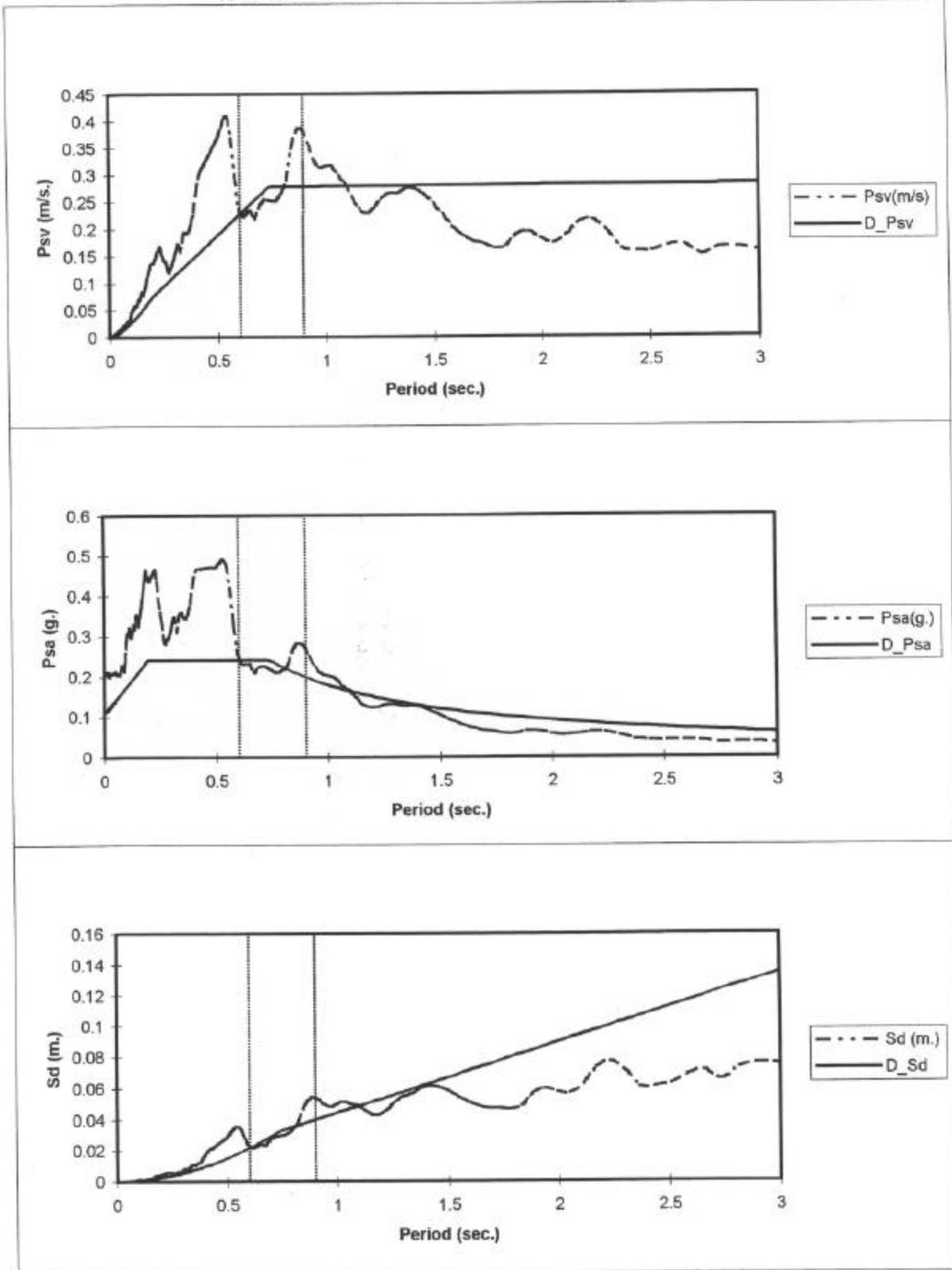


Figure 6.4 Scaling of the Earthquake Spectra for Knox County, Soil Type D.

NORHNTN.V2 CHANNEL3 Northridge Earthquake 1994

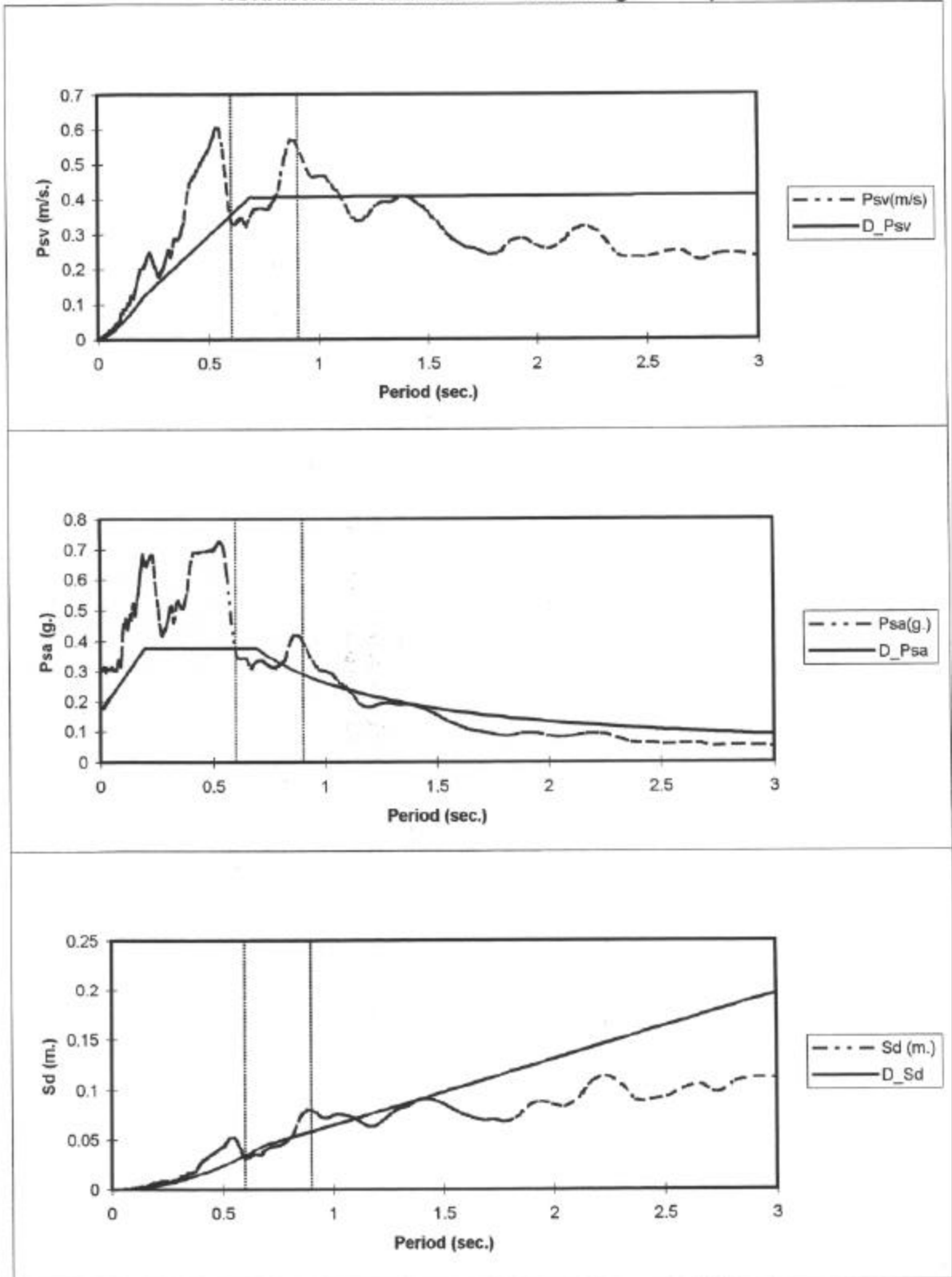


Figure 6.5 Scaling of the Earthquake Spectra for Knox County, Soil Type E.

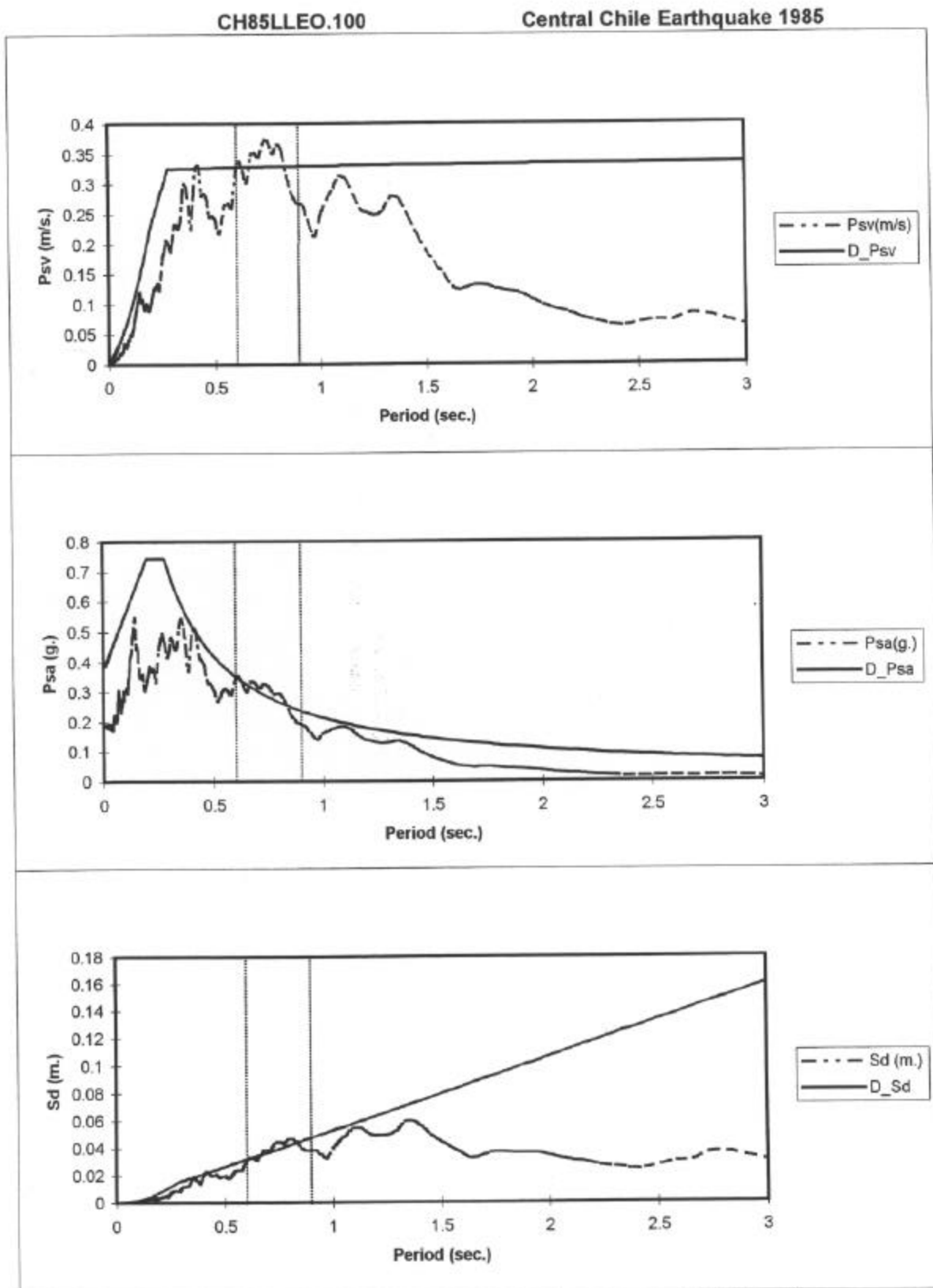


Figure 6.6 Scaling of the Earthquake Spectra for Marion County, Soil Type B.

CH85LLEO.100

Central Chile Earthquake 1985

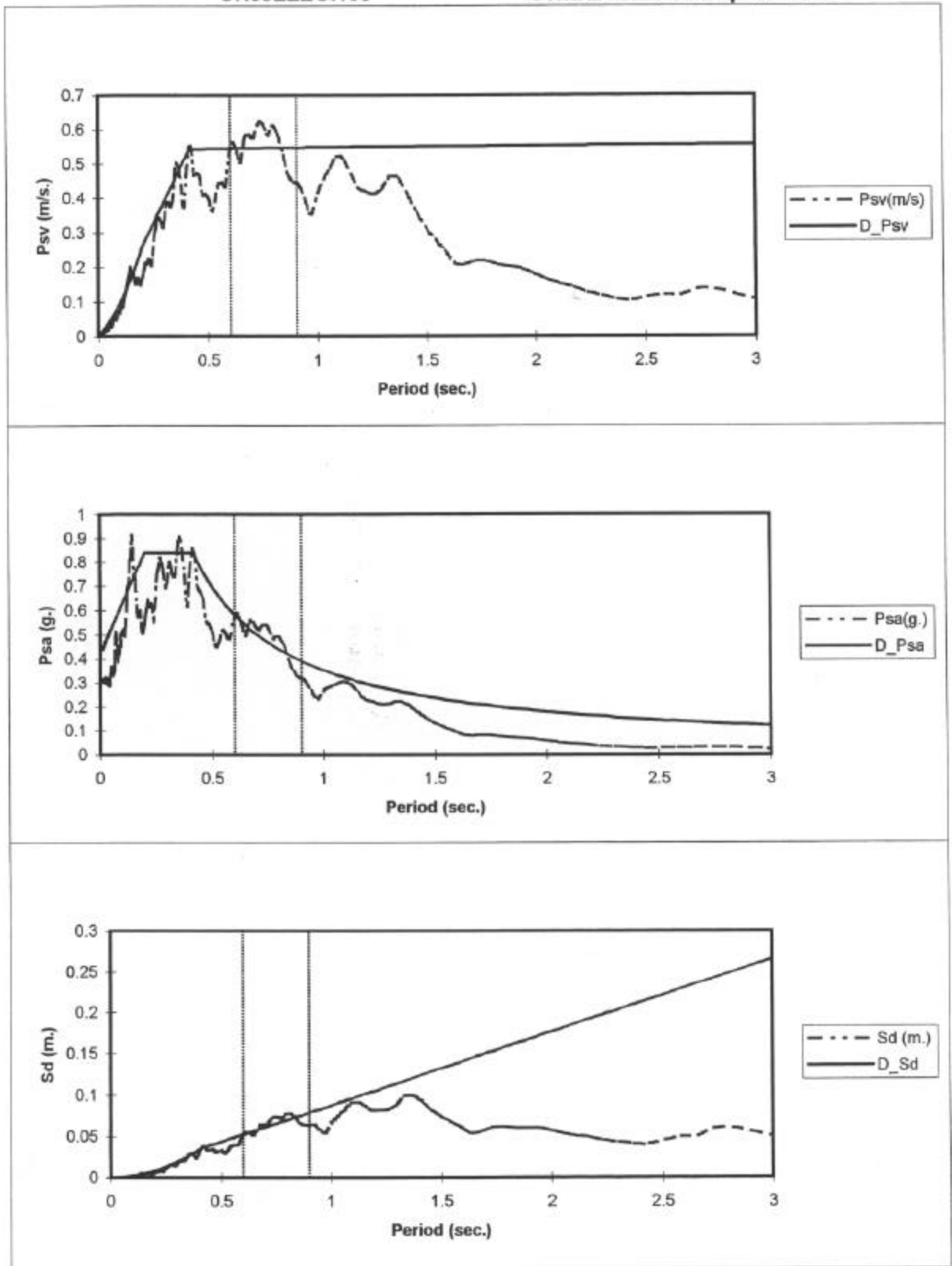


Figure 6.7 Scaling of the Earthquake Spectra for Marion County, Soil Type D.

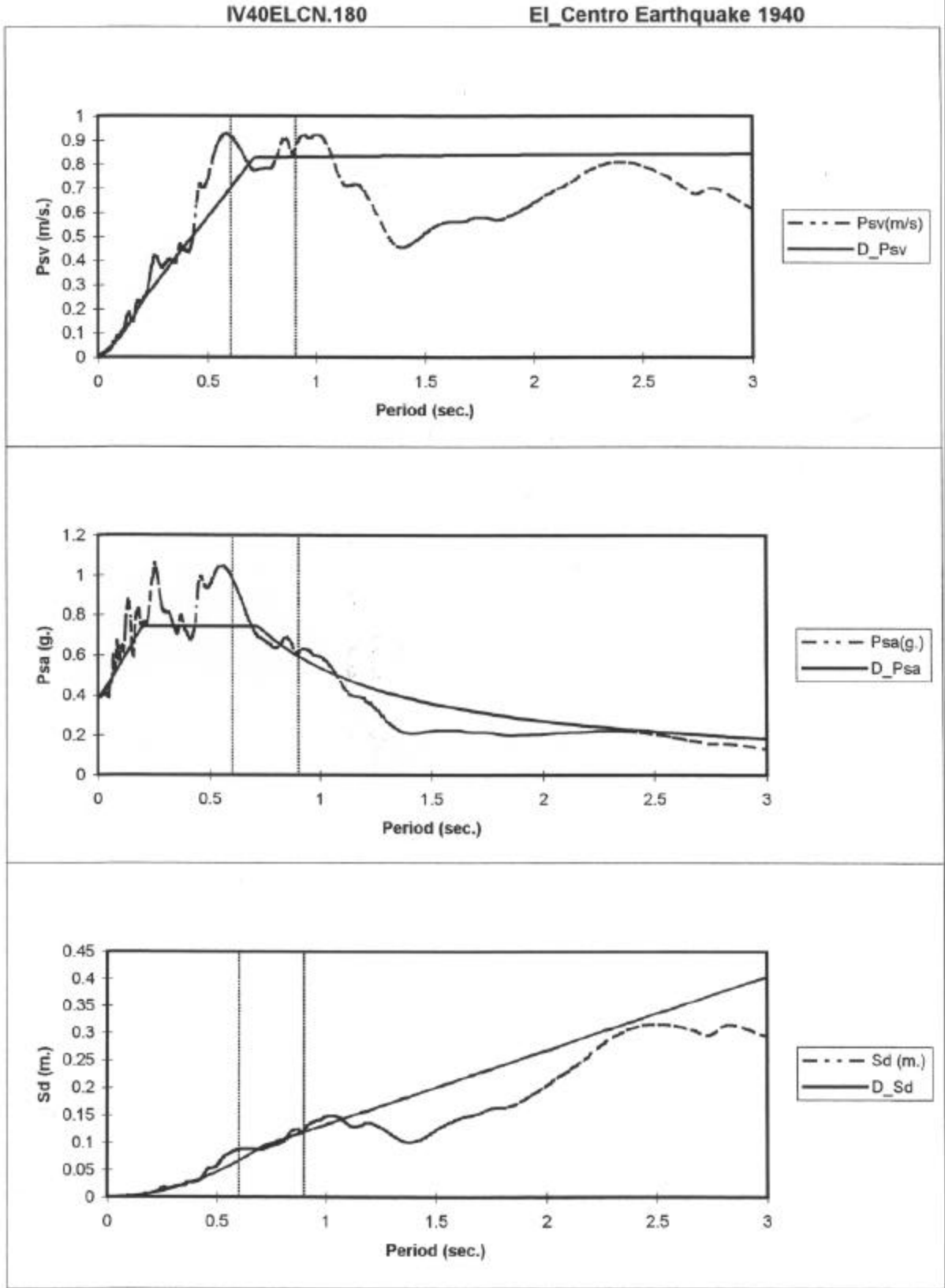


Figure 6.8 Scaling of the Earthquake Spectra for Marion County, Soil Type E.



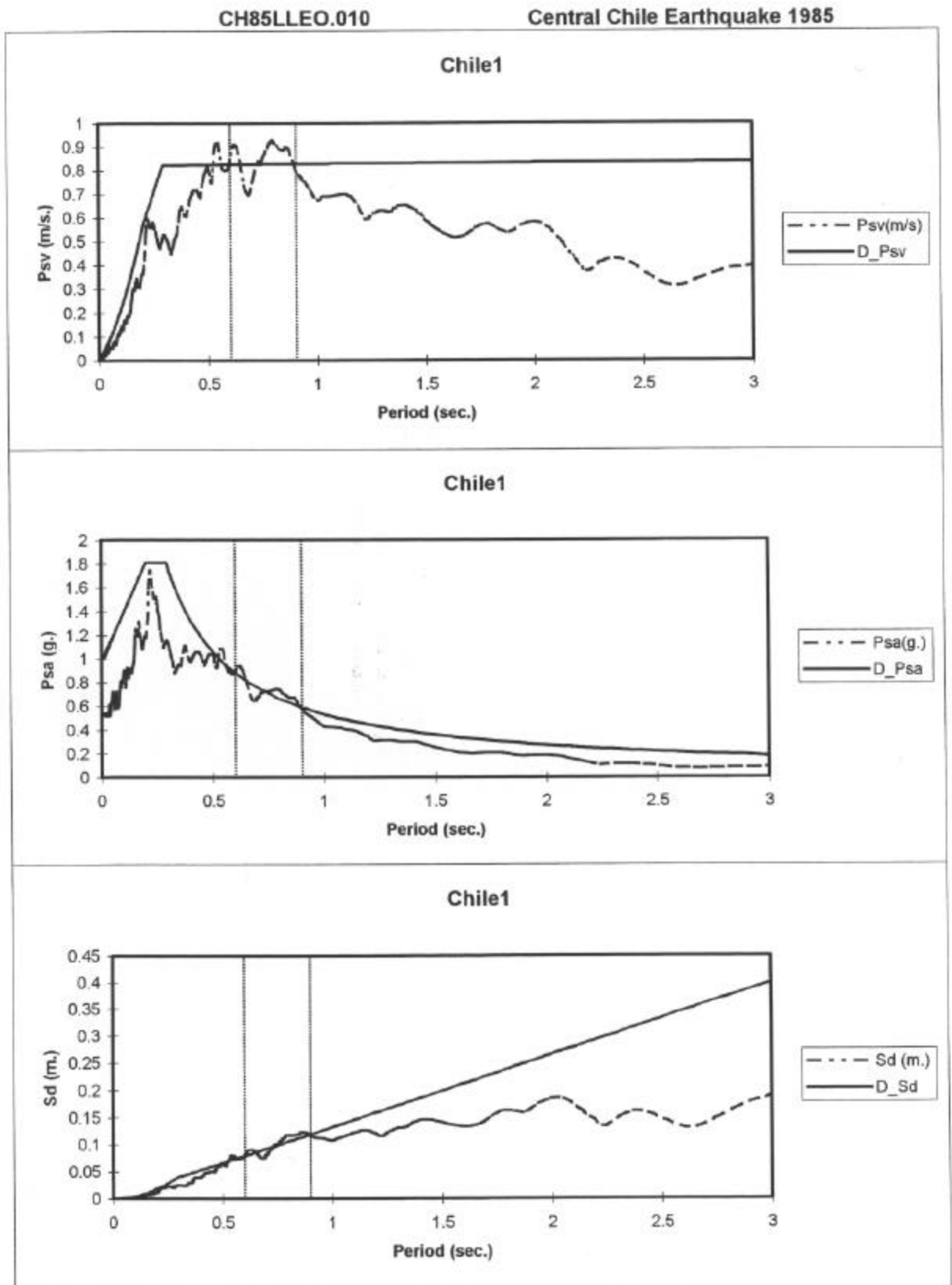


Figure 6.9 Scaling of the Earthquake Spectra for Massac County, Soil Type B.

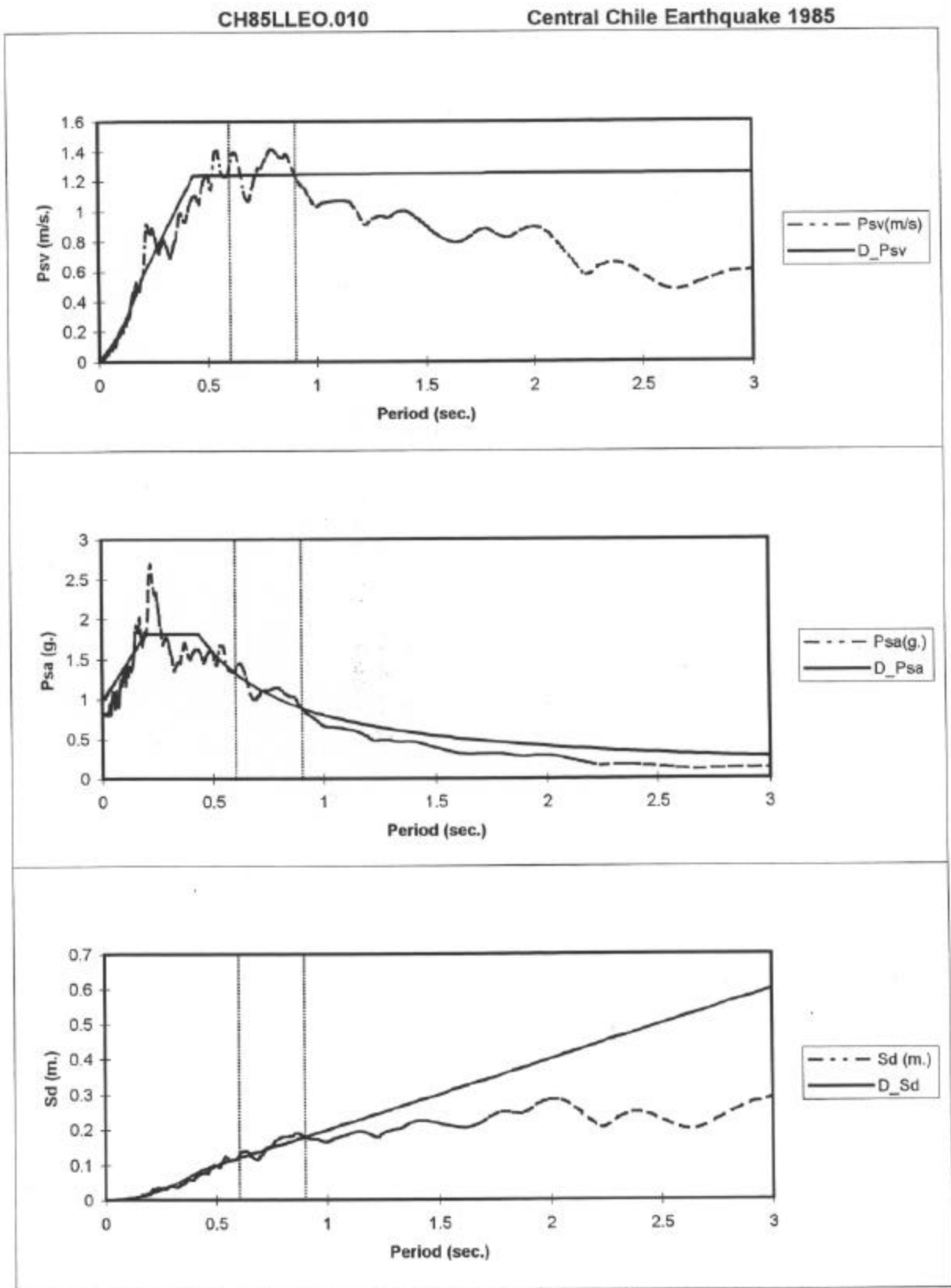


Figure 6.10 Scaling of the Earthquake Spectra for Massac County, Soil Type D.

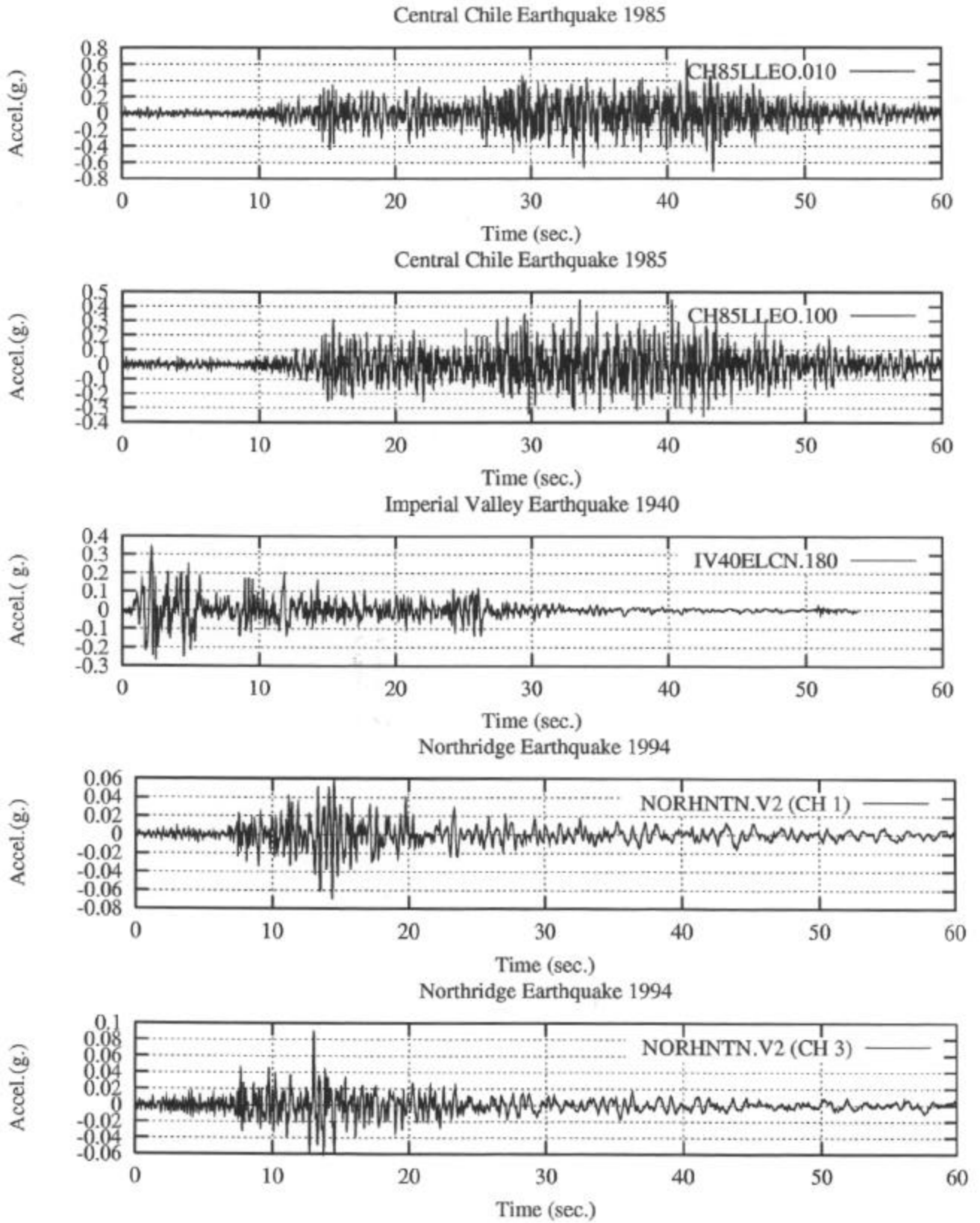


Figure 6.11 Original Time-History Records

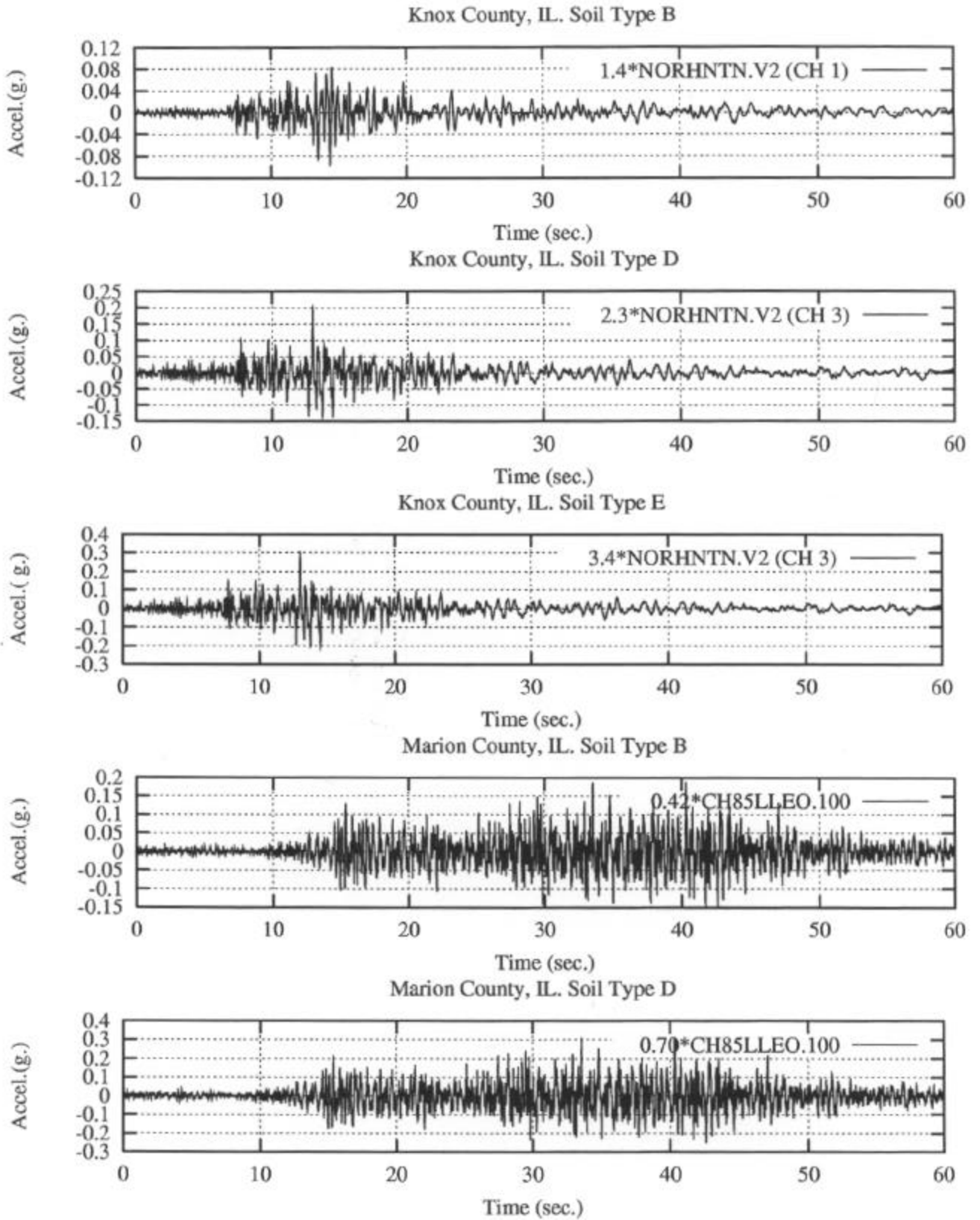


Figure 6.12 Scaled Time-History Records

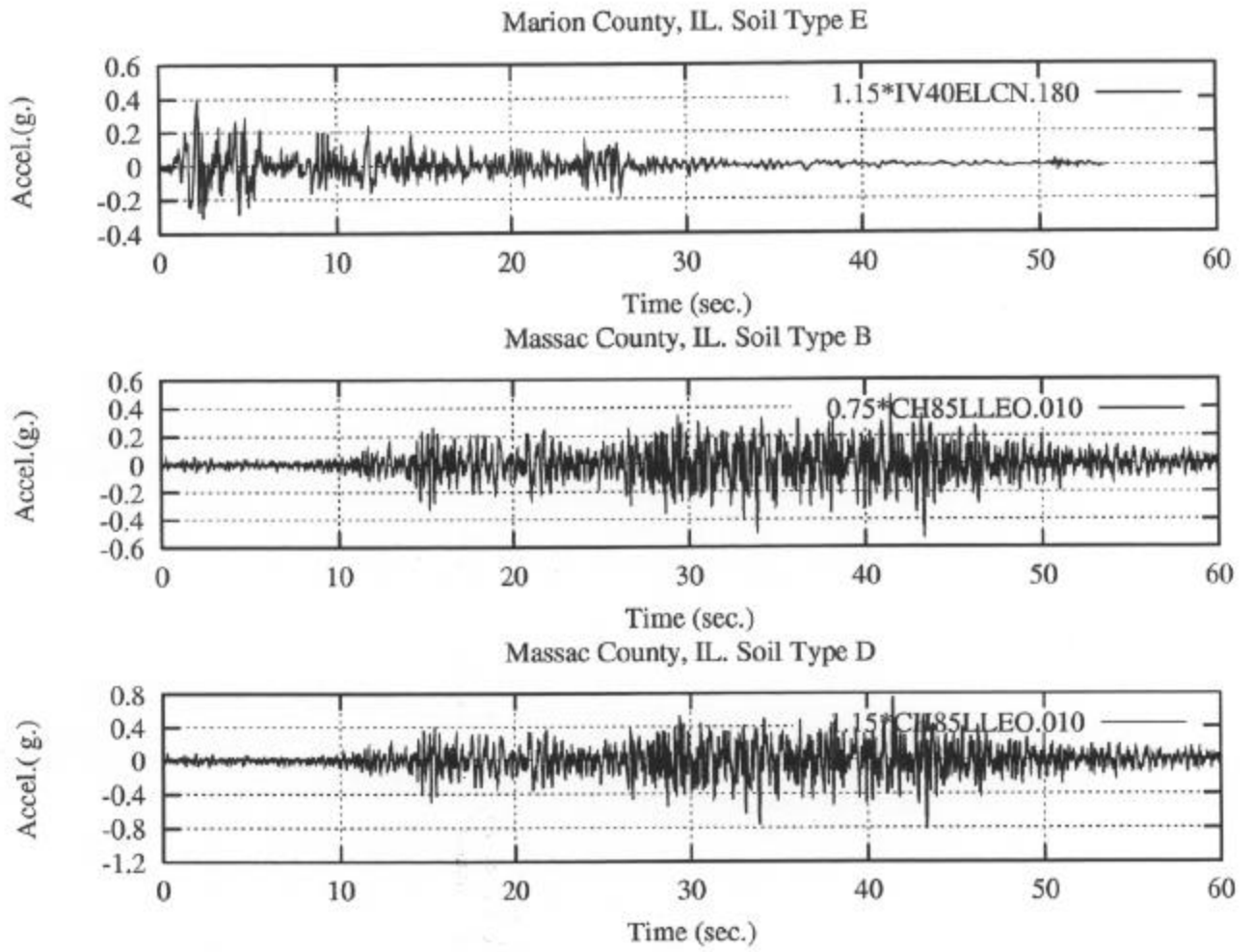


Figure 6.12 (Continued) Scaled Time-History Records

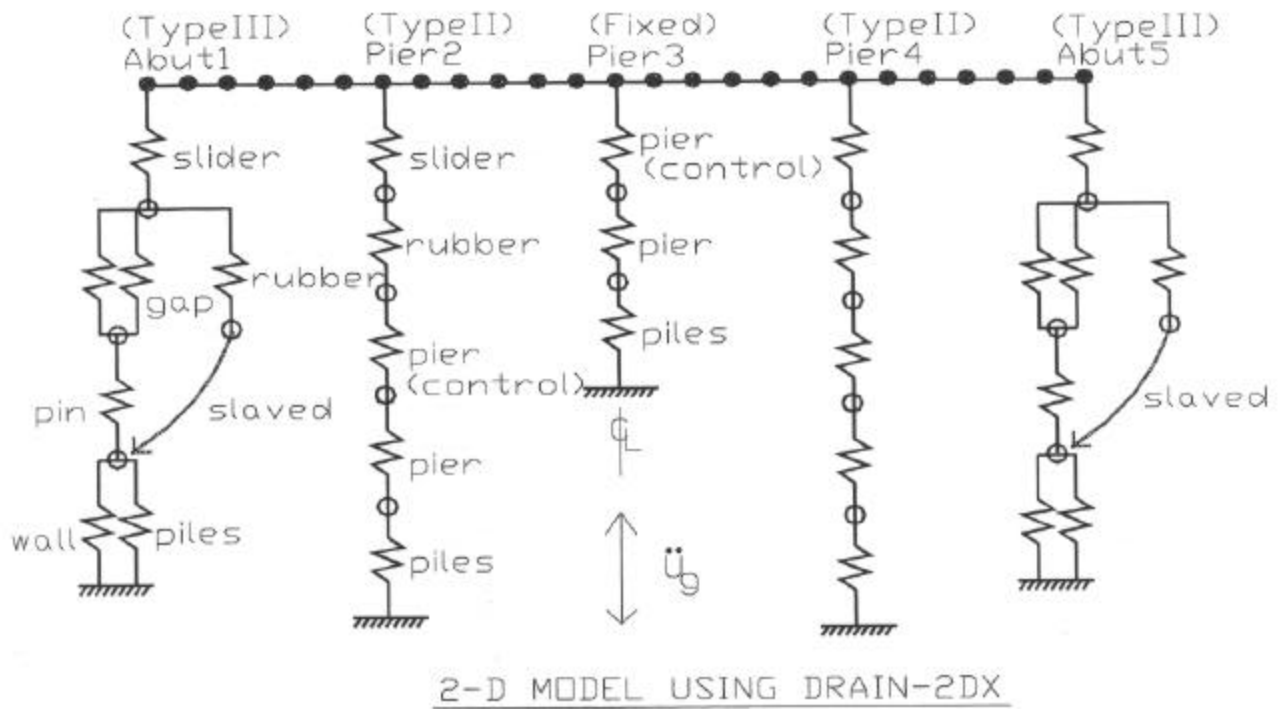


Figure 6.13 Two-Dimensional Bridge Model for the "As-Built" Bridge.

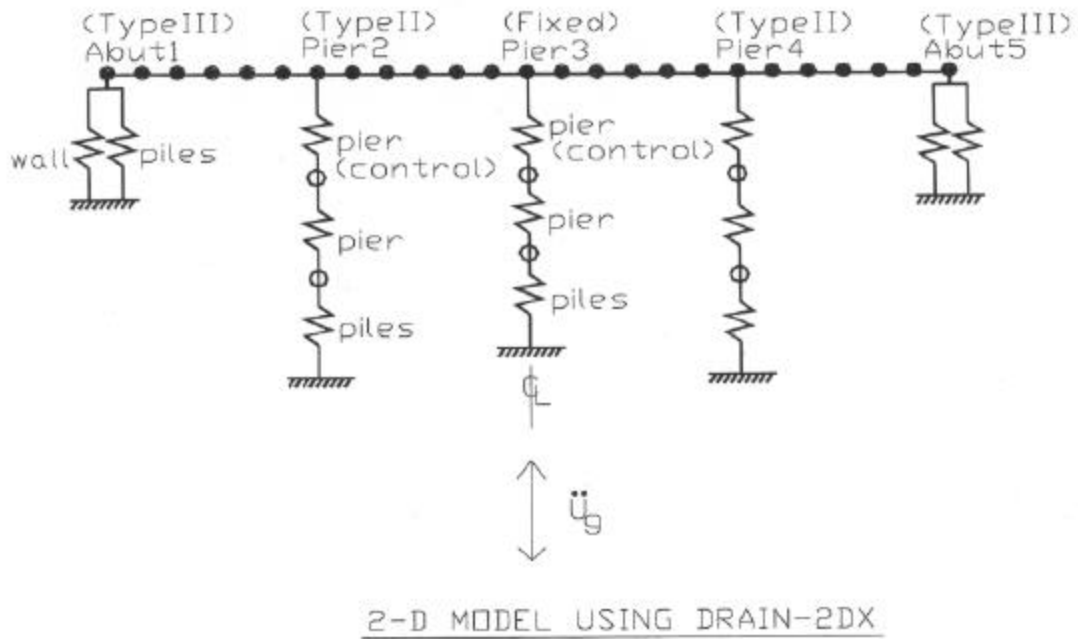


Figure 6.14 Two-Dimensional Bridge Model for the "Fixed Bearing" Bridge.






mode	as-built	T(sec.)	effective modal mass
1		0.915	18.4%
2		0.881	0
3		0.671	41.3%
4		0.631	0
5		0.594	38.4%

Figure 6.15 Elastic Mode Shapes of the “As-Built” Bridge.






mode	fixed	T(sec.)	effective modal mass
1		0.772	14.4%
2		0.659	0
3		0.643	83.8%
4		0.604	0
5		0.397	0.2%

Figure 6.16 Elastic Mode Shapes of the “Fixed Bearing” Bridge.

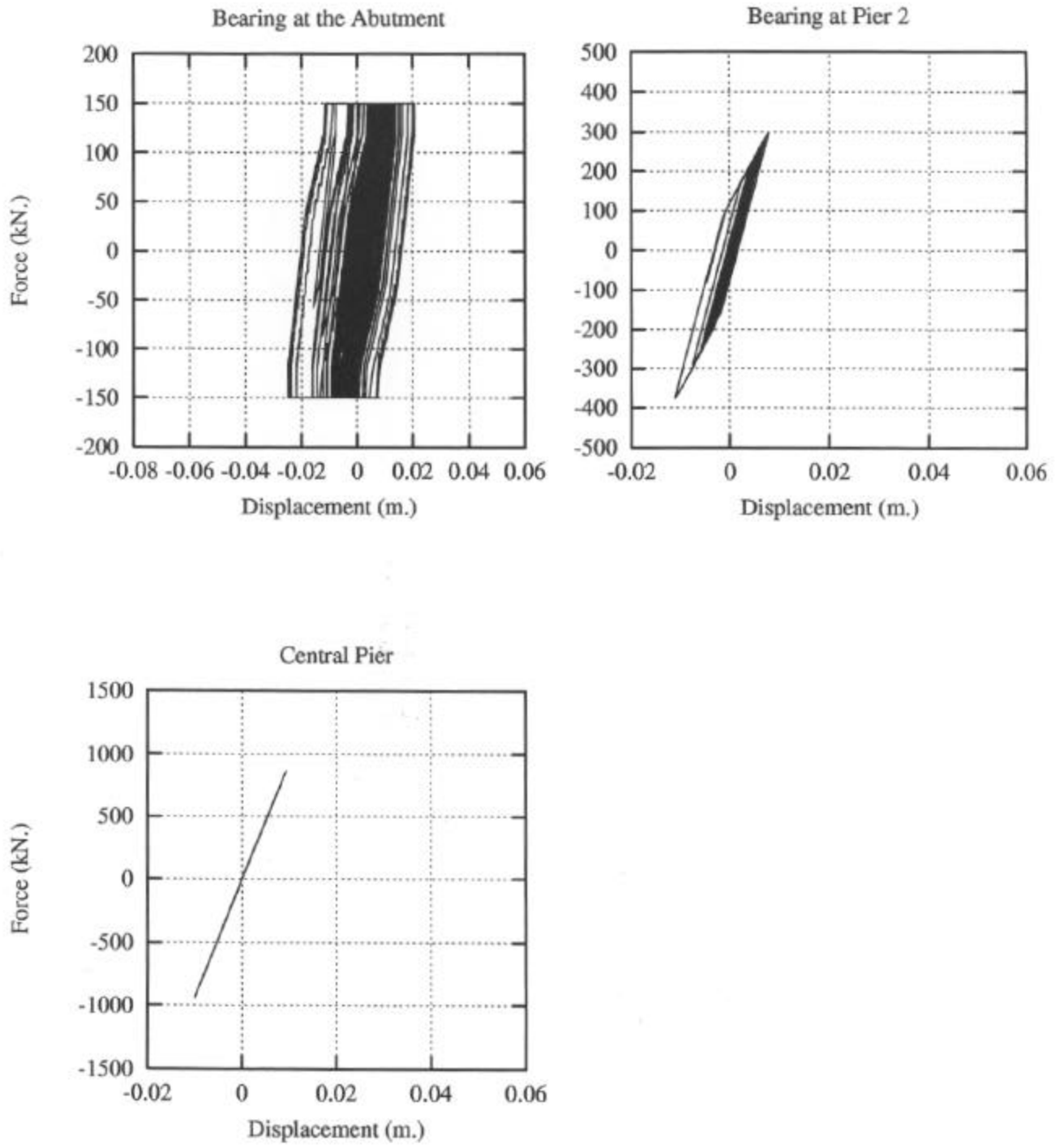


Figure 6.17 Hysteresis for the "As-Built" Bridge at Knox County, IL. Soil Type B



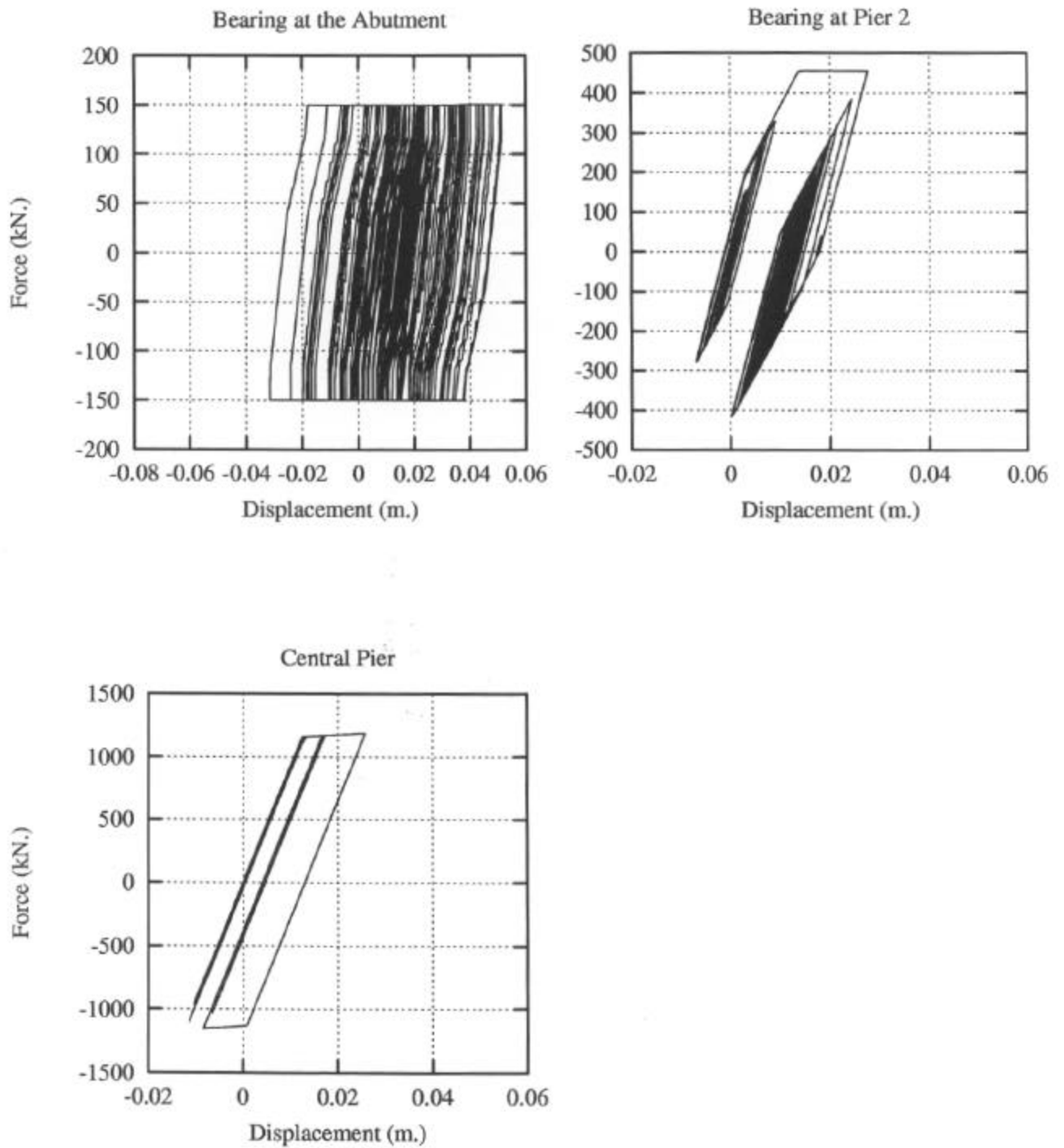


Figure 6.18 Hysteresis for the "As-Built" Bridge at Knox County, IL. Soil Type D

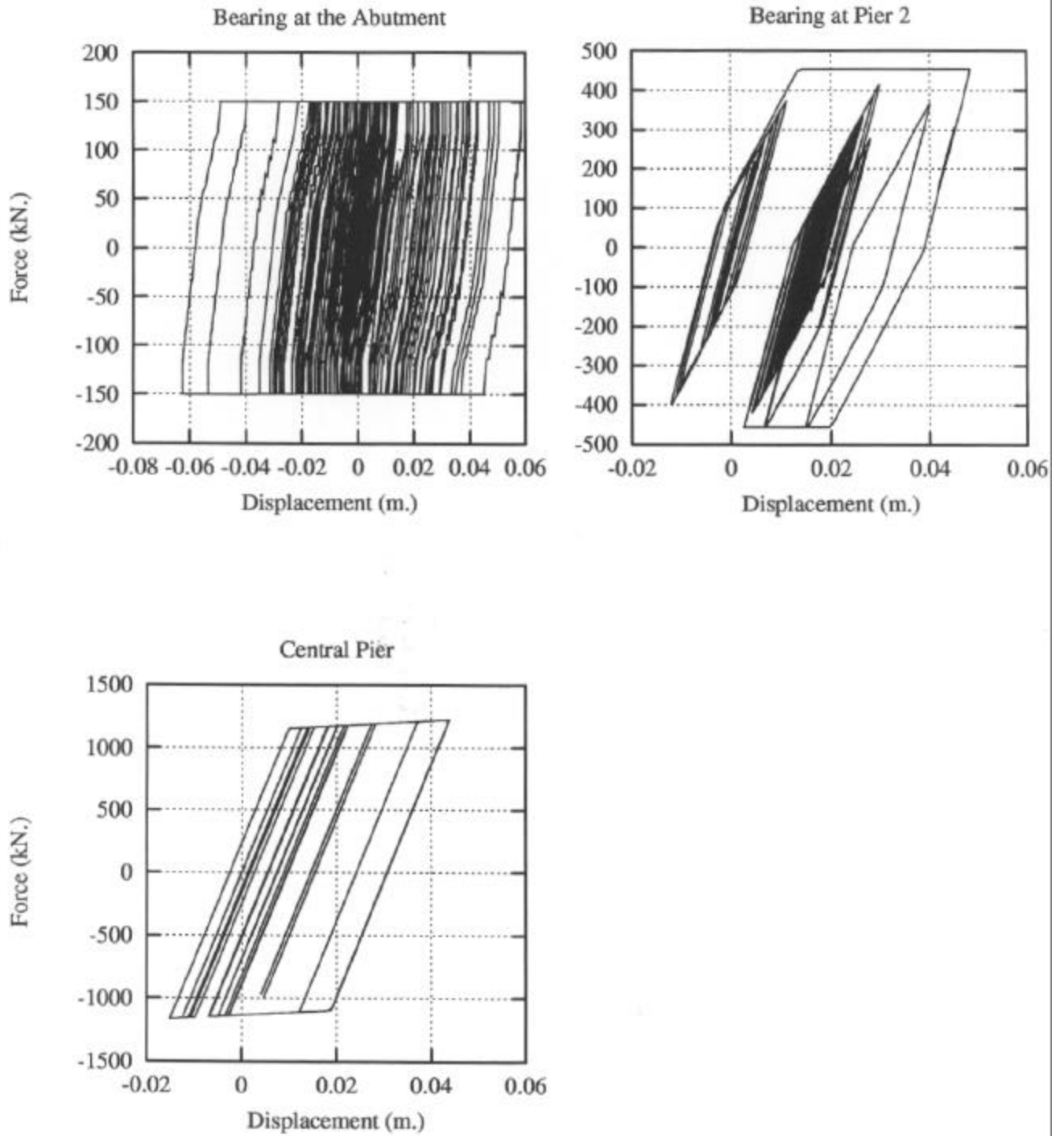


Figure 6.19 Hysteresis for the "As-Built" Bridge at Knox County, IL. Soil Type E

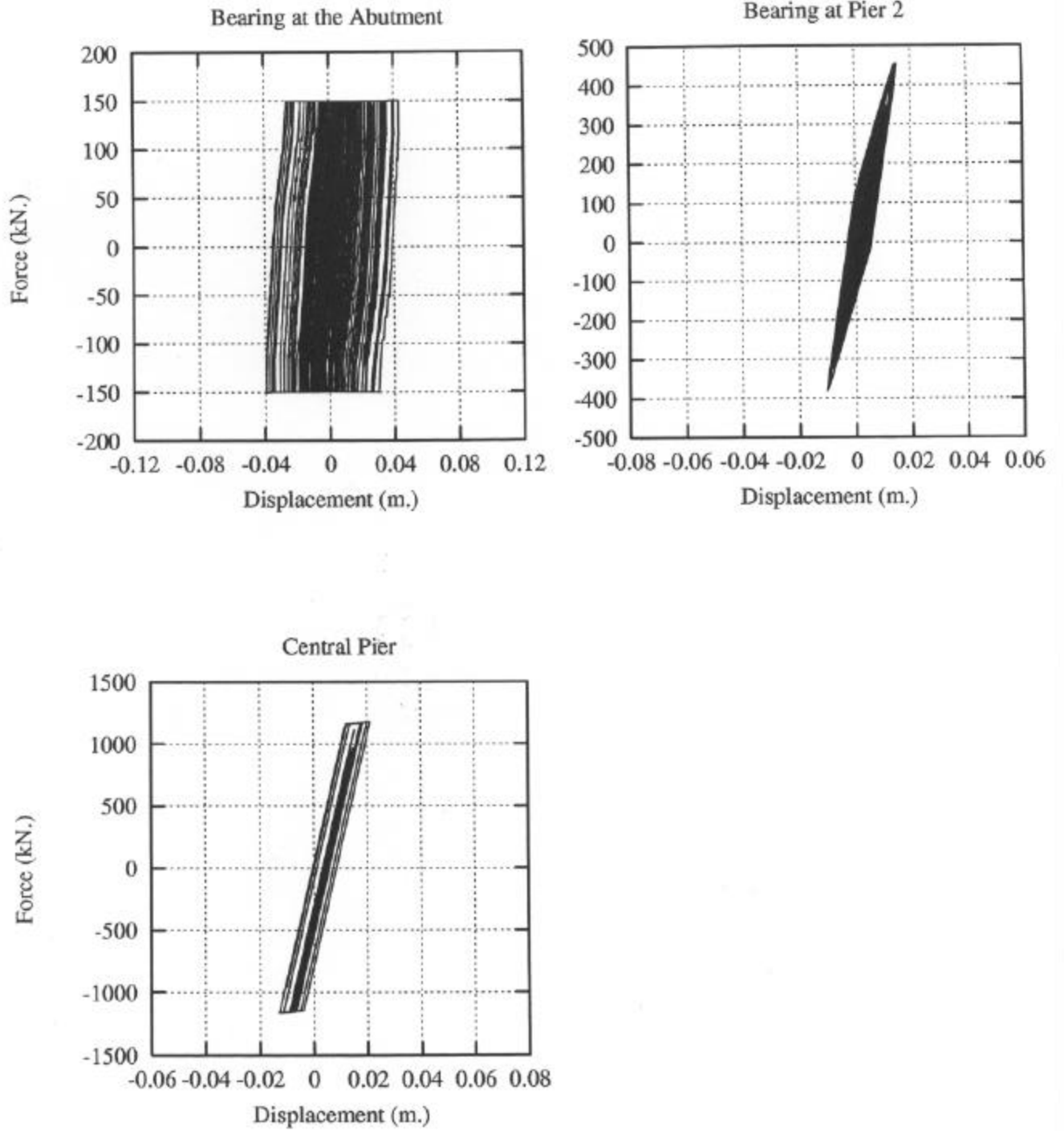


Figure 6.20 Hysteresis for the "As-Built" Bridge at Marion County, IL. Soil Type B

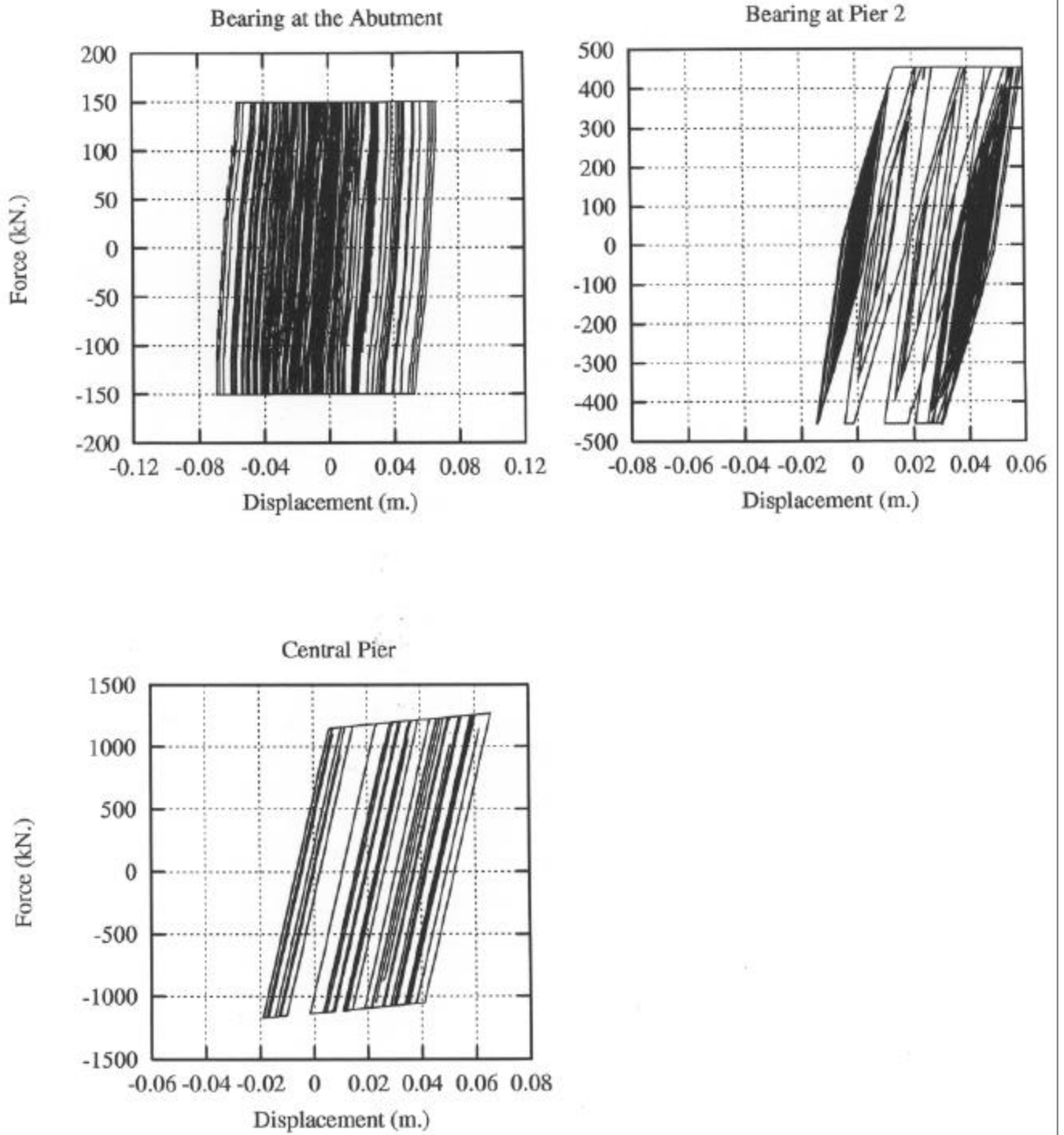


Figure 6.21 Hysteresis for the "As-Built" Bridge at Marion County, IL. Soil Type D

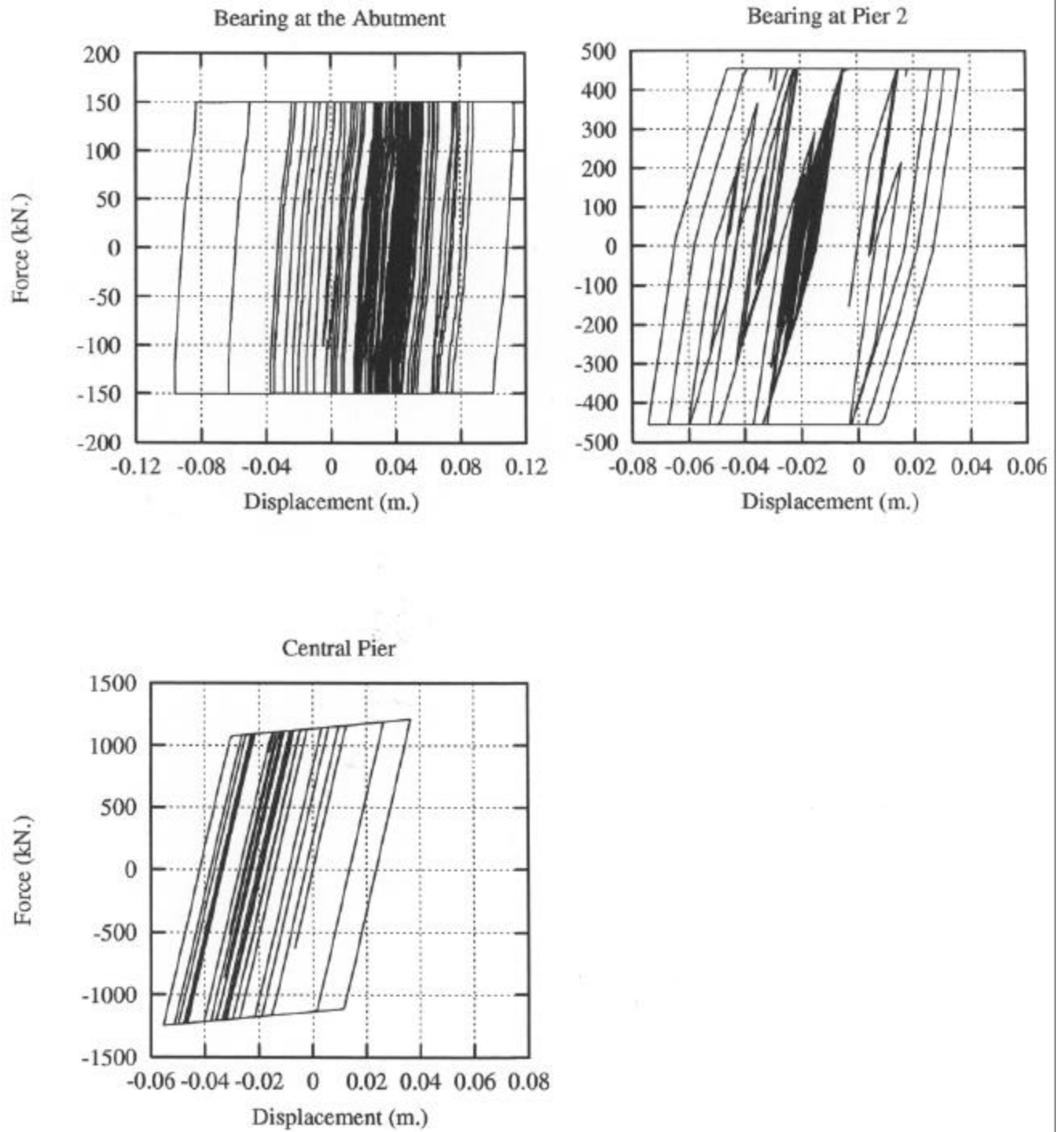


Figure 6.22 Hysteresis for the "As-Built" Bridge at Marion County, IL. Soil Type E

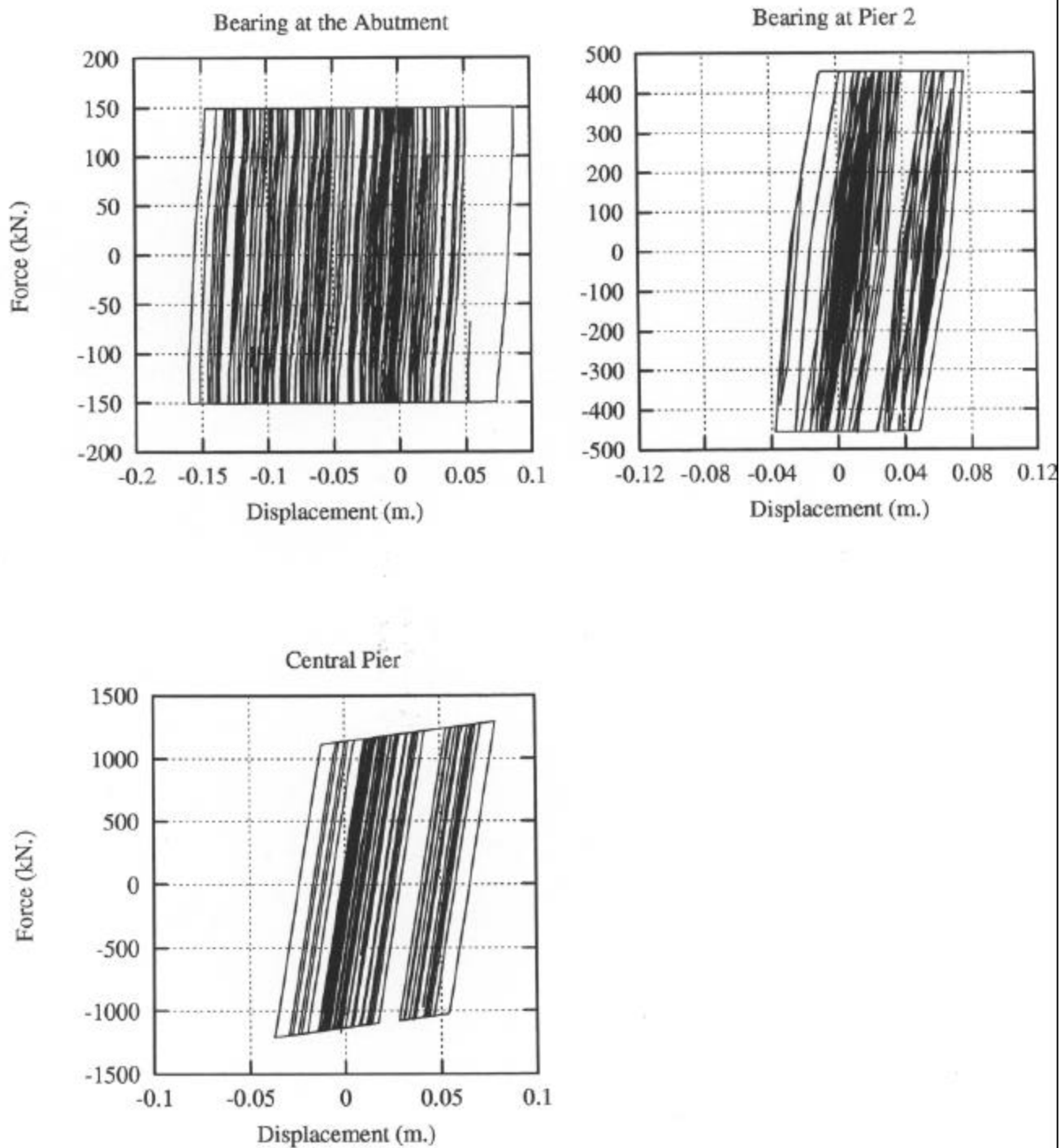


Figure 6.23 Hysteresis for the "As-Built" Bridge at Massac County, IL. Soil Type B

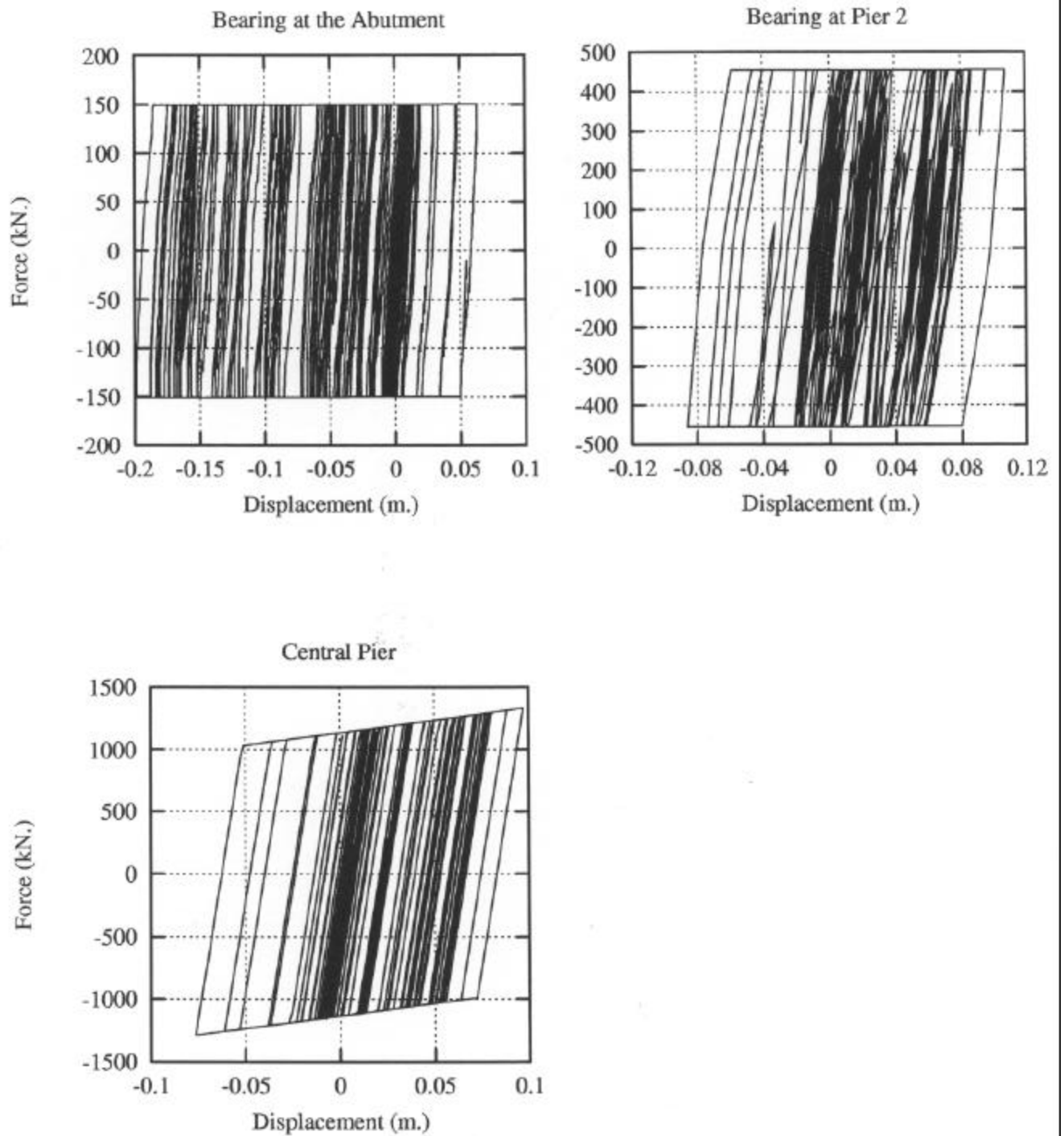


Figure 6.24 Hysteresis for the "As-Built" Bridge at Massac County, IL. Soil Type D

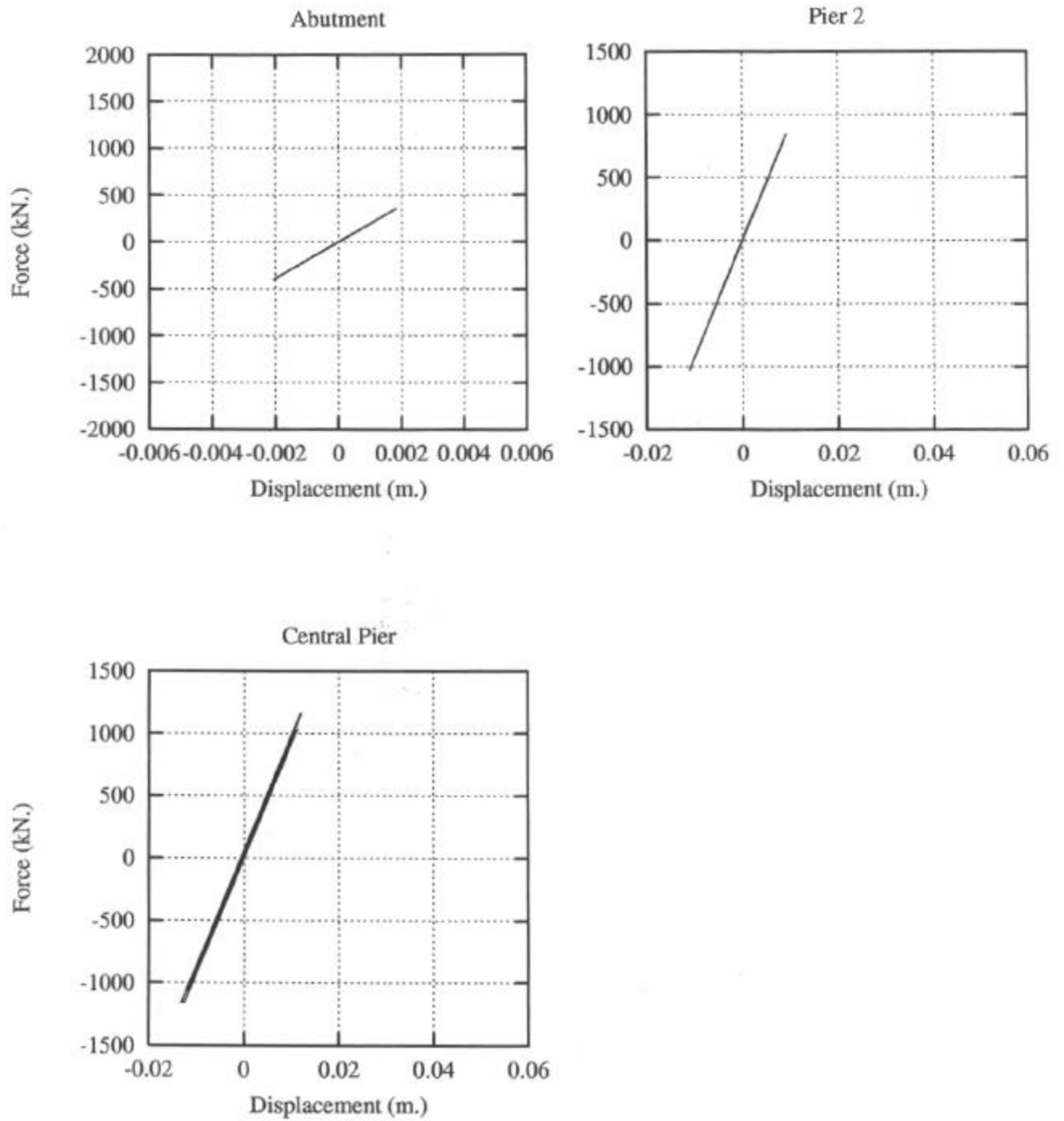


Figure 6.25 Hysteresis for the "Fixed Bearing" Bridge at Knox County, IL. Soil Type B



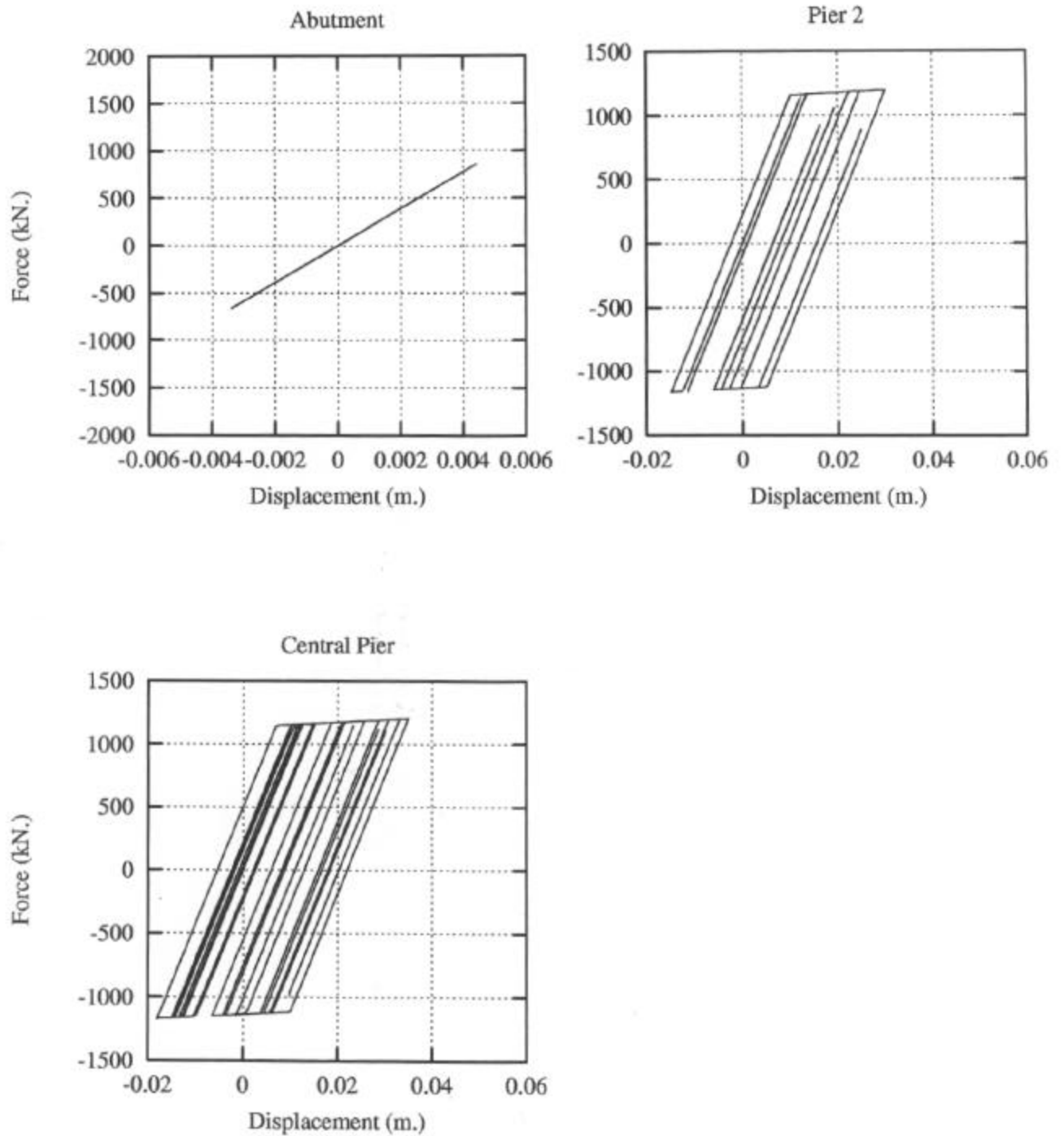


Figure 6.26 Hysteresis for the "Fixed Bearing" Bridge at Knox County, IL. Soil Type D

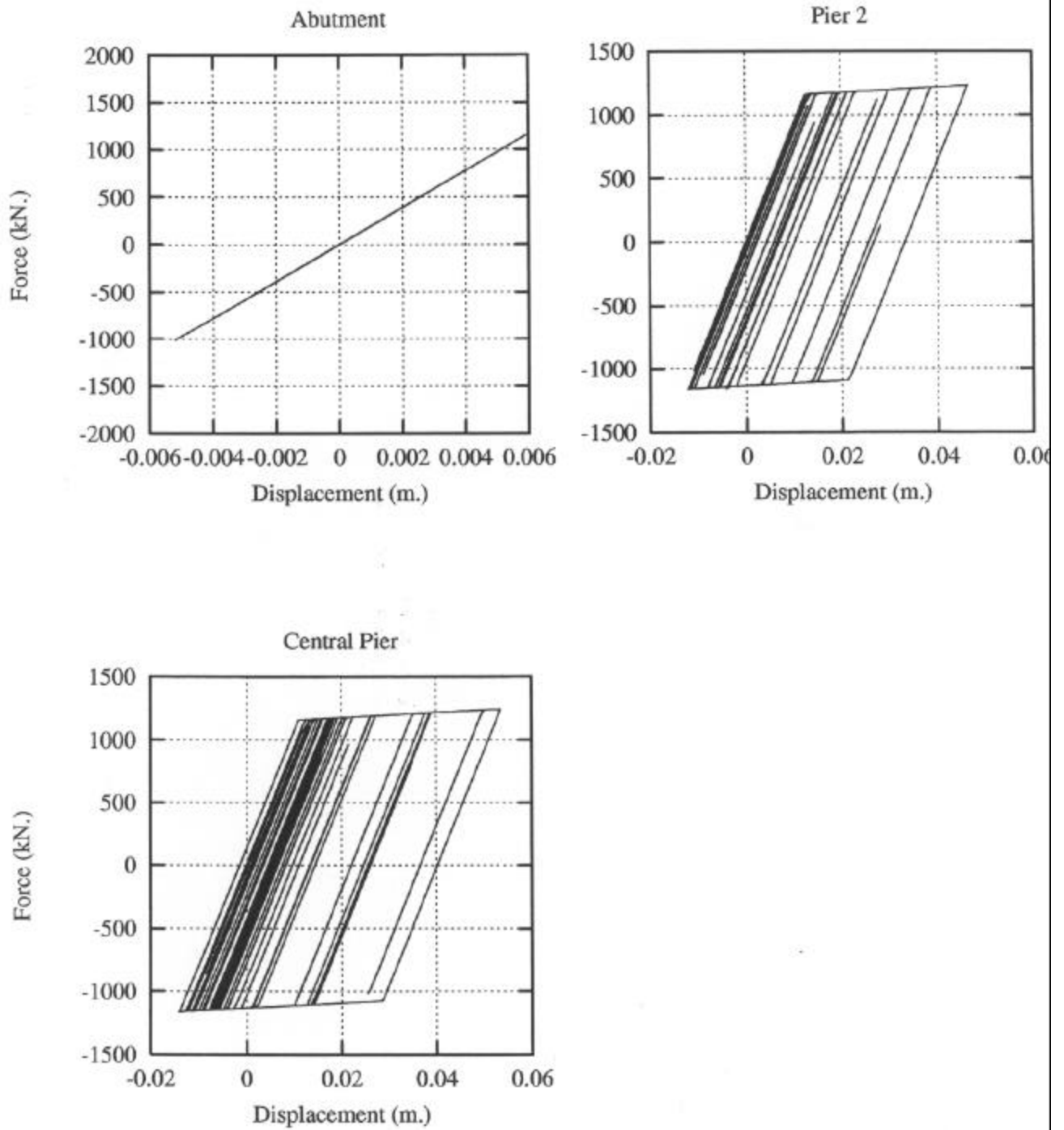


Figure 6.27 Hysteresis for the "Fixed Bearing" Bridge at Knox County,IL. Soil Type E

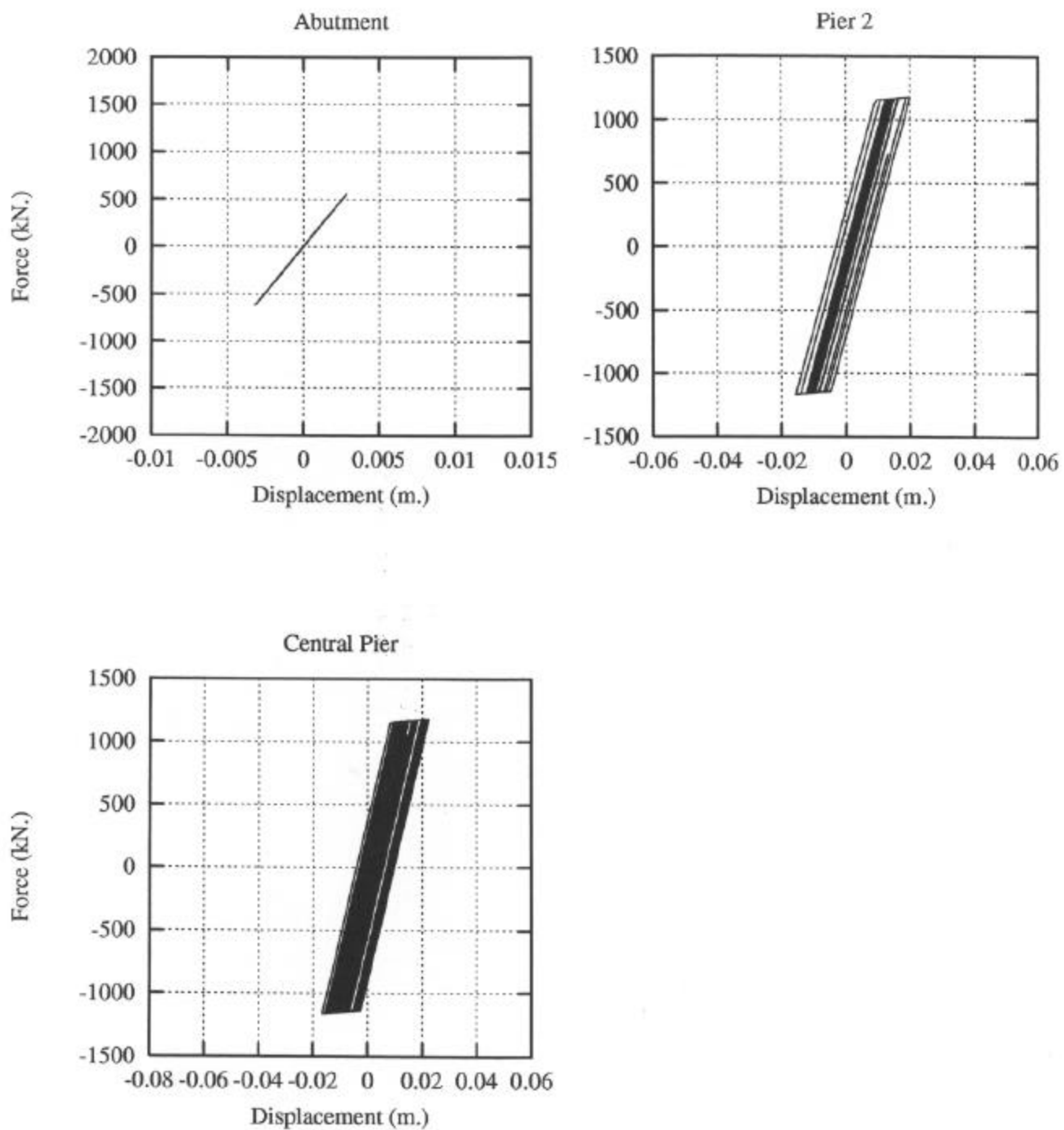


Figure 6.28 Hysteresis for the "Fixed Bearing" Bridge at Marion County, IL. Soil Type B

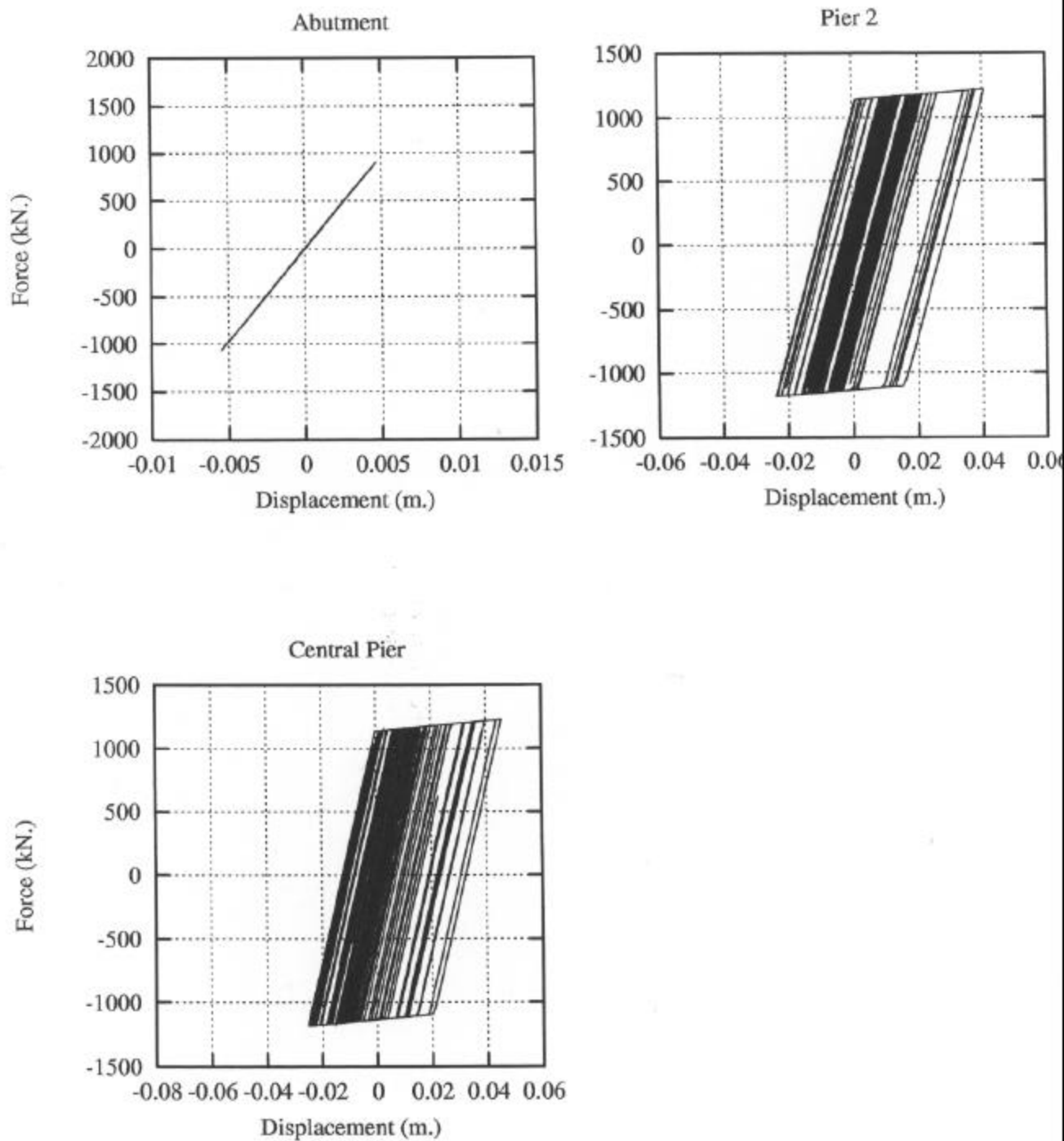


Figure 6.29 Hysteresis for the "Fixed Bearing" Bridge at Marion County, IL. Soil Type D

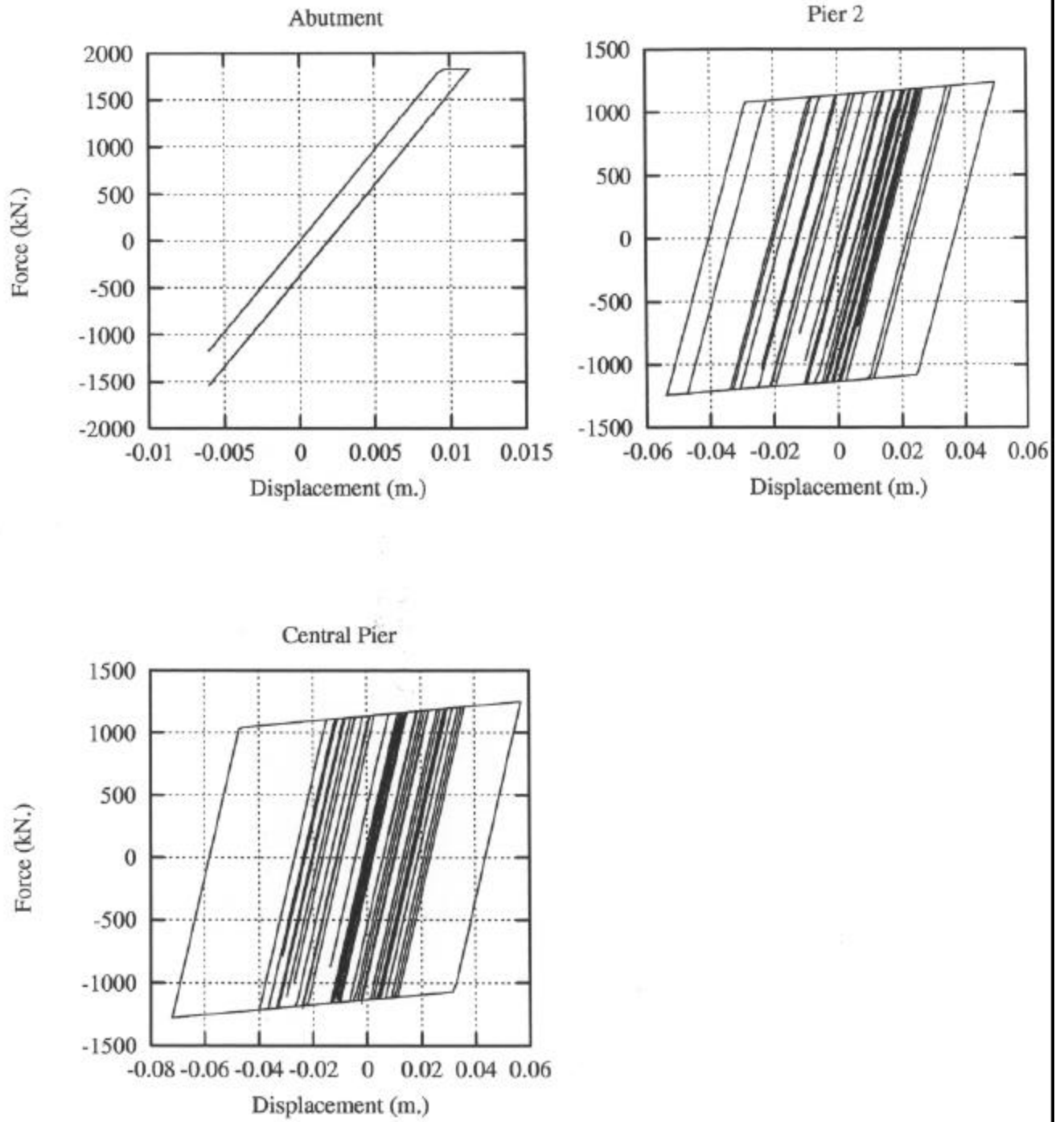


Figure 6.30 Hysteresis for the "Fixed Bearing" Bridge at Marion County, IL. Soil Type E

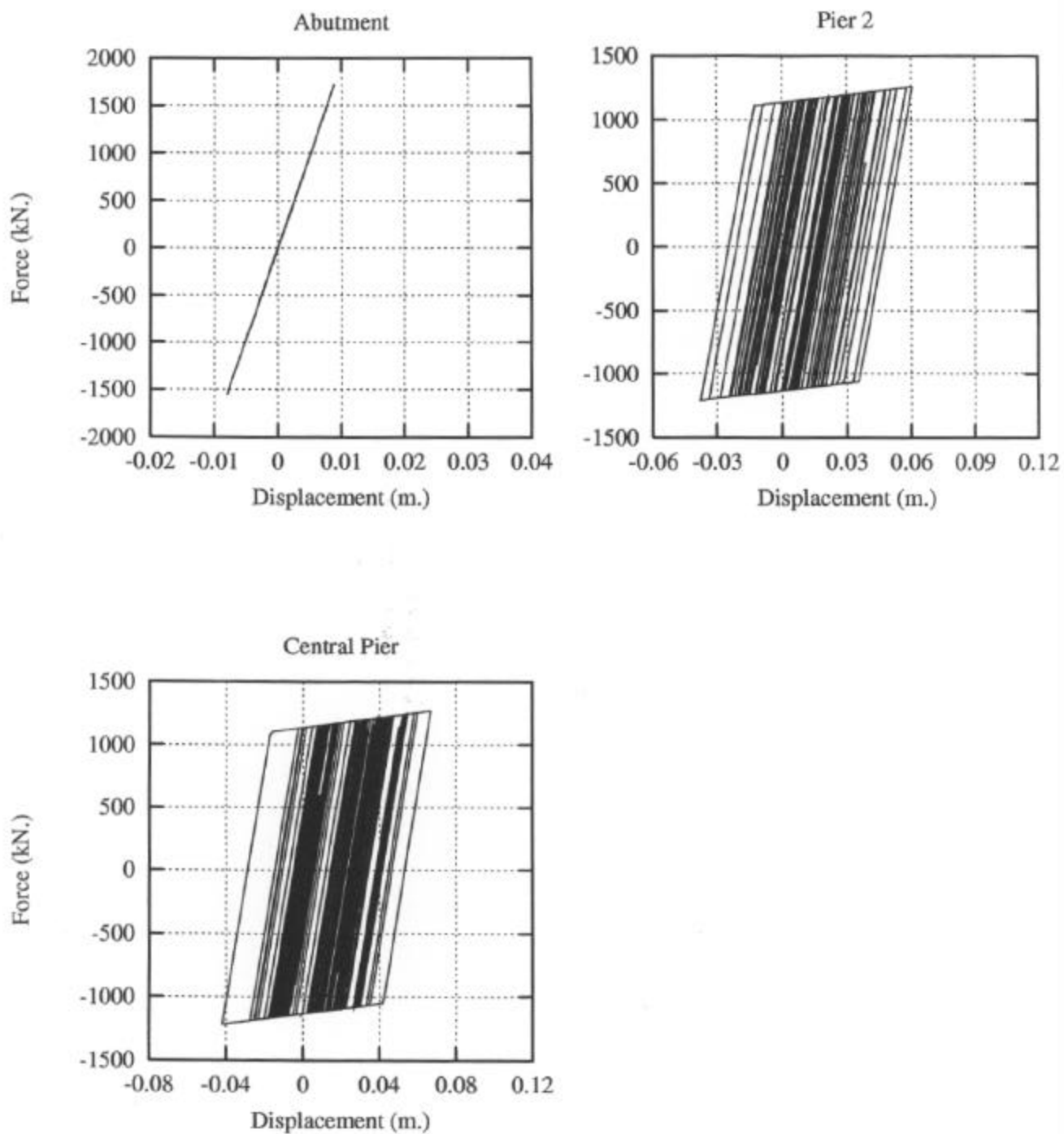


Figure 6.31 Hysteresis for the "Fixed Bearing" Bridge at Massac County, IL. Soil Type B

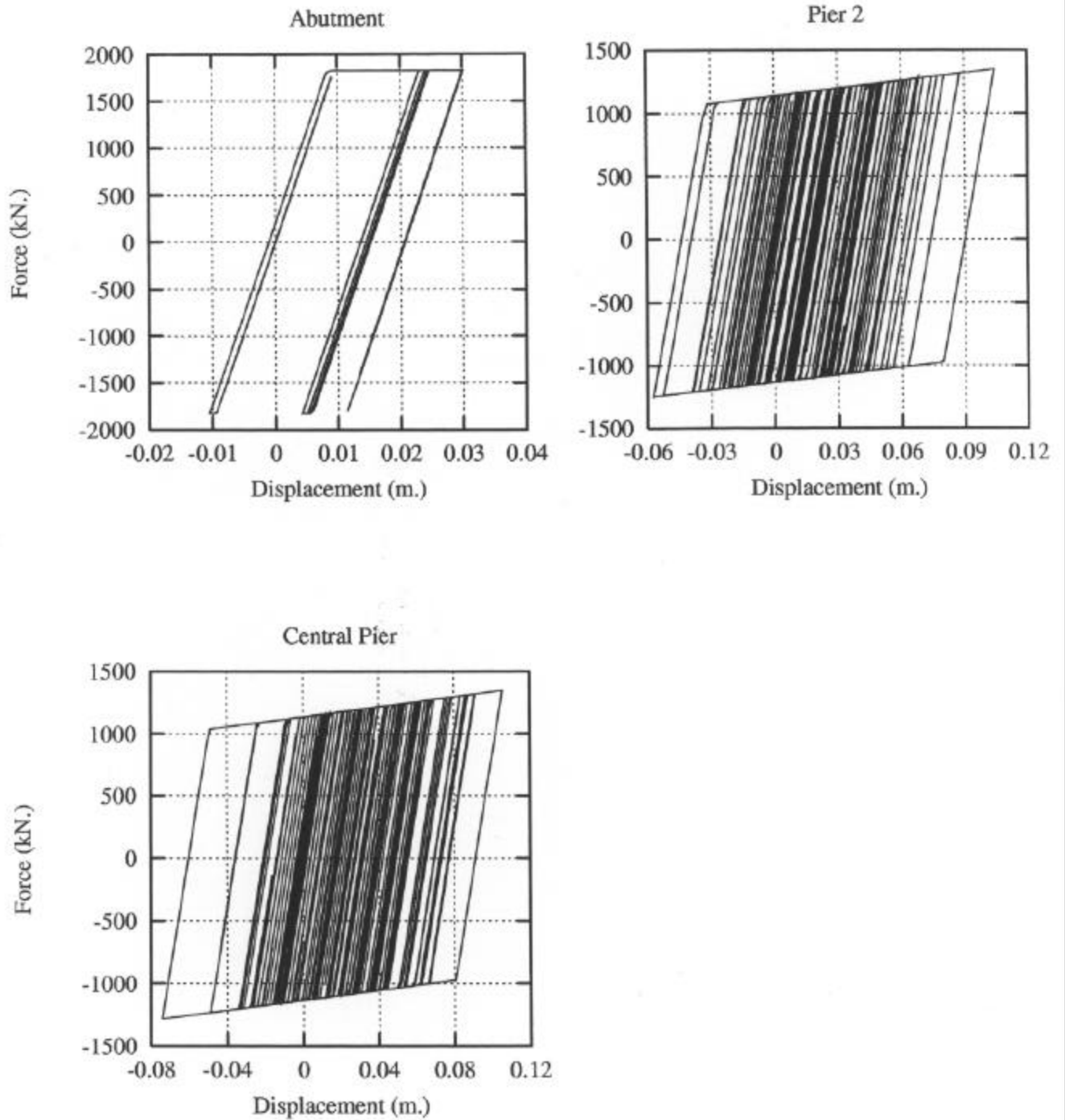


Figure 6.32 Hysteresis for the "Fixed Bearing" Bridge at Massac County, IL. Soil Type D

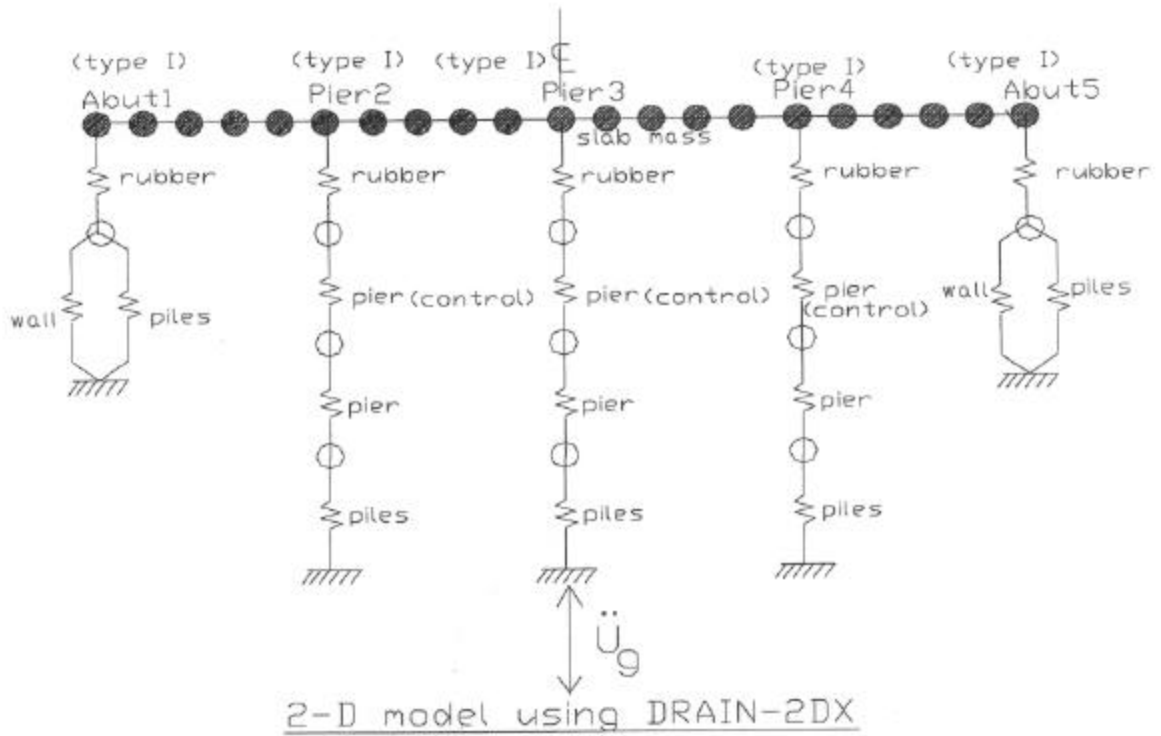


Figure 6.33 Two-Dimensional Bridge Model with ATC-32 Abutment

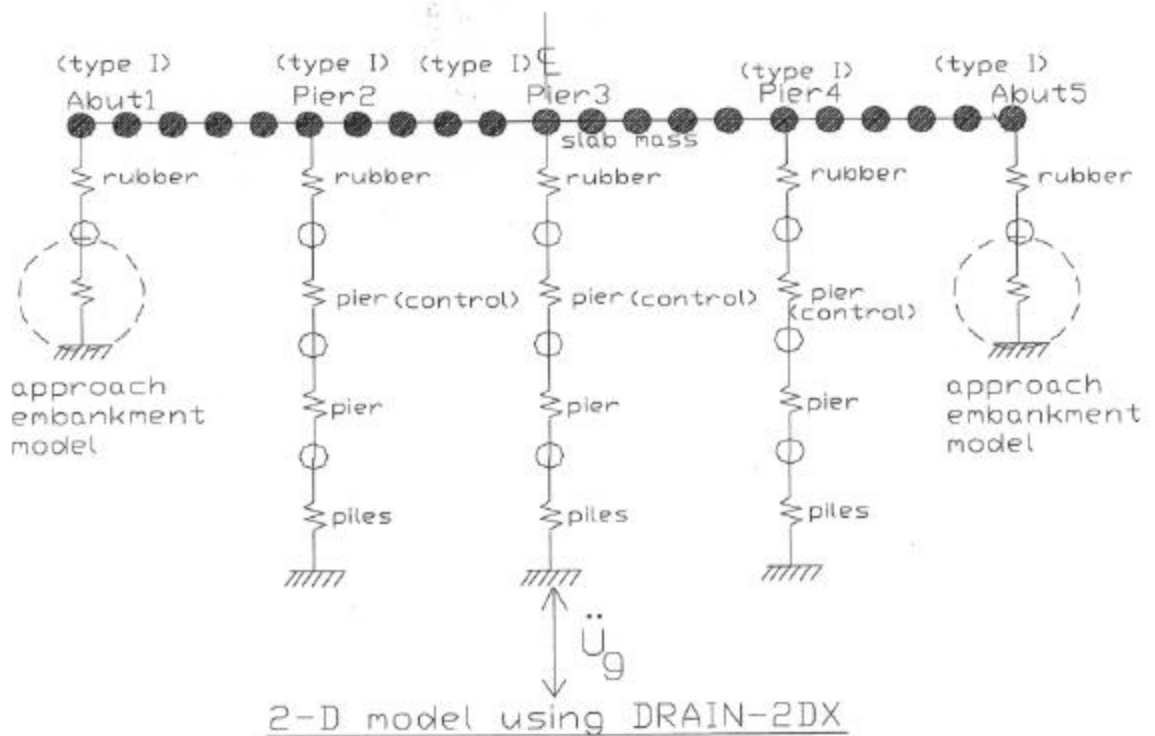


Figure 6.34 Two-Dimensional Bridge Model with Approach-Embankment Model



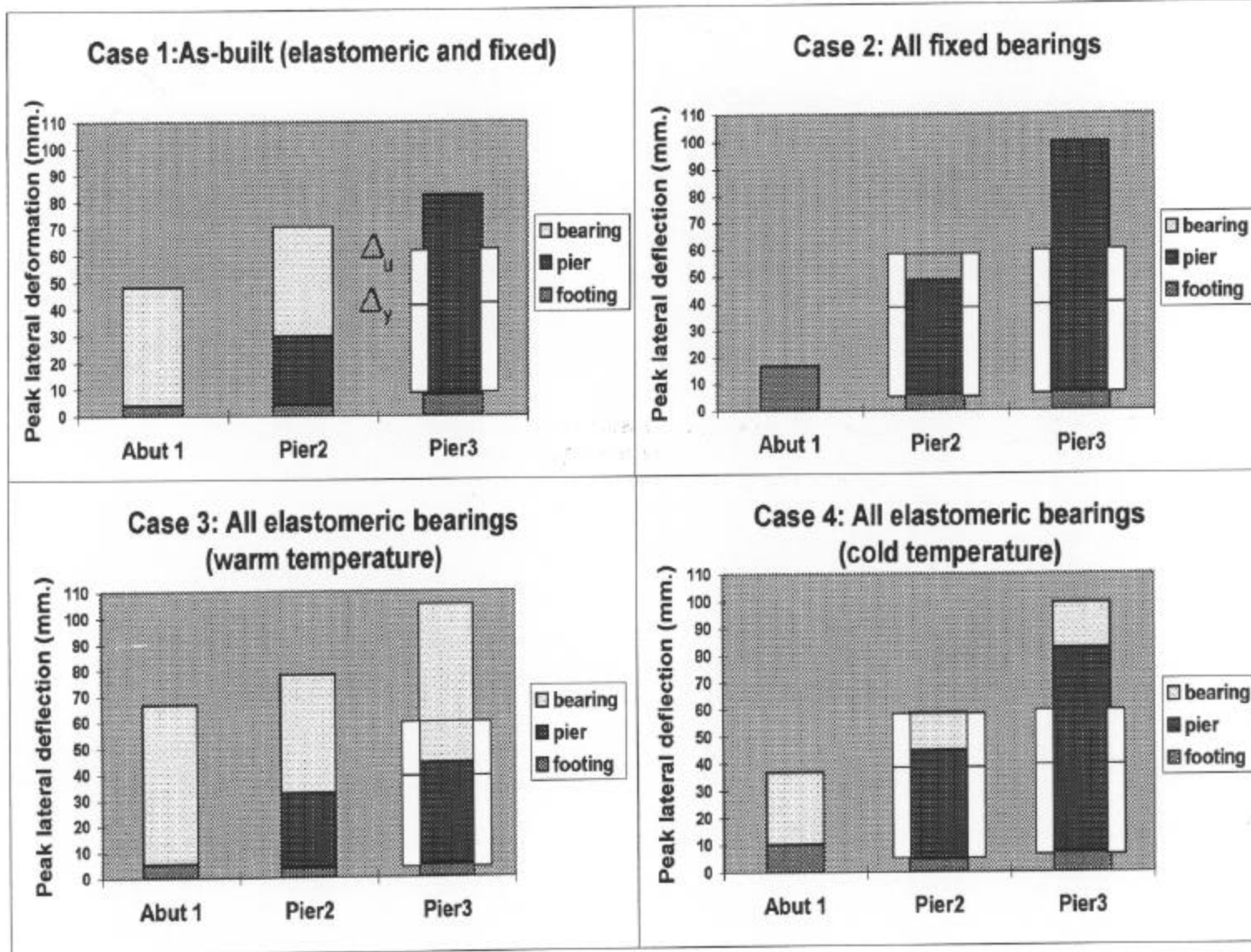


Figure 6.35 Peak Transverse Displacement Responses of Various Bridge Components (Cases 1-4 -- ATC-32 Model)

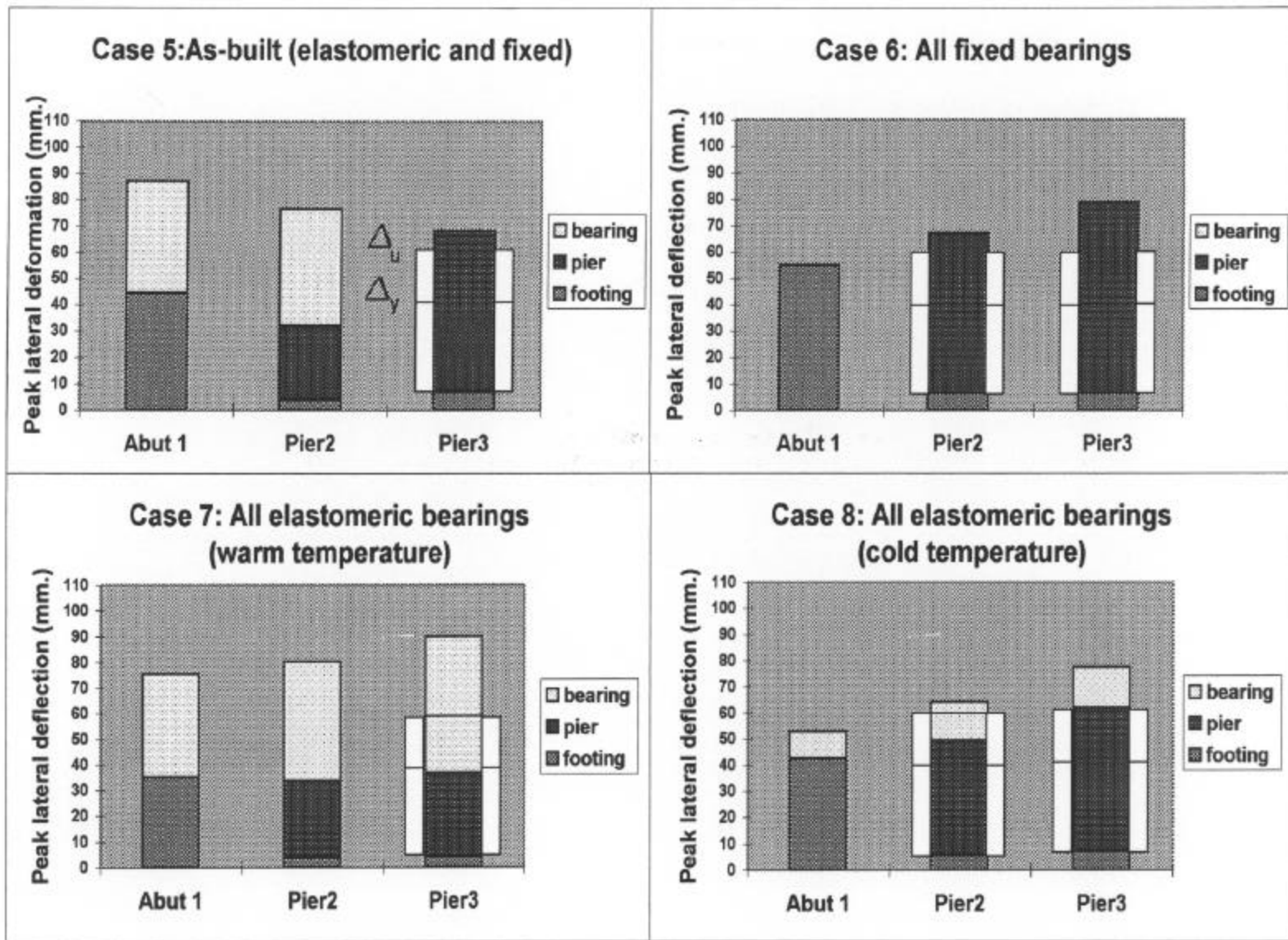


Figure 6.36 Peak Transverse Displacement Responses of Various Bridge Components (Cases 5-8 -- Soil-Slice Model)

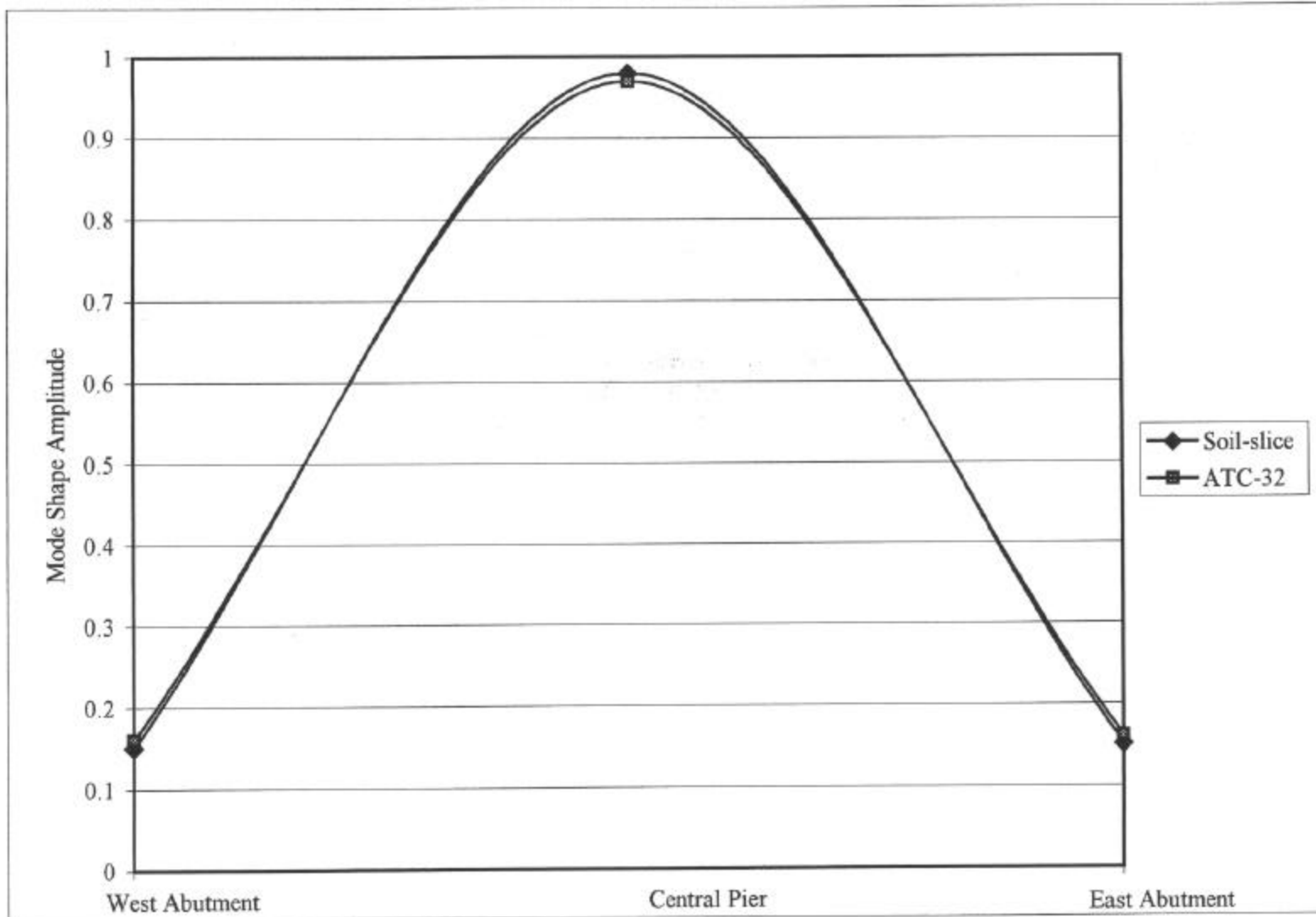


Figure 6.37 Comparison of First PCA Mode Shape for "Low" Level of Shakings

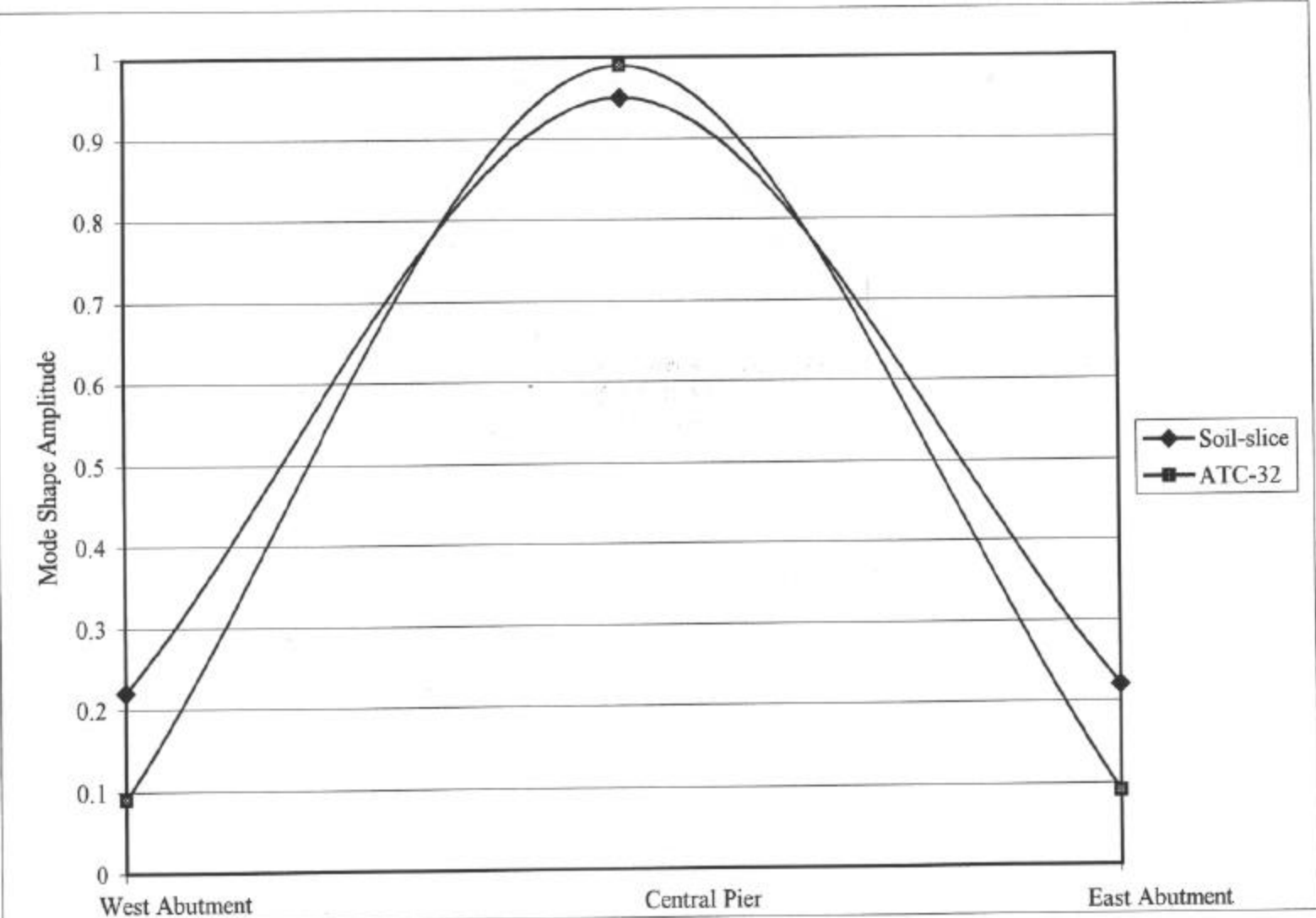


Figure 6.38 Comparison of First PCA Mode Shape for "High" Level of Shakings

## CHAPTER 7

## SUMMARY

7.1 Overview

The transverse response of short bridges is often critical because displacement demands may exceed substructure column displacement capacities. This study focused on modeling of the approach-embankment to predict pier displacement demands in short bridges subjected to seismic excitations, and the reduction of these demands using conventional elastomeric bearings to isolate the superstructure. The following results were obtained:

- (1) The column displacement demand is dominated by the dynamic response of the approach-embankment. An improved approach-embankment model (a soil-pile model) was developed; this incorporates nonlinear hysteretic properties of the soil and accounts for the dynamic response of the approach-embankment and pile-soil interaction at the abutment.
- (2) A simplified version of the approach-embankment model (a soil-slice model) was introduced and calibrated to two California bridges and a representative slab-on-girder bridge. The simplified model is capable of giving a good match between the recorded and the computed bridge displacement response, but the first PCA mode shapes of the two models differ somewhat (Figures 3.42-3.43).
- (3) Iterative nonlinear bearing models for Illinois Type I, II, and III elastomeric bearings were developed for use in nonlinear dynamic response analysis. These models were used to investigate the effectiveness of elastomeric bearings for reducing column displacement demands in Illinois bridges, in conjunction with

various abutment and embankment models. These bearings were found to reduce column displacement demands at warm ambient temperatures. Their effectiveness is reduced at cold temperatures, but low temperature stiffening characteristics vary widely, and experimental data are needed to quantify this behavior for specific cases.

## 7.2 Development of Approach-Embankment Models

An approach-embankment model (a soil-pile model) was developed to explicitly model the dynamic response of the approach-embankment and pile-soil interaction at the abutment. The embankment soil is modeled as nonlinear and the strain-dependent characteristics of the soil are implemented based on normalized modulus reduction curves (Sun et al. 1988). Material damping is accounted for directly in the hysteretic response of the material model. The inertial mass of the embankment soil is included.

The model requires information on the embankment dimensions, basic soil properties such as unit weight, plasticity index, and low-strain shear wave velocity of soil, and the properties of the soil below the abutment piles. Below the abutment, the interaction between the piles and soil is modeled by nonlinear p-y springs, determined using conventional engineering approaches.

The thickness of the embankment slice is the only unknown in this formulation, and is determined empirically to match the recorded response of the Painter Street Overcrossing and the Meloland Road Overpass bridges. The length of approach-embankment to be modeled was found from calibration studies to depend on the intensity of earthquake shaking. The first PCA mode shapes obtained with this model correlated

well to those obtained from recorded response data. Displacement estimates obtained with this model at the central pier were within 20 percent of recorded values in 5 of the 7 cases studied.

### 7.3 A Simplified Version of the Approach-Embankment Model

A simplified model (a soil-slice model) was developed to model the dynamic response of the approach-embankment but without explicitly modeling soil-pile interaction at the abutment. It is calibrated to the recorded response at the MRO and PSO bridges, and to analytically determined responses computed using the soil-pile model for slab-on-girder bridges typical of Illinois and possibly other central U.S. states. Despite its simplicity, the computed bridge response based on a soil-slice model closely matches the recorded bridge response. The recommended thickness of the approach-embankment wedge is generally less than that for the soil-pile model. The reduced thickness results in lower stiffness, compensating for the lack of pile flexibility present in the soil-pile model.

### 7.4 Development of the Bearing Models

A nonlinear iterative model for elastomeric bearings was developed based on observation of test results from Kelly and Quiroz (1992). The hysteretic curve of the bearings is approximated by a bilinear force-displacement relationship. Iterations are required to approximately account for energy dissipation at large amplitude excursions.

Type II and Type III Illinois bridge bearings are modeled using a combination of nonlinear springs. These models can be implemented using nonlinear dynamic response analysis programs such as DRAIN-2DX and DRAIN-3DX (Prakash et al. 1993).

## 7.5 Effectiveness of Elastomeric Bearings for Reducing Illinois Bridge Column

### Displacement Demand

The elastomeric bearing models were used to investigate the effectiveness of the bearings for reducing pier displacements. Several scenarios with different bearing types were studied. Type I, Type II and Type III Illinois bridge bearings were found to reduce column displacement demands relative to bridges employing bearings that fully restrain transverse movement. The increase in bearing stiffness at low temperatures was found to have a significant effect on bridge response and column displacement demands. Stiffness increases with low temperatures depend highly on the formulation of the elastomeric bearing.

## 7.6 Recommendations for Future Research

Approach-embankment models for use in seismic analysis of short bridges were calibrated against the recorded data from instrumented California bridges and extrapolated to Illinois bridges. This was necessary because there is no such recorded data for slab-on-girder bridges. Slab-on-girder bridges that are representative of Illinois bridge construction should be instrumented so that the approach-embankment models proposed herein can be confirmed or refined in the future.

Bearing stiffness increases with reductions in temperature. The stiffness increase is highly dependent on the elastomer formulation. No data on stiffness increase is available for conventional elastomeric bearings commonly used in the central U.S. Low



temperature tests of these bearings should be encouraged to allow their use for isolation to be evaluated using accurate information.

## APPENDIX A

## MODULUS REDUCTION AND DAMPING CURVE FROM THE MODEL

Shear springs in the soil-pile model of Section 3.4.1, derived based on the Iwan (1973) model, are evaluated in this Appendix. To do so, a layer of soil is subject to sinusoidal force with varying amplitude. After one complete cycle, the maximum shear modulus is calculated and the equivalent viscous damping is computed. Three types of soil with varying plasticity indices are used. The maximum shear modulus at  $10^{-4}$  percent shear strain ( $G_0$ ) is kept constant at 76800 kPa.

The equivalent viscous damping ( $\zeta$ ) is computed from

$$\zeta = \frac{A_L}{2pG_{\max}g_{\max}^2} \quad (\text{A-1})$$

as shown in Figure A1 where

$A_L$  = area enclosed by the hysteresis loop

$\gamma_{\max}$  = maximum shear strain

$G_{\max}$  = maximum secant shear modulus at strain  $\gamma_{\max}$

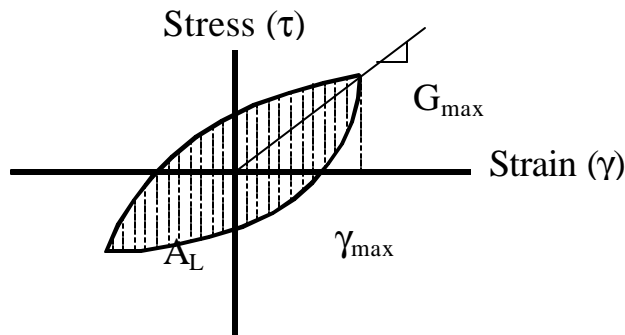


Figure A1. Stress-Strain Relationship for Damping Calculation.

The results are summarized in Table A1.

Table A1. Three Types of Soil with Varying Plasticity Indices.

Case	Plasticity Index	$\gamma_{\max}$ (%)	$G_{\max}/G_0$	$\zeta$ (%)
C1_a	5-10	$6.2 \times 10^{-1}$	0.09	29
C1_b	5-10	$8.2 \times 10^{-2}$	0.35	19
C1_c	5-10	$2.6 \times 10^{-2}$	0.57	11
C1_d	5-10	$4.0 \times 10^{-3}$	0.90	2
C3_a	20-40	$6.9 \times 10^{-1}$	0.20	22
C3_b	20-40	$9.6 \times 10^{-2}$	0.56	11
C3_c	20-40	$6.2 \times 10^{-3}$	0.92	1.5
C5_a	>80	$9.8 \times 10^{-1}$	0.33	16
C5_b	>80	$1.0 \times 10^{-1}$	0.71	5
C5_c	>80	$1.0 \times 10^{-2}$	0.92	1

The hysteresis loops of the first four cases are shown in Figure A2.

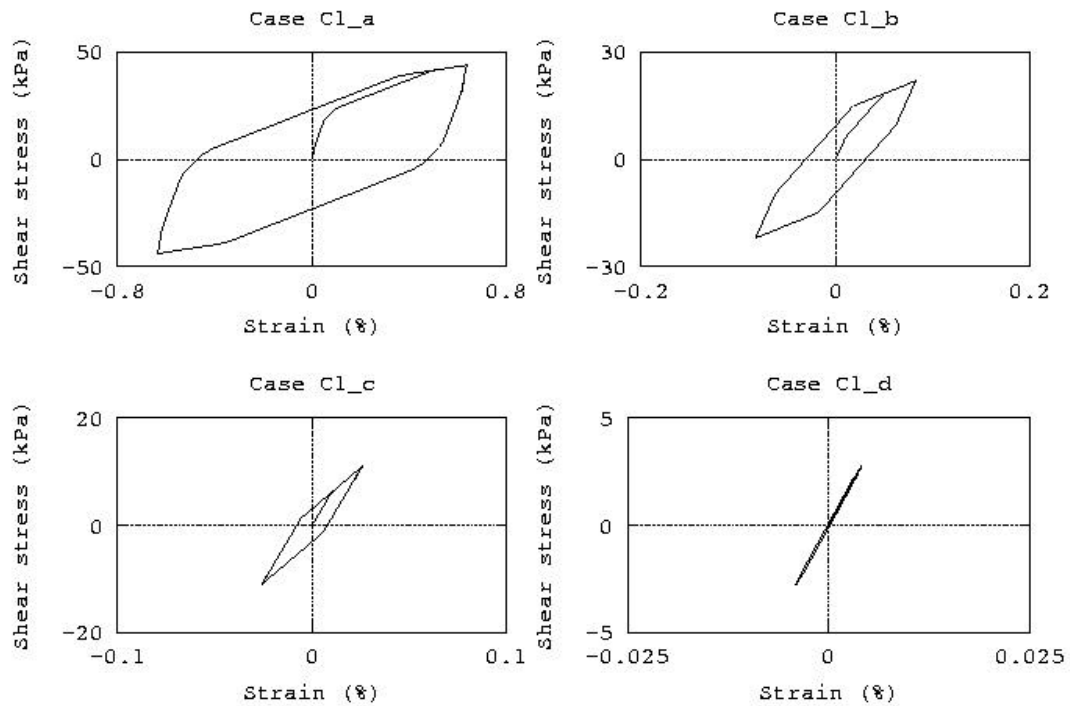


Figure A2. Hysteresis Loop of the First Four Cases

The modulus reduction curves and the damping ratio in each case are plotted on top of the curve from Sun's report (Sun et al. 1988) as shown in Figure A3 and A4.

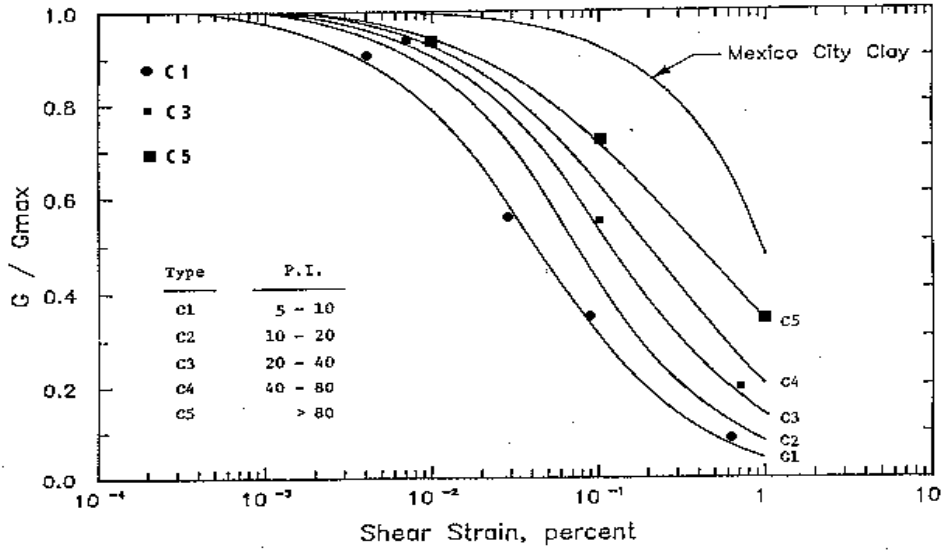


Figure A3. Normalized Modulus Reduction Curves for Clays with Different Plasticity Indices. (from Sun et al.1988)

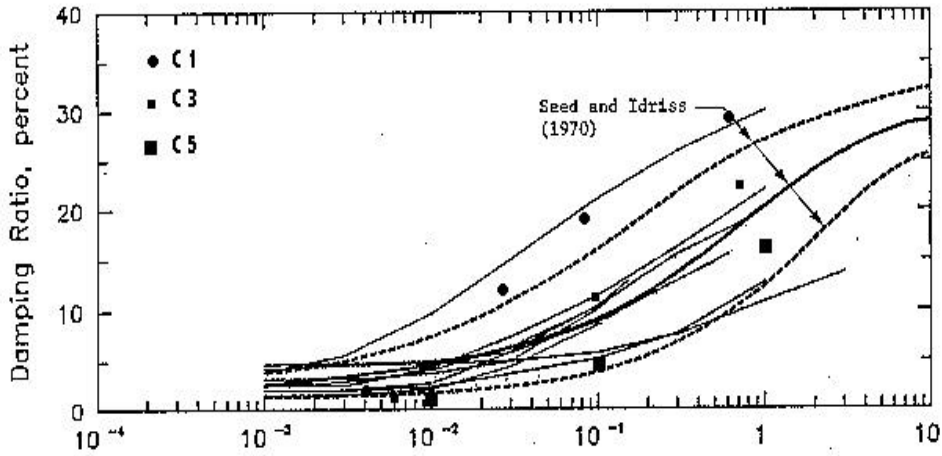


Figure A4. Strain Dependent Damping Ratio for Clays. (from Sun et al. 1988)

The calculated  $G/G_{max}$  versus strain and damping versus strain are also plotted against Vucetic and Dobry curves (Vucetic and Dobry 1991) as shown in Figures A5 and A6.

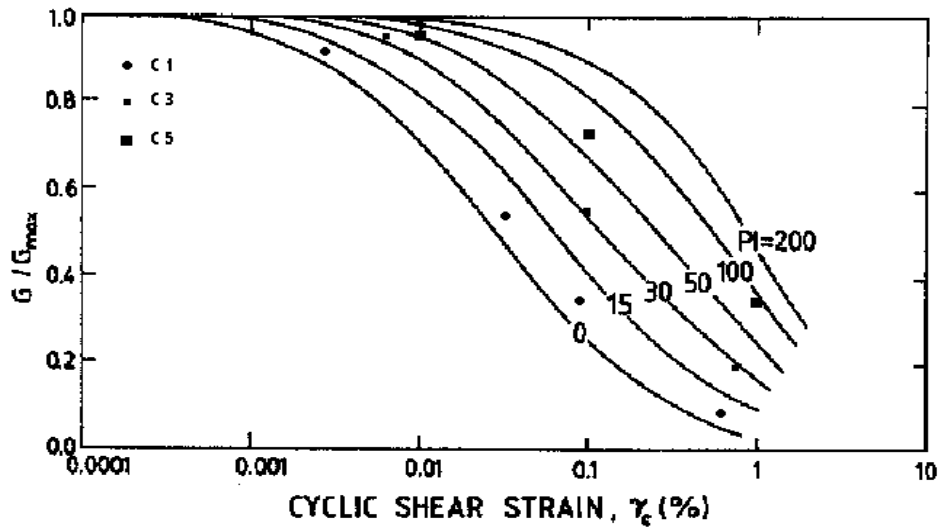


Figure A5. Modulus Reduction Curves for Fine-grained Soils of Different Plasticity. (from Vucetic and Dobry 1991).

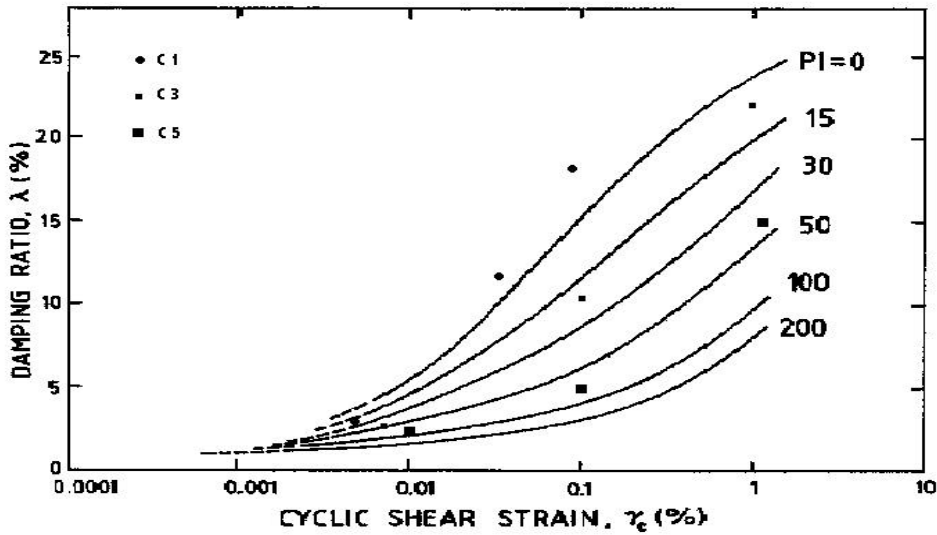


Figure A6. Damping Ratio of Fine-grained Soil with Cyclic Shear Strain Amplitude and Plasticity Index. (from Vucetic and Dobry 1991).

Sun et al. 1988 reported that plasticity index is the most dominant and consistent factor on the form of the normalized modulus reduction relationships for cohesive soils. It

is evident that the higher the plasticity indices, the slower the rate of modulus reduction with increasing shear strain. The model is able to represent the modulus reduction curves reasonably well over the range of shear strain. For damping characteristics of cohesive soils, the calculated damping ratio also fell within the range as indicated by Seed and Idriss (1970) as well as Vucetic and Dobry (1991).

## APPENDIX B

## EXAMPLE FILES

The following files are presented as examples:

- B.1 Three-Dimensional Modeling of PSO in DRAIN-3DX using a Soil-Pile Model
- B.2 Three-Dimensional Modeling of MRO in DRAIN-3DX using a Soil-Slice Model
- B.3 Three-Dimensional Modeling of IL-1 in DRAIN-3DX using a Soil-Slice Model
- B.4 Matlab Routine Used to Determine Parameters for the Elastoplastic Elements  
(Shear Springs in Chapter 3)
- B.5 Nonlinear Push-Over Analysis of Multiple Pier-Columns using DRAIN-2DX  
(Figure 5.3)
- B.6 Two-Dimensional Modeling of a Representative Illinois Bridge in  
DRAIN-2DX (Figure 6.13)

### B.1 Three-Dimensional Modeling of PSO in DRAIN-3DX using a Soil-Pile Model

```

! CHATDANAI WISSAWAPAISAL. DRAIN 3DX INPUT FILE
! ANALYSIS OF PAINTER STREET OVERPASS USING A SOIL-PILE MODEL
! ALL UNITS IN kN, m, sec.
!
!   5   10   15   20   25   30   35   40   45   50   55   60   65   70
!UNITS L m F kn
*STARTXX                P-DELTA
      PSO                0 1 1 1                PAINTER STREET
! CONSIDER P-DELTA EFFECT
*NODECOORDS
C     1000      0.0      0.0      0.0
C     2000     44.5      0.0      0.0
L     1000     2000     100     9     0.0
C     3000     80.8      0.0      0.0
C     2700     76.3      0.0      0.0
L     2000     2700     100     6     0.0
C     2001     40.86     4.5     -8.185
C     2002     40.86     4.5     -5.745
C     2003     40.86     4.5     -3.305
C     4008     40.86     4.5      0.0
C     2005     48.14     -4.5     -8.185
C     2006     48.14     -4.5     -5.745
C     2007     48.14     -4.5     -3.305
C     2008     48.14     -4.5      0.0
C     9000      0.0      1.0      0.0
C     3011     80.8      0.0      0.0
C     2009     40.86     4.5     -8.185
C     2010     40.86     4.5     -8.185
C     2011     40.86     4.5     -8.185
C     2012     48.14     -4.5     -8.185
C     2013     48.14     -4.5     -8.185
C     2014     48.14     -4.5     -8.185
!reference nodes
C     9990      0.0      1.0      0.0
C     9991      1.0      0.0      0.0
C     9992     80.8      1.0      0.0
C     9993     81.8      0.0      0.0
!west abutment- y direction
C     7005      0.0      0.0     -1.78
C     7010      0.0     0.0000    -3.56
C     7011      0.0     0.0000    -3.56
C     7020      0.0     0.0000   -4.435
C     7021      0.0     0.0000   -4.435
C     7025      0.0     0.0000   -5.310
C     7026      0.0     0.0000   -5.310
C     7030      0.0     0.0000   -6.185
C     7031      0.0     0.0000   -6.185
C     7035      0.0     0.0000   -7.060
C     7036      0.0     0.0000   -7.060
C     7040      0.0     0.0000   -7.935
C     7041      0.0     0.0000   -7.935
C     7045      0.0     0.0000   -8.810
C     7046      0.0     0.0000   -8.810
C     7050      0.0     0.0000   -9.685

```



C	7051	0.0	0.0000	-9.685
C	7060	0.0	0.0000	-11.435
C	7061	0.0	0.0000	-11.435
C	7070	0.0	0.0000	-13.185
C	7071	0.0	0.0000	-13.185
C	7080	0.0	0.0000	-14.935
C	7081	0.0	0.0000	-14.935
!west abutment - x direction				
C	7111	0.0	0.0000	-3.56
C	7121	0.0	0.0000	-4.435
C	7125	0.0	0.0000	-5.310
C	7126	0.0	0.0000	-5.310
C	7131	0.0	0.0000	-6.185
C	7135	0.0	0.0000	-7.060
C	7136	0.0	0.0000	-7.060
C	7141	0.0	0.0000	-7.935
C	7145	0.0	0.0000	-8.810
C	7146	0.0	0.0000	-8.810
C	7151	0.0	0.0000	-9.685
C	7161	0.0	0.0000	-11.435
C	7171	0.0	0.0000	-13.185
C	7181	0.0	0.0000	-14.935
!east abutment - y direction				
C	8005	80.8	0.0000	-1.78
C	8010	80.8	0.0000	-3.56
C	8011	80.8	0.0000	-3.56
C	8020	80.8	0.0000	-4.435
C	8021	80.8	0.0000	-4.435
C	8025	80.8	0.0000	-5.310
C	8026	80.8	0.0000	-5.310
C	8030	80.8	0.0000	-6.185
C	8031	80.8	0.0000	-6.185
C	8035	80.8	0.0000	-7.060
C	8036	80.8	0.0000	-7.060
C	8040	80.8	0.0000	-7.935
C	8041	80.800	0.0000	-7.935
C	8045	80.800	0.0000	-8.810
C	8046	80.800	0.0000	-8.810
C	8050	80.800	0.0000	-9.685
C	8051	80.800	0.0000	-9.685
C	8060	80.800	0.0000	-11.435
C	8061	80.800	0.0000	-11.435
C	8070	80.800	0.0000	-13.185
C	8071	80.800	0.0000	-13.185
C	8080	80.800	0.0000	-14.935
C	8081	80.800	0.0000	-14.935
!east abutment - x direction				
C	8111	80.800	0.0000	-3.56
C	8121	80.800	0.0000	-4.435
C	8125	80.800	0.0000	-5.310
C	8126	80.800	0.0000	-5.310
C	8131	80.800	0.0000	-6.185
C	8135	80.800	0.0000	-7.060
C	8136	80.800	0.0000	-7.060
C	8141	80.800	0.0000	-7.935
C	8145	80.800	0.0000	-8.810
C	8146	80.800	0.0000	-8.810

```

C      8151      80.800      0.0000      -9.685
C      8161      80.800      0.0000     -11.435
C      8171      80.800      0.0000     -13.185
C      8181      80.800      0.0000     -14.935
!
*RESTRAINTS
S      001100      1000
S      001100      3000
S      111111      3011
S      111111      2009
S      111111      2010
S      111111      2011
S      111111      2012
S      111111      2013
S      111111      2014
S      111111      2001
S      111111      2005
!reference nodes
S      111111      9990
S      111111      9991
S      111111      9992
S      111111      9993
!west abutment
S      001001      7005
S      001001      7010      7080      10
!west abutment - y direction
S      101111      7011      7041      10
S      101111      7025      7026      1
S      101111      7035      7036      1
S      101111      7045
S      111111      7046
S      111111      7051      7081      10
!west abutment - x direction
S      011111      7111      7141      10
S      011111      7125      7126      1
S      011111      7135      7136      1
S      011111      7145
S      111111      7146
S      111111      7151      7181      10
!east abutment
S      001001      8005
S      001001      8010      8080      10
!east abutment - y direction
S      101111      8011      8041      10
S      101111      8025      8026      1
S      101111      8035      8036      1
S      101111      8045
S      111111      8046
S      111111      8051      8081      10
!east abutment - x direction
S      011111      8111      8141      10
S      011111      8125      8126      1
S      011111      8135      8136      1
S      011111      8145
S      111111      8146
S      111111      8151      8181      10
!

```

## \*MASSES

```

! SLAB MASS
! ALL MASS IS CONSIDERED.
S 111 2110.0 1000 9.81 1.0
S 111 2110.0 3000
S 111 923.0 1100 2700 100
! EMBANKMENT SOIL MASS IN EACH LAYER
S 110 7.69e+002 7005
S 010 1.10e+003 7021
S 010 1.44e+003 7031
S 010 1.77e+003 7041
S 100 1.10e+003 7121
S 100 1.44e+003 7131
S 100 1.77e+003 7141
S 110 7.69e+002 8005
S 010 1.10e+003 8021
S 010 1.44e+003 8031
S 010 1.77e+003 8041
S 100 1.10e+003 8121
S 100 1.44e+003 8131
S 100 1.77e+003 8141
! CENTRAL PIER MASS
S 111 110.0 2002 2003 1
S 111 110.0 2006 2007 1
S 111 55.0 4008
S 111 55.0 2008
S 111 474.0 2001
S 111 474.0 2005
*ELEMENTGROUP
!
! --PD- --beta---- -
17 1 0 0.000970 SLAB
! CONTROL INFORMATION
! 5 10 15 20 25 30 35 40 45 50 55 60 65 70
1 1 1 0
! MATERIAL PROPERTIES
1 2.62E7 1.14E7
! CROSS SECTION PROPERTIES
1 10.1 3.3 156.0 7.9 4.81 2.98
! STIFFNESS FACTORS
1 4.0 4.0 2.0
! ELEMENT GENERATION COMMANDS
1 1000 1100 100 9000 1 1 0 0 0
17 2600 2700 100 9000 1 1 0 0 0
18 2700 3000 300 9000 1 1 0 0 0
*ELEMENTGROUP
!
! --PD- --beta---- -
17 1 0 0.000970 BENT
! CONTROL INFORMATION
! 5 10 15 20 25 30 35 40 45 50 55 60 65 70
1 1 1 0
! MATERIAL PROPERTIES
1 2.62E7 1.14E7
! CROSS SECTION PROPERTIES
1 1060.0 720.0 680.0 2.91

```

```

! STIFFNESS FACTORS
  1      4.0      4.0      2.0
! ELEMENT GENERATION COMMANDS
  1      2008      2000      9000      1      1      0      0      0
  2      2000      4008      9000      1      1      0      0      0
*ELEMENTGROUP
!
!      --PD- --beta----      -
  17     1      1      0.000970      PIER
! CONTROL INFORMATION
!   5   10   15   20   25   30   35   40   45   50   55   60   65   70
  1     1     1     1
! MATERIAL PROPERTIES
  1     2.62E7     1.14E7
! CROSS SECTION PROPERTIES
  1     0.59     0.15     0.15     1.92     1.92     1.92
! STIFFNESS FACTORS
  1      4.0      4.0      2.0
! RIGID END ZONES
  1     0.0     0.0    -0.865
! ELEMENT GENERATION COMMANDS
  1      2001      2002      1      2000      1      1      0      0      0
  2      2002      2003      1      2000      1      1      0      0      0
  3      2003      4008      1      2000      1      1      0      0      0
  4      2005      2006      1      2000      1      1      0      0      0
  5      2006      2007      1      2000      1      1      0      0      0
  6      2007      2008      1      2000      1      1      0      0      0
*ELEMENTGROUP
! (restrain the nodes for fixed base pier)
!      --PD- --beta----      -
  4     1     0     0.000970      BASE PIER SPRINGS
! CONTROL INFORMATION
!   5   10   15   20   25   30   35   40   45   50   55   60   65   70
  2     3
! PROPERTY TYPES
! ELASTIC SPRING
  1     6.0E5     1E-06     1.000E7     1.000E7     1.0     1     1
  2     2.5E5     1E-06     1.000E7     1.000E7     1.0     1     1
! DIRECTION TYPES
!   5   10   15   20   25   30   35   40   45   50   55   60   65   70
  1     0.777     0.629     0.000     -0.629     0.777     0.0
  2     0.629     -0.777     0.000     0.777     0.629     0.0
  3     0.000     0.000     -1.000     1.000     0.000     0.0
! ELEMENT GENERATION COMMANDS
  1      2001      2011      2      1      1
  2      2001      2010      2      2      1
  3      2001      2009      1      3      1
  4      2005      2014      2      1      1
  5      2005      2013      2      2      1
  6      2005      2012      1      3      1
*ELEMENTGROUP
!
!      --PD- --beta----      -
  4     1     0     0.000970      BACKWALL SPRINGS
! CONTROL INFORMATION
!   5   10   15   20   25   30   35   40   45   50   55   60   65   70
  1     1

```

```

! PROPERTY TYPES
! ELASTIC SPRING
   1   8.80E4   1E-06   1.00E7   1.00E7   1.0   1   1
! DIRECTION TYPES
!   5   10   15   20   25   30   35   40   45   50   55   60   65   70
   1   0.777   0.629   0.000   -0.629   0.777   0.0
! ELEMENT GENERATION COMMANDS
   1   3000   3011   1   1   1
*ELEMENTGROUP
!
!           --PD- --beta----
   4   1   0   0.000000   EMBANKMENT SOILS
! CONTROL INFORMATION
!   5   10   15   20   25   30   35   40   45   50   55   60   65   70
   40   2
! PROPERTY TYPES
! INELASTIC SPRING
   1 1.78e+005 1.00e-006 2.75e+001 2.75e+001 0.01 1 0
   2 1.27e+005 1.00e-006 5.65e+001 5.65e+001 0.01 1 0
   3 9.67e+004 1.00e-006 1.12e+002 1.12e+002 0.01 1 0
   4 5.27e+004 1.00e-006 1.98e+002 1.98e+002 0.01 1 0
   5 1.18e+004 1.00e-006 4.03e+002 4.03e+002 0.01 1 0
   6 2.56e+005 1.00e-006 3.94e+001 3.94e+001 0.01 1 0
   7 1.83e+005 1.00e-006 8.11e+001 8.11e+001 0.01 1 0
   8 1.39e+005 1.00e-006 1.61e+002 1.61e+002 0.01 1 0
   9 7.56e+004 1.00e-006 2.84e+002 2.84e+002 0.01 1 0
  10 1.69e+004 1.00e-006 5.79e+002 5.79e+002 0.01 1 0
  11 3.34e+005 1.00e-006 5.14e+001 5.14e+001 0.01 1 0
  12 2.38e+005 1.00e-006 1.06e+002 1.06e+002 0.01 1 0
  13 1.81e+005 1.00e-006 2.10e+002 2.10e+002 0.01 1 0
  14 9.86e+004 1.00e-006 3.71e+002 3.71e+002 0.01 1 0
  15 2.21e+004 1.00e-006 7.55e+002 7.55e+002 0.01 1 0
  16 4.12e+005 1.00e-006 6.33e+001 6.33e+001 0.01 1 0
  17 2.93e+005 1.00e-006 1.30e+002 1.30e+002 0.01 1 0
  18 2.23e+005 1.00e-006 2.59e+002 2.59e+002 0.01 1 0
  19 1.22e+005 1.00e-006 4.57e+002 4.57e+002 0.01 1 0
  20 2.72e+004 1.00e-006 9.31e+002 9.31e+002 0.01 1 0
  21 1.78e+005 1.00e-006 2.22e+001 2.22e+001 0.01 1 0
  22 1.27e+005 1.00e-006 4.58e+001 4.58e+001 0.01 1 0
  23 9.67e+004 1.00e-006 9.10e+001 9.10e+001 0.01 1 0
  24 5.27e+004 1.00e-006 1.60e+002 1.60e+002 0.01 1 0
  25 1.18e+004 1.00e-006 3.27e+002 3.27e+002 0.01 1 0
  26 2.56e+005 1.00e-006 3.19e+001 3.19e+001 0.01 1 0
  27 1.83e+005 1.00e-006 6.57e+001 6.57e+001 0.01 1 0
  28 1.39e+005 1.00e-006 1.31e+002 1.31e+002 0.01 1 0
  29 7.56e+004 1.00e-006 2.30e+002 2.30e+002 0.01 1 0
  30 1.69e+004 1.00e-006 4.69e+002 4.69e+002 0.01 1 0
  31 3.34e+005 1.00e-006 4.16e+001 4.16e+001 0.01 1 0
  32 2.38e+005 1.00e-006 8.56e+001 8.56e+001 0.01 1 0
  33 1.81e+005 1.00e-006 1.70e+002 1.70e+002 0.01 1 0
  34 9.86e+004 1.00e-006 3.00e+002 3.00e+002 0.01 1 0
  35 2.21e+004 1.00e-006 6.11e+002 6.11e+002 0.01 1 0
  36 4.12e+005 1.00e-006 5.13e+001 5.13e+001 0.01 1 0
  37 2.93e+005 1.00e-006 1.06e+002 1.06e+002 0.01 1 0
  38 2.23e+005 1.00e-006 2.10e+002 2.10e+002 0.01 1 0
  39 1.22e+005 1.00e-006 3.70e+002 3.70e+002 0.01 1 0
  40 2.72e+004 1.00e-006 7.54e+002 7.54e+002 0.01 1 0

```

```

! DIRECTION TYPES
!   5   10   15   20   25   30   35   40   45   50   55   60   65   70
    1     0.0     1.0     0.0     -1.0     0.0  0.0
    2     1.0     0.0     0.0     0.0     1.0  0.0
! ELEMENT GENERATION COMMANDS
    1     7010     7011     1     1     1
    2     7010     7011     2     1     1
    3     7010     7011     3     1     1
    4     7010     7011     4     1     1
    5     7010     7011     5     1     1
    6     7025     7026     6     1     1
    7     7025     7026     7     1     1
    8     7025     7026     8     1     1
    9     7025     7026     9     1     1
   10     7025     7026    10     1     1
   11     7035     7036    11     1     1
   12     7035     7036    12     1     1
   13     7035     7036    13     1     1
   14     7035     7036    14     1     1
   15     7035     7036    15     1     1
   16     7045     7046    16     1     1
   17     7045     7046    17     1     1
   18     7045     7046    18     1     1
   19     7045     7046    19     1     1
   20     7045     7046    20     1     1
   21     7010     7111    21     2     1
   22     7010     7111    22     2     1
   23     7010     7111    23     2     1
   24     7010     7111    24     2     1
   25     7010     7111    25     2     1
   26     7125     7126    26     2     1
   27     7125     7126    27     2     1
   28     7125     7126    28     2     1
   29     7125     7126    29     2     1
   30     7125     7126    30     2     1
   31     7135     7136    31     2     1
   32     7135     7136    32     2     1
   33     7135     7136    33     2     1
   34     7135     7136    34     2     1
   35     7135     7136    35     2     1
   36     7145     7146    36     2     1
   37     7145     7146    37     2     1
   38     7145     7146    38     2     1
   39     7145     7146    39     2     1
   40     7145     7146    40     2     1
   41     8010     8011     1     1     1
   42     8010     8011     2     1     1
   43     8010     8011     3     1     1
   44     8010     8011     4     1     1
   45     8010     8011     5     1     1
   46     8025     8026     6     1     1
   47     8025     8026     7     1     1
   48     8025     8026     8     1     1
   49     8025     8026     9     1     1
   50     8025     8026    10     1     1
   51     8035     8036    11     1     1
   52     8035     8036    12     1     1

```

53	8035	8036	13	1	1
54	8035	8036	14	1	1
55	8035	8036	15	1	1
56	8045	8046	16	1	1
57	8045	8046	17	1	1
58	8045	8046	18	1	1
59	8045	8046	19	1	1
60	8045	8046	20	1	1
61	8010	8111	21	2	1
62	8010	8111	22	2	1
63	8010	8111	23	2	1
64	8010	8111	24	2	1
65	8010	8111	25	2	1
66	8125	8126	26	2	1
67	8125	8126	27	2	1
68	8125	8126	28	2	1
69	8125	8126	29	2	1
70	8125	8126	30	2	1
71	8135	8136	31	2	1
72	8135	8136	32	2	1
73	8135	8136	33	2	1
74	8135	8136	34	2	1
75	8135	8136	35	2	1
76	8145	8146	36	2	1
77	8145	8146	37	2	1
78	8145	8146	38	2	1
79	8145	8146	39	2	1
80	8145	8146	40	2	1

\*ELEMENTGROUP  
! P-Y SPRINGS  
! IGNORE P-DELTA            BETA = ---  
   4    1    0            0.000000            P-Y SPRINGS  
! INPUT SPECIFIC TO ELEMENT TYPE 4 (# OF PROPERTY TYPES)  
   16    2

! PROPERTY TYPE , ELASTIC UNLOADING							
1	1524.	1E-6	24.9	24.9	0.01	1	1
2	140.	1E-6	6.8	6.8	0.01	1	1
3	92.	1E-6	10.5	10.5	0.01	1	1
4	53.	1E-6	16.2	16.2	0.01	1	1
!							
5	1524.	1E-6	20.1	20.1	0.01	1	1
6	140.	1E-6	5.5	5.5	0.01	1	1
7	92.	1E-6	8.5	8.5	0.01	1	1
8	53.	1E-6	13.2	13.2	0.01	1	1
!							
9	2666.	1E-6	43.5	43.5	0.01	1	1
10	245.	1E-6	12.0	12.0	0.01	1	1
11	158.	1E-6	18.2	18.2	0.01	1	1
12	92.	1E-6	28.2	28.2	0.01	1	1
!							
13	2666.	1E-6	35.2	35.2	0.01	1	1
14	245.	1E-6	9.7	9.7	0.01	1	1
15	158.	1E-6	14.7	14.7	0.01	1	1
16	92.	1E-6	22.8	22.8	0.01	1	1

! DIRECTION TYPES  
! 5 10 15 20 25 30 35 40 45 50 55 60 65 70  
   1    0.0            1.0            0.0            -1.0            0.0    0.0

	2	1.0	0.0	0.0	0.0	0.0	1.0	0.0						
!	5	10	15	20	25	30	35	40	45	50	55	60	65	70
!	ELEMENT GENERATION COMMANDS west abutment-y,x east abutment-y,x													
!	west abutment-y													
	1		7020		7021			1	1	1				
	2		7020		7021			2	1	1				
	3		7020		7021			3	1	1				
	4		7020		7021			4	1	1				
	5		7030		7031			9	1	1				
	6		7030		7031			10	1	1				
	7		7030		7031			11	1	1				
	8		7030		7031			12	1	1				
	9		7040		7041			9	1	1				
	10		7040		7041			10	1	1				
	11		7040		7041			11	1	1				
	12		7040		7041			12	1	1				
	13		7050		7051			9	1	1				
	14		7050		7051			10	1	1				
	15		7050		7051			11	1	1				
	16		7050		7051			12	1	1				
	17		7060		7061			9	1	1				
	18		7060		7061			10	1	1				
	19		7060		7061			11	1	1				
	20		7060		7061			12	1	1				
	21		7070		7071			9	1	1				
	22		7070		7071			10	1	1				
	23		7070		7071			11	1	1				
	24		7070		7071			12	1	1				
	25		7080		7081			9	1	1				
	26		7080		7081			10	1	1				
	27		7080		7081			11	1	1				
	28		7080		7081			12	1	1				
!	west abutment-x													
	29		7020		7121			5	2	1				
	30		7020		7121			6	2	1				
	31		7020		7121			7	2	1				
	32		7020		7121			8	2	1				
	33		7030		7131			13	2	1				
	34		7030		7131			14	2	1				
	35		7030		7131			15	2	1				
	36		7030		7131			16	2	1				
	37		7040		7141			13	2	1				
	38		7040		7141			14	2	1				
	39		7040		7141			15	2	1				
	40		7040		7141			16	2	1				
	41		7050		7151			13	2	1				
	42		7050		7151			14	2	1				
	43		7050		7151			15	2	1				
	44		7050		7151			16	2	1				
	45		7060		7161			13	2	1				
	46		7060		7161			14	2	1				
	47		7060		7161			15	2	1				
	48		7060		7161			16	2	1				
	49		7070		7171			13	2	1				
	50		7070		7171			14	2	1				
	51		7070		7171			15	2	1				
	52		7070		7171			16	2	1				



53	7080	7181	13	2	1
54	7080	7181	14	2	1
55	7080	7181	15	2	1
56	7080	7181	16	2	1
! east abutment - y					
57	8020	8021	1	1	1
58	8020	8021	2	1	1
59	8020	8021	3	1	1
60	8020	8021	4	1	1
61	8030	8031	9	1	1
62	8030	8031	10	1	1
63	8030	8031	11	1	1
64	8030	8031	12	1	1
65	8040	8041	9	1	1
66	8040	8041	10	1	1
67	8040	8041	11	1	1
68	8040	8041	12	1	1
69	8050	8051	9	1	1
70	8050	8051	10	1	1
71	8050	8051	11	1	1
72	8050	8051	12	1	1
73	8060	8061	9	1	1
74	8060	8061	10	1	1
75	8060	8061	11	1	1
76	8060	8061	12	1	1
77	8070	8071	9	1	1
78	8070	8071	10	1	1
79	8070	8071	11	1	1
80	8070	8071	12	1	1
81	8080	8081	9	1	1
82	8080	8081	10	1	1
83	8080	8081	11	1	1
84	8080	8081	12	1	1
! east abutment-x					
85	8020	8121	5	2	1
86	8020	8121	6	2	1
87	8020	8121	7	2	1
88	8020	8121	8	2	1
89	8030	8131	13	2	1
90	8030	8131	14	2	1
91	8030	8131	15	2	1
92	8030	8131	16	2	1
93	8040	8141	13	2	1
94	8040	8141	14	2	1
95	8040	8141	15	2	1
96	8040	8141	16	2	1
97	8050	8151	13	2	1
98	8050	8151	14	2	1
99	8050	8151	15	2	1
100	8050	8151	16	2	1
101	8060	8161	13	2	1
102	8060	8161	14	2	1
103	8060	8161	15	2	1
104	8060	8161	16	2	1
105	8070	8171	13	2	1
106	8070	8171	14	2	1
107	8070	8171	15	2	1

108	8070	8171	16	2	1
109	8080	8181	13	2	1
110	8080	8181	14	2	1
111	8080	8181	15	2	1
112	8080	8181	16	2	1

```

*ELEMENTGROUP
!
!
!      --PD- --beta----      -
  17   1   0   0.000970      RIGID LINK
! CONTROL INFORMATION
!   5  10  15  20  25  30  35  40  45  50  55  60  65  70
!   1   1   1   0
! MATERIAL PROPERTIES
!   1  2.60E7  1.13E7
! CROSS SECTION PROPERTIES
!   1  264.0  132.0  132.0  1.6E4
! STIFFNESS FACTORS
!   1   4.0   4.0   2.0
! ELEMENT GENERATION COMMANDS
! west abutment - y
!   1   7005   1000   9990   1   1   0   0   0
!   2   7010   7005   9990   1   1   0   0   0
!   3   7021   7011   9990   1   1   0   0   0
!   4   7025   7021   9990   1   1   0   0   0
!   5   7031   7026   9990   1   1   0   0   0
!   6   7035   7031   9990   1   1   0   0   0
!   7   7041   7036   9990   1   1   0   0   0
!   8   7045   7041   9990   1   1   0   0   0
! west abutment - x
!   9   7121   7111   9991   1   1   0   0   0
!  10   7125   7121   9991   1   1   0   0   0
!  11   7131   7126   9991   1   1   0   0   0
!  12   7135   7131   9991   1   1   0   0   0
!  13   7141   7136   9991   1   1   0   0   0
!  14   7145   7141   9991   1   1   0   0   0
! east abutment - y
!  15   8005   3000   9992   1   1   0   0   0
!  16   8010   8005   9992   1   1   0   0   0
!  17   8021   8011   9992   1   1   0   0   0
!  18   8025   8021   9992   1   1   0   0   0
!  19   8031   8026   9992   1   1   0   0   0
!  20   8035   8031   9992   1   1   0   0   0
!  21   8041   8036   9992   1   1   0   0   0
!  22   8045   8041   9992   1   1   0   0   0
! east abutment - x
!  23   8121   8111   9993   1   1   0   0   0
!  24   8125   8121   9993   1   1   0   0   0
!  25   8131   8126   9993   1   1   0   0   0
!  26   8135   8131   9993   1   1   0   0   0
!  27   8141   8136   9993   1   1   0   0   0
!  28   8145   8141   9993   1   1   0   0   0
*ELEMENTGROUP
!
!
!      --PD- --beta----      -
  17   1   1   0.000970      PILES
! CONTROL INFORMATION
!   5  10  15  20  25  30  35  40  45  50  55  60  65  70

```

```

    1    1    1    0
! MATERIAL PROPERTIES
    1    2.60E7    1.13E7
! CROSS SECTION PROPERTIES
    1    2.64E-2    1.32E-2    1.32E-2    0.163E1
! STIFFNESS FACTORS
    1    4.0    4.0    2.0
! ELEMENT GENERATION COMMANDS
! west abutment
    1    7020    7010    9990    1    1    0    0    0
    2    7030    7020    9990    1    1    0    0    0
    3    7040    7030    9990    1    1    0    0    0
    4    7050    7040    9990    1    1    0    0    0
    5    7060    7050    9990    1    1    0    0    0
    6    7070    7060    9990    1    1    0    0    0
    7    7080    7070    9990    1    1    0    0    0
! east abutment
    8    8020    8010    9992    1    1    0    0    0
    9    8030    8020    9992    1    1    0    0    0
   10    8040    8030    9992    1    1    0    0    0
   11    8050    8040    9992    1    1    0    0    0
   12    8060    8050    9992    1    1    0    0    0
   13    8070    8060    9992    1    1    0    0    0
   14    8080    8070    9992    1    1    0    0    0
*RESULTS
! NODE DATA
NSD    001    4008
NSA    001    4008
NSA    001    9000
*ACCNREC
LONG    192.acn    (8f10.0)    '1.00*long'
! CONTROL INFORMATION
3000    8    0    2    1.00    0.02    0.00
! 5 10 15 20 25 30 35 40 45 50 55 60 65 70
*ACCNREC
VERT    v92.acn    (8f10.0)    '1.00*vert'
! CONTROL INFORMATION
3000    8    0    2    1.00    0.02    0.00
! 5 10 15 20 25 30 35 40 45 50 55 60 65 70
*ACCNREC
TRAN    t92.acn    (8f10.0)    '1.00*trans'
! CONTROL INFORMATION
3000    8    0    2    1.00    0.02    0.00
! 5 10 15 20 25 30 35 40 45 50 55 60 65 70
*MODE
! PRINT MODE SHAPES, PRINT TO .OUT FILE
    6    0    1    0
*PARAMETERS
! DEFINE ALPHA AND BETA
VS    1.146000    1.0
! PRINT TO .OUT
OD    0    0.    0    0.    1    0    0.99999
! 5 10 15 20 25 30 35 40 45 50 55 60 65 70
! TURN OFF OPTIONS TO CORRECT VELOCITY AND ACCELERATION
DC 1 0 0 0
! TIME STEP PARAMETERS
DT    0.01    0.02    0.01

```

```
DA          0.01                0.5                2          2.0
*ACCN
!          99999 = max.# of steps
60.0      99999    2
! GROUND ACCELERATION RECORD
1      LONG      0.01      1.0
3      VERT      0.01      1.0
2      TRAN      0.01      1.0
!   5   10   15   20   25   30   35   40   45   50   55   60   65   70
*STOP
```

## B.2 Three-Dimensional Modeling of MRO in DRAIN-3DX using a Soil-Slice Model

```

! CHATDANAI WISSAWAPAISAL. DRAIN 3DX INPUT FILE
! ANALYSIS OF MELOLAND ROAD OVERPASS using a soil-slice model
! ALL UNITS IN kN, m, sec.
!
!   5   10   15   20   25   30   35   40   45   50   55   60   65   70
!UNITS L m F kn
*STARTXX                P-DELTA
      mro                0 1 1 1                MELOLAND
! CONSIDER P-DELTA EFFECT
*NODECOORDS
C   9000      15.0      0.0      -6.306
C   9001      0.0       1.0       0.0
C   1000      0.0       0.0       0.0
C   1001      0.0       0.0       0.0
C   1002      0.0       0.0       0.0
C   1003      0.0       0.0       0.0
C   1004      0.0       0.0       0.0
C   1005      0.0       0.0       0.0
C   2000      31.7      0.0       0.0
L   1000      2000      100       9       0.0
C   3000      63.4      0.0       0.0
C   3001      63.4      0.0       0.0
C   3002      63.4      0.0       0.0
C   3003      63.4      0.0       0.0
C   3004      63.4      0.0       0.0
C   3005      63.4      0.0       0.0
L   2000      3000      100       9       0.0
C   2010      31.7      0.0      -1.969
C   2020      31.7      0.0      -2.989
C   2030      31.7      0.0      -4.009
C   2040      31.7      0.0      -5.029
C   2050      31.7      0.0      -6.049
C   2060      31.7      0.0      -7.069
C   2070      31.7      0.0      -7.255
C   2071      31.7      0.0      -7.255
C   2072      31.7      0.0      -7.255
C   2073      31.7      0.0      -7.255
*RESTRAINTS
S   101100     1000
S   101111     1001
S   101111     1002
S   101111     1003
S   101111     1004
S   111111     1005
S   101100     3000
S   101111     3001
S   101111     3002
S   101111     3003
S   101111     3004
S   111111     3005
S   111111     2070
S   111111     2071
S   111111     2072
S   111111     2073

```

```

*SLAVING
S 010000      1000      1001
S 010000      3000      3001
*MASSES
! SLAB MASS
! ALL MASS IS CONSIDERED.
S 111      773.0      1000      9.81 1.0
S 111      773.0      3000
S 111      358.0      1100      2900      100
! CENTRAL PIER MASS
S 111      44.0      2010      2050      10
S 111      30.0      2060
S 111      266.0      2070
! EMBANKMENT SOIL MASS IN EACH LAYER
S 010 6.26e+002      1001
S 010 8.77e+002      1002
S 010 1.13e+003      1003
S 010 1.38e+003      1004
S 010 6.26e+002      3001
S 010 8.77e+002      3002
S 010 1.13e+003      3003
S 010 1.38e+003      3004
*ELEMENTGROUP
!
!          --PD- --beta----      -
   17    1    1    0.000970      COLUMN
! CONTROL INFORMATION
!   5   10   15   20   25   30   35   40   45   50   55   60   65   70
   1    1    1    1
! MATERIAL PROPERTIES
   1    2.74E7    1.19E7
! CROSS SECTION PROPERTIES
   1    0.52960    0.1324    0.1324    1.8240    1.8240    1.8240
! STIFFNESS FACTORS
   1    4.0      4.0      2.0
! RIGID END ZONES
   1    0.0      0.0    -0.949
! ELEMENT GENERATION COMMANDS
   1    2070      2060      9000    1    1    0    0    0
   2    2060      2050      9000    1    1    0    0    0
   3    2050      2040      9000    1    1    0    0    0
   4    2040      2030      9000    1    1    0    0    0
   5    2030      2020      9000    1    1    0    0    0
   6    2020      2010      9000    1    1    0    0    0
   7    2010      2000      9000    1    1    0    0    0
*ELEMENTGROUP
!
!          --PD- --beta----      -
   17    1    0    0.000970      SLAB
! CONTROL INFORMATION
!   5   10   15   20   25   30   35   40   45   50   55   60   65   70
   1    1    1    1
! MATERIAL PROPERTIES
   1    2.74E7    1.19E7
! CROSS SECTION PROPERTIES
! USE 0.75*Igross , Full J , 5/6*Agross for shear
   1    5.288    1.4586    26.916    4.346    2.716    2.716

```

```

! STIFFNESS FACTORS
  1      4.0      4.0      2.0
! RIGID END ZONES
  1      0.9145      0.0      0.0
! ELEMENT GENERATION COMMANDS
  1      1000      1100      100      9001      1      1      0      0      0
  9      1800      1900      100      9001      1      1      0      0      0
 10      1900      2000      100      9001      1      1      0      0      0
 11      2000      2100      100      9001      1      1      0      0      1
 12      2100      2200      100      9001      1      1      0      0      0
 20      2900      3000      100      9001      1      1      0      0      0
*ELEMENTGROUP
!
!      --PD- --beta----      -
  4      1      0      0.000970      PIER FOUNDATION
! CONTROL INFORMATION
!   5   10   15   20   25   30   35   40   45   50   55   60   65   70
  3     3
! PROPERTY TYPES
! ELASTIC SPRING
  1      7.30E5      1.0E-6      1.0E7      1.0E7      1.0      1      1
  2      6.57E5      1.0E-6      1.0E7      1.0E7      1.0      1      1
  3      5.56E6      1.0E-6      1.0E7      1.0E7      1.0      2      1
! DIRECTION TYPES
!   5   10   15   20   25   30   35   40   45   50   55   60   65   70
  1      0.0      0.0      1.0      1.0      0.0      0
  2      0.0      1.0      0.0      0.0      0.0      1
  3      1.0      0.0      0.0      0.0      1.0      0
! ELEMENT GENERATION COMMANDS
  1      2071      2070      1      1      1
  2      2070      2072      2      2      1
  3      2070      2073      3      3      1
*ELEMENTGROUP
!
!      --PD- --beta----      -
  4      1      0      0.000000      EMBANKMENT SOILS
! CONTROL INFORMATION
!   5   10   15   20   25   30   35   40   45   50   55   60   65   70
 20     1
! PROPERTY TYPES
! INELASTIC SPRING
  1 2.98e+005 1.00e-006 5.43e+001 5.43e+001      0.01      1      0
  2 2.02e+005 1.00e-006 1.84e+002 1.84e+002      0.01      1      0
  3 6.14e+004 1.00e-006 1.12e+002 1.12e+002      0.01      1      0
  4 2.82e+004 1.00e-006 2.57e+002 2.57e+002      0.01      1      0
  5 1.79e+004 1.00e-006 8.50e+002 8.50e+002      0.01      1      0
  6 4.17e+005 1.00e-006 7.60e+001 7.60e+001      0.01      1      0
  7 2.82e+005 1.00e-006 2.58e+002 2.58e+002      0.01      1      0
  8 8.60e+004 1.00e-006 1.57e+002 1.57e+002      0.01      1      0
  9 3.94e+004 1.00e-006 3.60e+002 3.60e+002      0.01      1      0
 10 2.51e+004 1.00e-006 1.19e+003 1.19e+003      0.01      1      0
 11 5.36e+005 1.00e-006 9.78e+001 9.78e+001      0.01      1      0
 12 3.63e+005 1.00e-006 3.31e+002 3.31e+002      0.01      1      0
 13 1.11e+005 1.00e-006 2.02e+002 2.02e+002      0.01      1      0
 14 5.07e+004 1.00e-006 4.63e+002 4.63e+002      0.01      1      0
 15 3.23e+004 1.00e-006 1.53e+003 1.53e+003      0.01      1      0
 16 6.55e+005 1.00e-006 1.20e+002 1.20e+002      0.01      1      0

```

```

17 4.44e+005 1.00e-006 4.05e+002 4.05e+002 0.01 1 0
18 1.35e+005 1.00e-006 2.47e+002 2.47e+002 0.01 1 0
19 6.20e+004 1.00e-006 5.65e+002 5.65e+002 0.01 1 0
20 3.94e+004 1.00e-006 1.87e+003 1.87e+003 0.01 1 0
! DIRECTION TYPES
! 5 10 15 20 25 30 35 40 45 50 55 60 65 70
1 0.0 1.0 0.0 -1.0 0.0 0.0
! ELEMENT GENERATION COMMANDS
1 1002 1001 1 1 1
2 1002 1001 2 1 1
3 1002 1001 3 1 1
4 1002 1001 4 1 1
5 1002 1001 5 1 1
6 1003 1002 6 1 1
7 1003 1002 7 1 1
8 1003 1002 8 1 1
9 1003 1002 9 1 1
10 1003 1002 10 1 1
11 1004 1003 11 1 1
12 1004 1003 12 1 1
13 1004 1003 13 1 1
14 1004 1003 14 1 1
15 1004 1003 15 1 1
16 1005 1004 16 1 1
17 1005 1004 17 1 1
18 1005 1004 18 1 1
19 1005 1004 19 1 1
20 1005 1004 20 1 1
21 3002 3001 1 1 1
22 3002 3001 2 1 1
23 3002 3001 3 1 1
24 3002 3001 4 1 1
25 3002 3001 5 1 1
26 3003 3002 6 1 1
27 3003 3002 7 1 1
28 3003 3002 8 1 1
29 3003 3002 9 1 1
30 3003 3002 10 1 1
31 3004 3003 11 1 1
32 3004 3003 12 1 1
33 3004 3003 13 1 1
34 3004 3003 14 1 1
35 3004 3003 15 1 1
36 3005 3004 16 1 1
37 3005 3004 17 1 1
38 3005 3004 18 1 1
39 3005 3004 19 1 1
40 3005 3004 20 1 1
*RESULTS
! GET DISPLACEMENT PROFILE
NSA 001 1000
NSV 001 1000
NSD 001 1000
NSA 001 2000
NSV 001 2000
NSD 001 2000
NSD 001 2070

```



```

NSA      001      2070
*ACCNREC
EQ14     quake14.acn      (f10.2,f10.3)      '1.00*vert'
! CONTROL INFORMATION
1001     1      1      2      1.00
!   5   10   15   20   25   30   35   40   45   50   55   60   65   70
*ACCNREC
EQ15     quake15.acn      (f10.2,f10.3)      '1.00*long'
! CONTROL INFORMATION
1001     1      1      2      1.00
!   5   10   15   20   25   30   35   40   45   50   55   60   65   70
*ACCNREC
EQ24     quake24.acn      (f10.2,f10.3)      '1.00*trans'
! CONTROL INFORMATION
1001     1      1      2      1.00
!   5   10   15   20   25   30   35   40   45   50   55   60   65   70
*MODE
! PRINT MODE SHAPES, PRINT TO .OUT FILE
      8      0      1      0
*PARAMETERS
! DEFINE ALPHA AND BETA
VS      1.146000      1.0
! PRINT TO .OUT
OD      0      0.      0      0.      1      0      0.99999
!   5   10   15   20   25   30   35   40   45   50   55   60   65   70
! TURN OFF OPTIONS TO CORRECT VELOCITY AND ACCELERATION
DC 1    0      0      0
! TIME STEP PARAMETERS
DT      0.01      0.02      0.01
DA      0.01      0.5      2      2.0
*ACCN
!          99999 = max.# of steps
60.0    99999      1      0.02
! GROUND ACCELERATION RECORD
1      EQ15      0.01      1.0
2      EQ24      0.01      1.0
3      EQ14      0.01      1.0
!   5   10   15   20   25   30   35   40   45   50   55   60   65   70
*STOP

```

### B.3 Three-Dimensional Modeling of IL-1 in DRAIN-3DX using a Soil-Slice Model

```

! CHATDANAI WISSAWAPAISAL. DRAIN 3DX INPUT FILE
! ANALYSIS OF IL-1 using a soil-slice model
! ALL UNITS IN kN, m, sec.
!
!   5   10   15   20   25   30   35   40   45   50   55   60   65   70
!UNITS L m F kn
*STARTXX                P-DELTA
      ill                0 1 1 1                SCOTT COUNTY
! CONSIDER P-DELTA EFFECT
*NODECOORDS
C   9001                0.0                1.0                0.0
C   9002                0.0                2.0                0.0
C   9003                80.0               2.0                0.0
C   1000                0.0                0.0                0.0
C   1001                0.0                0.0                0.0
C   1002                0.0                0.0                0.0
C   1003                0.0                0.0                0.0
C   1004                0.0                0.0                0.0
C   1005                0.0                0.0                0.0
!
C   401                 2.6                0.0                0.0
C   409                 23.4               0.0                0.0
L   401                 409                1                7                0.0
C   410                 26.0               0.0                0.0
C   510                 26.0               0.0                0.0
C   411                 28.8               0.0                0.0
C   419                 51.2               0.0                0.0
L   411                 419                1                7                0.0
C   420                 54.0               0.0                0.0
C   520                 54.0               0.0                0.0
C   421                 56.6               0.0                0.0
C   429                 77.4               0.0                0.0
L   421                 429                1                7                0.0
C   3000                80.0               0.0                0.0
C   3001                80.0               0.0                0.0
C   3002                80.0               0.0                0.0
C   3003                80.0               0.0                0.0
C   3004                80.0               0.0                0.0
C   3005                80.0               0.0                0.0
*RESTRAINTS
S   101100              1000
S   101111              1001
S   101111              1002
S   101111              1003
S   101111              1004
S   111111              1005
!
S   101100              3000
S   101111              3001
S   101111              3002
S   101111              3003
S   101111              3004
S   111111              3005
!

```

```

S 111111 510
S 111111 520
!
S 111111 9001
S 111111 9002
S 111111 9003
*SLAVING
S 010000 1000 1001
S 010000 3000 3001
*MASSES
! ABUTMENT ADD 1000 kN., PIER NODE ADD 400 kN.
! SLAB MASS
! ALL MASS IS CONSIDERED.
S 111 1267.0 1000 9.81 1.0
S 111 1267.0 3000
S 111 667.0 410
S 111 667.0 420
S 111 267.0 401 409 1
S 111 267.0 411 419 1
S 111 267.0 421 429 1
! EMBANKMENT SOIL MASS IN EACH LAYER
S 010 5.28e+002 1001
S 010 7.92e+002 1002
S 010 1.06e+003 1003
S 010 1.32e+003 1004
S 010 5.28e+002 3001
S 010 7.92e+002 3002
S 010 1.06e+003 3003
S 010 1.32e+003 3004
*ELEMENTGROUP
!
! --PD- --beta---- -
17 1 0 0.000970 SLAB
! CONTROL INFORMATION
! 5 10 15 20 25 30 35 40 45 50 55 60 65 70
1 1 1 0
! MATERIAL PROPERTIES
1 2.00E8 7.70E7
! CROSS SECTION PROPERTIES
1 0.5 0.12 4.3 0.5 0.4 0.4
! STIFFNESS FACTORS
1 4.0 4.0 2.0
! RIGID END ZONES
! ELEMENT GENERATION COMMANDS
1 1000 401 9001 1 1 0 0 0
2 401 402 1 9001 1 1 0 0 0
29 428 429 1 9001 1 1 0 0 0
30 429 3000 9001 1 1 0 0 0
*ELEMENTGROUP
!
! --PD- --beta---- -
4 1 0 0.000970 PIER SPRING
! CONTROL INFORMATION
! 5 10 15 20 25 30 35 40 45 50 55 60 65 70
1 1
! PROPERTY TYPES

```

```

! ELASTIC SPRING
  1  1.50E5      0.03   1300.0   1300.0      0.01   1   0
! DIRECTION TYPES
!   5   10   15   20   25   30   35   40   45   50   55   60   65   70
  1      0.0      1.0      0.0      1.0      0.0   0
! ELEMENT GENERATION COMMANDS
  1      410      510      1   1   1
  2      420      520      1   1   1
*ELEMENTGROUP
!
!      --PD- --beta----      -
  4   1   0      0.000000      EMBANKMENT SOILS
! CONTROL INFORMATION
!   5   10   15   20   25   30   35   40   45   50   55   60   65   70
  20   1
! PROPERTY TYPES
! INELASTIC SPRING
  1  1.86e+005  1.00e-006  3.72e+001  3.72e+001      0.01   1   0
  2  1.26e+005  1.00e-006  1.26e+002  1.26e+002      0.01   1   0
  3  3.84e+004  1.00e-006  7.68e+001  7.68e+001      0.01   1   0
  4  1.76e+004  1.00e-006  1.76e+002  1.76e+002      0.01   1   0
  5  1.12e+004  1.00e-006  5.82e+002  5.82e+002      0.01   1   0
  6  2.79e+005  1.00e-006  5.58e+001  5.58e+001      0.01   1   0
  7  1.89e+005  1.00e-006  1.89e+002  1.89e+002      0.01   1   0
  8  5.76e+004  1.00e-006  1.15e+002  1.15e+002      0.01   1   0
  9  2.64e+004  1.00e-006  2.64e+002  2.64e+002      0.01   1   0
 10  1.68e+004  1.00e-006  8.74e+002  8.74e+002      0.01   1   0
 11  3.72e+005  1.00e-006  7.44e+001  7.44e+001      0.01   1   0
 12  2.52e+005  1.00e-006  2.52e+002  2.52e+002      0.01   1   0
 13  7.68e+004  1.00e-006  1.54e+002  1.54e+002      0.01   1   0
 14  3.52e+004  1.00e-006  3.52e+002  3.52e+002      0.01   1   0
 15  2.24e+004  1.00e-006  1.16e+003  1.16e+003      0.01   1   0
 16  4.65e+005  1.00e-006  9.30e+001  9.30e+001      0.01   1   0
 17  3.15e+005  1.00e-006  3.15e+002  3.15e+002      0.01   1   0
 18  9.60e+004  1.00e-006  1.92e+002  1.92e+002      0.01   1   0
 19  4.40e+004  1.00e-006  4.40e+002  4.40e+002      0.01   1   0
 20  2.80e+004  1.00e-006  1.46e+003  1.46e+003      0.01   1   0
! DIRECTION TYPES
!   5   10   15   20   25   30   35   40   45   50   55   60   65   70
  1      0.0      1.0      0.0      -1.0      0.0   0.0
! ELEMENT GENERATION COMMANDS
  1      1002      1001      1   1   1
  2      1002      1001      2   1   1
  3      1002      1001      3   1   1
  4      1002      1001      4   1   1
  5      1002      1001      5   1   1
  6      1003      1002      6   1   1
  7      1003      1002      7   1   1
  8      1003      1002      8   1   1
  9      1003      1002      9   1   1
 10      1003      1002     10   1   1
 11      1004      1003     11   1   1
 12      1004      1003     12   1   1
 13      1004      1003     13   1   1
 14      1004      1003     14   1   1
 15      1004      1003     15   1   1
 16      1005      1004     16   1   1

```

17	1005	1004	17	1	1
18	1005	1004	18	1	1
19	1005	1004	19	1	1
20	1005	1004	20	1	1
21	3002	3001	1	1	1
22	3002	3001	2	1	1
23	3002	3001	3	1	1
24	3002	3001	4	1	1
25	3002	3001	5	1	1
26	3003	3002	6	1	1
27	3003	3002	7	1	1
28	3003	3002	8	1	1
29	3003	3002	9	1	1
30	3003	3002	10	1	1
31	3004	3003	11	1	1
32	3004	3003	12	1	1
33	3004	3003	13	1	1
34	3004	3003	14	1	1
35	3004	3003	15	1	1
36	3005	3004	16	1	1
37	3005	3004	17	1	1
38	3005	3004	18	1	1
39	3005	3004	19	1	1
40	3005	3004	20	1	1

```

*RESULTS
! NODE DATA
NSD 001 410
NSA 001 410
NSA 001 9001
*ACCNREC
LONG 192.acn (8f10.0) '1.00*long'
! CONTROL INFORMATION
3000 8 0 2 1.00 0.02 0.00
! 5 10 15 20 25 30 35 40 45 50 55 60 65 70
*ACCNREC
VERT v92.acn (8f10.0) '1.00*vert'
! CONTROL INFORMATION
3000 8 0 2 1.00 0.02 0.00
! 5 10 15 20 25 30 35 40 45 50 55 60 65 70
*ACCNREC
TRAN t92.acn (8f10.0) '1.00*ttrans'
! CONTROL INFORMATION
3000 8 0 2 1.00 0.02 0.00
! 5 10 15 20 25 30 35 40 45 50 55 60 65 70
*MODE
! PRINT MODE SHAPES, PRINT TO .OUT FILE
6 0 1 0
*PARAMETERS
! DEFINE ALPHA AND BETA
VS 1.146000 1.0
! PRINT TO .OUT
OD 0 0. 0 0. 1 0 0.99999
! 5 10 15 20 25 30 35 40 45 50 55 60 65 70
! TURN OFF OPTIONS TO CORRECT VELOCITY AND ACCELERATION
DC 1 0 0 0
! TIME STEP PARAMETERS
DT 0.01 0.02 0.01

```

```
DA          0.01                0.5                2          2.0
*ACCN
!          99999 = max.# of steps
60.0       99999    2
! GROUND ACCELERATION RECORD
1    LONG      0.01      1.0
3    VERT      0.01      1.0
2    TRAN      0.01      1.0
!   5   10   15   20   25   30   35   40   45   50   55   60   65   70
*STOP
```

## B.4 Matlab Routine Used to Determine Parameters for the Elastoplastic Elements

### (Shear Springs in Chapter 3)

```

% M-file
% iwan model
% embankment wedge is divided into 4 layers (MRO)
% When approach-embankment thickness (L*) changes, both mass and
% stiffness of approach-embankment changes too.
delete iwan_d.out
diary iwan_d.out
clear
% embankment dimension (all units are in kN, m.)
unit_weight = 18.8; %kN/m^3
length = 2.0; %approach-embankment thickness (L*)
w(1,1)= 18.25; dz(1,1) = 1.825; %width and depth of each layer
w(2,1)= 25.55; dz(2,1) = 1.825;
w(3,1)= 32.85; dz(3,1) = 1.825;
w(4,1)= 40.15; dz(4,1) = 1.825;

% find mass of each layer
m(1,1) = unit_weight*w(1,1)*dz(1,1)*length;
m(2,1) = unit_weight*w(2,1)*dz(2,1)*length;
m(3,1) = unit_weight*w(3,1)*dz(3,1)*length;
m(4,1) = unit_weight*w(4,1)*dz(4,1)*length;

embk_mass = m'

% soil properties
gmax = 76800; %low strain shear modulus

% modulus reduction
strain = [0.01;0.05;0.1;0.5;2.6]/100;
gfrac = [.79;.48;.31;.11;.04];
G = gmax*gfrac; %G is a 5x1 matrix

for j = 1:4
    for i = 1:5
        KE(i,j) = (w(j,1)*length/dz(j,1))*G(i,1);
%KE is a 5x4 matrix
        y(i,j) = dz(j,1)*strain(i,1); %Y is an 5x4 matrix
    end
end

    KE; %secant stiffness
    y; %displacement

for p = 1:4
    A = [1 1 1 1 1
y(1,p)/y(2,p) 1 1 1 1
y(1,p)/y(3,p) y(2,p)/y(3,p) 1 1 1
y(1,p)/y(4,p) y(2,p)/y(4,p) y(3,p)/y(4,p) 1 1
y(1,p)/y(5,p) y(2,p)/y(5,p) y(3,p)/y(5,p) y(4,p)/y(5,p) 1 ];

% A is a 5x5 matrix (5 elastoplastic elements are used to represent

```

```
% each shear spring)
    KEFF = KE(:,p);    %KEFF is a 5x1 matrix
    KK = A\KEFF;      %KK is a 5x1 matrix
    K_y(:,p) = KK;
    YY = y(:,p);      %yy is a 5x1 matrix
    for m = 1:5
        RR(m,1) = KK(m,1)*yy(m,1);    %RR is an 5x1 matrix
    end
    R_y(:,p) = RR;
end

K_y %initial stiffness of elastoplastic elements

R_y %yield force of elastoplastic elements

diary off
```



## B.5 Nonlinear Push-Over Analysis of Multiple Pier-Columns using DRAIN-2DX

(Figure 5.3)

```

! CHATDANAI WISSAWAPAISAL. DRAIN 2DX INPUT FILE
! NONLINEAR PUSH-OVER ANALYSIS OF MULTIPLE PIER-COLUMNS
! ALL UNITS IN kN, m, sec.
!
!   5   10   15   20   25   30   35   40   45   50   55   60   65   70
!UNITS L m F kn   [Inserted by DrainPro]--Pre-processing of DRAIN-2DX
*STARTXX
  PIER_2          0 1 1 1          PIER_GEOMETRY
! CONSIDER P-DELTA EFFECT
*NODECOORDS
C   0001          0.0          0.0
C   0011          0.0          6.365
C   0005          10.24         0.0
C   0015          10.24         6.365
! GENERATE NODES ALONG HORIZONTAL AXES
L   0001          0005          1   3   2.56
L   0011          0015          1   3   2.56
*RESTRAINTS
! FIXED ALL BASE NODES.
S 111          0001          0005          1
*MASSES
! ONLY X MASS IS CONSIDERED.
S 100          1500.0          0011          0015          1          9.81 1.0
*ELEMENTGROUP
! DEFINE PIER (CONSIDER P-DELTA FOR STATIC ANALYSIS ONLY)
!
!           --beta----          -
!   2   1   1           0.000162          PIER SECTIONS
! INPUT SPECIFIC TO ELEMENT TYPE 2
!   1   1   1
! STIFFNESS TYPES (USE I AS 0.50*Ig)
!
!           I-col
!   1  25.222E6          0.03          0.4536          0.00819          4.0          4.0          2.0
! RIGID END ZONE TYPES
!   1           0.0          0.0          1.440          -0.6250
! YIELD SURFACE TYPES
!   1   3           587.0          587.0          11532.0          2400.0          1.8          0.403          1.8          0.403
! ELEMENT GENERATION COMMANDS
!   1           0001          0011          1   1   1   1   1
!   2           0002          0012          1   1   1   1   1
!   3           0003          0013          1   1   1   1   1
!   4           0004          0014          1   1   1   1   1
!   5           0005          0015          1   1   1   1   1
*ELEMENTGROUP
! NEGLECT P-DELTA EFFECT IN BENT
!
!           --beta----          -
!   2   1   0           0.000162          BENT
! INPUT SPECIFIC TO ELEMENT TYPE 2
!   1   1   1
! STIFFNESS TYPES ( use I as 1.00*Ig )
!
!           I-bent
!   1  25.222E6          0.03          1.075          0.1400          4.0          4.0          2.0

```

```

! RIGID END ZONE TYPES
  1    0.380   -0.380     0.0     0.0
! YIELD SURFACE TYPES
  1    1    1321.0   1321.0
! ELEMENT GENERATION COMMANDS
  1    0011    0012     1    1    1    1    1
  2    0012    0013     1    1    1    1    1
  3    0013    0014     1    1    1    1    1
  4    0014    0015     1    1    1    1    1
*RESULTS
! GET DISPLACEMENT PROFILE
NSD   011    0011
! PRINT OUT ELEMENT DATA
E     011
*NODALOAD
! TRANSVERSE LOAD APPLIED AT BENT
TRAN                                TRANSVERSE LOAD
S     1.0    0.0    0.0    0011
*PARAMETERS
! DO NOT SAVE STRUCTURE STATE AT END OF ANALYSIS FOR FUTURE USE
! DO NOT SAVE EACH STEP FOR .RXX AND .OUT
OS    0    0    0    0    0
*MODE
! PRINT MODE SHAPES, PRINT TO .OUT FILE
  1                0    1    0
*GRAV
! GRAVITY LOAD AT NODE WITH MASS
I     9.81    0.0    -1.0
*PARAMETERS
! DO NOT SAVE STRUCTURE STATE AT END OF ANALYSIS FOR FUTURE USE
! SAVE EACH STEP FOR .RXX AND .OUT
OS    0    1    1    0    500
*STAT                                NONLINEAR PUSH-OVER
N     TRAN    1.0
! DISPLACEMENT CONTROL (UNIT IN M.)
! INCREMENT OF 0.1 cm UNTIL 7.0 cm
!
!           --increm--           -
D     0015    1    0.001    0.070
*STOP

```

## B.6 Two-Dimensional Modeling of a Representative Illinois Bridge in

### DRAIN-2DX (Figure 6.13)

```

! CHATDANAI WISSAWAPAISAL. DRAIN 2DX INPUT FILE
! Analysis of a representative Illinois bridge (original)
! (4 SPANS BRIDGE)-- ATC-32 abutment modeling
! ALL UNITS IN kN, m, sec.
!
!   5   10   15   20   25   30   35   40   45   50   55   60   65   70
!UNITS L m F kn   [Inserted by DrainPro]
*STARTXX           ! IGNORE P-DELTA EFFECT
  knox1           0 1 0 1           knox county bridge
*NODECOORDS
C   1000           0.0           0.0
C   2000           56.34          0.0
L   1000           2000           100   9           0.0
C   3000           121.84          0.0
L   2000           3000           100   9           0.0
C   4000           187.34          0.0
L   3000           4000           100   9           0.0
C   5000           243.68          0.0
L   4000           5000           100   9           0.0
C   1001           0.0           0.0
C   1002           0.0           0.0
C   1003           0.0           0.1
C   1004           0.0           0.1
C   1005           0.0           0.1
C   1006           0.0           0.1
C   2001           56.34          0.0
C   2002           56.34          0.0
C   2003           56.34          0.0
C   2004           56.34          0.0
C   3001           121.84          0.0
C   3002           121.84          0.0
C   4001           187.34          0.0
C   4002           187.34          0.0
C   4003           187.34          0.0
C   4004           187.34          0.0
C   5001           243.68          0.0
C   5002           243.68          0.0
C   5003           243.68          0.1
C   5004           243.68          0.1
C   5005           243.68          0.1
C   5006           243.68          0.1
*RESTRAINTS
S 100           1000
S 111           1006
S 111           2004
S 111           3002
S 111           4004
S 111           5006
*SLAVING
S 111           1004           1002
S 111           5004           5002
!   5   10   15   20   25   30   35   40   45   50   55   60   65   70

```

```

*MASSES ! alpha = 1.0
! SLAB MASS
S 010 303.5 1000 9.81 1.0
S 010 607.0 1100 1900 100 9.81 1.0
S 010 656.5 2000 9.81 1.0
S 010 706.0 2100 2900 100 9.81 1.0
S 010 1150.4 3000 9.81 1.0
S 010 706.0 3100 3900 100 9.81 1.0
S 010 656.5 4000 9.81 1.0
S 010 607.0 4100 4900 100 9.81 1.0
S 010 303.5 5000 9.81 1.0
! ABUTMENT MASS
S 010 547.0 1004 9.81 1.0
S 010 547.0 5004 9.81 1.0
! BENT MASS & PIER (ABOVE)
S 010 444.4 2002 9.81 1.0
S 010 444.4 4002 9.81 1.0
! CRASH WALL & FOOTING & PIER (BELOW)
S 010 1781.0 2003
S 010 1781.0 4003
*ELEMENTGROUP
! SLIDER
!IGNORE P-DELTA BETA = 0.0
4 1 0 0.0 SLIDER
! INPUT SPECIFIC TO ELEMENT TYPE 4 (# OF PROPERTY TYPES)
2
! PROPERTY TYPE
1 5E06 1E-06 150 150 0.01 2 0
2 5E06 1E-06 455 455 0.01 2 0
! 5 10 15 20 25 30 35 40 45 50 55 60 65 70 75
! ELEMENT GENERATION COMMANDS
1 1000 1001 1
2 2000 2001 2
3 4000 4001 2
4 5000 5001 1
*ELEMENTGROUP
! ELASTOMER
!IGNORE P-DELTA BETA = ---
4 1 0 0.001486 RUBBER
! INPUT SPECIFIC TO ELEMENT TYPE 4 (# OF PROPERTY TYPES)
2
! PROPERTY TYPE
1 24800 0.50 75 75 0.01 2 0
2 47355 0.50 227.5 227.5 0.01 2 0
! 5 10 15 20 25 30 35 40 45 50 55 60 65 70 75
! ELEMENT GENERATION COMMANDS
1 1001 1002 1
2 2001 2002 2
3 4001 4002 2
4 5001 5002 1
*ELEMENTGROUP
! gap element
!IGNORE P-DELTA BETA = 0.0
9 1 0 0.0 GAP
! INPUT SPECIFIC TO ELEMENT TYPE 9 (# OF PROPERTY TYPES)
2

```

```

! PROPERTY TYPE, 1=COMP, 2=TEN
  1  -2  0.5E-3  1E-3  5E06  5E06  5E06  0.01
  2   2  0.5E-3  1E-3  5E06  5E06  5E06  0.01
!  5  10  15  20  25  30  35  40  45  50  55  60  65  70  75
! ELEMENT GENERATION COMMANDS
  1   1001   1003   1   -6.5E-3
  2   1001   1003   2   -6.5E-3
  3   5001   5003   1   -6.5E-3
  4   5001   5003   2   -6.5E-3
*ELEMENTGROUP
! PIN
! IGNORE P-DELTA      BETA = ---
  4   1   0   0.001486      PIN
! INPUT SPECIFIC TO ELEMENT TYPE 4 (# OF PROPERTY TYPES)
  1
! PROPERTY TYPE , INELASTIC UNLOADING
  1   7.8E6   1E-06   1220   1220   0.01   2   0
!  5  10  15  20  25  30  35  40  45  50  55  60  65  70  75
! ELEMENT GENERATION COMMANDS
  1   1003   1004   1
  2   5003   5004   1
*ELEMENTGROUP
! ABUTMENT WALL
! IGNORE P-DELTA      BETA = ---
  4   1   0   0.001486      ABUTMENT WALL
! INPUT SPECIFIC TO ELEMENT TYPE 4 (# OF PROPERTY TYPES)
  1
! PROPERTY TYPE , ELASTIC UNLOADING
  1   7.5E4   1E-6   1824   1824   0.01   2   1
!  5  10  15  20  25  30  35  40  45  50  55  60  65  70  75
! ELEMENT GENERATION COMMANDS
  1   1004   1005   1
  2   5004   5005   1
*ELEMENTGROUP
! PIER
! IGNORE P-DELTA      BETA = ---
  4   1   0   0.001486      PIER
! INPUT SPECIFIC TO ELEMENT TYPE 4 (# OF PROPERTY TYPES)
  1
! PROPERTY TYPE , INELASTIC UNLOADING
  1   1.73E5  3.18E-2   1384   1384   0.01   2   0
!  5  10  15  20  25  30  35  40  45  50  55  60  65  70  75
! ELEMENT GENERATION COMMANDS
  1   2002   2003   1
  2   3000   3001   1
  3   4002   4003   1
*ELEMENTGROUP
! PILES
! IGNORE P-DELTA      BETA = ---
  4   1   0   0.001486      PILES
! INPUT SPECIFIC TO ELEMENT TYPE 4 (# OF PROPERTY TYPES)
  2
! PROPERTY TYPE , ELASTIC UNLOADING
  1   2.72E5  0.263   1020   1020   0.01   2   1
  2   9.73E5  0.161   1836   1836   0.01   2   1
!  5  10  15  20  25  30  35  40  45  50  55  60  65  70  75

```

```

! ELEMENT GENERATION COMMANDS
  1      1004      1005      1
  2      2003      2004      2
  3      3001      3002      2
  4      4003      4004      2
  5      5004      5005      1
*ELEMENTGROUP
! DEFINE SLAB
! IGNORE P-DELTA      BETA = ---
  2      1      0      0.001486      SLAB ELEMENT
! INPUT SPECIFIC TO ELEMENT TYPE 2
  1      0      1
! STIFFNESS TYPES
  1      2.0E8      0.03      0.553      5.16      4.0      4.0      2.0      0.01
! RIGID END ZONE TYPES
! YIELD SURFACE TYPES
  1      1      313804      313804
! ELEMENT GENERATION COMMANDS
  1      1000      1100      100      1      1      1
  40     4900      5000      100      1      1      1
*RESULTS
! GET DISPLACEMENT PROFILE
NSD      001      1000      1004      4
! 5 10 15 20 25 30 35 40 45 50 55 60 65 70 75
! GET ELEMENT DATA
E      001      1      1
*ACCNREC
  EQ      chile1.acn      (8f10.0)      '1.15*chile1'
! CONTROL INFORMATION
  5816      8      0      2      1.15      0.02      0.00
! 5 10 15 20 25 30 35 40 45 50 55 60 65 70 75
*PARAMETERS
! DEFINE ALPHA AND BETA TO ACHIEVE 5% DAMPING FOR CERTAIN MODES
VS      0.696339      1.0
! PRINT TO .OUT
OD      0      0.      0      0.      1      0      0.9999      0.
! 5 10 15 20 25 30 35 40 45 50 55 60 65 70 75
! TURN OFF OPTIONS TO CORRECT VELOCITY AND ACCELERATION
DC      1      0      0      0
! TIME STEP PARAMETERS
DT      0.01      0.02      0.005
DA      0.01      0.5      2      2.0
*MODE
! PRINT MODE SHAPES, PRINT TO .OUT FILE , PRINT MODAL DAMPING RATIOS.
  14      0      1      0
*ACCN
      99999 = max.# of steps
60.0      99999      2
! GROUND ACCELERATION RECORD
  2      EQ      0.01      1.0
! 5 10 15 20 25 30 35 40 45 50 55 60 65 70 75
*STOP

```

## BIBLIOGRAPHY

- ATC-32 (1996). "Improved Seismic Design Criteria for California Bridges: Provisional Recommendations," Applied Technology Council, Redwood City, California.
- Caltrans (1999). "Caltrans Seismic Design Criteria," Version 1.1, California Department of Transportation, July.
- Douglas, B.M., Maragakis, E.A., Vrontinos, S., and Douglas B.J. (1990). "Analytical Studies of the Static and Dynamic Response of the Meloland Road Overcrossing," Proceedings of the 4<sup>th</sup> U.S. National Conference on Earthquake Engineering, May 20-24, Palm Springs, California.
- Dynamic Isolation Systems (1993). "UBC Procedures for Seismically Isolated Buildings," DIS, Inc., California.
- Eyre, R., and Stevenson, A. (1991). "Characterisation of Rubber Vulcanizates for Bridge Bearings," Research Report 299, Transport and Road Research Laboratory, Department of Transport, Crowthorne, Berkshire, The United Kingdom.
- FEMA 273/274 (1996). "The NEHRP Guidelines for Seismic Rehabilitation of Buildings and Commentary," Federal Emergency Management Agency, Washington D.C.
- Foutch, D.A., Karshenas, M., and Tobias, D.H. (1997). "Design of Highway Bridges for Seismic Loads," CE 479 Class Notes, Department of Civil Engineering, University of Illinois at Urbana-Champaign.
- Goel, R.K. (1997). "Earthquake Characteristics of Bridges with Integral Abutments," Journal of Structural Engineering, pp. 1435-1443, November.
- Goel, R.K., and Chopra, A.K. (1997). "Evaluation of Bridge Abutment Capacity and Stiffness during Earthquakes," Earthquake Spectra, Vol.13, No.1, pp.1-23, February.
- Iwan W.D. (1973). "A Model for the Dynamic Analysis of Deteriorating Structures," Proceedings of the 5<sup>th</sup> World Conference on Earthquake Engineering, Paper No. 222, pp.1782-1791.
- Jacobsen, F.K. (1977). "TFE Expansion Bearings for Highway Bridges," Report No. FHWA-IL-PR-71, Illinois Department of Transportation.
- Katafygiotis, L.S. (1991). "Treatment of Model Uncertainties in Structural Dynamics," Report No. EERL-91-01, Earthquake Engineering Research Laboratory, California Institute of Technology, May.

Kelly, J.M. (1991). "Dynamic and Failure Characteristics of Bridgestone Isolation Bearings," Report No. UCB/EERC-91-04, Earthquake Engineering Research Center, University of California at Berkeley, April.

Kelly, J.M. (1996). "High-Damping Rubber Seismic Isolation Bearings Ten Years After Manufacture," Earthquake Engineering Research Center News, Vol. 17, Number 3, July.

Kelly, J.M., Buckle, I.G., and Tsai, H.C. (1986). "Earthquake Simulator Testing of a Base-Isolated Bridge Deck," Report No. UCB/EERC-85-09, Earthquake Engineering Research Center, University of California at Berkeley, January.

Kelly, J.M., Buckle, I.G., and Koh, C.G. (1987). "Mechanical Characteristics of Base Isolation Bearings for a Bridge Deck Model Test," Report No. UCB/EERC-86-11, Earthquake Engineering Research Center, University of California at Berkeley, November.

Kelly, J.M., and Chalhoub, M.S. (1990). "Earthquake Simulator Testing of a Combined Sliding Bearing and Rubber Bearing Isolation System," Report No. UCB/EERC-87-04, Earthquake Engineering Research Center, University of California at Berkeley, December.

Kelly, J.M., and Quiroz, E. (1992). "Mechanical Characteristics of Neoprene Isolation Bearings," Report No. UCB/EERC-92-11, Earthquake Engineering Research Center, University of California at Berkeley, August.

Lin, Y. (1996). "Seismic Behavior of Bridge Pier Column Lap Splices," Ph.D.dissertation, University of Illinois at Urbana-Champaign, Champaign, IL.

Mander, J.B., Kim, D.K., Chen, S.S., and Premus, G.J. (1996). "Response of Steel Bridge Bearings to Reversed Cyclic Loading," Report No. NCEER-96-0014, National Center for Earthquake Engineering Research, State University of New York at Buffalo, January.

Maragakis, E.A., Douglas, B.M., and Abdel-Ghaffar, S.M. (1994). "An Equivalent Linear Finite Element Approach for the Estimation of Pile Foundation Stiffnesses," Earthquake Engineering and Structural Dynamics, Vol. 23, pp.1115-1124.

Maroney, B., Kutter, B., Romstad, K., Chai, Y.H., and Vanderbilt, E. (1994). "Interpretation of Large Scale Bridge Abutment Test Results," Proceedings of the 3<sup>rd</sup> Annual Seismic Research Workshop, June 27-29, Sacramento, California.

Martin, J.W. (1991). "Long Term Performance of Rubber in Seismic and Non-Seismic Bearings: A Literature Review," Report No. NISTIR 4613, National Institute of Standards and Technology, U.S. Department of Commerce, June.



- Matlock, H. (1970). "Correlations for Design of Laterally Loaded Piles in Soft Clay," Paper No. OTC 1204, Proceedings of the 2<sup>nd</sup> Annual Offshore Technology Conference, Houston, Texas, Vol. 1, pp. 577-594.
- McCallen, D.B., and Romstad, K.M. (1994a). "Dynamic Analyses of a Skewed Short-Span, Box-Girder Overpass," *Earthquake Spectra*, Vol.10, No. 4, pp. 729-754.
- McCallen, D.B., and Romstad, K.M. (1994b). "Seismic Response Computations for a Simple Overcrossing," Proceedings of the 3<sup>rd</sup> Annual Seismic Research Workshop, June 27-29, Sacramento, California.
- Murray, R.M., and Detenber, J.D. (1961). "First and Second Order Transitions in Neoprene," *Rubber Chemistry and Technology*, pp.668-685, April-June.
- NEHRP (1997). "NEHRP Recommended Provisions for Seismic Regulations for New Buildings and Other Structures," Federal Emergency Management Agency.
- Porter, L.D. (1983). "Processed Data from the Strong-Motion Records of the Imperial Valley Earthquake of 15 October 1979," Special Publication 65, California Department of Conservation, Division of Mines and Geology.
- Prakash, V., and Powell, G.H. (1993). "DRAIN-2DX, DRAIN-3DX and DRAIN-BUILDING: Base Program and Design Documentation," Report No. UCB/SEMM-93-16, December.
- Price, T.E. (1997). "Influence of Embankment/Superstructure Interaction on the Dynamic Response of Short Bridges," Ph.D.dissertation, University of Washington, Seattle.
- Pujol, S. (1997). "Drift Capacity of Reinforced Concrete Columns," Master Thesis, Purdue University, Indiana.
- Reese, L.C., Cox, W.R., and Koop, F.D. (1974). "Analysis of Laterally Loaded Piles in Sand," Paper No. OTC 2080, Proceedings of the 5<sup>th</sup> Annual Offshore Technology Conference, Houston, Texas, Vol. II, pp. 473-485.
- Reese, L.C., and Welch, R.C. (1975). "Lateral Loading of Deep Foundations in Stiff Clay," Proceedings of the American Society of Civil Engineers, Vol. 101, No. GT7, pp. 633-649, February.
- Reese, L.C., Cox, W.R., and Koop, F.D. (1975). "Field Testing and Analysis of Laterally Loaded Piles in Stiff Clay," Paper No. OTC 2312, Proceedings of the 7<sup>th</sup> Annual Offshore Technology Conference, Houston, Texas, Vol. II, pp. 672-690.

- Roeder, C.W., and Stanton, J.F. (1983). "Elastomeric Bearings: State-of-the-Art," ASCE Journal of Structural Engineering, Vol. 109, No. 12, pp. 2853-2871, December.
- Salveson, M.W. (1991). "Painter Street Overcrossing Linear-Elastic Finite Element Dynamic Analysis," UCRL-ID-108573, Lawrence Livermore National Laboratory.
- Seed, H.B., and Idriss, I.M. (1970). "Soil Moduli and Damping Factors for Dynamic Response Analyses," Report No. UCB/EERC-70-10, University of California, Berkeley.
- Seed, H.B., Wong, R.T., Idriss, I.M., and Tokimatsu, K. (1984). "Moduli and Damping Factors for Dynamic Analysis of Cohesionless Soils," Report No. UCB/EERC-84-14, University of California, Berkeley.
- Siddharthan, R.V., and El-Gamal, M. (1998). "Simplified Approach for Nonlinear Stiffness Characterization of Abutments on Piles," Proceedings of the 6<sup>th</sup> U.S. National Conference on Earthquake Engineering, Seattle, Washington, May 31-June 4.
- Stanton, J.F., and Roeder, C.W. (1982). "Elastomeric Bearings Design, Construction, and Materials," NCHRP Report 248, August.
- Sullivan, W.R. (1977). "Development and Evaluation of a Unified Method for the Analysis of Laterally Loaded Piles in Clay," Ph.D.dissertation, The University of Texas at Austin, Austin, Texas.
- Sullivan, W.R., and Reese, L.C. (1980). "Documentation of Computer Program COM624," Geotechnical Engineering Center, Department of Civil Engineering, University of Texas at Austin, Austin, Texas.
- Sultan, M., Sheng, L.H., and Onesto, A. (1998). "Summary of the FHWA/CALTRANS/HITEC Seismic Isolator and Energy Dissipator Evaluation Program for Highway Bridges," Proceedings of the 5<sup>th</sup> Caltrans Seismic Research Workshop, June 16-18, Sacramento, California.
- Sun, J.I., Golesorkhi, R., and Seed, H.B. (1988). "Dynamic Moduli and Damping Ratios for Cohesive Soils," Report No. UCB/EERC-88-15, Earthquake Engineering Research Center, University of California at Berkeley, August.
- Sweet, J., and Morrill, K.B. (1993). "Nonlinear Soil-Structure Interaction Simulation of the Painter Street Overcrossing," Proceedings of the 2<sup>nd</sup> Annual Seismic Research Workshop, March 16-18, California.
- Taylor, P.W., and Larkin, T.J. (1978). "Seismic Site Response of Nonlinear Soil Media," Journal of the Geotechnical Engineering Division, Vol. 104, No. GT3, pp. 369-383, March.

Vucetic, M., and Dobry, R. (1991). "Effect of Soil Plasticity on Cyclic Response," *Journal of Geotechnical Engineering*, Vol. 117, No. 1, pp. 89-107.

Werner, S.D. (1993). "Study of Caltrans' Seismic Evaluation Procedures for Short Bridge Overcrossing Structures," Dames and Moore, Inc., Oakland, CA.

Werner, S.D., Beck, J.L., and Levine, M.B. (1987). "Seismic Response Evaluation of Meloland Road Overpass Using 1979 Imperial Valley Earthquake Records," *Earthquake Engineering and Structural Dynamics*, Vol. 15, pp. 249-274.

Werner, S.D., Beck, J.L., and Nisar, A. (1990). "Dynamic Tests and Seismic Excitation of a Bridge Structure," *Proceedings of the 4<sup>th</sup> U.S. National Conferences on Earthquake Engineering*, Vol. 1, May 20-24, Palm Springs, California.

Wieser, P.F. (1980). "Steel Castings Handbook," 5<sup>th</sup> Edition, Steel Founders' Society of America.

Wilson, J.C., and Tan, B.S. (1990a). "Bridge Abutments: Formulation of Simple Model for Earthquake Response Analysis," *Journal of Engineering Mechanics*, Vol. 116, No. 8, pp.1828-1837, August.

Wilson, J.C., and Tan, B.S. (1990b). "Bridge Abutments: Assessing their Influence on Earthquake Response of Meloland Road Overpass," *Journal of Engineering Mechanics*, Vol. 116, No.8, pp. 1838-1856, August.